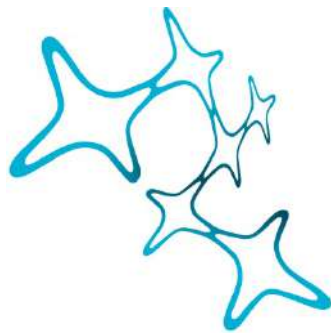


---

# UNRAVELING AND OVERCOMING HURDLES IN DIRECT NEURONAL REPROGRAMMING

---

Gianluca Luigi Russo



Graduate School of  
Systemic Neurosciences

LMU Munich



Dissertation der  
Graduate School of Systemic Neurosciences der  
Ludwig-Maximilians-Universität München

07<sup>th</sup> May, 2019

Supervisor  
Prof. Dr. Magdalena Götz  
Head of Department of Physiological Genomics  
BioMedical Center - BMC  
Ludwig-Maximilians-Universität München

Institute of Stem Cell Research  
Helmholtz Zentrum München

First Reviewer: Prof. Dr. Magdalena Götz  
Second Reviewer: Prof. Dr. Thomas Misgeld  
External Reviewer: Dr. Alessandro Prigione

Date of Submission: 07.05.2019  
Date of Defense: 06.09.2019

# Index

<b>Abstract</b> .....	<b>4</b>
<b>Introduction</b> .....	<b>6</b>
Metabolism in the CNS: astrocyte and neuron interplay .....	7
CNS damage and neuronal-glia response .....	11
CNS repair: strategies .....	15
Direct neuronal reprogramming <i>in vitro</i> and <i>in vivo</i> .....	17
Hurdles to direct neuronal reprogramming .....	19
<b>Results</b> .....	<b>24</b>
Aim of the study I .....	25
Region- and layer-specific differences in astrocyte-to-neuron reprogramming .....	26
Aim of the study II .....	59
Identification and successful negotiation of a metabolic checkpoint in direct neuronal reprogramming .....	60
Aim of the study III .....	98
Mitochondrial reprogramming using dCas9 boosts glia-to-neuron conversion .....	99
<b>Discussion</b> .....	<b>130</b>
Impact of viral vectors and inflammation on direct neuronal reprogramming .....	131
Role of ROS and metabolism in hampering direct neuronal reprogramming .....	135
Mitochondria reprogramming boosts astrocytes-to-glia conversion .....	139
<b>Bibliography</b> .....	<b>146</b>
Curriculum Vitae .....	160
Publications .....	162
Affidavit .....	163
Declaration of author contribution .....	164
Acknowledgements .....	165

## Abstract

Discovering new approaches to replace lost neurons following brain damage, as for traumatic injury, is one of the major goals in the field of regenerative medicine. Direct neuronal conversion of glial cells into neurons is emerging as a powerful strategy to achieve neuronal replacement. Despite large progress in the field, major limitations still exist before bringing this approach toward clinical translation. Major hurdles encompass epigenetic, metabolic and environmental barriers, which impede the newly generated neurons to properly integrate into the injured brain parenchyma, to substitute the lost neuronal networks and to fully replace the endogenous neuronal counterpart.

The pathological process includes a cascade of fast-occurring events, such as metabolic impairment, reactive oxygen species and inflammatory molecules production, cell death, reactive gliosis and recruitment of inflammatory cells, which can have devastating consequences for the survival of the endogenous and reprogrammed neurons. Thus, a deeper understanding of the interplay between these mechanisms and how key players in the injury environment regulate processes of cell fate decision is needed.

An important aspect fundamental to functional glia-to-neuron conversion in the injured brain is the viral vector used, especially in regard to the inflammatory reaction elicited in the tissue. Indeed we could observe that different viral vectors, routinely used in neuronal reprogramming studies, could induce diverse responses in the environment, independently from the transgene expressed. In particular, we noticed that retrovirus and lentivirus-mediated reprogramming elicited a strong inflammatory reaction, characterized by microglia and astrocyte reactivity, and massive immune cells infiltration, still persisting at the time when neurons start appearing. Conversely, adeno-associated virus (AAV)-mediated neuronal conversion had much a milder impact on the activation of the glial cells, with minimal immune cells recruitment. As using AAV greatly improved the rate of neuronal conversion, specification, integration and survival, compared to retroviral approaches, the environment plays a critical role in this successful reprogramming.

A secondary mechanism also associated with inflammation is reactive oxygen species (ROS) production. Indeed, astrocytes transitioning into neurons face a burst of ROS, which lead to drastic cell death by ferroptosis if not properly counteracted. Consequently, buffering ROS with scavengers and pro-survival genes could greatly ameliorate the conversion efficiency *in vitro* as well as *in vivo*. As ROS production is mostly related to functional metabolic changes, we investigated this so far neglected aspect of direct neuronal reprogramming.

I first demonstrated that a metabolic switch from glycolysis to oxidative phosphorylation is an essential requirement for a successful conversion to occur, as inhibiting the function of the electron transport chain did not improve the process despite the decrease in ROS, but actually entirely blocked the conversion of glia into neurons.

As we were further interested in understanding the roles played by the metabolism in the reprogramming paradigm, we decided to characterize the mitochondria proteome of astrocytes

and neurons, to identify differences in the mito-proteome between these cell types. We identified proteins enriched to each cell type, highlighting metabolic pathways relevant for their specific physiological functions. Interestingly, some of the specific mitochondrial proteins analyzed were correctly up-regulated or down-regulated during the transition from astrocytes to neurons, but at a relatively late stage in the reprogramming process. This finding further confirmed that a remodeling in mitochondrial proteins, and consequently metabolic pathways, occurs during the reprogramming process, even if partial and temporally delayed compared to the burst of ROS which converting neurons face. Early dCas9-mediated overexpression of anti-oxidant proteins in converting astrocytes, specific to the neuronal mitochondria proteome, could greatly improve the speed and efficiency of astrocyte-to-neuron conversion.

Thus, understanding how to properly modify converting glial cells into neurons, not only from an epigenetic, genetic and morphological point of view, is necessary. In fact evaluating the impact on direct neuronal reprogramming of extrinsic factors, such as viral vectors and the environmental inflammatory reaction, as well as intrinsic constraints, such as mitochondria remodeling, ROS production and metabolic switch, could greatly improve the quality of reprogrammed neurons.

The aim of my thesis is thus to unravel mechanisms involving inflammation, mitochondria and metabolic remodeling, which could increase our understanding of the glia-to-neuron conversion process, overall improving direct neuronal reprogramming.

## Introduction

The Central Nervous System (CNS) is probably the most complex and delicate organ of our body, yet the least understood. How trillions of cells intricately connect to each other, creating neuronal networks which shape our identity, is definitely a miracle of evolution and has been a long topic of debate amongst scientists and philosophers for centuries. Nevertheless, the advances in technology allowed us in the last decades to unravel many unknown functions of the brain and of the cells that constitute it, in physiological as well as in pathological conditions. In particular, understanding the interplay between fundamental components of the brain, namely neurons and glial cells, and how they react in pathological environment, interacting with local and invading inflammatory cells, is essential to treat neurodegenerative conditions affecting more than 50 million people worldwide, with huge health costs for society (Chen et al., 2016; Winblad et al., 2016).

As later discussed in detail, following an acute pathological insult an impairment in supply of oxygen and metabolic substrates leads to energy failure and cell death. The most sensitive cells are neurons, mostly due to their high energy demand usually met by ATP generated through oxidative phosphorylation (oxphos) (Harris et al., 2012). Glial cells, such as astrocytes and mature oligodendrocytes, further support neuronal metabolic needs, beyond performing a plethora of other functions in the CNS (Magistretti and Allaman, 2015; Saab et al., 2013). In this early phase of damage inflammatory signals, such as cytokines, chemokines and reactive oxygen species, spread, leading to recruitment of immune cells and proliferation of local cells (i.e. astrocytes, oligodendrocyte precursor cells (OPCs) and microglia). These activated cells in mammals form a glial scar that, despite debated function, limits the spreading of damage signals and contributes to clean up the cellular debris. The final phase of the process is mainly focused on tissue remodeling for functional restoration, encompassing blood-brain barrier (BBB) repair, scar reorganization and alternative neuronal connections rewiring and reinforcement (Burda and Sofroniew, 2014). Unfortunately, spontaneous restoration of lost neuronal functions has still very limited success, leading the patient to face severe disabilities or death (Grade and Götz, 2017).

The biggest barrier in the field of treating diseases related to damage of the CNS is indeed the very limited capacity of the brain for self-repair, as neurons and consequently functional circuits are irreversibly lost once an injury has occurred. A revolution in the field was the discovery of ongoing neurogenesis in the brain (*for historical review see Gage, 2002*), leading to great hopes to replace endogenous lost neurons. Despite that, the expectations have been disappointed, as endogenous neurogenesis is restricted to few neurogenic niches (Grade and Götz, 2017), leading to very small degrees of self-repair.

Another turn in the promises for neuronal replacement was the discovery that adult somatic cells can be forced to change fate through selective overexpression of master developmental-derived transcription factors (TFs) (*for historical review see Xu et al., 2015*), which lead to the discovery that adult somatic fate can be turned back to pluripotent state (Takahashi and

Yamanaka, 2006), opening the field of induced pluripotent stem cells (*see review* Avior et al., 2016; Shi et al., 2017).

Even prior to this breakthrough discovery, several somatic cell types have been reprogrammed into neurons, starting from glial cells (Heins et al., 2002) and extending to cells derived from different germinal layers, leading to the field of direct neuronal reprogramming (*see review* Amamoto and Arlotta, 2014; Heinrich et al., 2015). Especially in the last decade, enormous advances in technology and in the molecular understanding of the reprogramming process have drastically improved the generation of neurons (Grath and Dai, 2019; Masserdotti et al., 2016).

Despite the progress, the generation of specific neuronal subtypes that properly integrate, survive long-term and restore lost neuronal function in a pathological environment has still to overcome many hurdles. Indeed, gaps in understanding molecular, epigenetic and metabolic constraints to the process of direct neuronal reprogramming are the biggest challenges for its translation into clinical application (Gascón et al., 2017). As the role of the metabolism and inflammation in direct neuronal reprogramming has been barely investigated, a deeper understanding of the molecular and cellular interplay of these key factors with the converting neurons is fundamental.

With this aim, I will first discuss in details the delicate metabolic interplay between astrocytes and neurons in the brain, highlighting their response in physiological and pathological conditions. I will introduce the inflammatory response consequent to brain injury and how it can influence the metabolism of neuronal and glial cells. I will then move to the available strategies to induce neuronal replacement and repair. I will finish by evidencing the current state of the art of direct neuronal reprogramming, as a promising strategy for brain repair. I will at the end discuss the hurdles that direct neuronal reprogramming needs to overcome to improve the process, focusing on the metabolic, mitochondria and inflammatory interplay.

### **Metabolism in the CNS: astrocyte and neuron interplay**

Despite representing only 2% of the total body mass, the brain is responsible for the consumption of 20% of the oxygen (O<sub>2</sub>) and 25% of the glucose daily absorbed in the human body (Bélanger et al., 2011). Glucose is indeed the main energy substrate for most of the cells, and in particular for the brain, which requires higher amounts to sustain the intense electrical activity. The metabolism of glucose within the brain comprises sophisticated and not yet fully understood reactions and interchanges amongst glial cells and neurons.

Glucose is generally distributed throughout the body *via* blood vessels. Within the CNS, the expression of specific glucose transporters (GLUTs) on endothelial cells, glial cells and neurons allows its distribution (Benarroch, 2014). Glucose is mostly first processed within astrocytes and its intermediates are then distributed to other glial cells and neurons.

Astrocytes, accounting for about 20-40% of the total glial cells in the mammalian brain (Liddelow and Barres, 2017; Verkhratsky and Nedergaard, 2018), perform a plethora of functions, encompassing regulation of ion and neurotransmitter concentrations in the extrasynaptic space, setting brain blood flow rate, orchestrating synaptic pruning, contributing

to neuronal information processing, mediating phagocytic and inflammatory functions (Poskanzer and Molofsky, 2018; Sofroniew and Vinters, 2010). Most importantly, astrocytes are key player in regulating brain energy supply and storage. Indeed these cells metabolize glucose mainly through glycolysis and alternatively store it in the form of glycogen. Storing glycogen is a unique feature for astrocytes within the brain, which is released in condition of brain energy shortage, like upon intense neuronal activation and neurotransmitters induction (Magistretti and Allaman, 2015).

The preferred pathways for glucose utilization are glycolysis and subsequently oxidative phosphorylation. Glycolysis is the sequence of reactions catalyzed by 10 enzymes converting glucose in pyruvate, generating adenosine triphosphate (ATP) and important cofactors, as nicotinamide adenine dinucleotide reduced (NADH), flavin adenine dinucleotide reduced (FADH<sub>2</sub>), coenzyme A (CoA). Importantly, glycolysis also provides precursors for chemical constituents of amino acids, nucleotides and lipid synthesis. It is thus the preferred pathway for proliferating cells, with high requirements for metabolic intermediates to support biosynthesis (Lunt and Vander Heiden, 2011), and for glial cells, which require high lipid content (Montani and Suter, 2018). Glycolysis produces two molecules of pyruvate, which can take different metabolic routes depending on oxygen availability and cellular metabolic context.

When oxygen is available, pyruvate is converted to acetyl-coenzyme A (acetyl-coA) by pyruvate dehydrogenase complex, which then can enter mitochondria to feed the tricarboxylic (TCA) cycle, also known as Krebs's cycle or citric acid cycle. TCA cycle is fundamental for most of the anabolic and catabolic reactions within the cells, as central hub to produce many molecular intermediates, such as amino-acid and lipids (Akram, 2014). TCA cycle produces also highly energetic cofactors, as NADH and FADH<sub>2</sub>, to feed the oxidative phosphorylation.

Oxphos encompasses a series of enzymatic reactions that take place within mitochondria, requiring O<sub>2</sub> and high energetic releasing cofactors, as NADH and FADH<sub>2</sub>. These cofactors carry electrons to allow transfer redox reactions to occur and are produced from glycolysis, citric acid cycle and  $\beta$ -oxidation of fatty acid. The electrons deriving from these molecules are passed through a set of complex enzymes, present along the inner mitochondria membrane (IMM), forming the electron transport chain (ETC) (Wilson, 2017).

Five different complexes, constituted of 90 nuclear- and mitochondrial-encoded proteins, are responsible for coupling cofactor-derived electrons to ion transfer of protons (H<sup>+</sup>) across the IMM (Letts and Sazanov, 2017). This creates an electrochemical proton gradient that drives the synthesis of ATP and water (H<sub>2</sub>O) in the final ETC complex, ATP synthase, subsequently released in the mitochondrial matrix and exported to the cytoplasm. The process of aerobic respiration burns O<sub>2</sub> molecules, creating a proton gradient across the mitochondrial membrane, but also produces reactive oxygen species as a byproduct (Nath and Villadsen, 2015). The fundamental role of ROS in astrocytes or neurons is discussed later.

Importantly, ATP production from glucose catabolism is more efficient in oxphos than in glycolysis, as the net yield from each pathway is 30-36 versus 2 ATP molecules (Berg et al., 2002). Despite that, the preferred pathway within a cell is not necessarily the most energy

producing one, as this comes with the cost of higher ROS production and faster metabolism. Each cell type specifically regulates the preferential pathway for energy derivation according to specific function and cellular stage (Folmes et al., 2011). For example, higher and faster glycolytic rate can compensate for lower ATP production (Pfeiffer et al., 2001; Valvona et al., 2015), e.g. in dividing cells, which have high macromolecules demand, or stem cells, which require low ROS production (Zhang et al., 2012). ATP production also derives from alternative routes of acetyl-coA metabolism, such as fatty acid metabolism, amino-acids catabolism and lactate conversion (Berg et al., 2002).

$\beta$ -oxidation of fatty acid includes catabolic reactions leading to acetyl-coA and cofactor production, used as substrates for ATP generation. How much of the brain energy demand relies on this pathway is a matter of debate, but some data suggest that up to 20% of energy expenses might be dependent on oxidation of fatty acid, which almost exclusively occurs in mitochondria (Panov et al., 2014). Indeed the complete oxidation of one molecule of fatty acid, compared to one of glucose, can produce more than double the amount of ATP molecules, even if preferring this pathway over complete glycolysis may occur at the costs of higher oxygen requirements and presumably increased ROS production (Darvey, 1998; Perevoshchikova et al., 2013; Schönfeld and Reiser, 2013; Souza et al., 2019). In any case, a prominent role for fatty acid  $\beta$ -oxidation in brain homeostasis is undeniable. Indeed many studies underline high expression levels of key enzymes involved in this pathway within astrocytes (van Deijk et al., 2017; Hofmann et al., 2017).

Nevertheless astrocytes, despite their ability to perform glycogenesis, glycolysis, oxidative phosphorylation and fatty acid oxidation, absorb a disproportionately high amount of glucose, compared to their energy demand (Chuquet et al., 2010). A simple reason for this paradox is the well-established function of astrocytes as energy feeders for neurons.

Neurons indeed lack key enzymes involved in fundamental steps of glycolysis, such as the correct pyruvate kinase (PKM) isoform (Zhang et al., 2014) or the rate-limiting enzyme Pfk3b (Herrero-mendez et al., 2009), compared to astrocytes. Indeed, pioneer experiments where selective key components of the oxphos machinery were ablated in the brain further confirmed the low reliance of neurons, compared to other glial cells, on glycolysis, also when oxphos was impaired (Diaz et al., 2012; Fünfschilling et al., 2012; Supplie et al., 2017). Other reports suggest on the contrary that neurons, in particular conditions of stimulation, may perform glycolysis, even at higher rate compared to oxphos (Díaz-García and Yellen, 2018; Ivanov et al., 2014); indeed some GLUTs isoforms are also expressed on neuronal plasma membrane (Vannucci et al., 1998). Nevertheless, neuronal glucose uptake in physiological condition may happen, but likely has a different degradation pathway compared to astrocytes.

Indeed glucose in neurons is known to detour, at least partially, to the Penta-Phosphate Pathway (PPP) (Bélanger et al., 2011). PPP, divided in an oxidative and not-oxidative branch, is fundamental for defense against oxidative stress, generating nicotinamide adenine dinucleotide phosphate reduced (NAPDH) to fuel redox reaction of glutathione (GSSG, oxidized, or GSH, reduced), mainly involved in detoxifying from ROS (Bolaños and Almeida, 2009). PPP is further involved in maintaining carbon homeostasis providing

precursors for nucleotide and amino acid biosynthesis, according to specific cellular context needs (Stincone et al., 2015)

Even if glucose does not seem to be the main energetic source for neurons, the astrocyte-neuron lactate shuttle hypothesis (ANLSH) (Pellerin and Magistretti, 1994; Pellerin et al., 1998) seems to reasonably explain how this supply of substrate might happen. Indeed pyruvate, in lower oxygen availability or when it is needed for other purposes rather than TCA cycle, can be converted by lactate dehydrogenase (LDH) into lactate. Lactate is released in the extracellular matrix by astrocytes and taken up by specific neuronal transporters, then is converted back to pyruvate and utilized for aerobic respiration. This offers the selective advantage for neurons to have a ready-to-use substrate to meet their energetic requirements, while astrocytes perform the high energy producing steps of glycolysis (Amaral et al., 2013; Mächler et al., 2016).

Interestingly, also glutamate and glutamine have been shown to be potential substrates for ATP production within neurons. Glutamate is physiologically released following excitatory activity and it accumulates in the extracellular space. Astrocytes, through glial-specific glutamate transporters (EAATs), take up glutamate and convert it into glutamine, further released by astrocytes through glutamine transporter. Neurons then take up and recycle glutamine, converting it into glutamate through glutaminase (Gls) and reuse it as neurotransmitter or also to fuel the TCA cycle. Concomitantly, glutamate accumulation within astrocytes also triggers increase in glycolysis and lactate production (Calvetti and Somersalo, 2012; Fendt and Verstreken, 2017).

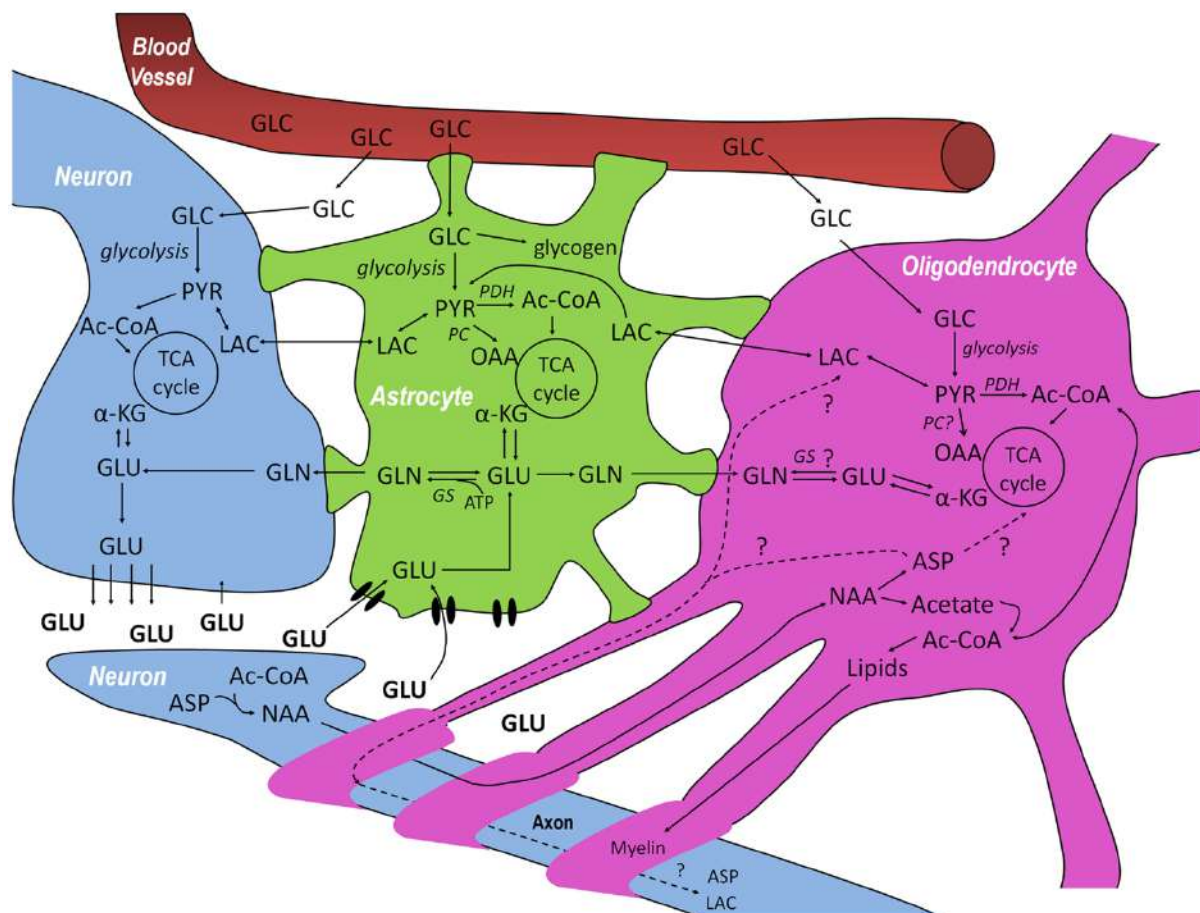


*Figure 1. Schematic overview of the metabolic interactions between neurons and glial cells (Amaral et al., 2013. This is an open-access article distributed under the terms of the Creative Commons Attribution License).*

It is worthwhile mentioning that despite more than a century of studies on the CNS metabolism, development of new technologies and techniques still surprise us with how few we actually know of what happens in the brain *in vivo*. Interestingly, deep proteomic studies are finding more and more proteins involved in mitochondrial homeostasis, whose effect in cellular context is still to be determined (Calvo et al., 2016). Mitochondrial composition varies hugely amongst different tissues and even cell types within the same tissue (Calvo and Mootha, 2010; Forner et al., 2006; Pagliarini et al., 2008). Excitingly also mitochondria and metabolic differences within different compartments of the same cell type have been determined (Graham et al., 2017; Völgyi et al., 2015). Development of new technologies, like CRISPR-Cas9, is helping us unraveling new molecular functions for well known mitochondrial proteins (Arroyo et al., 2016; Jo et al., 2015), fundamental to fully understand specific mitochondrial pathways within a cell (Johnson et al., 2007b, 2007a).

The importance of mitochondria in regulating broader and uninvestigated branches of metabolism is now being increasingly recognized (Spinelli and Haigis, 2018). This can have a great impact on unraveling new specific metabolic functions of astrocytes and neurons (Fiebig et al., 2019; Hayakawa et al., 2016).

To sum up, according to the cellular and environmental context, the metabolism of astrocytes and neurons within the brain is plastic and mitochondria play a pivotal role in this regulation. In particular, it seems that neurons have a limited capacity for glycolysis, while having an active TCA cycle and oxphos machinery. Oxphos requires the metabolic supply of substrates and cofactors, like lactate, glutamate, NADH and FADH<sub>2</sub>, from astrocytes and oligodendrocytes. On the contrary, astrocytes seem to have a more adaptable metabolism, relying mostly on glycolysis and glycogenesis for production and storage of energy. Furthermore, high reliance also on fatty acid metabolism and oxphos for ATP generation has been suggested to occur in this glial cell type. Notwithstanding, scarce knowledge still exists on how specific mitochondria composition of astrocytes and neurons might influence cell-specific function in physiological and pathological conditions.

Interestingly, in a pathological model of Huntington disease, astrocytes from different regions compensate for lack of glucose metabolizing different substrates (Polyzos et al., 2019). Indeed a further level of understanding of the metabolic reactions occurring within glial cells and neurons derives from evaluating these cell types in a pathological context. In fact, astrocytes and neurons have different abilities to survive upon damage and oxidative stress (Wang and Michaelis, 2010).

### **CNS damage and neuronal-glia response**

The delicate architecture and balance of functions within the CNS can be easily perturbed by a variety of different pathological insults. These diverse stimuli trigger a multifaceted cellular and molecular response, involving endogenous neuronal and glial cells, but also blood-derived immune cells, which cooperate for wound repair and tissue replacement.

Nevertheless, neurological damage often leads to severe cell death, causing disability and representing a major cause of death worldwide (Jassam et al., 2017; Winblad et al., 2016).

CNS injuries can be broadly defined as acute and focal, such as the ones consequent to ischemic stroke or traumatic brain injury (TBI), or diffuse and chronic neurodegenerative diseases, like Alzheimer's disease (AD), multiple sclerosis (MS), Parkinson's diseases (PD) and many more (Chen et al., 2016). The pathologies induce different response mechanisms in the brain, triggering wound repair and tissue replacement when the insult is acute, or more drastic tissue remodeling mechanisms when slow neurodegenerative diseases occur (Burda and Sofroniew, 2014). The adverse output for the recovery of the patient, in all these conditions, triggers the necessity for a deeper understanding of the molecular mechanisms regulating the pathological process, where metabolic deregulation represents one of the major challenges.

TBI, or stab-wound injury (SWI) when referring to animal models, can be considered as a typical model of acute and focal injury. It largely varies as output for the recovery of the patient according to the severity of the trauma, the injured area involved and how fast the medical treatment occurs. TBI contributes to 30% of all injury-related deaths, leading also to permanent disabilities in most of the millions of people yearly affected (Gyoneva and Ransohoff, 2015; Jassam et al., 2017). Overall, at molecular and cellular level, it can be divided into three temporal phases.

It is first characterized by disruption of blood vessels, inducing a lack of oxygen and glucose for the affected area. In seconds to minute after the failure in energy supply neurons depolarize, not being able to actively sustain their membrane potential. This has as a first consequence the inability to remove the released neurotransmitters, like glutamate, from the extracellular space, activating endogenous glutamatergic receptors triggering excitotoxicity. As consequence of excessive neuronal activation, free radicals species are generated, further damaging membranes, mitochondria and DNA, triggering caspase-mediated cell death (apoptosis) (Arundine and Tymianski, 2004; Leker and Shohami, 2002). Moreover, the extracellular concentration of potassium ( $K^+$ ) rises, further propagating waves of depolarization. According to the severity of the injury, accumulation of extracellular ions can induce swelling and edema, while intracellular calcium ( $Ca^{2+}$ ) within neurons can activate enzyme systems, like lipases, endonucleases and proteases, which further promote early neuronal death. Furthermore, early release of damage associated molecular patterns (DAMPs) together with free radicals from the injured tissue elicit the second phase of the pathological cascade, involving activation of microglia and recruitment of blood-derived leukocytes.

In this early phase, perturbed interactions among astrocytes and neurons play a key role in spreading the pathological insult. Particularly relevant is the reliance of neurons on astrocytes for anti-oxidants and substrates for survival. Thus, it is not surprising that when an energy failure occurs and basic astrocyte functions are impaired, neurons are the first cells to suffer, losing substrates as lactate and glutamate (Bélanger et al., 2011). It is rather surprising instead that neurons, despite being stronger users of oxphos, are the most sensitive cell to ROS-mediated damage in the brain.

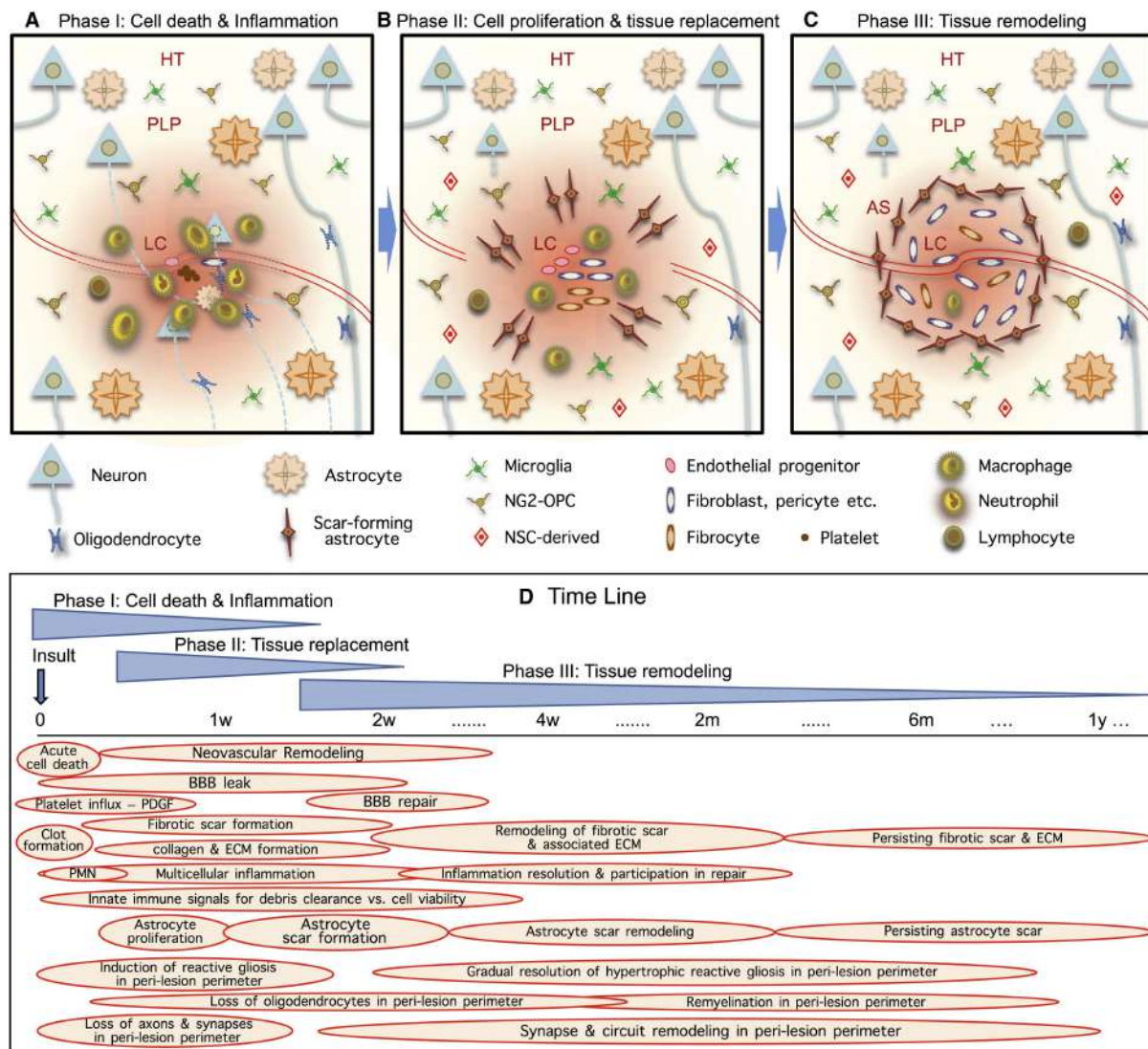


**Figure 2.** Phases and time course of multicellular responses following acute injury to the central nervous system (Burda and Sofroniew, 2014. License Number: 4565530405973).

The most represented ROS are mitochondrial-derived superoxide radical ( $O_2^-$ ), reactive hydroxyl radical ( $\cdot OH$ ), and hydrogen peroxide ( $H_2O_2$ ) (Murphy, 2009). Many antioxidant systems protect the cell from their action, such as superoxide dismutases (SOD), glutathione, thioredoxins (TRX), peroxiredoxins (PRX) and catalases (CAT) (Birben et al., 2012). Astrocytes possess higher amounts of these antioxidant molecules and couple their bioenergetics system to neurons also with defense against ROS. Indeed, in different models of injury, neurons rely on astrocytes to survive and cope with damage (Allaman et al., 2011; Anderson et al., 2016; Chen et al., 2009). For example, astrocytes mostly synthesize and provide GSH, through recycling of glutamate, which is then used within neurons as strong anti-oxidant molecule, together with NADPH produced through neuronal PPP (Fernandez-Fernandez et al., 2012). Neurons can anyway cope with stress relying on some self-produced antioxidant molecules, such as PRX and SOD, up-regulated in situation of stress, or produced through the PPP pathway (Boulos et al., 2007; Quaegebeur et al., 2016).

The second phase of events within the lesioned area occurs hours to days after the injury, and is mainly characterized by tissue remodeling processes, such as cell proliferation and

migration, ongoing inflammation and secondary cell death (Burda and Sofroniew, 2014). In particular, DAMPs and ROS lead to secretion of chemokines and pro-inflammatory cytokines from the brain resident microglia and astrocytes, leading to activation of chemokine receptors on endothelial cells, mediating recruitment and extravasation of leukocytes. Neutrophils and macrophages are the first subtypes of leukocytes infiltrating the tissue, modulating and decreasing the ongoing inflammation in the environment, actively secreting pro- and anti-inflammatory cytokines. Cytokines further increase in a positive loop the recruitment of other inflammatory cells on one side, and on the other side modulate glial function, activating phagocytosis to remove cell debris and resolve the ongoing inflammation (Chen et al., 2016; Gyoneva and Ransohoff, 2015; Silver et al., 2014). Shortly after early macrophage infiltration, microglia and astrocytes further increase their reactivity, up-regulating Iba1 and GFAP expression respectively, and acquiring a further activated amoeboid morphology. These glial cells start to proliferate, forming the so-called “reactive gliosis”, contributing to the resolution of ongoing inflammation and to the formation of a glial scar in the mammalian brain (Dimou and Götz, 2014).

In particular, the ambiguous role of reactive astrocytes in the injury environment has been long debated (Liddelow and Barres, 2017; Pekny and Pekna, 2014). It is known that astrocytes following an injury do not migrate to the injury site, unlike microglia or OPCs, but rather proliferate locally, mostly at the peri-vascular location (Bardehle et al., 2013; Robel et al., 2011). The local proliferation of astrocytes has been long considered as negative for the neuronal regeneration, leading to the formation of a scar in mammals that hampers neuronal axonal regrowth (Silver et al., 2014). However, growing pieces of evidence support beneficial effects of reactive astrocytes in neuroprotection and neurorepair, rather than being detrimental (Anderson et al., 2016; Frik et al., 2018; Tang, 2016).

In many paradigms of injury, innate immune infiltration characterized by macrophages and neutrophils is usually followed by active induction and recruitment of lymphocytes, characterizing the branch of the adaptive immunity. This feature is typical of insults where bacterial, virus or autoimmune reactivity occurs. T lymphocytes exert the function of actively recognizing specific antigens, which can belong to the invading pathogen, or in case of autoimmunity to the host. This specific recognition leads to activation of pathways inducing selective killing of the targeted cells. B lymphocytes, producing antigen-targeted antibodies, further contribute to the killing of compromised cells and support the survival of T cells (Koyuncu et al., 2013; Russo and McGavern, 2015). Usually in TBI lymphocyte infiltration is absent or minimal, as most of the immune functions are performed from the non-specific branch of innate immunity (Frik et al., 2018; Mattugini et al., 2018). Anyway, some degree of T cell infiltration has been described in animal models of TBI and in patients following injury, even if their role in the post-injury environment is not clear (McKee and Lukens, 2016).

The last phase of the recovery process occurs one week to months following injury, and is mainly characterized by scar injury formation, BBB closure and neuronal rewiring to compensate the lost network, according to the degree of damage (Burda and Sofroniew, 2014). Astrocytes orchestrate the process of BBB closure together with OPCs, microglia and

macrophages, through the extensive remodeling of the extracellular matrix (ECM) and neovasculogenesis (Dimou and Götz, 2014). By 2 weeks post-injury, the brain has almost no more infiltrating immune cells, however activated microglia and astrocytes, associated with high levels of inflammatory cytokines, may persist for months. Indeed, a well-organized compact glial scar usually surrounds the lesion core, physically limiting the inflammation and allowing recovery. This reactive gliosis scar is characterized by high glial fibrillary acidic protein (GFAP) and Vimentin reactivity, which partially reduce over time (Burda and Sofroniew, 2014). Macrophages play a pivotal role in modulating the glial scar formation, as a lack of their infiltration results in reduced scar formation, already one month after injury (Frik et al., 2018). Interestingly, the capacity of the CNS to form a permanent scar opposed to full scarless regeneration differs in evolution. Mammals have indeed the most complex but also less plastic, in term of regeneration, central nervous system (Alunni and Bally-Cuif, 2016).

In mammals, the viable neuronal tissue surrounding the scar also faces a remodeling phase, whose extent varies accordingly to the degree of damage. Depending on the neuronal network involved, compensatory mechanisms exist to restore, at least partially, the lost neuronal connections, for example by strengthening the contra-lateral ones or forming collateral fibers (Carron et al., 2016; Nudo, 2013).

It is worthwhile mentioning that the delicate metabolic balance disrupted within the brain following an injury has important consequence for mitochondria stability, which clearly plays an essential role in physiology and pathology. Indeed following an injury, drastic alteration of mitochondria morphology have been observed in astrocytes (Motori et al., 2013) as well as neurons (Misgeld and Schwarz, 2017), with fundamental consequences for ROS homeostasis and pathological progression (Knott et al., 2008; Sena and Chandel, 2012). Mitochondria are indeed the primary functional regulators of cell survival and cell death, and are commonly deregulated in diseases involving the CNS, consequently mainly affecting neuronal survival (Kasahara and Scorrano, 2014).

Despite the endogenous attempt of the brain to fully restore neuronal function following a brain injury, the outcome for the patient is often fatal. This is due to the fact that neurons cannot regenerate like other glial cell types. It is thus not surprising that restoring lost neuronal cells has always been the dream of regenerative medicine.

### **CNS repair: strategies**

The attempts to repair the central nervous system have been long focused on rescuing the remaining neurons, by providing chemicals and growth factors to stimulate neuronal outgrowth and activity, or by directly pushing neural plasticity to create compensatory networks for lost connection. Thus most of these treatments, including drugs and rehabilitation techniques, aim at alleviating symptoms and promote brain functional plasticity (Grade and Götz, 2017). Despite that, the rate of success has been extremely low, mainly restricted to combinatorial drug treatments in the very early phase after injury (Rajkovic et al., 2018).

The discovery that endogenous neurogenesis occurs also in mammals (Altman, 1962), even if at a lesser extent than in other vertebrates (Alunni and Bally-Cuif, 2016), opened the door for a new field of neuroregenerative medicine. The main limitation to the use of endogenous neural stem cells (NSCs), for neuronal replacement therapies, is the restriction of adult neurogenesis to only two neurogenic niches, the subventricular zone (SVZs) and the hippocampus (Gonçalves et al., 2016; Lim and Alvarez-Buylla, 2016), which give rise to a limited number of specific long-term surviving and integrating interneurons (Bergami and Berninger, 2012). Intriguingly, neurogenesis is increased to some extent in the lesion sites of some pathologies (Hou et al., 2008; Kandasamy et al., 2015), even if proper integration of these new neurons has been very limited or even detrimental (Cho et al., 2015). Furthermore, the notion that in ageing, where most of the neurological diseases occur, NSCs decrease in number and functionality, further cooled down the enthusiasm to apply this treatment for brain disorders (Calzolari et al., 2015; Lazarov et al., 2010).

Excitingly, injury seems to elicit plasticity in glial cells to replace degenerated neurons, to some extent. The discovery that reactive cortical astrocytes up-regulate some feature typical of NSCs, and have neurogenic potential *in vitro* (Sirko et al., 2013), suggest that a better understanding of the developmental origin and molecular cues regulating astrocyte fate may be the future to foster neurogenesis after injury (Götz et al., 2015). Interestingly, also other cells within different brain regions, such as ependymal cells and striatal glia (Carlén et al., 2009; Magnusson et al., 2014), or tanycytes in the hypothalamus (Goodman and Hajihosseini, 2015), have been proven to have some neurogenic potential.

More promising as strategy for brain repair has been transplantation of exogenous neurons or neural stem cells, with broader applications in term of source and targeted area. Diverse sources exist for neuronal replacement, such as primary fetal neurons and embryonic stem cells (ESCs)-derived neurons, which have proven excellent degree of differentiation, integration and survival in different mouse models (Falkner et al., 2016; Southwell et al., 2014), and also some degrees of success when tested in human clinical trials (Curtis et al., 2018; Politis and Lindvall, 2012; Yasuhara et al., 2017). Interestingly, transplantation of NSCs supports recovery in some injury models remaining undifferentiated rather than by differentiating into neurons, secreting molecules fostering the recovery; the so-called bystander effect (Bacigaluppi et al., 2016; Martino and Pluchino, 2006).

Another promising source for transplantation are induced pluripotent stem cells (iPSCs)-derived neurons. These cells have the advantages of reduced ethical concerns compared to ESCs, of deriving from a source easy to obtain (e.g. fibroblasts) and of being genetically matched with the patient, reducing the risks for immune response and rejection. The discovery that murine and human adult somatic cells, through the expression of specific embryonically-derived TFs, can be converted back to pluripotency, similarly to ESCs (Takahashi and Yamanaka, 2006; Takahashi et al., 2007), opened a new approach for the field of disease modeling and drug discovery, reaching nowadays the previously unthinkable possibility of generating organs-like structures *in vitro* (e.g. organoids) (Rowe and Daley, 2019). Indeed, iPSCs can be converted virtually into any kind of differentiated cell type and mature iPSCs-derived neurons were indeed amongst the first generated (Dimos et al., 2008).

Most importantly, iPSCs-derived neurons can be efficiently transplanted in murine and non-human primates disease models, leading to some extent of functional recovery (Hallett et al., 2015; Wernig et al., 2008).

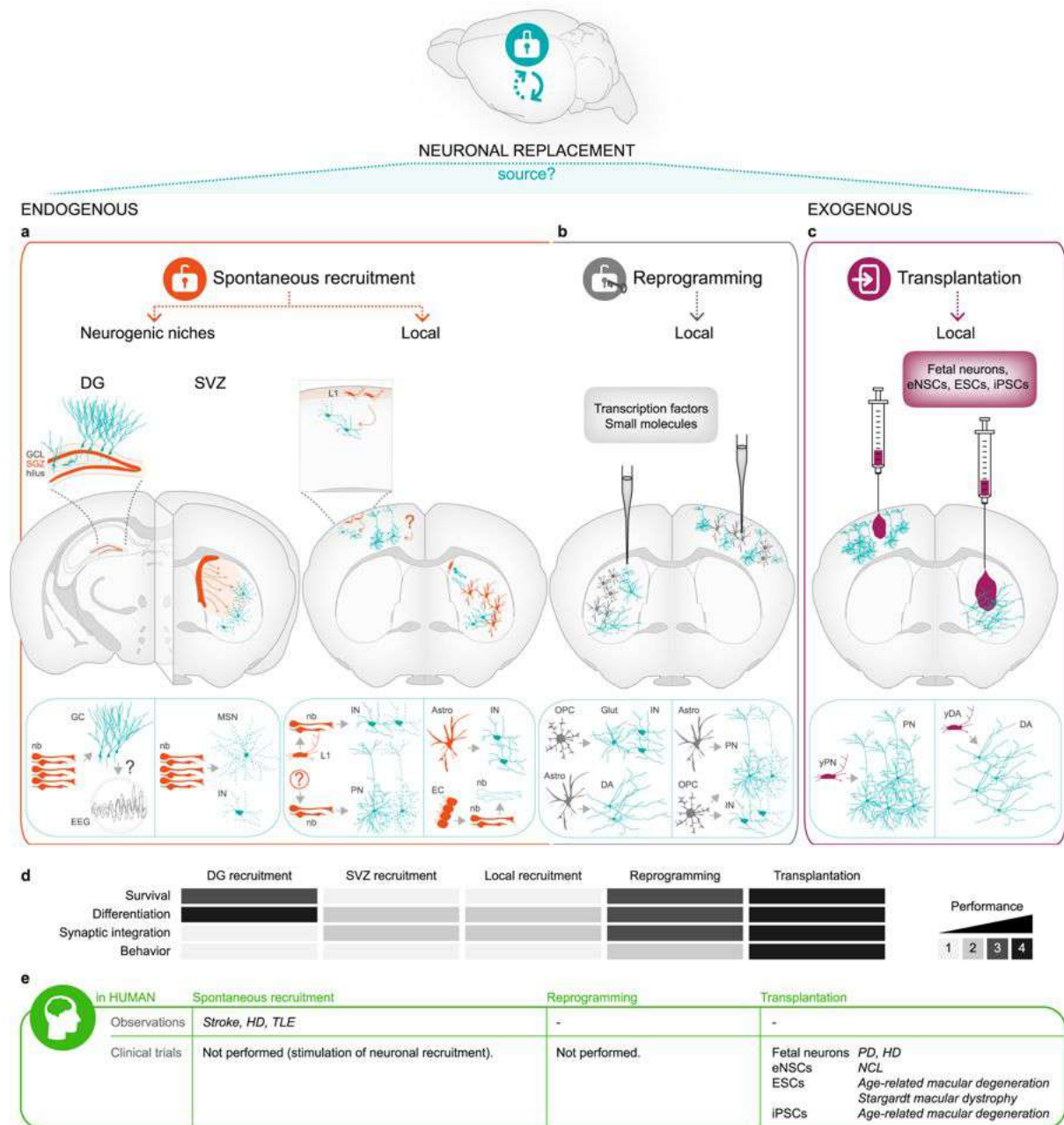


Figure 3. Overview of strategies for neuronal replacement following brain damage (Grade and Götz, 2017). Open Access: This article is licensed under a Creative Commons Attribution 4.0 International License).

The discovery that adult somatic cells can be directly converted into functional neurons, both *in vitro* and *in vivo*, opened the door to an alternative strategy for neuronal regeneration: direct neuronal reprogramming.

### Direct neuronal reprogramming *in vitro* and *in vivo*

The concept that adult somatic cells can be directly converted into other somatic cells was first demonstrated when overexpression of MyoD in fibroblasts induced their conversion to myoblasts (Davis et al., 1987). The first conversion of adult somatic cells into neurons, without passing through an intermediate pluripotent or proliferative stage, was proved when astrocytes were converted into neuronal cells through overexpression of Pax6, many years later (Heins et al., 2002). These discoveries inaugurated direct reprogramming or transdifferentiation.

Since then, the field has been boosted by the discovery that other cells, not necessarily deriving from the same germinal layer, can be converted into mature neurons, with different efficiencies and degrees of maturation (Masserdotti et al., 2016). Beyond astrocytes (Heins et al., 2002), fibroblasts (Vierbuchen et al., 2010), hepatocytes (Marro et al., 2011), pericytes (Karow et al., 2012), microglia (Matsuda et al., 2019) and even lymphocytes (Tanabe et al., 2018) have been reprogrammed into neurons, both of murine and/or human origin.

Overcoming the barrier of transitioning from one cell fate to another, even beyond germinal layer origin as for fibroblasts (Vierbuchen et al., 2010), proved how few we knew about the mechanisms regulating cell state, and how adult somatic cells can actually be plastic. Unraveling new molecular and epigenetic mechanisms involved in this process has also important applications for developmental neurogenesis (Masserdotti et al., 2016). Notably, most of these early reprogramming approaches have in common that TFs alone, involved in embryonic neurogenesis, were sufficient to generate mature neurons, like in the case of the master TFs Neurogenin 2 (Neurog2) or achaete-scute homolog 1 (Ascl1), inducing mostly glutamatergic or gabaergic neurons respectively (Heinrich et al., 2010; Masserdotti et al., 2015). Interestingly, while astrocytes are relatively easy to reprogram, this is not the same for other cells, such as fibroblasts or hepatocytes, where a combination of several TFs and molecules are required to generate a decent number of reprogrammed neurons (Pang et al., 2011). Intriguingly, recent reports also highlighted the direct generation of neurons from human and murine fibroblasts through microRNAs (miRNAs), alone or in combination with TFs (Victor et al., 2014; Yoo et al., 2011), or even through combination of small molecules alone (Hu et al., 2015; Li et al., 2015).

The biggest step forward was the proof of principle that *in vivo* direct neuronal conversion was possible (Buffo et al., 2005), even if early studies generated rather neuroblast-like cells, with short survival and rather immature morphology (Heinrich et al., 2014; Niu et al., 2013).

When translating to *in vivo* approaches, a fundamental consideration is the cell type we want to target and reprogram. This has indeed a profound impact on the environment, as we subtract functional cells from the brain. Thus, it is important we aim to target cells with proliferative and homeostatic capacity, as we do not want to generate neurons at the expenses of other important glial cell functions, as metabolic and trophic support.

The main cells targeted indeed are reactive and non-reactive astrocytes (Brulet et al., 2017), OPCs (Torper et al., 2013, 2015) or a mixture of both (Grande et al., 2013). Interestingly, according to the targeted region, usually striatum or cortex, as well as the targeted cells, OPCs or astrocytes, different efficiencies of reprogramming and survival of induced neurons have

been observed (Grade and Götz, 2017). Recent advances in genetic studies, taking advantage of transgenic mouse lines to selectively express the viral vectors carrying the neuronal TFs in one glial cell or the other, further allowed us to elucidate which cell is more amenable to neuronal reprogramming (Liu et al., 2015; Torper et al., 2015). The recent discovery that also microglia and pericytes can be reprogrammed into neurons opens new possibilities for *in vivo* studies, targeting these two CNS cell types. It would be further important to considerate which delivery strategy could be optimal for direct neuronal reprogramming, as different viral vectors can be modified to target specifically different brain cell populations, and have also been shown to elicit diverse immune responses within the CNS, which are potentially harmful for the newly generated neurons (Chew et al., 2016; Drokhlyansky et al., 2016; Mancini and Horvath, 2018).

Surprisingly, in fact, very few papers have tested the possibility of direct neuronal reprogramming in a pathological context, as most of the efforts so far focused on generating mature and long-term survival neurons. Anyway, pioneering studies in mouse models of PD and stroke showed first hints of improvement in motor functions, following *in vivo* neuronal direct reprogramming (Guo et al., 2014; Rivetti di Val Cervo et al., 2017).

Even if we are now able to produce neurons that functionally integrate into the CNS, showing electrophysiological properties and morphological features similar to the endogenous ones (Liu et al., 2015; Rivetti di Val Cervo et al., 2017), we still miss fundamental pieces of information to aim for proper neuronal replacement. Indeed, we are still lacking a comprehensive understanding of how specific neuronal subtype can be generated, how to foster their grafting and correct wiring within the lesioned area and which delivery method is optimal. Thus, many hurdles still exist before an efficient *in vivo* translation is possible.

A deeper understanding of the epigenetic, transcriptional and metabolic processes regulating reprogramming, and how the highly inflammatory and reactive pathological environment may impact the conversion, are essential aspects to fill this gap in knowledge and boost direct neuronal reprogramming to the next step (Gascón et al., 2017).

### **Hurdles to direct neuronal reprogramming**

Understanding what defines a cell identity is a central question in the field of reprogramming, which faces a further challenge when considering a neuron. Indeed, the advent of single cell genomics added a further layer of complexity, revealing dozens of unpredicted neuronal subtypes within the human and mouse brain (Lake et al., 2016; Luo et al., 2017), whose molecular characterization is not yet completed. As the aim of reprogramming is to regenerate *bona fide* neurons, a deeper understanding of which transcriptional and epigenetic networks regulate them is necessary. Interestingly, also astrocytes heterogeneity has been recently recognized as important for brain development and specification (John Lin et al., 2017; Lanjakornsiripan et al., 2018; Morel et al., 2017). Indeed, neuron and astrocyte heterogeneity seem to be intrinsically related and further associated to basic and specific cellular functions (Morel et al., 2017; Polyzos et al., 2019). Interestingly, different astrocyte subtypes are amenable to reprogramming with the same TFs, although generating different subtypes of neurons (Chouchane et al., 2017; Hu et al., 2019). Changing the molecular program

characterizing the starter cell is one of the greater challenges for the neuronal factors. Thus, a better understanding of the molecular mechanisms regulating cell fate specification of each starter cell can become an advantage to generate the correct neuronal subtype.

Indeed, recent papers highlighted how understanding and manipulating these genetic, epigenetic or even metabolic hurdles in a cell-specific context, not only offer the possibility to better understand the biology of the process, but can also greatly improve the neuronal conversion (Masserdotti et al., 2015; Zhou et al., 2018).

General hurdles to reprogramming can be subdivided as cell-specific and general. The second group encases mechanisms protecting genome stability, senescence or cell cycle re-entry (Gascón et al., 2017). Genome stability can refer to cell-type-specific transcriptional repressors or epigenetic barriers, which need to be manipulated for efficient neuronal reprogramming. For example, ablation of the RE-1 transcription repressor complex (REST) in astrocytes potently improves the conversion efficiency into neurons, as it competes for binding to targets of Neurog2 (Masserdotti et al., 2015); while the transcription factor Myt1l regulates neuronal program activation from fibroblasts by repressing all others somatic lineage programs (Mall et al., 2017). Understanding the epigenetic regulation of the reprogramming process, like was recently done for microglia converting into neurons (Matsuda et al., 2019), is essential, as epigenetic modulation has been shown to improve neurogenesis (Albert et al., 2017) and can have important consequences to boost neuron generation (Stricker and Götz, 2018). The discovery of CRISPR-Cas9 technology and its huge application for genome editing may offer great advantages in this regard (Barrangou et al., 2007).

CRISPR-Cas9 technology offers indeed an amazing tool for fast and efficient manipulation of gene expression, which has just been started to be exploited also in direct neuronal reprogramming *in vivo* and *in vitro* (Black et al., 2016; Zhou et al., 2018). The applications of Cas9 technology range from modulation of endogenous expression of multiple genes through guide-RNAs (gRNAs) co-expression targeting promoter regions (Breunig et al., 2018a; Chavez et al., 2015), screening of important proteins for neuronal metabolism and survival (Arroyo et al., 2016; Rubio et al., 2016), regulation of proteins important for mitochondria function and metabolic adaptation during reprogramming (Calvo-Garrido et al., 2019; Jo et al., 2015).

Also proteome regulation can be a barrier to reprogramming, as larger differences between the starter and induced cell type, in term of protein composition, may elicit metabolic and cellular stress. To sustain this hypothesis in iPSCs generation mitochondrial and protein autophagy is essential and beneficial for cell fate conversion (Ma et al., 2015; Wang et al., 2013). If Cas9 can be the future of reprogramming, the appropriate delivery method to mediate its expression deserves some thoughtful revision.

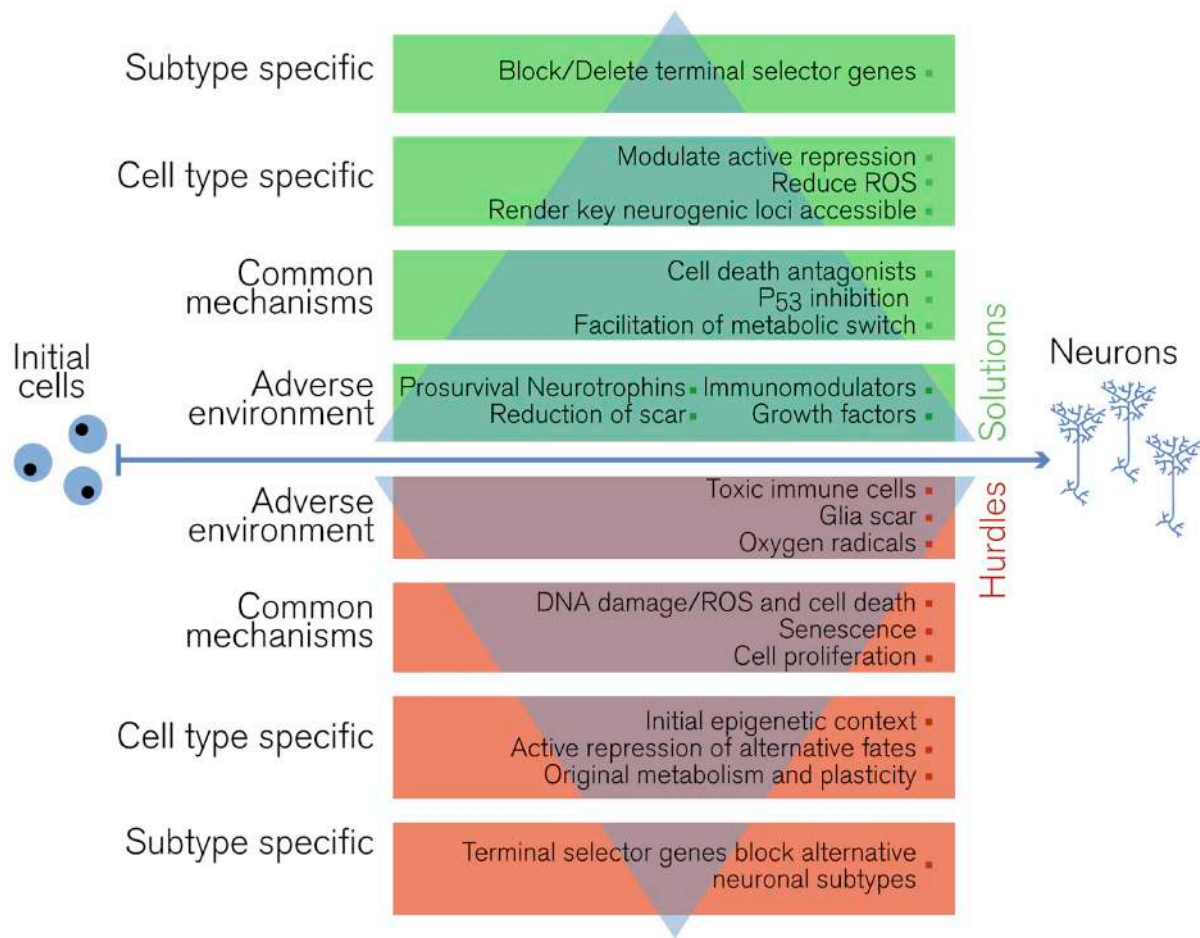


**Figure 4.** General hurdles common to direct neuronal reprogramming (Gascón et al., 2017).

Indeed, we know that most of the *in vivo* and *in vitro* reprogramming approaches so far discussed overexpress the factors mostly through Lentivirus (LV), Retrovirus (RV) and Adeno-associated virus (AAV). Each of these delivery methods have different advantages, mostly linked to the properties of the viral vector from which they derive.

Lentivirus and Retrovirus share most of their components, deriving both from *Retroviridae* and consisting of a linear positive-sense single-stranded RNA. The main difference amongst LV and RV consists in the fact that the first can infect and replicate within quiescent cells, as neurons, being able to cross the nuclear membrane and use the endogenous cell machinery for viral replication, while the second is duplicated only in replicating cells with open nuclear membrane. Both viruses have similar capacity in term of transgene, about 8kb, and can virtually transduce any cell types, when pseudo-typed with vesicular stomatitis virus G (VSV-G) envelope glycoprotein (Mancini and Horvath, 2018). A potential side effect for these viral vectors is their ability to integrate into the host genome, with increased risk for insertional mutagenesis and oncogenicity, although they tend to integrate distant from cellular promoters (Naldini, 2011). LVs have been broadly used to target specific glial cells, as pseudo-typing their envelope can restrict their selectivity (Buffo et al., 2008; Niu et al., 2013; Torper et al., 2013), but RVs offer fundamental advantages. Retroviral-mediated reprogramming reduces the risks for false positive neurons, as these post-mitotic cells do not express the transgene. Furthermore, RVs target proliferating glial cells that will not be depleted and have strong

homeostatic drive (Dimou and Götz, 2014; Gascón et al., 2017). Anyway, some of the limitations of LV and RV, like low efficiency of transduction and immunogenicity of the construct itself, can be overcome by AAV.

AAVs are small viruses of the *Parvoviridae* family, which require a co-helper virus to properly replicate. The DNA consists of a single-stranded DNA filament, which exists in the host nucleus in episomal state or selectively integrating in the chromosome 19. Limiting the risk for insertional mutagenesis. However, the size of the transgene that they can carry is relatively small, only 5kb. Interestingly, several AAV capsids have been generated allowing selective targeting of cells, with higher transduction efficiency than RV or LV (Mancini and Horvath, 2018). Furthermore, the overexpression of the transgene in AAV occurs slower than for RV or LV, reducing the risks for the converting neurons to cope with the early highly inflammatory injured environment (Burda and Sofroniew, 2014).

Indeed, an important factor to consider is that viral vector spreading, as it happens for pathogens attack in the CNS, can induce a strong immune response, which can be elicited both from the original viral components, as well as the transgene. This immune response can be first innate and then adaptive, limiting the expression of the new transgene, inducing even selective recognition and killing of the transduced cells. This can even increase inflammation and worsen the outcome (Drokhlyansky et al., 2016; Lowenstein et al., 2007), even if in the case of AAV this induced immune response does not seem to elicit cell death (Chew et al., 2016). New technologies in the field of gene therapy are aiming at reducing side effects of viral vectors, decreasing immunogenicity and increasing delivery rate (Ewer et al., 2016). All of these hallmarks would also be useful for direct neuronal reprogramming. Indeed broad immune reaction and selective killing of transduced cells, further increasing inflammatory reaction in the environment, would enhance the pathogenic process and are fundamental general hurdles to consider for efficient neuronal conversion.

Other general hurdles can be for example cell proliferation and DNA damage consequent to ROS production (Gascón et al., 2017). It is known that cells need to exit the cell cycle to efficiently convert into neurons, as for fibroblasts in which pushing the proliferation hampers the conversion (Fishman et al., 2015). The metabolism is also emerging as a relevant and preponderant mechanism regulating neuronal fate, which can be considered as cell-type specific hurdle.

Indeed, it was already shown in other fields of cell fate decision, like iPSCs generation and adult and developmental neurogenesis, that a switch from glycolytic to oxidative metabolism occurs and is essential for proper neuronal generation (Khacho et al., 2016; Llorens-bobadilla et al., 2015; Mlody and Prigione, 2016; Prigione et al., 2015). In fact down-regulation of key glycolytic enzymes, increased mitochondrial biogenesis and enhanced oxidative phosphorylation accompany the neuronal differentiation processes (Fang et al., 2016; Gascón et al., 2017). Also similar metabolic changes have been observed in iPSCs generation (Prigione et al., 2010; Zhu et al., 2010). Furthermore, direct blockage of oxphos pathway, or converse stimulation of glycolysis, further increased iPSCs generation from fibroblasts (Folmes et al., 2011; Panopoulos et al., 2011; Son et al., 2013). This suggests that acting directly on metabolic regulation might also improve neuronal generation, as modulation of

oxygen availability increases direct neuronal reprogramming from fibroblasts (Davila et al., 2013). Furthermore, modulation of oxygen availability is linked to increased iPSCs generation through activation of the transcription factor HIF1 $\alpha$ , which enhances the glycolytic rate (Papandreou et al., 2006; Prigione et al., 2014; Yoshida et al., 2009).

Interestingly, metabolic changes observed in iPSCs generation and developmental neurogenesis are also associated to ROS production, with direct and indirect effects on the converting cells (Le Belle et al., 2011; Khacho et al., 2016; Wu et al., 2013; Zhou et al., 2016), in most cases affecting their survival. As neurons are extremely sensitive cells to ROS-mediated damage (Wang and Michaelis, 2010), a better understanding of the consequences of metabolic transition for converting neurons is required. The role of ROS in impairing the generation of neurons might also have a big impact on the *in vivo* integration and survival of these cells. Indeed, the highly inflammatory environment characterized by ROS and immune cell infiltration might create a further barrier to the conversion process (Burda and Sofroniew, 2014). Furthermore, ROS might also interfere with other pathways and molecules required for neuronal differentiation, such as fatty acid generation (Knobloch et al., 2012), prone to suffer from ROS-mediated peroxidation. This leads to properly evaluate the best timing to apply direct reprogramming following the pathological insult. A delayed treatment might be beneficial, as ROS and inflammation are decreased, but the glial scar could interfere. Also the viral vector used can influence this choice, as different times for transgene expression are required (Gascón et al., 2017).

Notwithstanding, in the field of direct neuronal reprogramming not much is known on the impact that metabolic changes might pose on the transitioning neurons.

To sum up, direct neuronal reprogramming future lies in unraveling the mechanisms that burden its success application into pathological models first, and for clinical translation after. Indeed, generation of specific neuronal subtypes that successfully integrate and correctly project in the injured environment, replacing the lost ones from a functional, genetic and metabolic point of view, are the main goals of the field now.

My thesis aims to investigate and unravel common hurdles to the process of direct neuronal reprogramming, focusing on cell intrinsic and cell extrinsic properties. In particular, I investigate potential roles that metabolism, mitochondria and inflammation might play in the process, with the aim to find potential strategies to improve the conversion efficiency. To do so, I investigated *in vivo* the suitability of different viral vectors to direct neuronal reprogramming after TBI, evaluating in particular the effect that they exert on the environment and on the inflammatory processes. I then explored the mechanisms of metabolic conversion of glial cells to neurons. To do so, I first examined to which extent conversion to oxphos is required in the reprogramming process of astrocytes to neurons. Next, I asked how mitochondria protein composition differs between the starting glial cells and the end product of neuronal reprogramming, the neurons. I then investigated if mitochondria composition changes during glia-to-neuron conversion and how its modulation might impact direct neuronal reprogramming.

## **Results**

## **Aim of the study I**

The aim of the study is to investigate:

1. The effect that different viral vectors used to mediate *in vivo* direct neuronal reprogramming exert on the injured brain parenchyma.

## **Region- and layer-specific differences in astrocyte-to-neuron reprogramming**

Nicola Mattugini, Riccardo Bocchi, *Gianluca Luigi Russo*, Olof Torper, Chulan Lao and Magdalena Götz

For this paper I was involved in testing the environmental response to different viral vectors used for direct neuronal reprogramming. I was also involved in writing, editing and reviewing the paper.

*The paper is currently under second revision in Neuron.*

# Region- and layer-specific differences in astrocyte-to-neuron reprogramming

Nicola Mattugini <sup>1,2,3\*</sup>, Riccardo Bocchi <sup>1,2\*</sup>, Gianluca Luigi Russo <sup>1,2,3</sup>, Olof Torper <sup>1,2,4</sup>, Chulan Lao <sup>1,2</sup> and Magdalena Götz <sup>1,2,5</sup>

## AFFILIATIONS

1. Physiological Genomics, Biomedical Center (BMC), Ludwig-Maximilians-Universität (LMU), Großhaderner Str. 9, 82152 Planegg/Martinsried, Germany
2. Institute of Stem Cell Research, Helmholtz Center Munich, Biomedical Center (BMC), Großhaderner Str. 9, 82152 Planegg/Martinsried, Germany
3. Graduate School of Systemic Neuroscience, Ludwig-Maximilians-Universität (LMU), Großhaderner Str. 2, 82152 Planegg/Martinsried, Germany
4. Present address: Lund Stem Cell Center, Lund University, 221 84 Lund, Sweden
5. SyNergy Excellence Cluster, Germany

\* These authors contributed equally to this work.

## Lead contact:

Magdalena Götz, Physiological Genomics, Biomedical Center (BMC), Ludwig-Maximilians-Universität, Großhaderner Str. 9, 82152 Planegg/Martinsried, Germany

E-mail: [magdalena.goetz@helmholtz-muenchen.de](mailto:magdalena.goetz@helmholtz-muenchen.de)

## **SUMMARY**

Astrocytes are particularly promising candidates for reprogramming into neurons as they maintain the original patterning information from their radial glial ancestors. However, to which extent the position of astrocytes influences the fate of reprogrammed neurons remains unknown. To elucidate this, we performed stab wound injury covering an entire neocortical column, including the Grey Matter (GM) and White Matter (WM), and targeted local reactive astrocytes via injecting FLEx switch (Cre-On) adeno-associated viral vectors (AAV) into mGFAP-Cre mice. Single proneural factors were not sufficient for adequate reprogramming, while their combination with the nuclear receptor related 1 protein (Nurr1) potently improved reprogramming efficiency. Nurr1 and neurogenin 2 (Ngn2) in combination resulted in high efficiency reprogramming of targeted astrocytes into neurons that develop lamina-specific hallmarks including the appropriate long-distance axonal projections. Surprisingly, astrocytes in the WM entirely fail to become reprogrammed, thereby unveiling a crucial role of region- and layer-specific differences in astrocyte reprogramming.

## INTRODUCTION

The mammalian neocortex is a complex and highly organized structure containing many different types of neurons and glial cells. The intricate specificity of neuronal subtypes is established via a sequence of transcriptional regulators during development when neurons of different layer positions are generated in a sequential order from radial glial cells (Govindan and Jabaudon, 2017; Lodato and Arlotta, 2015; Greig et al., 2013). In the injured cerebral cortex, various combinations of transcription factors have been used to turn reactive glial cells (proliferating glia, NG2<sup>+</sup> oligodendrocyte progenitors or GFAP<sup>+</sup> cells; for review see (Gascón et al., 2017; Wang and Zhang, 2018)) into neurons. While much progress has been made since the first report describing *in vivo* glia-to-neuron reprogramming (Buffo et al., 2005), an efficient and reliable cocktail of regulators driving sustained and adequate reprogramming of cerebral cortex neurons is still to be revealed. Importantly, long distance axonal projections have never been reported for *in vivo* reprogrammed neurons and hence, little is known about the generation of adequate layer-specific neuronal subtypes achieved by such glia-to-neuron reprogramming in the cerebral cortex.

Recent data has shown that astrocytes display an amazing diversity in terms of positional identity, partly inherited from their radial glia ancestors (John Lin et al., 2017; Bayraktar et al., 2014) or instructed by surrounding neurons (Farmer et al., 2016; Lanjakornsiripan et al., 2018). Indeed, astrocytes at different positions within the neocortical Grey Matter (GM) differ in their morphology and gene expression through processes acquired during development that are associated with their neuronal laminar organization (Lanjakornsiripan et al., 2018). This suggests that either surrounding neurons, or intrinsic hallmarks of astrocytes at different laminar positions, may also influence the neuronal identity in direct reprogramming.

Indeed, laminar differences of excitatory projection neurons are key for cerebral cortex function. Pyramidal neurons differ in their identity according to their laminar position, molecular hallmarks, morphology and input-output connectivity (Molyneaux et al., 2007; Harris and Shepherd, 2015; Jabaudon, 2017). For instance, according to their laminar position, pyramidal projection neurons receive distinct inputs and project to different target regions in the brain, thereby exerting distinct roles in the cortical neuronal network (Tomassy et al., 2010; Lodato and Arlotta, 2015). For this reason, in order to functionally replace lost neurons upon injury, it is essential to obtain reprogrammed neurons recapitulating the original identity features. While this has been achieved with transplantation (Falkner et al., 2016), the characterization of specific neuronal subtype identities induced by reprogramming is still in its infancy, as only Gascon et al., 2016 reported expression of deep layer hallmarks in reprogrammed neurons. Thus, a comprehensive analysis of *in vivo* directly

reprogrammed neuron identity in the cerebral cortex is lacking. Moreover, we recently discovered profound differences in reactive gliosis between GM and White Matter (WM) in a stab wound injury lesion model covering the entire depth of the cortex without extending into the ventricle (Mattugini et al., 2018). Here, we use this model for direct reprogramming to determine if and how GM and WM astrocytes may differ in their reprogramming capacity.

## RESULTS

### **Nurr1 supports proneural factors to achieve high efficiency direct reprogramming of cortical astrocyte into neurons**

Different vectors, such as lentivirus (LV), retrovirus (RV) and adeno-associated-virus (AAV) have been used for *in vivo* reprogramming, achieving a great range of reprogramming efficiencies and neuronal survival (Gascón et al., 2017; Wang and Zhang, 2018). However, no direct comparison of these vectors on long-term immunogenicity in the injured brain has been performed despite previous data describing substantial differences in this regard (Nayak and Herzog, 2010; Lentz et al., 2012). We therefore injected viral vectors commonly used in direct reprogramming into our stab wound injury model. The injured site was then analyzed for infiltration of leukocytes (CD45<sup>+</sup>/Iba1<sup>-</sup> cells), microgliosis (Iba1<sup>+</sup> cells) and astrogliosis (GFAP<sup>+</sup> cells) at a time point when acute inflammation and reactive gliosis have normally already receded (13 days after injury; (Simon et al., 2011; Sirko et al., 2015)). When LV or RV were injected 3 days after stab wound and analyzed 10 days later (i.e. 13 days after stab wound injury and 10 days post viral vector injection, dpi), CD45<sup>+</sup> leukocytes were still abundant and reactive gliosis was very strong at the site of injection (Figure S1A). Conversely, AAVs injection shows very low levels of reactive gliosis and few immune cells in the brain parenchyma (Figure S1A). The low reactivity upon AAVs injection was independent of the number of vectors used (1 to 3) and whether or not they contained the reprogramming factors or only fluorescent proteins (data not shown).

Based on these results, we used AAVs for reprogramming for cell-type specific targeting, independent of the proliferation status (Lentz et al., 2012). To specifically target astrocytes we used FLEx (flip-excision) switch AAVs which are Cre-recombinase-dependent (Cre-On) as they are in inverted orientation and flanked by two pairs of loxP (Figure 1A; (Atasoy et al., 2008)). These constructs were injected 3 days after stab wound injury as described above into transgenic mice (mGFAP-Cre mice) expressing the Cre recombinase under the murine promoter of GFAP (Figure 1B; (Gregorian et al., 2009)). This lead to Green Fluorescence Protein (GFP) expression selectively in astrocytes (Torper et al., 2013; Wang et al., 2016) starting at 8-10 dpi (Figure S1B). To allow

sufficient time of gene expression we quantified GFP<sup>+</sup> cells at 24 dpi and found that virtually all had astrocyte morphology (Figure 1C for GM, for WM see below) and expressed the sex-determining region Y-box 9 (SOX9; Figure S1C; (Sun et al., 2017)). About 50% of these cells were also positive for GFAP (Figures 1D and 1E). Consistently, only a small fraction of cells (less than 10%) were positive for neuronal markers, such as RBFOX3 (NeuN; Figures 1D and 1E), suggesting a small degree of leakiness of the mGFAP-Cre expression. Importantly, this percentage did not increase at later time points (at 72 dpi) with mostly astrocytes and only less than 10% NeuN<sup>+</sup> cells amongst the GFP population (Figures 1F and 1G). Since injections into wild type mice did not result in any GFP<sup>+</sup> cells (data not shown), these controls confirm the tight Cre dependence and predominant astrocyte-specificity of the FLEEx-switch AAV constructs of this model.

In order to directly reprogram the local reactive astrocytes into neurons, we used FLEEx-switch AAVs containing either Neurogenin 2 (Ngn2) or Achaete-scute homolog 1 (Ascl1; Figure 1C). The proneural transcription factor Ngn2 is sufficient to convert astrocytes into glutamatergic neurons *in vitro* (Heinrich et al., 2010), but rather inefficient on its own in proliferating reactive glia using RVs (Gascón et al., 2016). Given the high leukocyte invasion and reactive gliosis elicited by the RV, we first tested if more neurons could be detected using the AAV-FLEEx-Ngn2, injected 3 days after stab wound injury. However, only a small percentage of GFP<sup>+</sup> cells was NeuN<sup>+</sup> (Figure S2A). We then chose to combine AAV-FLEEx-Ngn2 with AAV-FLEEx-Nurr1 (nuclear receptor related 1, Nr4a2), given the role of the later in improving reprogramming (Gascón et al., 2016) and neuroprotection (Saijo et al., 2009; Sousa et al., 2007). Indeed, when AAV-FLEEx vectors carrying GFP, Ngn2 and Nurr1 were injected simultaneously at 3 days after stab wound, a significant increase (about 53%) in the proportion of induced NeuN<sup>+</sup> neurons (iNs) was observed 24 dpi, with the remainder being largely astrocytes (determined by morphology or GFAP; (Figures 1D and 1E). To determine whether Nurr1 is also effective with other proneural factors, we tested this combination with GFP and Ascl1, previously used in other reprogramming cocktails (Masserdotti et al., 2016). AAV-FLEEx-Ascl1 injection with GFP resulted in only 20% NeuN<sup>+</sup> iNs (Figures S2B), while its combination with GFP and Nurr1 doubled the proportion of iNs to about 40% (Figures 1D and 1E). Conversely, injection of AAV-FLEEx-Nurr1 alone (Figure S2C) or the combination of AAV-FLEEx-GFP, AAV-FLEEx-RFP and AAV-FLEEx-Ngn2 showed low efficiency in direct neuronal reprogramming (data not shown), indicating that the combination of a proneural factor with Nurr1 is necessary to achieve efficient reprogramming. Analysis of long-term survival at 72 dpi showed even higher proportions of neurons induced by Ngn2 and Nurr1 (80% NeuN<sup>+</sup>) or Ascl1 and Nurr1 (70% NeuN<sup>+</sup>; Figures 1F and 1G), indicating that the combination of proneural factors with Nurr1 provides a powerful and highly

efficient *in vivo* reprogramming protocol. Notably, Ngn2/Nurr1 iNs exhibited a very mature pyramidal cell morphology, prompting us to examine their identity in more detail.

### **Neurons induced with Ngn2 and Nurr1 acquire mature pyramidal neuron hallmarks and molecular identities according to their laminar position**

To examine the identity of these Ngn2/Nurr1 iNs in more detail, we analyzed the origin, laminar identity, morphology and axonal projections using an AAV-FLE<sub>x</sub> expressing the fluorescent reporter mScarlet-I under the human synapsin (hSyn) promoter, to selectively visualize the converted neurons (Figure 1A). To determine if and how iNs derive from proliferating astrocytes, EdU was provided directly after stab wound for 10 days, i.e. during the entire period of reactive astrocyte proliferation in this injury model (Mattugini et al., 2018; Buffo et al., 2008). At 24 dpi, about 1/5<sup>th</sup> (21%) of Syn-Scarlet<sup>+</sup> iNs were derived from proliferating EdU<sup>+</sup> astrocytes (Figure S3A), consistent with the overall proliferation rate of reactive astrocytes (Buffo et al., 2008). Thus, the origin of iNs is not restricted or skewed to, but includes, the proliferating astrocyte population.

As the lesion paradigm extended throughout all cortex layers, we next compared the distribution of iNs (labeled with a AAV-FLE<sub>x</sub>-hSyn-mScarlet-I) and endogenous neurons (labeled with a AAV-hSyn-mScarlet-I) and found that reprogrammed neurons distribute within an entire cortical column (i.e. upper and lower layers), similarly to endogenous neurons (Figure S3B). In order to molecularly discriminate subtypes of pyramidal cells, we stained for CUX1, characteristic for upper layer neurons, and CTIP2 for lower layer neurons (Lodato et al., 2015). CUX1- and CTIP2-immunoreactivity was only weakly detected in few iNs at 24 dpi, while many more were strongly positive at 72 dpi (Figure S3C). Interestingly, most iNs expressing CUX1 were located in upper layers and virtually all CTIP2<sup>+</sup> iNs were found at deeper positions, closely resembling the distribution of the endogenous neurons (Figure 2A). Remarkably, both CUX1<sup>+</sup> and CTIP2<sup>+</sup> iNs display a stereotypical pyramidal shaped cell soma, a large apical dendrite oriented radially towards the pial surface, and an elaborated basal dendritic arbor (Figure 2B) similar to endogenous neurons (Harris and Shepherd, 2015). This was not the case when combining *Ascl1* and *Nurr1*, which instead generated iNs of more variable morphologies (Figure 1F) and marker expression (Figure S3D). Notably, Ngn2/Nurr1 iNs matured over time (Figure 2B). The number of Ngn2/Nurr1 iNs with an apical dendrite was significantly lower at 24 dpi compared to the endogenous neurons, while this difference was reduced at 72 dpi (Figure 2C). Likewise, the thickness of the iN apical process grew between 24 and 72 dpi (Figure 2D), and the soma was initially significantly more circular at 24 when compared to both iNs at 72 dpi and endogenous neurons (Figure 2E), demonstrating that iNs had acquired a pyramidal neuron shape. Moreover, the number of primary basal dendrites was reduced between 24 and 72 dpi, indicating

pruning processes as observed in transplanted neurons (Falkner et al., 2016) reaching a mean number (Figure 2F) and orientation, highly reminiscent to the basal dendritic arbor of endogenous pyramidal cells (Figure 2G). Together these data show that iNs adopt over time the congruent assignment of laminar, molecular and morphological features of mature pyramidal neurons.

### **Neurons induced with Ngn2 and Nurr1 develop mature spine numbers and axonal projections**

Given the morphological maturation of the iNs described above, we next examined parameters indicative of connectivity and synaptic integration. As spines act as postsynaptic sites, we assessed their number on secondary dendrites and found a significant increase from 24 to 72 dpi with Ngn2/Nurr1 iNs reaching numbers comparable to endogenous pyramidal neurons (Figure 3A).

Importantly, pyramidal neurons located at different laminar positions project to distinct target regions (Harris and Shepherd, 2015; Molyneaux et al., 2007): neurons in lower layers predominantly send ipsilateral corticofugal projections, towards the striatum, thalamus, midbrain or corticospinal tract, while many upper layer 2/3 neurons and a subpopulation of layer 5 neurons send callosal projections to the contralateral cortex hemisphere (Figure 3B). Following the axonal projections from mScarlet- $I^+$  (Figure 3) and GFP $^+$  (Figure S4) iNs at 72 dpi, we observed subcortical axons in the striatum (Figure 3C), thalamus and midbrain (Figure S4A) as well as axons travelling through the corpus callosum and reaching the contralateral cortex (Figure 3D; Figure S4A). In order to investigate the neuronal subtype-specific origin of these projections, we performed retrograde labelling from the contralateral hemisphere by Fluorogold injection and stained for SATB2 that is characteristic of callosal projection neurons in layers 2/3 and 5. This confirmed that most Fluorogold $^+$  iNs (were SATB2 $^+$  most often located in L2/3 but also in L5, while fewer were CTIP2 $^+$  cells in L5 (Figure 3E). Together these data reveal for the first time a consistent reassignment of axonal target selection by reprogrammed neurons after cortical injury *in vivo*.

### **White Matter astrocytes fail to undergo neuronal reprogramming**

Given the amazing specificity of neuronal reprogramming seen in the GM, we turned our attention to cells in the WM. Surprisingly, we virtually never detected any iNs in the WM at both 24 and 72 dpi (Figure 4). Some animals did not even display a single GFP $^+$  cell in the WM when using the neurogenic constructs (i.e. Ngn2/Nurr1 and Ascl1/Nurr1), despite GFP $^+$  cells present in all animals injected with the control virus containing only GFP (Figure 4A). In the few animals, where GFP $^+$  cells were detectable in the WM, the majority had maintained their astrocyte identity despite the expression of neurogenic factors Ngn2/Nurr1 (Figure 2B) or Ascl1/Nurr1 (Figure 4C). Thus, the injections and astrocyte targeting worked well also for WM astrocytes, but upon transduction with

neurogenic factors many seem to die rather than reprogram. Taken together, these data suggest that both neurogenic combinations were not sufficient to successfully convert WM astrocytes into neurons, while they were very efficient to reprogram GM astrocytes.

## **DISCUSSION**

Direct neuronal reprogramming from local glial cells after injury represents a promising strategy for brain repair (Barker et al., 2018; Grade and Götz, 2017). However, acquisition of adequate neuronal subtype identity and target region innervation is key for functional repair. Here we describe a novel reprogramming protocol using Ngn2 and Nurr1 sufficient to turn astrocytes with high efficiency into mature pyramidal neurons with different laminar and axonal projection identities after stab wound injury. Strikingly, Nurr1 is necessary for proneural factors to achieve the high reprogramming efficiency and this is specific for GM astrocytes, with WM astrocytes failing to be efficiently reprogrammed with these factors in the same lesion paradigm. These data therefore unravel a great specificity for *in vivo* direct neuronal reprogramming that is beneficial in achieving correct neuronal subtypes at different layer positions, but deleterious as observed in the WM.

### **Nurr1 is required for highly efficient astrocyte-to-neuron reprogramming**

In the cerebral neocortex, proliferating glial cells have been targeted for reprogramming into neurons (Gascón et al., 2017). In contrast to striatal glia that could be converted into neurons using only Sox2 (Niu et al., 2013; Wang and Zhang, 2018) cortical glia require a combination of proneural factors with Sox2 or Bcl-2 to improve the reprogramming efficiency (Gascón et al., 2016; Heinrich et al., 2014). While Sox2 resulted in immature young neurons (Heinrich et al., 2014), Ngn2 and Bcl2 (Gascón et al., 2016) or NeuroD1 (Guo et al., 2014) achieved more mature neurons from proliferating GFAP- or NG2-expressing glia. However, none of these protocols have achieved adequate axonal projections and pyramidal neuronal hallmarks. Here, we tested several combinations of proneural factors and unveiled a relevant role of the orphan nuclear receptor Nurr1 in direct neuronal reprogramming. The combination of Nurr1 with the proneural factor Ngn2 achieved over 80% efficiency in converting reactive astrocytes into neurons. Notably, efficiency and maturity of the converted neurons was much higher when Nurr1 was combined with Ngn2, compared to the proneural factor Ascl1. Nurr1 has also been previously used in reprogramming cocktails *in vivo* and *in vitro* towards generating dopaminergic neurons (Torper et al., 2015; Rivetti di Val Cervo et al., 2017) and although it is a well-known factor in specifying dopaminergic neurons in the ventral midbrain, it is also expressed in cortical and olfactory bulb neurons (Perlmann and Wallén-Mackenzie, 2004; Watakabe et al., 2007; Saino-Saito et al., 2004). Moreover, Nurr1 belongs to the orphan NR4A family

exerting anti-inflammatory effects in different tissues (Rodríguez-Calvo et al., 2017). In the central nervous system Nurr1 is recruited by the NF- $\kappa$ B promoter to regulate inflammatory genes and inhibit inflammatory signals in microglia and astrocytes (Saijo et al., 2009). This may be crucial for reprogramming given the sensitivity of this process to reactive oxygen species (Gascón et al., 2016). Indeed, Nurr1 overexpression in neural stem cells upregulates trophic and survival signals to improve their response to oxidative stress, while downregulating cell cycle genes (Sousa et al., 2007). These multiple pathways controlled by Nurr1 may be key in its potent role in improving the efficiency and efficacy of cortical astrocyte-to-neuron reprogramming as uncovered here.

### **Distinct reprogramming efficiencies of astrocytes from Gray and White Matter**

Astrocytes located in the GM and the WM are known to differ in many aspects and are generally discriminated as protoplasmic (GM) and fibrous (WM) astrocytes, respectively (Lundgaard et al., 2014). While the former wrap synapses in the GM, the latter are more in contact with nodes of Ranvier in the WM. This functional difference is also reflected by many molecular differences. They express different levels of GFAP (Lundgaard et al., 2014) and Olig2 deletion decreases the number of WM, but not GM astrocytes (Cai et al., 2007). Glial cell heterogeneity significantly affects the outcome of brain injury (Adams and Gallo, 2018; Dimou and Götz, 2014). However, astrocyte proliferation is similar between WM and GM after stab wound injury during the course of the first week, after which it quickly declines (Mattugini et al., 2018).

Surprisingly, WM astrocytes differ profoundly from GM astrocytes in their capability to be reprogrammed into neurons. One possible cause for the reprogramming failure could be an adverse environment as stab wound injury elicits a wave of monocyte invasion close to the WM (Mattugini et al., 2018). Additionally, activated microglia cells are still present in the WM 14 dpi (Mattugini et al., 2018), possibly contributing to render the WM environment less permissive for survival of iNs. In addition, the failure of iN survival in the WM may be due to the lack of neuronal input as there are fewer neurons surrounding the iNs in WM. Finally, given the profound differences in astrocyte gene expression in different brain regions (Boisvert et al., 2018; John Lin et al., 2017) WM astrocytes may exhibit expression profiles less amenable to neuronal reprogramming. Indeed, reactive astrocytes in GM increase the expression of some neurogenic transcription factors, such as Pax6, Sox4 and Sox11 (Götz et al., 2015) that help in neuronal reprogramming (Buffo et al., 2005; Ninkovic et al., 2013). Thus, both intrinsic and extrinsic factors may contribute to the profoundly different outcome in the reprogramming capacity of GM and WM astrocytes.

## **The combination Ngn2/Nurr1 converts Gray Matter astrocytes into neurons acquiring neuronal subtype identities according to their laminar position**

The mammalian neocortex is a complex structure, radially organized in six layers populated by different subtypes of projection neurons. Each subtype exhibits unique pyramidal morphology, has a specific gene expression profile, and accordingly serves distinct functions (Harris and Shepherd, 2015; Lodato and Arlotta, 2015). We report here that the combination of Ngn2 with Nurr1 not only achieved high efficiency in direct neuronal reprogramming, but also that the resulting iNs displayed mature molecular, morphological and axonal projections adequate for their laminar position. iNs expressed CTIP2 and CUX1 according to their laminar position. Both these iNs developed the typical morphology of pyramidal cells, with a prominent apical dendrite and an elaborated basal dendritic arbor which gradually developed to resemble that of endogenous neurons. Finally, iNs acquired spine density and long distance axonal projections to the striatum, midbrain and thalamus as well as the contralateral cerebral cortex hemisphere. Most strikingly, these projections were not random, but rather iNs expressing SATB2 were found to project through the callosum, as is the case normally. Thus, these data show for the first time adequate neuronal subtype specification by direct *in vivo* reprogramming.

The precise identity reassignment according to the iN location raises concerns about possible viral labelling artefacts. However, neither GFP on its own (Figure 1), nor Ngn2 or Nurr1 combined with GFP (Figure S2), nor GFP and RFP combined with Ngn2 (control for use of 3 viral vectors) resulted in any substantial labelling of mature pyramidal neurons. Moreover, pyramidal neuron maturation was achieved gradually with e.g. initially more dendrites than at later mature stages, a phenotype difficult to explain by labelling artefactual a mature neuron. These data, together with the 20% of iNs achieved by Ngn2/Nurr1 transduction deriving from proliferating EdU-incorporating cells leads us to exclude the possibility of artefactual labelling of mature neurons and favor the conclusion that the targeted astrocytes convert into neurons. This then prompts the question the intriguing question of whether the region- and layer-specific reprogramming is driven by cell-intrinsic mechanisms or environmental cues. Interestingly, astrocytes located in upper versus lower layers differ not only in their morphology but also in gene expression (Lanjakornsiripan et al., 2018). Surrounding neurons may play a key role in this process, as demonstrated in the cerebellum where neuron-released Sonic hedgehog influenced local astrocyte transcriptional activity (Farmer et al., 2016). This supports the intriguing hypothesis that layer-dependent differences in cortical astrocytes might affect the outcome of reprogramming in terms of neuronal subtype identity. Together, these results highlight the potential of astrocytes as promising starting cell population for direct neuronal reprogramming upon brain

injury and highlight the fundamental importance of astrocyte subtypes not only to determine the efficiency of direct neuronal reprogramming, but also the emerging neuronal subtype.

## **ACKNOWLEDGEMENTS**

We are very grateful to Malin Parmar for providing the plasmids of the AAV-FLEx constructs. We would like to thank Sabine Ulbricht, Manja Thorwirth and Gabi Jaeger for the excellent technical help and Alexandra Lepier and Ines Muehlhahn for establishing the AAV production in the lab. We would like to thank Adam O'Neill for excellent comments on the manuscript. This work was financed by the German Research Foundation for the Collaborative Research Center 870 Neural Circuits projects A06, and Z04 and the advanced ERC grant ChroNeuroRepair to M.G.. R.B. was supported by SNF post-doctoral fellowship (P2GEP3\_174900).

## **AUTHOR CONTRIBUTIONS**

M.G., N.M. and R.B. conceived the experiments, discussed the data and wrote the manuscript. N.M. and R.B. performed almost all experiments and analyzed the data. G.L.R. tested the immune response to viral vectors. O.T. provided AAV expertise and scientific inputs. C.L. prepared viral vectors.

## **DECLARATION OF INTERESTS**

The authors declare no conflict of interest

## REFERENCES

- Adams, K. L., and Gallo, V. (2018). The diversity and disparity of the glial scar. *Nat Neurosci* 21, 9-15.
- Atasoy, D., Aponte, Y., Su, H. H., and Sternson, S. M. (2008). A FLEX switch targets Channelrhodopsin-2 to multiple cell types for imaging and long-range circuit mapping. *J Neurosci* 28, 7025-7030.
- Barker, R. A., Götz, M., and Parmar, M. (2018). New approaches for brain repair-from rescue to reprogramming. *Nature* 557, 329-334.
- Bayraktar, O. A., Fuentealba, L. C., Alvarez-Buylla, A., and Rowitch, D. H. (2014). Astrocyte development and heterogeneity. *Cold Spring Harb Perspect Biol* 7, a020362.
- Boisvert, M. M., Erikson, G. A., Shokhirev, M. N., and Allen, N. J. (2018). The Aging Astrocyte Transcriptome from Multiple Regions of the Mouse Brain. *Cell Rep* 22, 269-285.
- Buffo, A., Rite, I., Tripathi, P., Lepier, A., Colak, D., Horn, A. P., Mori, T., and Götz, M. (2008). Origin and progeny of reactive gliosis: A source of multipotent cells in the injured brain. *Proc Natl Acad Sci U S A* 105, 3581-3586.
- Buffo, A., Vosko, M. R., Ertürk, D., Hamann, G. F., Jucker, M., Rowitch, D., and Götz, M. (2005). Expression pattern of the transcription factor Olig2 in response to brain injuries: implications for neuronal repair. *Proc Natl Acad Sci U S A* 102, 18183-18188.
- Cai, J., Chen, Y., Cai, W. H., Hurlock, E. C., Wu, H., Kernie, S. G., Parada, L. F., and Lu, Q. R. (2007). A crucial role for Olig2 in white matter astrocyte development. *Development* 134, 1887-1899.
- D'Costa, S., Blouin, V., Broucq, F., Penaud-Budloo, M., François, A., Perez, I. C., Le Bec, C., Moullier, P., Snyder, R. O., and Ayuso, E. (2016). Practical utilization of recombinant AAV vector reference standards: focus on vector genomes titration by free ITR qPCR. *Mol Ther Methods Clin Dev* 5, 16019.
- Dimou, L., and Götz, M. (2014). Glial cells as progenitors and stem cells: new roles in the healthy and diseased brain. *Physiol Rev* 94, 709-737.
- Falkner, S., Grade, S., Dimou, L., Conzelmann, K. K., Bonhoeffer, T., Götz, M., and Hübener, M. (2016). Transplanted embryonic neurons integrate into adult neocortical circuits. *Nature* 539, 248-253.
- Farmer, W. T., Abrahamsson, T., Chierzi, S., Lui, C., Zaelzer, C., Jones, E. V., Bally, B. P., Chen, G. G., Thérout, J. F., Peng, J., Bourque, C. W., Charron, F., Ernst, C., Sjöström, P. J., and Murai, K. K. (2016). Neurons diversify astrocytes in the adult brain through sonic hedgehog signaling. *Science* 351, 849-854.
- Gascón, S., Masserdotti, G., Russo, G. L., and Götz, M. (2017). Direct Neuronal Reprogramming: Achievements, Hurdles, and New Roads to Success. *Cell Stem Cell* 21, 18-34.
- Gascón, S., Murenu, E., Masserdotti, G., Ortega, F., Russo, G. L., Petrik, D., Deshpande, A., Heinrich, C., Karow, M., Robertson, S. P., Schroeder, T., Beckers, J., Irmeler, M., Berndt, C., Angeli, J. P., Conrad, M., Berninger, B., and Götz, M. (2016). Identification and Successful Negotiation of a Metabolic Checkpoint in Direct Neuronal Reprogramming. *Cell Stem Cell* 18, 396-409.
- Götz, M., Sirko, S., Beckers, J., and Irmeler, M. (2015). Reactive astrocytes as neural stem or progenitor cells: In vivo lineage, In vitro potential, and Genome-wide expression analysis. *Glia* 63, 1452-1468.
- Govindan, S., and Jabaudon, D. (2017). Coupling progenitor and neuronal diversity in the developing neocortex. *FEBS Lett* 591, 3960-3977.
- Grade, S., and Götz, M. (2017). Neuronal replacement therapy: previous achievements and challenges ahead. *NPJ Regen Med* 2, 29.
- Gregorian, C., Nakashima, J., Le Belle, J., Ohab, J., Kim, R., Liu, A., Smith, K. B., Groszer, M., Garcia, A. D., Sofroniew, M. V., Carmichael, S. T., Kornblum, H. I., Liu, X., and Wu, H. (2009). Pten deletion in adult neural stem/progenitor cells enhances constitutive neurogenesis. *J Neurosci* 29, 1874-1886.
- Greig, L. C., Woodworth, M. B., Galazo, M. J., Padmanabhan, H., and Macklis, J. D. (2013). Molecular logic of neocortical projection neuron specification, development and diversity. *Nat Rev Neurosci* 14, 755-769.
- Guo, Z., Zhang, L., Wu, Z., Chen, Y., Wang, F., and Chen, G. (2014). In vivo direct reprogramming of reactive glial cells into functional neurons after brain injury and in an Alzheimer's disease model. *Cell Stem Cell* 14, 188-202.
- Hack, M. A., Saghatelian, A., de Chevigny, A., Pfeifer, A., Ashery-Padan, R., Lledo, P. M., and Götz, M. (2005). Neuronal fate determinants of adult olfactory bulb neurogenesis. *Nat Neurosci* 8, 865-872.
- Harris, K. D., and Shepherd, G. M. (2015). The neocortical circuit: themes and variations. *Nat Neurosci* 18, 170-181.

- Heinrich, C., Bergami, M., Gascón, S., Lepier, A., Viganò, F., Dimou, L., Sutor, B., Berninger, B., and Götz, M. (2014). Sox2-mediated conversion of NG2 glia into induced neurons in the injured adult cerebral cortex. *Stem Cell Reports* 3, 1000-1014.
- Heinrich, C., Blum, R., Gascón, S., Masserdotti, G., Tripathi, P., Sánchez, R., Tiedt, S., Schroeder, T., Götz, M., and Berninger, B. (2010). Directing astroglia from the cerebral cortex into subtype specific functional neurons. *PLoS Biol* 8, e1000373.
- Heinrich, C., Gascón, S., Masserdotti, G., Lepier, A., Sanchez, R., Simon-Ebert, T., Schroeder, T., Götz, M., and Berninger, B. (2011). Generation of subtype-specific neurons from postnatal astroglia of the mouse cerebral cortex. *Nat Protoc* 6, 214-228.
- Holtmaat, A., Bonhoeffer, T., Chow, D. K., Chuckowree, J., De Paola, V., Hofer, S. B., Hübener, M., Keck, T., Knott, G., Lee, W. C., Mostany, R., Mrcic-Flogel, T. D., Nedivi, E., Portera-Cailliau, C., Svoboda, K., Trachtenberg, J. T., and Wilbrecht, L. (2009). Long-term, high-resolution imaging in the mouse neocortex through a chronic cranial window. *Nat Protoc* 4, 1128-1144.
- Jabaudon, D. (2017). Fate and freedom in developing neocortical circuits. *Nat Commun* 8, 16042.
- John Lin, C. C., Yu, K., Hatcher, A., Huang, T. W., Lee, H. K., Carlson, J., Weston, M. C., Chen, F., Zhang, Y., Zhu, W., Mohila, C. A., Ahmed, N., Patel, A. J., Arenkiel, B. R., Noebels, J. L., Creighton, C. J., and Deneen, B. (2017). Identification of diverse astrocyte populations and their malignant analogs. *Nat Neurosci* 20, 396-405.
- Lanjakornsiripan, D., Pior, B. J., Kawaguchi, D., Furutachi, S., Tahara, T., Katsuyama, Y., Suzuki, Y., Fukazawa, Y., and Gotoh, Y. (2018). Layer-specific morphological and molecular differences in neocortical astrocytes and their dependence on neuronal layers. *Nat Commun* 9, 1623.
- Lentz, T. B., Gray, S. J., and Samulski, R. J. (2012). Viral vectors for gene delivery to the central nervous system. *Neurobiol Dis* 48, 179-188.
- Lodato, S., and Arlotta, P. (2015). Generating neuronal diversity in the mammalian cerebral cortex. *Annu Rev Cell Dev Biol* 31, 699-720.
- Lodato, S., Shetty, A. S., and Arlotta, P. (2015). Cerebral cortex assembly: generating and reprogramming projection neuron diversity. *Trends Neurosci* 38, 117-125.
- Lundgaard, I., Osório, M. J., Kress, B. T., Sanggaard, S., and Nedergaard, M. (2014). White matter astrocytes in health and disease. *Neuroscience* 276, 161-173.
- Mattugini, N., Merl-Pham, J., Petrozziello, E., Schindler, L., Bernhagen, J., Hauck, S. M., and Götz, M. (2018). Influence of white matter injury on gray matter reactive gliosis upon stab wound in the adult murine cerebral cortex. *Glia*
- Molyneaux, B. J., Arlotta, P., Menezes, J. R., and Macklis, J. D. (2007). Neuronal subtype specification in the cerebral cortex. *Nat Rev Neurosci* 8, 427-437.
- Nayak, S., and Herzog, R. W. (2010). Progress and prospects: immune responses to viral vectors. *Gene Ther* 17, 295-304.
- Ninkovic, J., Steiner-Mezzadri, A., Jawerka, M., Akinci, U., Masserdotti, G., Petricca, S., Fischer, J., von Holst, A., Beckers, J., Lie, C. D., Petrik, D., Miller, E., Tang, J., Wu, J., Lefebvre, V., Demmers, J., Eisch, A., Metzger, D., Crabtree, G., Irmeler, M., Poot, R., and Götz, M. (2013). The BAF complex interacts with Pax6 in adult neural progenitors to establish a neurogenic cross-regulatory transcriptional network. *Cell Stem Cell* 13, 403-418.
- Niu, W., Zang, T., Zou, Y., Fang, S., Smith, D. K., Bachoo, R., and Zhang, C. L. (2013). In vivo reprogramming of astrocytes to neuroblasts in the adult brain. *Nat Cell Biol* 15, 1164-1175.
- Perlmann, T., and Wallén-Mackenzie, A. (2004). Nurr1, an orphan nuclear receptor with essential functions in developing dopamine cells. *Cell Tissue Res* 318, 45-52.
- Rivetti di Val Cervo, P., Romanov, R. A., Spigolon, G., Masini, D., Martín-Montañez, E., Toledo, E. M., La Manno, G., Feyder, M., Pifl, C., Ng, Y. H., Sánchez, S. P., Linnarsson, S., Wernig, M., Harkany, T., Fisone, G., and Arenas, E. (2017). Induction of functional dopamine neurons from human astrocytes in vitro and mouse astrocytes in a Parkinson's disease model. *Nat Biotechnol* 35, 444-452.
- Rodríguez-Calvo, R., Tajés, M., and Vázquez-Carrera, M. (2017). The NR4A subfamily of nuclear receptors: potential new therapeutic targets for the treatment of inflammatory diseases. *Expert Opin Ther Targets* 21, 291-304.
- Saijo, K., Winner, B., Carson, C. T., Collier, J. G., Boyer, L., Rosenfeld, M. G., Gage, F. H., and Glass, C. K. (2009). A Nurr1/CoREST pathway in microglia and astrocytes protects dopaminergic neurons from inflammation-induced death. *Cell* 137, 47-59.

- Saino-Saito, S., Sasaki, H., Volpe, B. T., Kobayashi, K., Berlin, R., and Baker, H. (2004). Differentiation of the dopaminergic phenotype in the olfactory system of neonatal and adult mice. *J Comp Neurol* *479*, 389-398.
- Simon, C., Götz, M., and Dimou, L. (2011). Progenitors in the adult cerebral cortex: cell cycle properties and regulation by physiological stimuli and injury. *Glia* *59*, 869-881.
- Sirko, S., Irmeler, M., Gascón, S., Bek, S., Schneider, S., Dimou, L., Obermann, J., De Souza Paiva, D., Poirier, F., Beckers, J., Hauck, S. M., Barde, Y. A., and Götz, M. (2015). Astrocyte reactivity after brain injury-: The role of galectins 1 and 3. *Glia* *63*, 2340-2361.
- Sousa, K. M., Mira, H., Hall, A. C., Jansson-Sjöstrand, L., Kusakabe, M., and Arenas, E. (2007). Microarray analyses support a role for *Nurr1* in resistance to oxidative stress and neuronal differentiation in neural stem cells. *Stem Cells* *25*, 511-519.
- Sun, W., Cornwell, A., Li, J., Peng, S., Osorio, M. J., Aalling, N., Wang, S., Benraiss, A., Lou, N., Goldman, S. A., and Nedergaard, M. (2017). SOX9 Is an Astrocyte-Specific Nuclear Marker in the Adult Brain Outside the Neurogenic Regions. *J Neurosci* *37*, 4493-4507.
- Tomassy, G. S., Lodato, S., Traves-Gibson, Z., and Arlotta, P. (2010). Development and regeneration of projection neuron subtypes of the cerebral cortex. *Sci Prog* *93*, 151-169.
- Torper, O., Ottosson, D. R., Pereira, M., Lau, S., Cardoso, T., Grealish, S., and Parmar, M. (2015). In Vivo Reprogramming of Striatal NG2 Glia into Functional Neurons that Integrate into Local Host Circuitry. *Cell Rep* *12*, 474-481.
- Torper, O., Pfisterer, U., Wolf, D. A., Pereira, M., Lau, S., Jakobsson, J., Björklund, A., Grealish, S., and Parmar, M. (2013). Generation of induced neurons via direct conversion in vivo. *Proc Natl Acad Sci U S A* *110*, 7038-7043.
- Wang, L. L., Su, Z., Tai, W., Zou, Y., Xu, X. M., and Zhang, C. L. (2016). The p53 Pathway Controls SOX2-Mediated Reprogramming in the Adult Mouse Spinal Cord. *Cell Rep* *17*, 891-903.
- Wang, L. L., and Zhang, C. L. (2018). Engineering new neurons: in vivo reprogramming in mammalian brain and spinal cord. *Cell Tissue Res* *371*, 201-212.
- Watakabe, A., Ichinohe, N., Ohsawa, S., Hashikawa, T., Komatsu, Y., Rockland, K. S., and Yamamori, T. (2007). Comparative analysis of layer-specific genes in Mammalian neocortex. *Cereb Cortex* *17*, 1918-1933.
- Zolotukhin, S., Byrne, B. J., Mason, E., Zolotukhin, I., Potter, M., Chesnut, K., Summerford, C., Samulski, R. J., and Muzyczka, N. (1999). Recombinant adeno-associated virus purification using novel methods improves infectious titer and yield. *Gene Ther* *6*, 973-985.

## MAIN FIGURES TITLES AND LEGENDS

### **Figure 1. Neurogenic factors reprogram cortical Grey Matter astrocytes into neurons after traumatic brain injury.**

(A) Scheme of the AAV-FLEX constructs. (B) Timeline of the experimental design. (C) Photomicrographs showing an overview with GFP<sup>+</sup> cells at 24 dpi of AAV encoding for GFP, GFP/*Ngn2/Nurr1* and GFP/*Ascl1/Nurr1*. (D) Photomicrographs showing GFP<sup>+</sup>/*NeuN*<sup>+</sup> neurons (yellow arrowheads) and GFP<sup>+</sup>/*GFAP*<sup>+</sup> astrocytes (white arrowheads) at 24 dpi of GFP, *Ngn2/Nurr1* and *Ascl1/Nurr1*. (E) Histograms showing the percentage of *NeuN*<sup>+</sup> (top) and *GFAP*<sup>+</sup> (middle) among the GFP<sup>+</sup> cells at 24 dpi of the viral vectors indicated on the x-axis. The lower panel show a Z-projection of *NeuN* and GFP colocalization at 24 dpi of GFP/*Ngn2/Nurr1* neuron (dashed square). (F) Photomicrographs showing GFP<sup>+</sup>/*NeuN*<sup>+</sup> neurons (yellow arrowheads) and GFP<sup>+</sup>/*GFAP*<sup>+</sup> astrocytes (white arrowheads) at 72 dpi. (G) Histograms of *NeuN*<sup>+</sup> (top) and *GFAP*<sup>+</sup> (middle)

percentage and Z-projection as described above. Each dot represents one experimental animal; n = 3, 4 and 4 for GFP, Ngn2/Nurr1 and Ascl1/Nurr1, respectively. Data are shown as median  $\pm$  IQR. Significance between mean was tested using the t-test after testing for normal distribution with the Shapiro test, \*  $p \leq 0.05$  \*\*  $p \leq 0.01$ , \*\*\*\*  $p \leq 0.0001$ . AAV: adeno-associated virus; dpi: days post injection. Scale bars: 100  $\mu\text{m}$  (C left), 50  $\mu\text{m}$  (C right), 10  $\mu\text{m}$  (D, F). See also Figure S1 and S2.

**Figure 2. Neurons reprogrammed from astrocytes with Ngn2/Nurr1 acquire adequate laminar identity and pyramidal morphology.**

(A) Photomicrographs of endogenous (top) and reprogrammed (bottom) neurons 72 dpi of AAV-mScarlet-I and AAV-FLEX-mScarlet-I/Ngn2/Nurr1, respectively. CUX1 and CTIP2 intensity levels are layer specific. The vertical dashed line in the right panel represents the intensity threshold (intensity of 0.2) defining positive cells. High magnification shows the co-localization of mScarlet-I<sup>+</sup> with CUX1 in upper L2/3 neurons and with CTIP2 in lower L5/6 neurons outlining a mScarlet-I<sup>+</sup> neuron. The heatmap shows the cell distribution in ten bins. The color-coded columns represent the percentage of mScarlet-I<sup>+</sup>/CUX1<sup>+</sup> or mScarlet-I<sup>+</sup>/CTIP2<sup>+</sup> cells per bin, of the total number of mScarlet-I<sup>+</sup>/CUX1<sup>+</sup> or mScarlet-I<sup>+</sup>/CTIP2<sup>+</sup>, respectively, in an entire column. Histograms illustrate the average of percentage for each bin; n = 5 animals. (B) Photomicrographs showing pyramidal morphology of mScarlet-I<sup>+</sup> endogenous and reprogrammed neurons at 24 and 72 dpi. (C-F) Histograms depicting the morphological analyses of endogenous neurons, younger (24 dpi) and older (72 dpi) iNs for the parameters indicated in the panels, supporting the maturation process of reprogrammed neurons. Each dot represents one experimental animal; n = 4. Data are shown as median  $\pm$  IQR. Significance between median was tested using the Kruskal-Wallis test followed by the Dunn's multiple comparisons test, \*  $p \leq 0.05$ , \*\*  $p \leq 0.01$ . dpi: days post injection, L: layer. Scale bars: 100  $\mu\text{m}$  (A and B; overview), 20  $\mu\text{m}$  (A; close up), 5  $\mu\text{m}$  (G). See also Figure S3.

**Figure 3. Neurons reprogrammed with Ngn2/Nurr1 develop spines and project to the appropriate brain regions.**

(A) Photomicrographs of secondary dendrite segments of endogenous (top) and reprogrammed (bottom) neurons at 24 and 72 dpi of mScarlet-I/Ngn2/Nurr1. Histogram on the right displays the number of spines per  $\mu\text{m}$  (spines density). Each dot represents one experimental animal; n = 4. (B) Cartoon summarizing examples of cerebral cortex efferent projections. (C-D) Photomicrographs illustrating axons of iNs at 72 dpi in the ipsilateral (C) and contralateral (D) cortical hemisphere. (E) Schematic drawing indicates the experimental schedule and positions of callosal neurons to the left with a low power overview photomicrograph depicting the Fluorogold injection site. Retrogradely

traced iNs at 72 dpi are mainly located in L2/3 and L5. Histograms illustrate the percentage of Fluorogold<sup>+</sup> endogenous or reprogrammed neurons in L2/3 that are SATB2<sup>+</sup>/CTIP2<sup>-</sup> and in L5 that are SATB2<sup>+</sup>/CTIP2<sup>-</sup> or SATB2<sup>-</sup>/CTIP2<sup>+</sup> neurons. Each dot represents one experimental animal; n = 3. Data are shown as median ± IQR. Significance between median was tested using the Kruskal-Wallis test followed by the Dunn's multiple comparisons test, \* p ≤ 0.05. cc: corpus callosum, Crb: cerebellum, Ctx: cortex, dpi: days post injection, ic: internal capsule, OB: olfactory bulb, LV: lateral ventricle, SC: spinal cord, Str: striatum Th: thalamus. Scale bars: 100 μm (C left and D left), 50 μm (C right), 10 μm (D right). See also Figure S4.

**Figure 4. Neocortex White Matter astrocytes are not reprogrammed into neurons by Ngn2, Ascl1 and Nurr1 after traumatic brain injury.**

(A-C) Photomicrographs showing GFP<sup>+</sup> cells at 24 and 72 dpi of GFP (A), GFP/Ngn2/Nurr1 (B) and GFP/Ascl1/Nurr1 (C). Histograms show the percentage of NeuN<sup>+</sup>, GFAP<sup>+</sup> and NeuN<sup>-</sup>/GFAP<sup>-</sup> cells among the GFP<sup>+</sup> cells for each experimental animal (3 or 4 per condition). Data are shown as median ± IQR of different technical replicates, i.e. immunostainings of different sections. Note that in some animals (B and C) GFP<sup>+</sup> cells were either not detectable or they were largely positive for GFAP (grey), but virtually none are NeuN<sup>+</sup> (black) neurons. dpi: days post injection. Scale bars: 20 μm.

# Figure 1

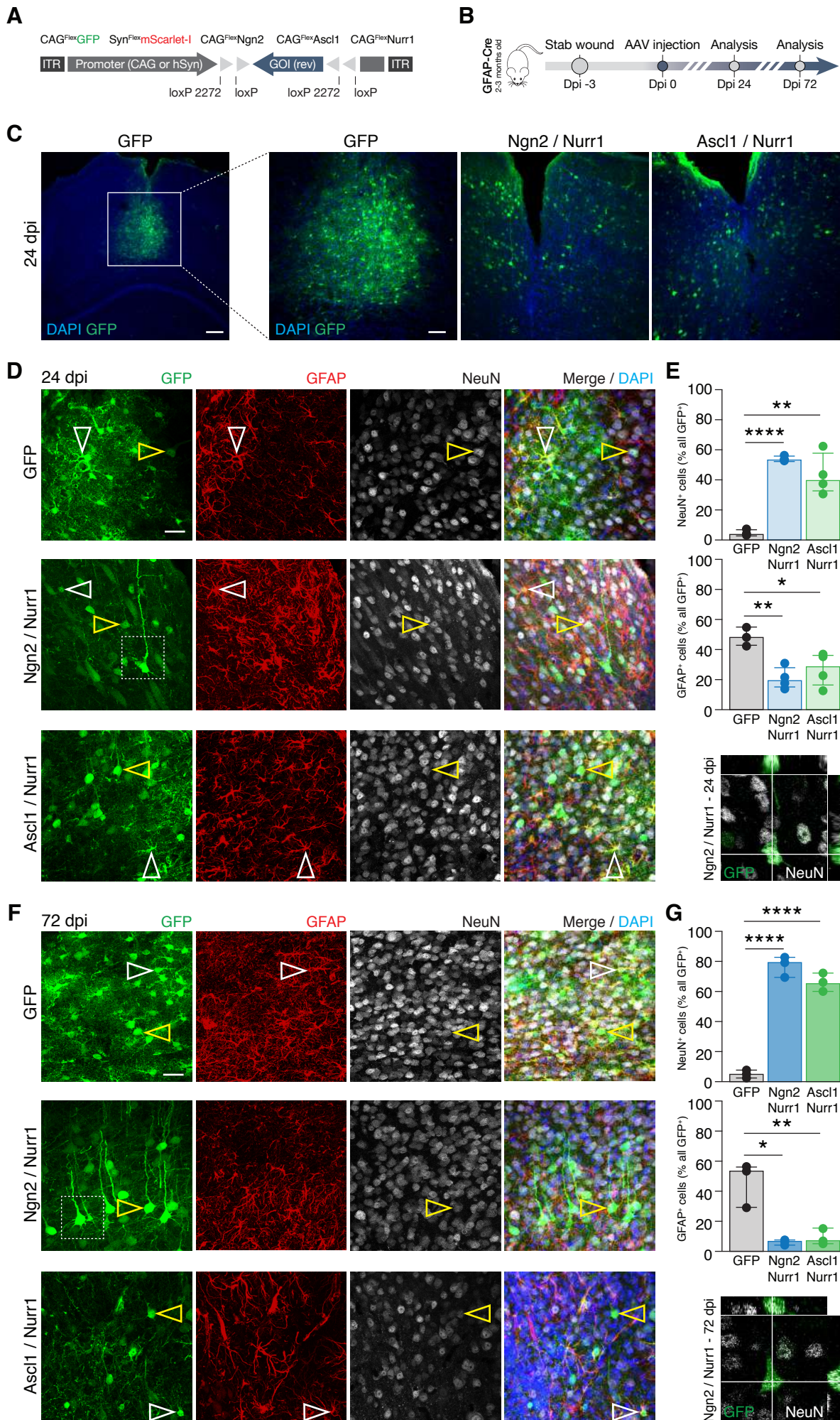


# Figure 2

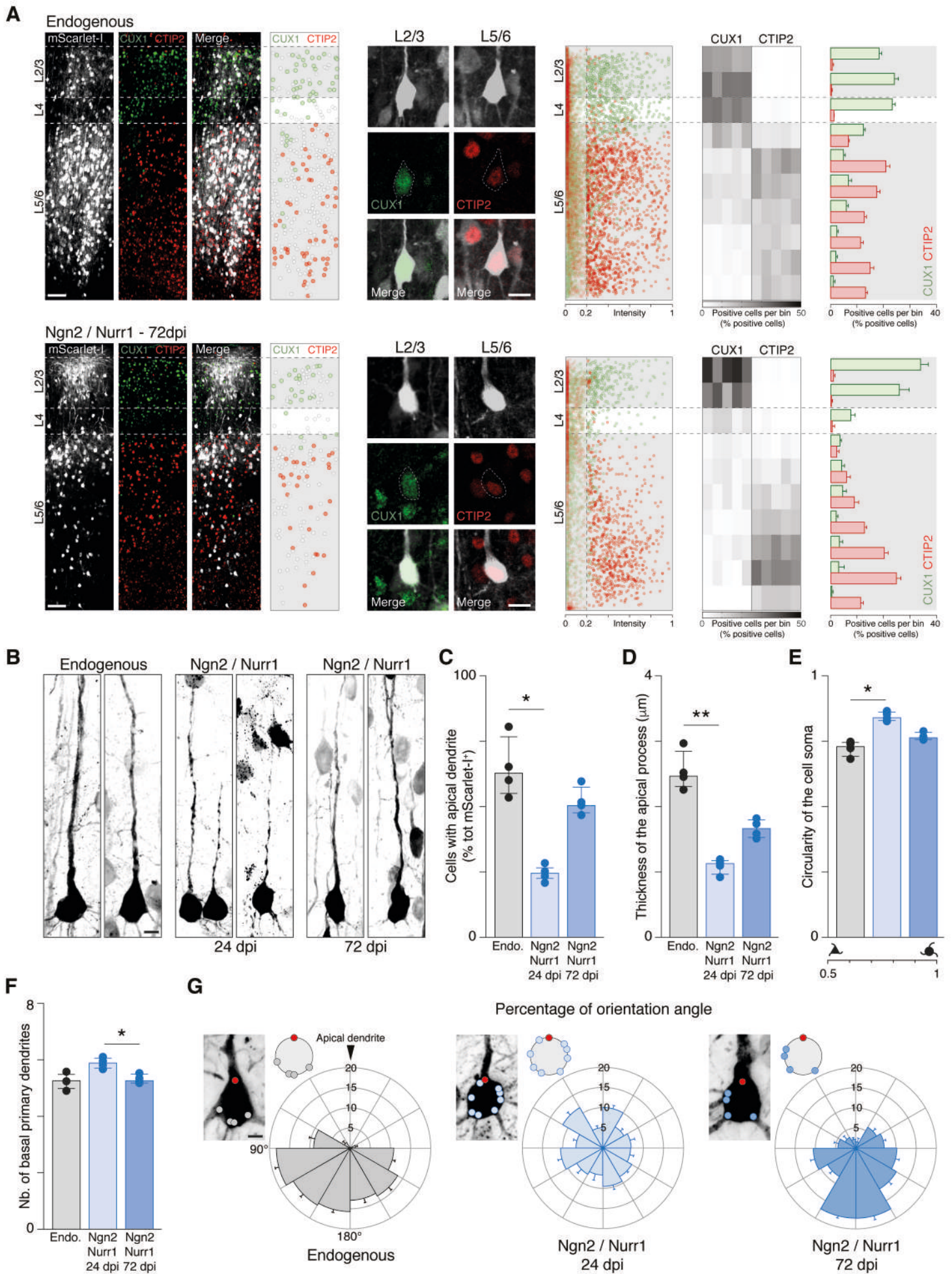


# Figure 3

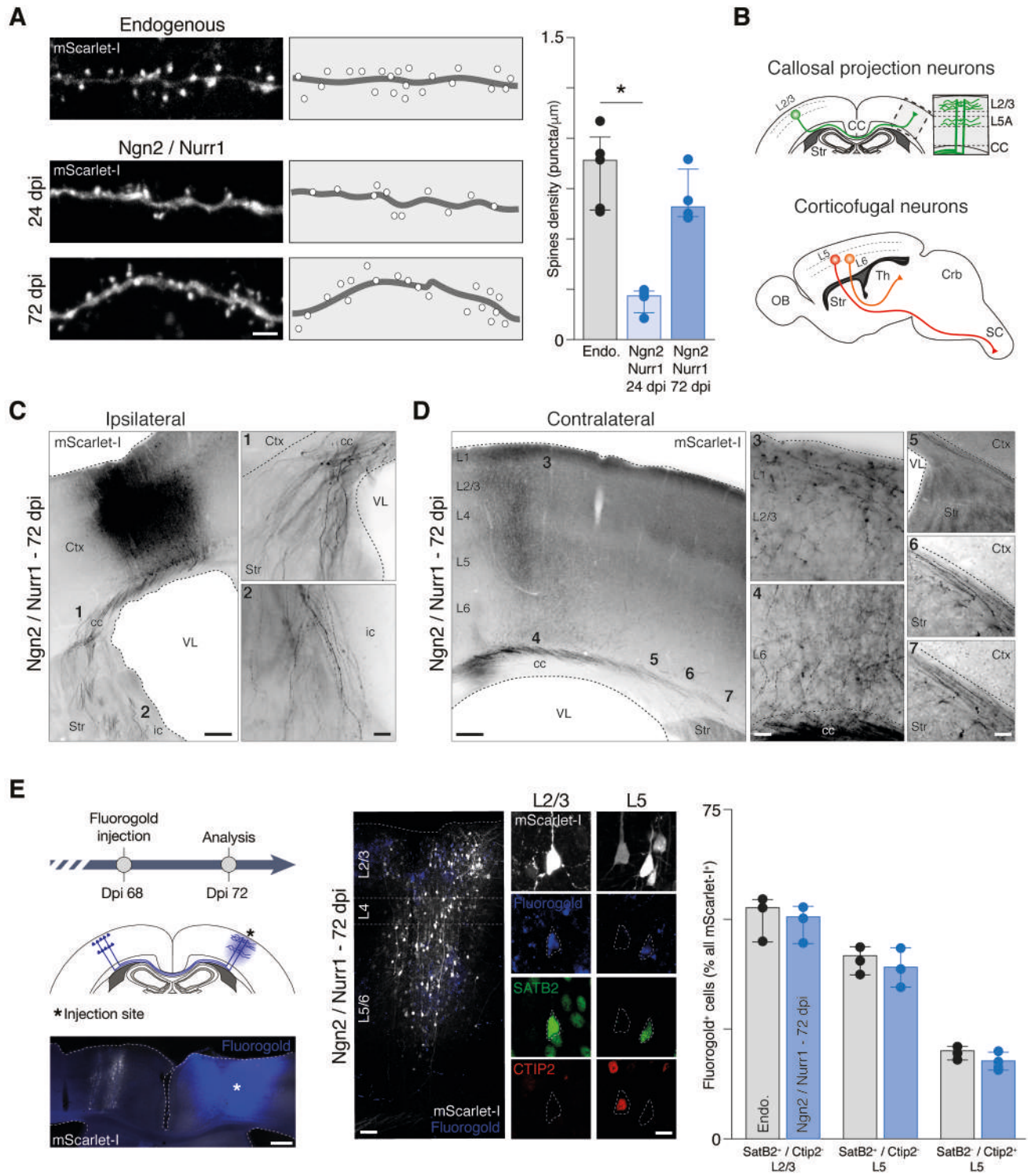




# Figure S1 - Related to Figure 1

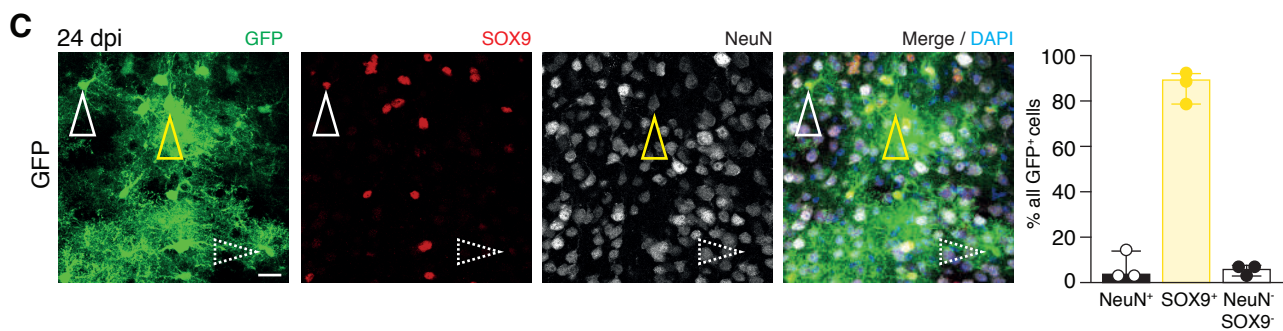
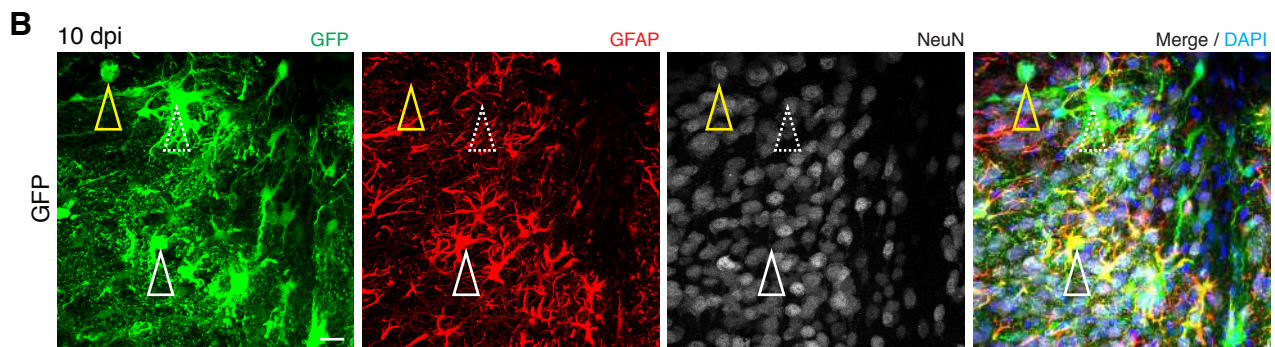
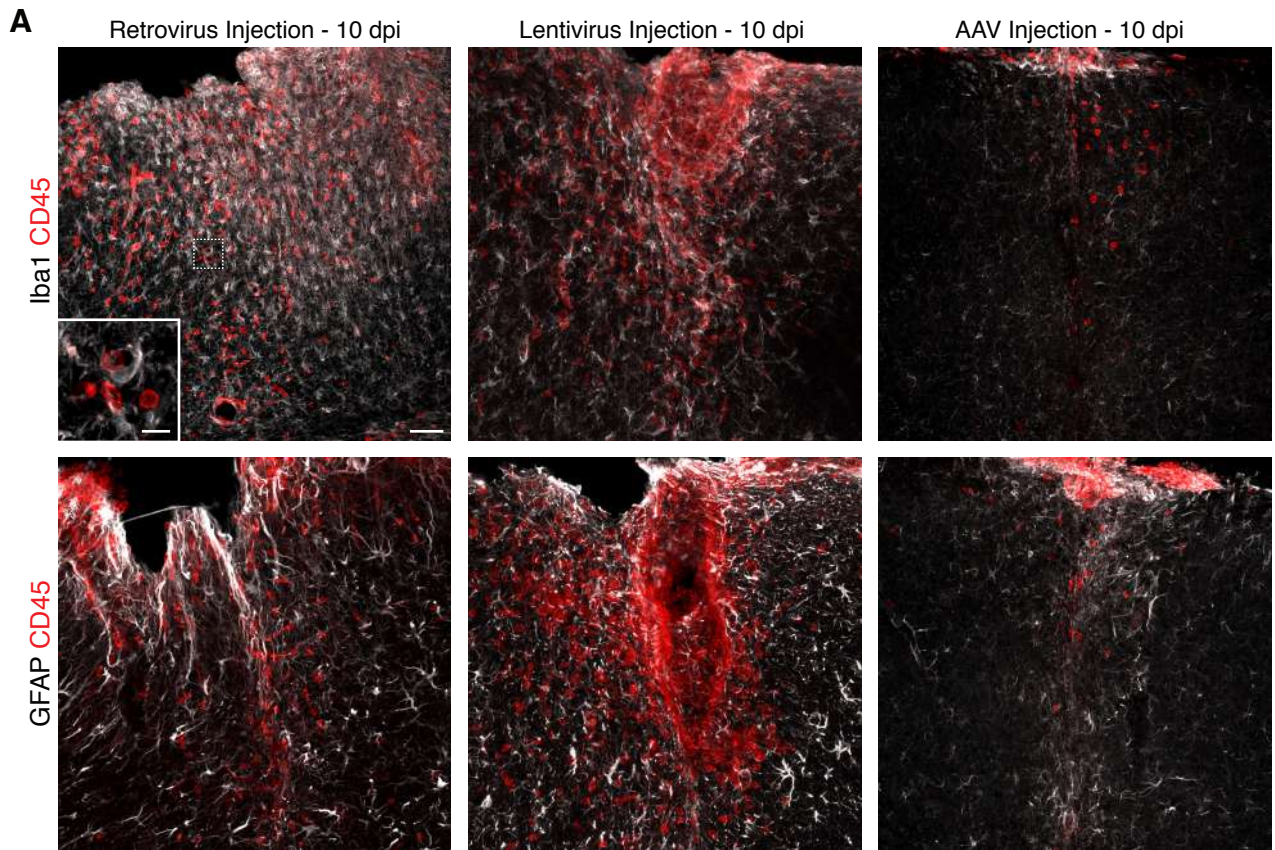


# Figure S2 - Related to Figure 1

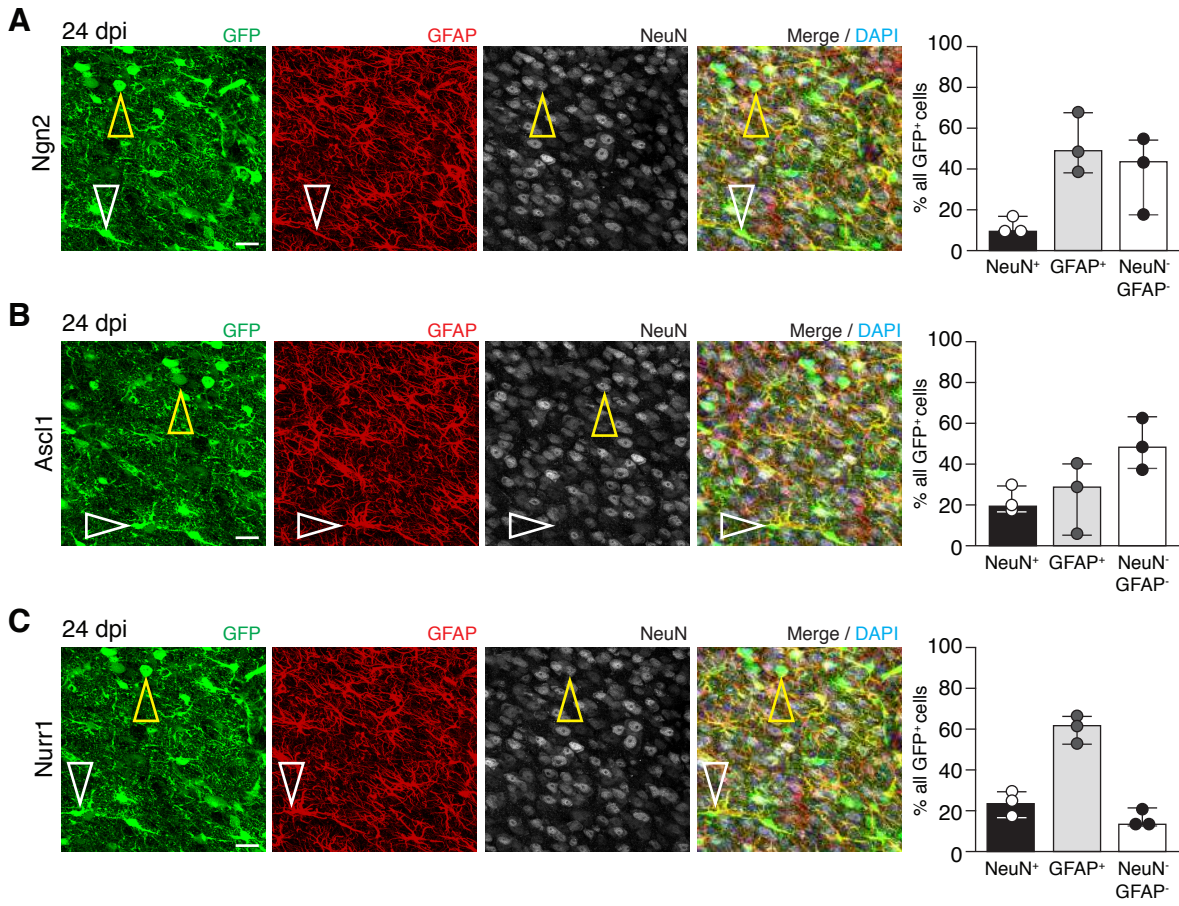


# Figure S3 - Related to figure 2

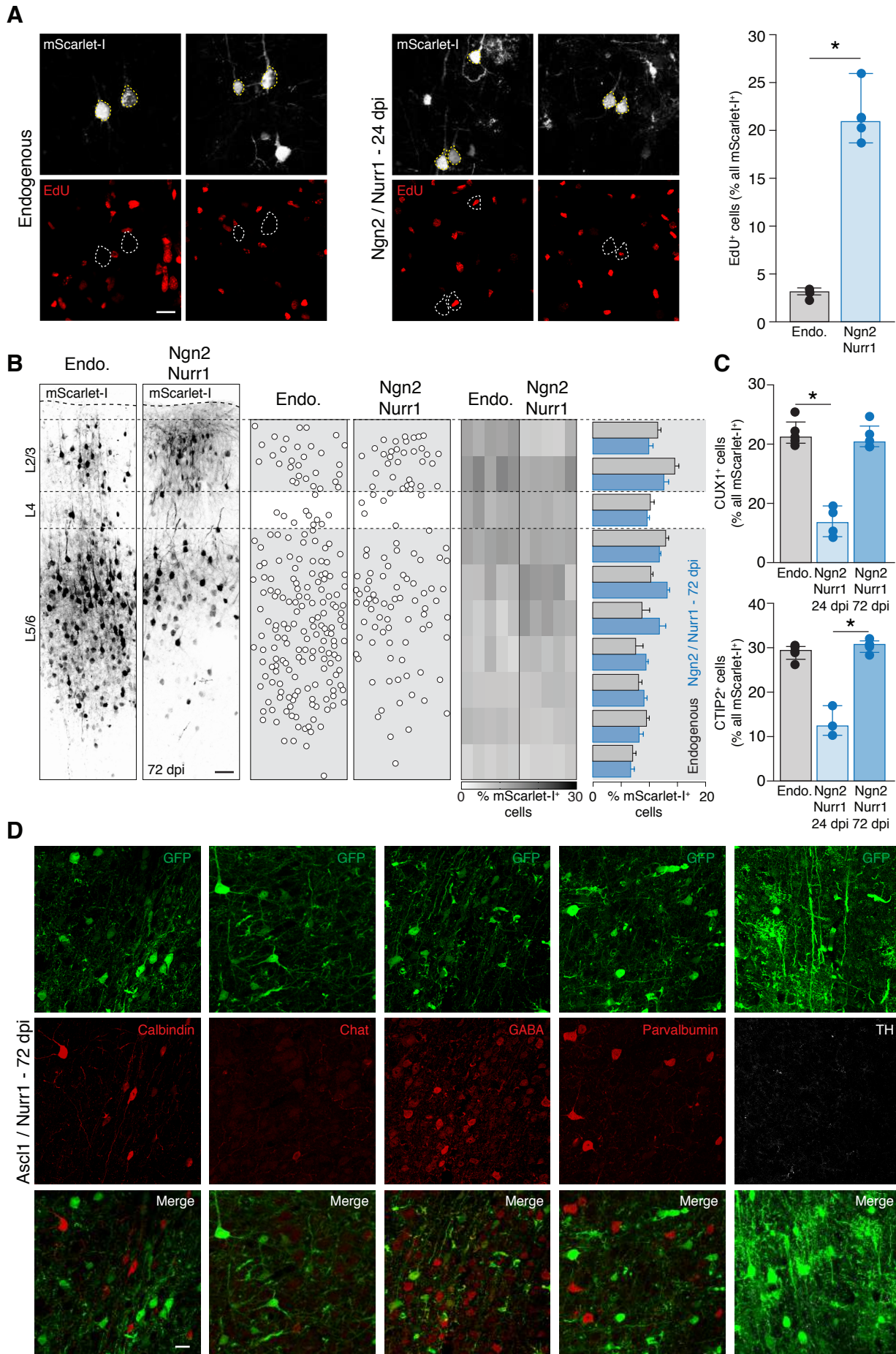
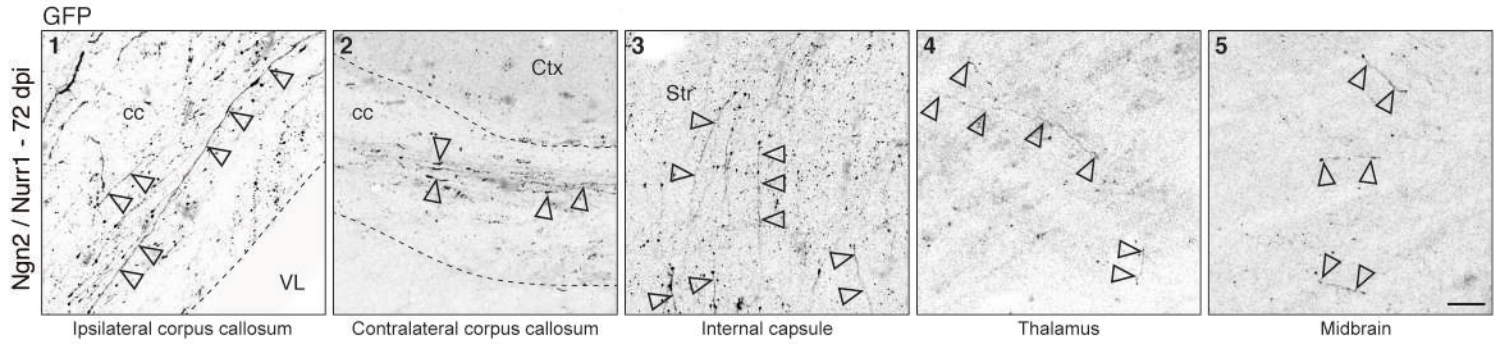
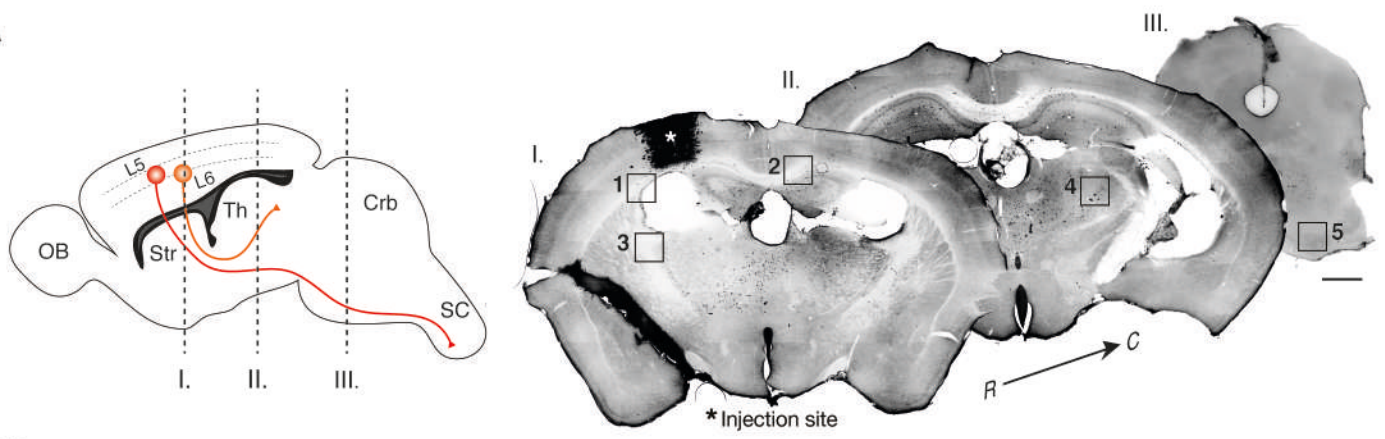


# Figure S4 - Related to figure 3

A



## SUPPLEMENTAL FIGURES TITLES AND LEGENDS

### **Supplementary Figure 1. Immune response to different viral vectors and identity of GFP<sup>+</sup> cells after injection of only AAV-FLEX-GFP.**

(A) Photomicrographs comparing immune cells infiltration (CD45<sup>+</sup>); microglia (Iba1<sup>+</sup>) and astrocyte reactivity (GFAP<sup>+</sup>) in the GM of mice injected with three types of viral vectors at 3 days after stab wound injury and analyzed 10 days post injection (dpi). Note that the high degree of reactive gliosis after MLV-based retrovirus (for virus see: Heinrich et al., 2014; Gascón et al., 2016) or differentially pseudotyped lentivirus (see Buffo et al., 2008; Heinrich et al., 2014) versus low reactive gliosis after rAAV2/5 injection was independent from the transgene carried by the viral vectors (Ngn2 or GFP control). (B-C) Photomicrographs showing GFP<sup>+</sup> cells at 10 (B) or 24 dpi of AAV-FLEX-GFP, double-stained for GFAP (or for SOX9) and NeuN. White arrowheads indicate GFP<sup>+</sup>/GFAP<sup>+</sup> or GFP<sup>+</sup>/SOX9<sup>+</sup> astrocytes, dashed white arrowheads indicate cells with an astrocytic morphology that is only GFP<sup>+</sup> and yellow arrowhead indicate GFP<sup>+</sup>/NeuN<sup>+</sup> neurons that are GFAP<sup>-</sup> or Sox9<sup>-</sup>. Histogram on the right in (C) shows the percentage of NeuN<sup>+</sup>, SOX9<sup>+</sup> and NeuN<sup>-</sup>/SOX9<sup>-</sup> among the GFP<sup>+</sup> cells. Note that most of GFP<sup>+</sup> cells are GFAP<sup>+</sup> or SOX9<sup>+</sup> indicating their astrocyte identity. Each dot represents one experimental animal; n = 3. Data are shown as median ± IQR. dpi: days post injection. Scale bars: 50 μm (A; overview), 20 μm (B and C), and 10 μm (A; close up).

### **Supplementary Figure 2. Identity of GFP<sup>+</sup> cells at 24 dpi of AAVs containing GFP and single neurogenic reprogramming factors**

(A-C) Photomicrographs show GFP<sup>+</sup> cells at 24 dpi of AAV-FLEX expressing single neurogenic factor: Ngn2 (A), Ascl1 (B) and Nurr1 (C). White arrowheads indicate GFP<sup>+</sup>/GFAP<sup>+</sup>/NeuN<sup>-</sup> astrocytes, yellow arrowheads indicate GFP<sup>+</sup>/NeuN<sup>+</sup>/GFAP<sup>-</sup> neurons. Histograms on the right show the percentage of NeuN<sup>+</sup> neurons, GFAP<sup>+</sup> astrocytes and NeuN<sup>-</sup>/GFAP<sup>-</sup> cells (that are mostly astrocytes based on their morphology) among the GFP<sup>+</sup> cells. Each dot represents one experimental animal; n = 3. Data are shown as median ± IQR. dpi: days post injection. Scale bars: 20 μm.

### **Supplementary Figure 3. Neurons reprogrammed with Ngn2/Nurr1 distribute along the entire cortical column.**

(A) Photomicrographs of endogenous (left) and reprogrammed (middle) neurons 24 dpi of mScarlet-I and mScarlet-I/Ngn2/Nurr1 respectively, showing the co-localization with EdU.

Quantification (right) of EdU<sup>+</sup> cells among mScarlet-I<sup>+</sup> neurons showing that after injury only reprogrammed, but not endogenous neurons incorporated EdU, confirming that some iNs derive from proliferating astrocytes. As the proportion of EdU<sup>+</sup> iNs corresponds well with the overall proportion of proliferating astrocytes amongst reactive astrocytes, we conclude that proliferating astrocytes are not more likely to convert into neurons than non-proliferating astrocytes. Each dot represents one experimental animal; n = 3 and 5 for Endo. and Ngn2/Nurr1, respectively). (B) Photomicrographs and drawings show the laminar position of endogenous and reprogrammed neurons 72 dpi of AAVs-FLE<sub>x</sub> expressing mScarlet-I, Ngn2 and Nurr1. The heatmap shows the cell distribution at ten different bins. The color-coded columns represent the percentage of cells per bin (n = 5 animals). Histogram illustrates the average percentage of cells per bin. (C) Histograms show the percentage of CUX1<sup>+</sup> (top) and CTIP2<sup>+</sup> cells (bottom) among mScarlet-I<sup>+</sup> endogenous neurons (grey) and mScarlet-I<sup>+</sup> reprogrammed neurons (blue) at 24 (light blue) and 72 dpi (dark blue). Each dot represents one experimental animal; n = 4. Data are shown as median ± IQR. Significance between median was tested using the Kruskal-Wallis test followed by the Dunn's multiple comparisons test (C) or the Mann-Whitney test (A), \* p ≤ 0.05. (D) Photomicrographs showing GFP<sup>+</sup> cells at 72 dpi of AAV encoding for GFP, Ascl1 and Nurr1 double-stained for various neuronal markers as indicated. Note that GFP<sup>+</sup> cells are negative for interneuron markers. dpi: days post injection. Scale bars: 100 μm (B) and 20 (A and D).

#### **Supplementary Figure 4. Neurons reprogrammed with Ngn2/Nurr1 project to the appropriate brain regions**

Photomicrographs showing axonal processes of reprogrammed neurons at 72 dpi in the ipsilateral and contralateral hemisphere. Overview sections are shown on the top left with squares indicating the high power magnifications shown in the bottom row. C: caudal, cc: corpus callosum, Crb: cerebellum, Ctx: cortex, dpi: days post injection, OB: olfactory bulb, R: rostral, VL: lateral ventricle, SC: spinal cord, Str: striatum Th: thalamus. Scale bars: 1 mm (overview), 20 μm (close up).

## STAR METHODS

REAGENT or RESOURCE	SOURCE	IDENTIFIER
Antibodies		
Rabbit anti-GFAP	Dako	Cat#Z0334
Mouse IgG1 anti-NeuN	Merk/Millipore	Cat#MAB377
Rabbit anti-CUX1	Santa Cruz	Cat#Sc-13024
Mouse anti-SATB2	Abcam	Cat# Ab51502
Rat anti- CTIP2	Abcam	Cat#Ab18465
Chicken anti-GFP	Aves Labs	Cat#GFP-1020
Goat anti-Choline Acetyltransferase	Merk/Millipore	Cat#AB 144P
Rabbit anti-Calbindin	Merk/Millipore	Cat#AB1778
Rabbit anti-GABA	Sigma	Cat#A2052
Mouse IgG1 anti-Parvalbumin	Sigma	Cat#P3088
Mouse IgG1 anti-TH	Merk/Millipore	Cat#MAB318
Rabbit anti-Iba1	BD/Bioscience	Cat#550539
Rat anti-CD45	Wako	Cat#019-19741
Guinea pig anti-SOX9		Professor Palle Serup NNF Center for Stem Cell Biology (DanStem), Copenhagen University,Denmark
Goat anti-Chicken IgY (H+L) Secondary Antibody, Alexa Fluor 488	Thermo Fischer scientific	Cat#A11039
Goat IgG anti-Rabbit IgG (H+L)-Cy3	Dianova	Cat#11-165-144
Goat anti-Mouse IgG1 Cross-Adsorbed Secondary Antibody, Alexa Fluor 647	Thermo Fischer scientific	Cat#A21121
Donkey anti-Goat IgG (H+L) Alexa Fluor 647	Jackson immunoresearch	Cat#705-605-003
DAPI	Sigma	Cat#28718-90-3
Recombinant DNA		
Plasmid: pAAV-CAG-FLE <sub>x</sub> -EGFP	(Torper et al., 2015)	

Plasmid: pAAV-hSyn-FLEEx-pmScarletI-P2A-GCaMP6		Tobias Rose Project Group Leader at Max Planck Institute of Neurobiology, Munich
Plasmid: pAAV-hSyn-pmScarletH-P2A-GCaMP6s		Tobias Rose Project Group Leader at Max Planck Institute of Neurobiology, Munich
Plasmid: pAAV-CAG-FLEEx-Ngn2		Professor Malin Parmar at Developmental and Regenerative Neurobiology, Lund University
Plasmid: pAAV-CAG-FLEEx-Nurr1		(Torper et al., 2015)
Plasmid: pAAV-CAG-FLEEx-Ascl1		(Torper et al., 2015)
Plasmid: pHelper	Cell Biolabs	Cat#gb AF369965.1
Plasmid: pAAV-RC5	Cell Biolabs	Cat#VPK-425
Plasmid:LV- PRSVLTR-psi-CAG-GFP-WPRE-LTRSIN	(Buffo et al., 2008)	
Plasmid: RV- CAG-Ngn2-IRES-Dsred	(Heinrich et al., 2011)	
<b>Bacterial and Virus Strains</b>		
Stable Competent E. coli (High Efficiency)	NEB	Cat#C3040
rAAV2/5 CAG-FLEEx-EGFP	SFB 870 Viral Vector Facility	N/A
rAAV2/5 CAG-FLEEx-Ngn2	SFB 870 Viral Vector Facility	N/A
rAAV2/5 CAG-FLEEx-Nurr1	SFB 870 Viral Vector Facility	N/A

rAAV2/5 CAG-FLEX-Ascl1	SFB 870 Viral Vector Facility	N/A
rAAV2/1 hSyn-FLEX-pmScarletI-P2A-GCaMP6s	SFB 870 Viral Vector Facility	N/A
rAAV2/1 hSyn-pmScarletH-P2A-GCaMP6s	SFB 870 Viral Vector Facility	N/A
Chemicals, Peptides, and Recombinant Proteins		
OptiPrep Density Gradient Medium	Sigma	Cat#D1556
SYBR Green Real-Time PCR Master Mixes	Thermo Fisher scientific	Cat#4385612
Fluorogold dye (Hydroxystilbamidine)	Sigma	Cat#223769-64-0
EdU (5-ethynyl-2'-deoxyuridine)	Invitrogen	Cat#E10187
Click-iT™ EdU Alexa Fluor™ 647 Imaging Kit	Invitrogen	Cat#C10340
Experimental Models: Cell Lines		
293T	ATCC	CRL-3216
Experimental Models: Organisms/Strains		
Mouse: B6.Cg-Tg(Gfap-cre)77.6Mvs/2J also known as GFAP-cre line 77.6	The jackson laboratory	Stock No: 024098
Mouse: C57BL/6J	The jackson laboratory	Stock No: 000664
Oligonucleotides		
SV40 Forward primer	5'AGCAATAGCATCACAA ATTTACAAA3'	(D'Costa et al., 2016)
SV40 reverse primer	5'CCAGACATGATAAGAT ACATTGATGAGTT3'.	(D'Costa et al., 2016)
GFP Forward primer	5'GATGTTGTGGCGGATC TTGA3'	(D'Costa et al., 2016)
GFP reverse primer	5'CAACAGCCACAACGTC TATATCATG3'	(D'Costa et al., 2016)
Software and Algorithms		
Zen software 2.3 lite	Carl Zeiss	

ImageJ 1.48v	NIH	<a href="https://imagej.nih.gov/ij/">https://imagej.nih.gov/ij/</a>
Photoshop	Adobe	<a href="https://www.adobe.com/en/products/photoshop.html">https://www.adobe.com/en/products/photoshop.html</a>
Illustrator	Adobe	<a href="https://www.adobe.com/en/products/illustrator.html">https://www.adobe.com/en/products/illustrator.html</a>
GraphPad Prism 7.04	GraphPad Software	
Other		
FPLC	GE healthcare	ÄKTA prime plus
HiTrap Q FF anion exchange chromatography column	GE healthcare	Cat#17505301

### **Animals and surgery**

Animal handling and experimental procedures were performed in accordance with German and European Union guidelines and were approved by the State of upper Bavaria. All efforts were made to minimize suffering and number of animals. Mice were maintained in specific pathogen-free conditions in the animal facility, upon 12:12 hour light/dark cycles.

Adult (2-3 months) heterozygous GFAP-cre mice from both genders were used for stab wound injury as described in Mattugini et al., 2018 with slight modifications. Briefly, animals were anesthetized and injured on one hemisphere from Bregma: RC: -0.4 to -1.4 mm; ML: -1.0 mm; DV: -1.2 mm. Three days after stab wound injury mice were injected with AAV virus in the site of the lesion using a microinjector at the speed of 40-50 nl/min. For control experiments we injected 200-300 nl of -AAV-FLEX-GFP. To label endogenous neurons we injected 200-300 nl of AAV-mScarlet-I (non- FLEX). For reprogramming experiments, we injected 800-1000 nl of the following mixes containing 1/2 or 1/3 of each virus: AAV- FLEX -GFP/ AAV- FLEX -Ngn2; AAV- FLEX -GFP/ AAV- FLEX -Ascl1; AAV- FLEX -GFP/ AAV- FLEX -Nurr1; AAV- FLEX -GFP/ AAV- FLEX -Ngn2/ AAV- FLEX -Nurr1; AAV- FLEX -GFP/ AAV- FLEX -Ascl1/ AAV- FLEX -Nurr1; AAV- FLEX -mScarlet-I/ AAV- FLEX -Ngn2/ AAV- FLEX -Nurr1. For retro- and lenti-viral vectors testing, wild type animals were injured at the following coordinates from Bregma: RC: -0.4 to -1.4 mm; ML: -1.0 mm; DV: -0.6 mm. Three days after stab wound injury mice were injected with 300nl of LV-GFP (VSV-G) or 800nl of RV-Ngn2-ires-dsRed.

Where indicated, EdU (0,2 mg/ml) was administrated in 1% sucrose drinking water for 10 consecutives days following the stab wound lesion (between -3 and 7 dpi).

### **Immunohistochemistry**

Mice were anesthetized and trans-cardially perfused with 4% paraformaldehyde (PFA). Brains were post-fixed for 24 hours in 4% PFA and then cryo-protected in 30% sucrose in Phosphate Buffered Saline (PBS). Fifty-micrometer-thick brain sections were cut at the vibratome and incubated with blocking solution composed of PBS, 2% bovine serum albumin (BSA Sigma Aldrich), 0,5 % Triton X-100 (Sigma Aldrich) for 20 minutes and overnight with primary antibodies diluted in blocking solution. The day after, free-floating sections were washed in PBS and incubated with appropriate secondary antibodies, diluted in the blocking solution for 2 hours. Finally, sections were washed and stained with 4', 6-diamidino-2-phenylindole (DAPI; Sigma Aldrich) for 5 minutes. EdU was detected using the Click-iT EdU imaging kit (Invitrogen) following the protocol from the kit.

### **Viral vectors preparation**

High-titer preparations of rAAV2/5 were produced based on Zolotukhin and colleagues (Zolotukhin et al., 1999) protocol with minor modifications. In brief, HEK 293T cells were transfected with the CaPO<sub>4</sub> precipitate method, pRC5, Ad helper and pAAV plasmid at a 1:1:1 molar ratio. After 72 h, cell pellets were harvested with AAV release solution, 50 U/ml benzonase was added, then incubated for 2 h at 37°C in a water bath. Cells were frozen and thawed in liquid nitrogen to allow rAAV release. Purification of rAAV vector was done with iodixanol densities gradient (consisting of 15, 25, 40 and 56% iodixanol), followed by gradient spinning at 50,000 rpm for 2 h 17 min at 22°C in a Ti70 rotor (Beckman, Fullerton, CA, USA). rAAVs were collected at 40% iodixanol with 5-ml-syringe. rAAVs were dialyzed (Slide-A-Lyzer 10,000 MWCO 5ml) in buffer A overnight to remove iodixanol. Anion exchange chromatography column HiTrap Q FF sepharose column and superloop were connected with the ÄKTAprius plus chromatography system to collect the eluted fraction. To measure rAAV concentration, the eluted fraction was spun and washed once in PBS-MK Pluronic-F68 buffer with Millipore 30K MWCO 6ml filter unit. rAAVs were stored in glass vial tube in 4°C. rAAVs were titered by SYBR Green qPCR with GFP or SV40 primer (D'Costa et al., 2016). Usual titer was 3 x10<sup>14</sup> to 5x10<sup>15</sup> gc/ml. Retrovirus and Lentivirus were prepared as already described in (Gascón et al., 2016; Hack et al., 2005; Heinrich et al., 2011).

## **Retrograde labeling**

Anesthetized animals were placed in a stereotaxic apparatus and injected with Fluoro-Gold (300 nl) into the contralateral homotypic somatosensory cortex 68 dpi, in order to retrogradely label callosal projection neurons. Animals were sacrificed 4 days later (72 dpi) and analysed.

## **Quantification and data analysis**

All images (30-40  $\mu\text{m}$  thick z-stacks) were acquired on a confocal laser scanning (Zeiss LSM710) microscope. At least three sections from each animal (at least 3) were analyzed for quantifications. All quantifications were done using Zen or ImageJ software. The proportions of neurons and astrocytes were obtained by counting NeuN<sup>+</sup>, GFAP<sup>+</sup>, SOX9<sup>+</sup>, NeuN<sup>-</sup>/GFAP<sup>-</sup> and NeuN<sup>-</sup>/SOX9<sup>-</sup> cells among the transduced GFP<sup>+</sup> population. For CUX1/CTIP2 analysis, the intensities of CUX1 and CTIP2 were measured on the cells soma of both endogenous and reprogrammed neurons (> 2000 mScarlet-I<sup>+</sup> cells per condition were measured) and plotted on the Y axis according to their laminar position. The normalized intensity threshold defining positive cells for CUX1 or CTIP2 was arbitrary fixed at 0.2. The number of positive (CUX1<sup>+</sup> or CTIP2<sup>+</sup>) cells was divided by the total number of m-Scarlet-I<sup>+</sup> cells in each bin, representative of ten different cortical levels. For morphological analysis, 50 cells per conditions (endogenous and reprogrammed m-Scarlet-I<sup>+</sup> neurons) were analyzed. The presence of the apical dendrite was defined by the presence of a prominent primary dendrite oriented to the pial surface. The thickness of the apical leading process was measured in its proximal part (5 $\mu\text{m}$  from the cell soma). The circularity was measured using an ImageJ plugin drawing the cell soma. The number of primary processes was calculated as the number of processes leaving the cell soma in each neuron. The polarization was analyzed by measuring angles between the apical dendrite (red dots in Figure 2) and all the others primary dendrites (gray or blue dots) and plotted into a circular diagram divided in 12 different bins corresponding to the 360° orientation angles. For spine density, high power images were acquired and quantifications were done by counting only laterally emanating protrusions longer than 0.4  $\mu\text{m}$  (Holtmaat et al., 2009).

Statistical analyses of data were performed using the GraphPad Prism 7.0 software. All data are plotted as median  $\pm$  IQR and each dot represent one animal. Normal distribution was tested using the Shapiro-Wilk test. If not rejected, we performed the t-test (unpaired two-tailed) for the group comparison. If rejected, significance between groups was analyzed using of Kruskal-Wallis test followed by Dunn's multiple comparisons test or Mann-Whitney U-test.

Significance is based on the P-value indicated in the figures as \*  $p \leq 0.05$ , \*\*  $p \leq 0.01$ , \*\*\*  $p \leq 0.001$ , \*\*\*\*  $p \leq 0.0001$ .

## **Aim of the study II**

The aim of the study is to investigate:

1. How modulating metabolism can affect direct neuronal reprogramming *in vitro*, acting on glycolysis or oxidative phosphorylation.

## **Identification and Successful Negotiation of a Metabolic Checkpoint in Direct Neuronal Reprogramming**

Sergio Gascon, Elisa Murenu, Giacomo Masserdotti, Felipe Ortega, ***Gianluca L. Russo***, David Petrik, Aditi Deshpande, Christophe Heinrich, Marisa Karow, Stephen P. Robertson, Timm Schroeder, Johannes Beckers, Martin Irmeler, Carsten Berndt, José P. Friedmann Angeli, Marcus Conrad, Benedikt Berninger, and Magdalena Götz

For this paper I was involved in performing *in vitro* experiments to investigate the role of different metabolic medium on direct neuronal reprogramming. I was also involved in writing, editing and reviewing the paper.

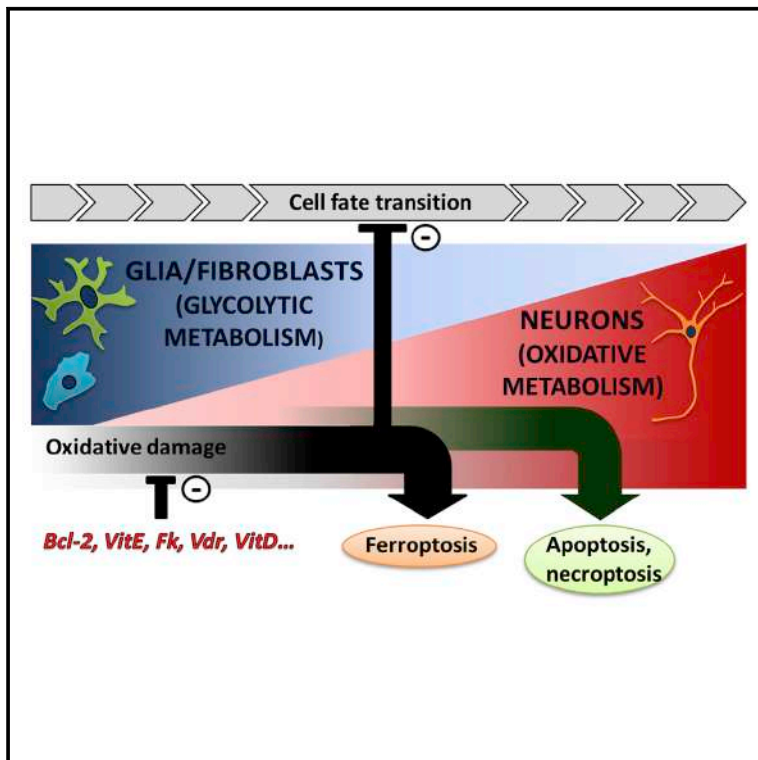
*The paper is published on Cell Stem Cell, 3 March 2016, pages 396-409*  
<http://doi.org/10.1016/j.stem.2015.12.003>

*As open access paper and author of this Elsevier article, I have the right to include it in a thesis or dissertation, provided it is not published commercially.*

# Cell Stem Cell

## Identification and Successful Negotiation of a Metabolic Checkpoint in Direct Neuronal Reprogramming

### Graphical Abstract



### Highlights

- Oxidative stress is a major hurdle in converting different cell types into neurons
- Ferroptosis inhibitors and antioxidants improve direct neuronal reprogramming
- Bcl-2 reduces ROS and promotes direct neuronal reprogramming also in vivo
- Antioxidants potently improve maturation of induced neurons in vitro and in vivo

### Authors

Sergio Gascón, Elisa Murenu, Giacomo Masserdotti, ..., Marcus Conrad, Benedikt Berninger, Magdalena Götz

### Correspondence

sergio.gascon@med.uni-muenchen.de (S.G.),  
magdalena.goetz@helmholtz-muenchen.de (M.G.)

### In Brief

By imaging cell fate conversion over time, Gascón, Murenu, and colleagues find that high levels of oxidative stress prevent successful direct neuronal reprogramming, instead causing extensive cell death. They identify inhibitors of ferroptosis, antioxidants, and Bcl-2 as key metabolic agents in improving generation of iNs from a range of somatic cells and in vivo after brain injury.

### Accession Numbers

GSE70921



# Identification and Successful Negotiation of a Metabolic Checkpoint in Direct Neuronal Reprogramming

Sergio Gascón,<sup>1,2,14,\*</sup> Elisa Murenu,<sup>1,2,14</sup> Giacomo Masserdotti,<sup>1,2</sup> Felipe Ortega,<sup>1,3,4</sup> Gianluca L. Russo,<sup>1,2</sup> David Petrik,<sup>1,2</sup> Aditi Deshpande,<sup>1,15</sup> Christophe Heinrich,<sup>1,16</sup> Marisa Karow,<sup>1</sup> Stephen P. Robertson,<sup>5</sup> Timm Schroeder,<sup>6,17</sup> Johannes Beckers,<sup>7,8,9</sup> Martin Irmeler,<sup>8</sup> Carsten Berndt,<sup>10</sup> José P. Friedmann Angeli,<sup>11</sup> Marcus Conrad,<sup>11</sup> Benedikt Berninger,<sup>1,3,12</sup> and Magdalena Götz<sup>1,2,13,\*</sup>

<sup>1</sup>Physiological Genomics, Biomedical Center Ludwig-Maximilians-University Munich, 80336 Munich, Germany

<sup>2</sup>Institute for Stem Cell Research, Helmholtz Center Munich, 85764 Neuherberg, Germany

<sup>3</sup>Institute of Physiological Chemistry, University Medical Center of the Johannes Gutenberg University Mainz, 55128 Mainz, Germany

<sup>4</sup>Biochemistry and Molecular Biology Department, Faculty of Veterinary Medicine, Complutense University, Avenue Puerta de Hierro, 28040 Madrid, Spain

<sup>5</sup>Department of Women's and Children's Health, Dunedin School of Medicine, University of Otago, 9016 Dunedin, New Zealand

<sup>6</sup>Research Unit Stem Cell Dynamics, Helmholtz Center Munich, Neuherberg, 85764 Neuherberg, Germany

<sup>7</sup>German Center for Diabetes Research (DZD), 85764 Neuherberg, Germany

<sup>8</sup>Institute of Experimental Genetics, Helmholtz Center Munich GmbH, 85764 Neuherberg, Germany

<sup>9</sup>Center of Life and Food Sciences Weihenstephan, Technical University Munich, 85354 Freising, Germany

<sup>10</sup>Department of Neurology, Medical Faculty, Heinrich-Heine University Düsseldorf, Merowingerplatz 1a, 40225 Düsseldorf, Germany

<sup>11</sup>Institute of Developmental Genetics, Helmholtz Center Munich, 85764 Neuherberg, Germany

<sup>12</sup>Focus Program Translational Neuroscience, Johannes Gutenberg University Mainz, 55128 Mainz, Germany

<sup>13</sup>Excellence Cluster of Systems Neurology (SYNERGY), 80336 Munich, Germany

<sup>14</sup>Co-first author

<sup>15</sup>Present address: Department of Psychiatry and Institute for Human Genetics, University of California San Francisco, San Francisco, CA 94143, USA

<sup>16</sup>Present address: INSERM, U1216, University Grenoble Alpes, Grenoble Institut des Neurosciences, GIN, F-38000 Grenoble, France

<sup>17</sup>Present address: Department of Biosystems Science and Engineering, ETH Zurich, Mattenstrasse 26, 4058 Basel, Switzerland

\*Correspondence: [sergio.gascon@med.uni-muenchen.de](mailto:sergio.gascon@med.uni-muenchen.de) (S.G.), [magdalena.goetz@helmholtz-muenchen.de](mailto:magdalena.goetz@helmholtz-muenchen.de) (M.G.)

<http://dx.doi.org/10.1016/j.stem.2015.12.003>

## SUMMARY

Despite the widespread interest in direct neuronal reprogramming, the mechanisms underpinning fate conversion remain largely unknown. Our study revealed a critical time point after which cells either successfully convert into neurons or succumb to cell death. Co-transduction with Bcl-2 greatly improved negotiation of this critical point by faster neuronal differentiation. Surprisingly, mutants with reduced or no affinity for Bax demonstrated that Bcl-2 exerts this effect by an apoptosis-independent mechanism. Consistent with a caspase-independent role, ferroptosis inhibitors potently increased neuronal reprogramming by inhibiting lipid peroxidation occurring during fate conversion. Genome-wide expression analysis confirmed that treatments promoting neuronal reprogramming elicit an anti-oxidative stress response. Importantly, co-expression of Bcl-2 and anti-oxidative treatments leads to an unprecedented improvement in glial-to-neuron conversion after traumatic brain injury in vivo, underscoring the relevance of these pathways in cellular reprogramming irrespective of cell type in vitro and in vivo.

## INTRODUCTION

Direct reprogramming of somatic cells has proven to be an extraordinary method to generate cell populations such as neurons that are otherwise difficult to obtain for research purposes (Amamoto and Arlotta, 2014). In addition, replenishing neuronal populations in the injured brain using reprogramming-based therapies is an exciting future prospect (Buffo et al., 2005; Heinrich et al., 2014). However, the cellular and molecular basis underlying direct reprogramming remains poorly understood. Most studies are restricted to the function of neurogenic reprogramming factors (Masserdotti et al., 2015; Ninkovic et al., 2013; Wapinski et al., 2013), while little is known about other aspects, such as metabolic changes or proliferation. As the function of neurogenic factors is context dependent, this also prompts the question to which extent there may be mechanisms common to all cells types converting into neurons. For example, Neurogenin2 (Neurog2) efficiently induces neuronal conversion of mouse post-natal astrocytes in culture (Berninger et al., 2007; Blum et al., 2011; Heinrich et al., 2010) but is rather ineffective in mouse embryonic fibroblasts (MEFs) (Chanda et al., 2014) or adult reactive glial cells in vivo (Grande et al., 2013). While the starting cell type may dictate conversion efficiency by providing transcriptional accessibility of target genes (Wapinski et al., 2013), other cellular processes shown to influence reprogramming into induced pluripotent stem cells (iPSCs) such as cell death (Kawamura et al., 2009), proliferation rate (Halley-Stott et al., 2014; Ruiz

et al., 2011), or metabolic state (Zhang et al., 2012) may also be important in direct neuronal reprogramming. Among them, the metabolic state is particularly relevant for the conversion into neurons, which rely on oxidative metabolism, while astroglia, fibroblasts, and proliferative cells rather utilize anaerobic glycolysis and  $\beta$ -oxidation (McKay et al., 1983; Tsacopoulos and Magistretti, 1996). Moreover, metabolic factors such as reactive oxygen species (ROS) have been implicated in cell fate regulation (Maryanovich and Gross, 2013). Here, we used continuous single-cell live imaging to monitor direct reprogramming of fibroblasts and glia into neurons. We identify stage-specific barriers and metabolic regulators increasing conversion efficiency both in vitro and in vivo.

## RESULTS

### A Critical Checkpoint Eliciting Cell Death in Neuronal Conversion

To target also postmitotic cells, we transfected astroglial cells isolated from mouse cerebral cortex at postnatal day (P) 5–7 with a dual red fluorescent protein (RFP) and *Ascl1*-encoding vector (Heinrich et al., 2010; Masserdotti et al., 2015) and tracked RFP+ cells starting at 26–29 hr after transfection (Figure 1A). In this model, neuronal conversion is achieved within 7 days and can be monitored by continuous single-cell imaging. Images were taken every 5 min in phase contrast and 5 hr in the fluorescence channel (RFP+; Figure 1B shows stills from such movies; Movie S1). To follow the fate conversion we used three methods: neuronal morphology (Figures 1B–1H and S1A; Movie S1), GFP driven by the Doublecortin promoter (*DCX-GFP*; Figures S2A–S2C; Movie S2), and immunostaining for neuron-specific antigens (Figure 1B, lower panels; Figures S2D and S2E). The first signs of neuronal conversion were visible by weak *DCX-GFP* signals at around 24 hr of live imaging (i.e., about 2 days after transfection, see Figure 1A; Figure S2, blue line) and most cells that became *DCX-GFP*+ did so within the first 2 days of imaging (Figures S2A1, S2B1, and S2C, blue line), i.e., about 3 days after transfection (Figure 1A). Thus, the regulation of key neuronal genes occurs rapidly and is implemented within few days (see also Masserdotti et al., 2015). Within 50 hr of imaging, i.e., about 3 days after transfection, the first *Ascl1/RFP*+ cells changed from flat astrocyte to neuronal morphology (Figures 1B1 and 1C1). Noteworthy, more than 90% of cells classified with a neuronal morphology were accordingly immuno-reactive for  $\beta$ -III-tubulin and MAP2. The more mature neuronal marker NeuN was present only in 60% of cells with neuronal morphology (Figures S1B and S1C). Among the cells with non-neuronal morphology we found cells in fate transition immunoreactive for both neuronal ( $\beta$ -III-tubulin) and astroglia (GFAP) markers (Figure S1E, upper). Cells with a neuronal morphology were never found to be double positive for GFAP and neuronal markers (Figure S1E, lower), confirming the stringency of these criteria.

By about 150 hr of imaging (7 days post-transfection [DPT]) most RFP+ cells had developed a neuronal morphology (Figures 1B1, 1C1, and 1D, left bars) or *DCX*-reporter activity (see example in Figures S2A1, S2B1, and S2C, blue line). However, at that time, the number of RFP+ cells had decreased dramatically, with only about 18% of all RFP+ cells observed at the

beginning of the time lapse (see Movie S1) surviving to the end (Figures 1B1, 1C1, and 1D, left bars). The peak of cell death occurred between 50- and 100-hr imaging (Figures 1B1, 1C1, and 1D, left bars), when fate conversion manifests by morphological changes (Figures 1B1 and 1C1). Most (94%) transfected cells that did not acquire a neuronal morphology underwent cell death at some point during the observation period (Figures 1D and 1G, left bars), while only 48% of the cells with neuronal morphology died (Figure 1H, left bar). Accordingly, most cells surviving until the end of imaging were reprogrammed into neurons (Figures 1B1, 1C1, and 1D, left bars; Figures S2A1, S2B1, and S2C, blue line). Thus, cell death is a main limiting factor of neuronal reprogramming and peaks at the time of fate conversion. Conversely, proliferation is limited in this paradigm (Figure 1F, left bar), with most astrocytes directly converting into neurons (Figure 1C1).

### Bcl-2 Improves Fate Conversion and Survival

To improve survival during reprogramming, we first examined the effect of the anti-apoptotic protein Bcl-2. Indeed, co-expression of *Bcl-2* with *Ascl1/RFP* in astrocytes not only increased the total number of surviving cells, but also the number of induced neurons (iNs), based on morphological analysis (Figures 1B–1D), *DCX*-reporter activity (Figures S2A–S2C), and immunostaining for  $\beta$ -III-tubulin and MAP2 at 5 DPT (Figures S2D and S2E). Furthermore, continuous single cell imaging revealed a faster conversion of *Ascl1/Bcl-2* co-transfected astrocytes, with a significant increase in the proportion of cells with neuronal morphology in the initial phases (8-fold at 50 hr of tracking time; Figures 1C–1E; Movie S1) and faster acquisition of *DCX*-reporter (Figures S2A–S2C; Movie S2) but no effect on cell proliferation (Figure 1F). Bcl-2 expression increased the proportion of surviving cells in the whole transfected population (Figures 1B–1D and S2A–S2C), while each class of cells, i.e., those with neuronal and non-neuronal morphology, still died as much as cells not co-expressing Bcl-2 (Figures 1G and 1H). Thus, the main effect of Bcl-2 is to facilitate fate transition from astrocytes to neurons, which then have a lower death rate (Figure 1I).

Continuous live imaging results were further corroborated by immunostaining and electrophysiology. Indeed, neuronal morphology faster acquired by *Bcl-2* co-expression correlated with lower resting membrane potential (RMP =  $-60$  to  $-40$  mV; Figures S2F and S2G) typical for immature neurons (Pedroni et al., 2014), while astrocytes have a RMP of  $-90$  to  $-80$  mV (Anderová et al., 2004) (Figures S2F and S2G). Notably, at 5DPT, when most reprogrammed cells have already acquired *DCX-GFP*,  $\beta$ -III-tubulin, MAP2, and NeuN expression (Figures S1C and S1D), their electrophysiological properties are still immature, and only 10% of *Ascl1/Bcl-2* co-transfected cells exhibited some very immature action potential-like features (Figure S2F3). However, iNs recorded at 15 DPT showed action potentials consistent with fully developed neurons (Figure S2H). Taken together, these results demonstrate that Bcl-2 improves reprogramming by faster fate conversion.

### Bcl-2 Promotes the Efficiency of Neuronal Conversion via a Non-canonical Pathway

As the Bcl-2 effect seems not only related to its anti-apoptotic role, we examined the contribution of its canonical function via

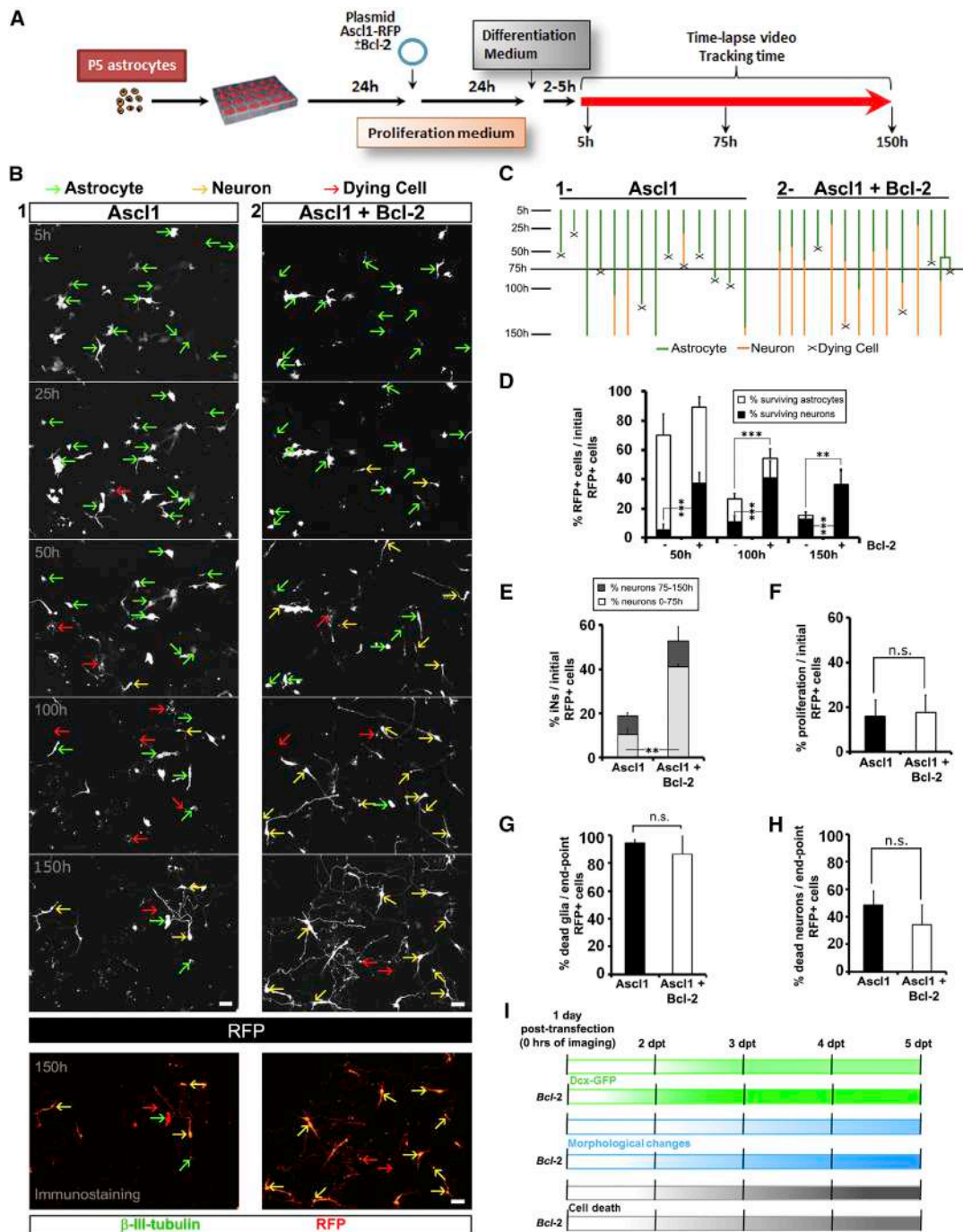


**Figure 1. Time-Lapse Analysis of Astrocyte-to-Neuron Reprogramming**

(A) Schematic of the experimental protocol used for time-lapse video analysis.

(B) Still images from video-time lapse movies (see [Movie S1](#)) showing cells classified as non-neuronal/astroglial (green arrows), neuronal (yellow arrows), and dying (red arrows) at the time in vitro indicated transfected with the constructs indicated.

(C) Progeny-trees of single cells tracked from example in B showing astrocytes (green lines), dead cells (depicted with “x”) and neurons (yellow lines).

(D–H) Histograms depicting cell survival and neuronal conversion from movies (n = 5 for control; 339 cells tracked; n = 4 with Bcl-2, 237 cells tracked) based on morphological classification, as detailed and verified by immunostaining in [Figures S1A–S1D](#). The percentage of neurons is normalized to the initial number of transfected cells in (D) and (E).

(I) Schematic summary of reprogramming and cell death as indicated by gradients of the respective color.

Error bars indicate  $\pm$  SD. \*\*p < 0.01, \*\*\*p < 0.001, p  $\geq$  0.05, no statistically significant difference (n.s.); ANOVA Tukey’s post hoc test in (D); t test in (E)–(G) and (H). Scale bars represent 40  $\mu$ m. See also [Figure S1](#) and [Movies S1](#) and [S2](#).

the interaction with the pro-apoptotic Bax/Bak. Bcl-2 inhibits apoptosis by sequestering Bax/Bak when phosphorylated at serine 69/70 (Deng et al., 2006) (Figure 2A). The replacement of both Ser69/70 by glutamic acid (EE-*Bcl-2*) mimics the constitutively phosphorylated form of Bcl-2 that sequesters Bax (Figure 2A), while substitution of Ser70 by alanine (A(70)-*Bcl-2*; Figure 2A) mimics the un-phosphorylated form of Bcl-2, reducing the binding to Bax (Deng et al., 2006). Likewise, A(145)-*Bcl-2* is unable to bind Bax due to a Glycine145/alanine substitution (Figure 2A; Yin et al., 1994).

Co-expression of EE-*Bcl-2* increased survival of cells transfected with *Ascl1* (Figure 2B), but did not alter the proportion of iNs (blue bars in Figure 2C). As expected, A(145)-*Bcl-2* had no significant effect in promoting cell survival during reprogramming (Figure 2B), but surprisingly still increased the proportion of *Ascl1*-transfected cells that turned into neurons (blue bars in Figure 2C). Co-transduction with A(70)-*Bcl-2* still retained some effect on cell survival (comparable to WT-*Bcl-2*; Figure 2B) and was most efficient in neuronal conversion, due to the added effect of rescuing non-converted cells from death and allowing them to convert more efficiently (Figure 2C, gray and blue bars, respectively). Moreover, we also observed increased length and complexity of the neuronal processes in cultures co-transfected with WT-*Bcl-2*, A(70)-*Bcl-2*, or A(145)-*Bcl-2*, but not with EE-*Bcl-2* (Figure 2D), further supporting an additional non-apoptotic role of Bcl-2 in neuronal reprogramming.

Importantly, Bcl-2 also enhanced conversion efficiency obtained from astrocytes transduced with *Neurog2* (Figure 2E), which induced mature glutamatergic neurons (vGlut1+ cells, Figure 2F). Both WT-*Bcl-2* and, to a greater extent, A(70)-*Bcl-2* potentially enhanced reprogramming of MEFs in combination with a single neurogenic fate determinant (*Ascl1*, Figures 2H, 2I, S3A, and S3C; *Neurog2*, Figures S3B, S3E, and S3F), giving rise to functional neurons able to fire action potentials (Figure S3D). Notably, Bcl-XL, a member of the Bcl-2 family, had a similar effect on reprogramming as WT-*Bcl-2* (data not shown). However, in the absence of a neurogenic factor neither A(70)-*Bcl-2* nor any other *Bcl-2* construct nor Bcl-XL alone were able to induce neuronal conversion (Figures 2G and S3C; data not shown). We thus conclude that Bcl-2-related proteins act as a potent facilitators of direct neuronal reprogramming for different transcription factors in different cell types and do so most potently in the A(70)-*Bcl-2* mutant form.

### Mode of Cell Death in Neuronal Reprogramming

As EE-*Bcl-2*, the mutant that exhibits an improved anti-apoptotic function, increases cell survival but does not improve the proportion of iNs, we tested how different modes of cell death affect neuron numbers. The pan-caspase/apoptosis inhibitor Z-VAD-FMK (ZVAD, 20  $\mu$ M) was added once at day 2 to *Ascl1*-transfected astrocytes, resulting in a significant increase in surviving cells (Figure 3A) without affecting the proportion of iNs neither among the initially transfected cells (Figure 3B, gray bars) nor at the end point (Figure 3B, blue bars). Thus, like EE-*Bcl-2*, blocking caspase activation does not improve neuronal conversion. We then tested the effects of RIP-K dependent necroptosis and the oxidative stress-dependent ferroptosis (Dixon et al., 2012) by using their respective in-

hibitors Necrostatin-1 (Degterev et al., 2005) and Liproxstatin-1 (Friedmann Angeli et al., 2014). While Necrostatin-1 had similar effects to ZVAD in rescuing some cells from death (Figure 3A), but no effects on iNs (Figure 3B), Liproxstatin-1 had a potent effect on conversion efficiency (Figure 3B). Thus, while apoptosis and necroptosis inhibitors protect cells from death, only the ferroptosis inhibitor liproxstatin-1 promotes both survival and neuronal conversion.

### Increased Lipid Peroxidation during Neuronal Reprogramming

Given the positive effects of Liproxstatin-1 treatment on reprogramming efficiency, we next examined lipid peroxidation (Lip-Ox) as a hallmark of ferroptosis (Dixon et al., 2012) by using two different reporters: Click-iT lipid peroxidation kit based on linoleamide alkyne (LAA) reagent (Life technologies) and C11-Bodipy (Drummen et al., 2002). Astrocyte cultures treated with cumene hydroperoxide as a positive control for Lip-Ox had increased signal from the LAA-based reporter in almost all cells (Figure 3C, upper row). Without any additional treatment, 60% of *Ascl1*-transfected cells exhibited the signal for Lip-Ox at 3 DPT, in contrast to 25% of cells transfected with the control plasmid (Figures 3C and 3D), suggesting that Lip-Ox occurs primarily during neuronal reprogramming. Similar results were obtained with C11-Bodipy, which integrates into phospholipid-containing membranes and shifts from red to green fluorescence upon oxidation (Drummen et al., 2002). We also tested  $\alpha$ -Tocopherol ( $\alpha$ Toc, one of the forms of vitamin E, 20 $\mu$ M), known to protect against Lip-Ox (Buettner, 1993), and found that it strongly reduces Lip-Ox LAA-signal in astrocytes undergoing neuronal conversion (Figures 3C and 3D).

Given the non-canonical effect of Bcl-2 on neuronal reprogramming, we examined its effect on Lip-Ox. Indeed, all forms of Bcl-2 significantly reduced Lip-Ox, with EE-*Bcl-2* being the weakest and A(70)-*Bcl-2* the strongest (Figure 3D). This result was observed with both reporters (Figures 3D and 3E), demonstrating a novel role of Bcl-2 in protecting from Lip-Ox most potently in the A(70)-*Bcl-2* mutant form. Consequently, we hypothesized that any condition that reduces Lip-Ox should be beneficial for direct neuronal reprogramming. Indeed,  $\alpha$ Toc treatment, almost doubled the proportion of *Ascl1/RFP* reprogrammed neurons obtained from astrocytes at 5DPT (Figures 4A–4C) and improved conversion efficiency of cells co-treated with ZVAD or co-expressing *Ascl1/EE-Bcl-2* (Figures 4A and 4B). Thus, the anti-oxidant vitamin E improves direct neuronal reprogramming.

### Forskolin Promotes the Efficiency of Neuronal Conversion and Reduces Lipid Peroxidation

We next tested whether other molecules known to improve reprogramming such as forskolin (Fk; Liu et al., 2013a) may also alleviate Lip-Ox. First, we verified its positive effects on reprogramming in astrocytes aiming to determine whether it would act similarly from what we had observed with Bcl-2. Both in continuous live imaging (Figures S4A–S4D) and after immunostaining at 5DPT (Figures 4D and 4E) we observed more cells surviving and efficiently converting after addition of 20  $\mu$ M Fk to *Ascl1*-transfected astrocyte cultures. As for Bcl-2, we also observed a faster conversion (Figures S4A–S4D) without any

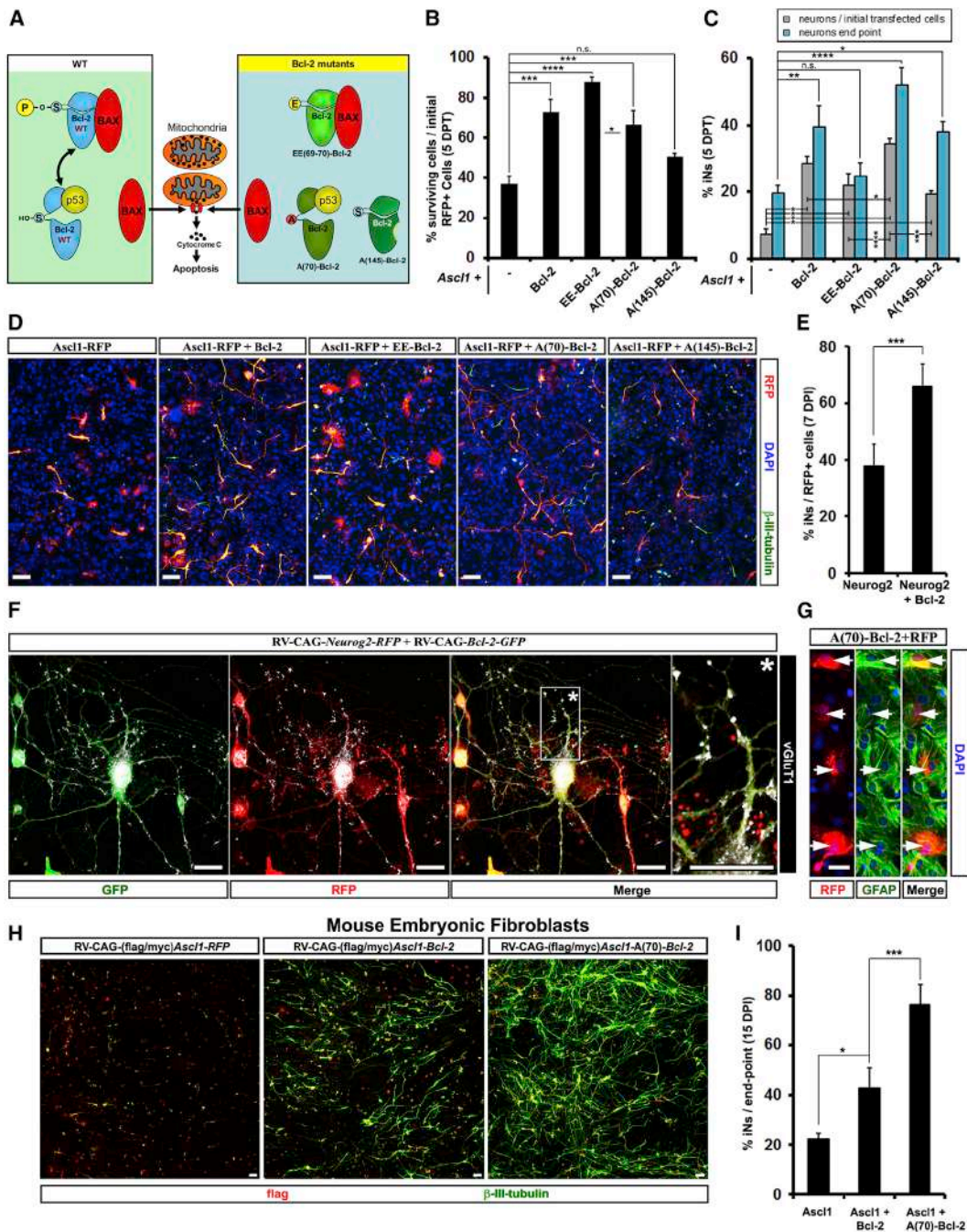


**Figure 2. Non-canonical, BAX-Independent Effect of Bcl-2 on Neuronal Reprogramming**

(A) Cartoon depicting previously described interactions of Bcl-2 and its mutant forms with several molecular partners as described in the text. (B–D) Histograms (with corresponding micrographs showing immunostaining for  $\beta$ -III-tubulin, in D) depicting the survival and fate conversion rate at 5DPT (for details, see [Supplemental Information](#)) in astroglial cultures transfected with the constructs indicated ( $n = 3$ ; cells = 900–2,500 for each condition). (E and I) Histograms showing the proportion of  $\beta$ -III-tubulin+ neurons at 7 days post infection (DPI) of astrocytes with a viral vector containing Neurog2 alone or with Bcl-2 (E,  $n = 3$ ; cells = 1,500–2,000 for each condition) or 15 DPI of MEFs with the vector indicated (I,  $n = 3$ ; cells = 340–700 for each condition). (F) Confocal micrographs showing that iNs from E are immunoreactive for vGlut1 at 15 DPI. (G) Arrows indicate astrocytes co-transfected with Bcl-2 and RFP (Red cells) being immuno-positive for GFAP (green) and retaining astroglial morphology at 7 DPT. (H) Micrographs of fibroblast conversion into neurons ( $\beta$ -III-tubulin+ cells; green) at 15 DPI upon transduction with retroviral vectors of the constructs indicated. Error bars indicate  $\pm$  SD. \* $p < 0.05$ , \*\* $p < 0.01$ , \*\*\* $p < 0.001$ ; ANOVA with Tukey’s post hoc test in (B), (C), and (I); t test in (E). Scale bars represent 50  $\mu$ m in (D) and (H) and 10  $\mu$ m in (F). See also [Figure S2](#).

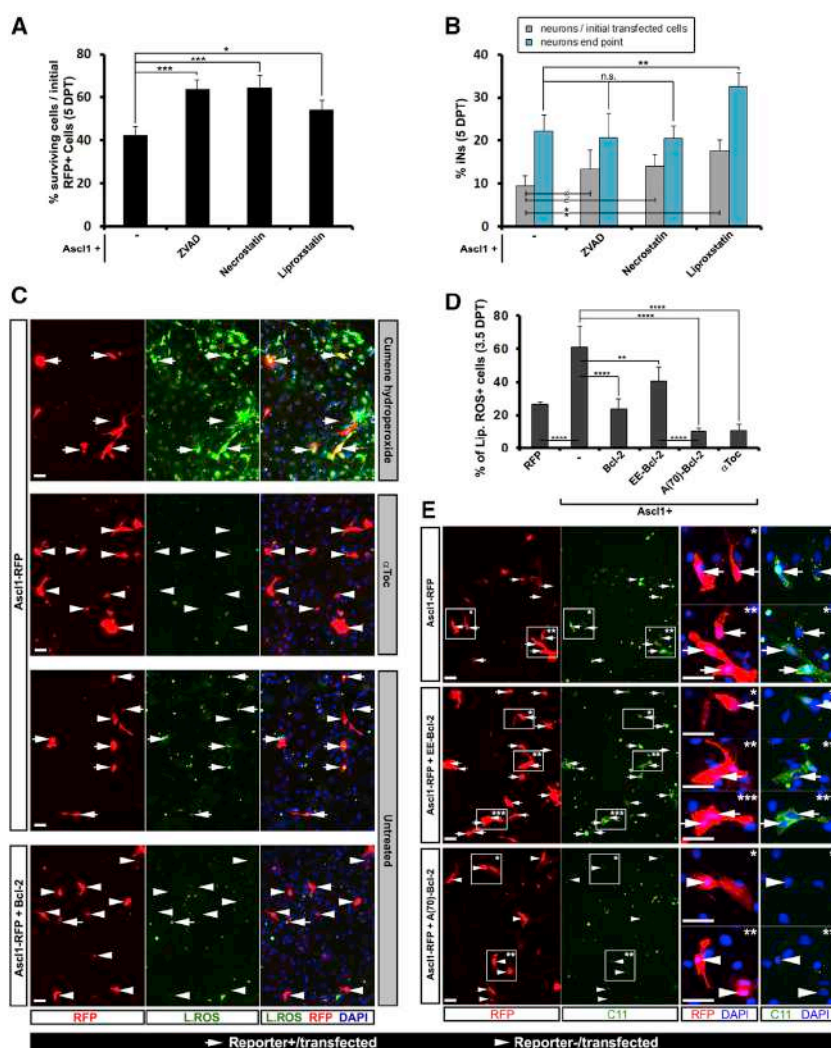


**Figure 3. Ferroptosis and Lipid Peroxidation Are Key Limiting Factors during Neuronal Reprogramming**

(A, B, and D) Histograms showing the percentage of survival and iNs (A and B) or Lipid ROS+ cells (D, n = 3, for RFP, Bcl-2, A(70)-Bcl-2,  $\alpha$ Toc; n = 4 for EE-Bcl-2 and Ascl1; cells = 80–500 each condition) in astroglial cultures treated as indicated on the x axis. Treatment with ZVAD (20  $\mu$ M), Necrostatin (10  $\mu$ M), or Liproxstatin-1 (200 nM) was performed at 1 DPT (n = 4, A and B; cells = 1,500–2,000).

(C and E) Confocal micrographs of Lip-Ox (Life Technologies, green reporter) staining (C, treatment with cumene hydroperoxide 100  $\mu$ M; positive control for Lip-Ox, or  $\alpha$ Toc 10  $\mu$ M; negative control for Lip-Ox, at 1 DPT) or C11-Bodipy (E) in astrocytes transfected as indicated at 3.5 DPT. Arrows indicate transfected cells (red) with increased levels of Lip-Ox (green); arrowheads show transfected cells without green signal.

Error bars indicate  $\pm$  SD. \*p < 0.05, \*\*p < 0.01, \*\*\*p < 0.001; ANOVA with Tukey’s post hoc test in (B) and (D); ANOVA with Dunnett’s post hoc test in (A). Scale bars represent 40  $\mu$ m. See also Figure S3.

oxidative stress during reprogramming facilitates neuronal conversion.

**Genome-wide Expression Analysis Reveals Anti-oxidative Stress Response in Improved Neuronal Reprogramming**

To identify candidate genes regulated by non-canonical Bcl-2 function and by Fk treatment that may promote neuronal conversion, we collected mRNA from different batches of MEF cultures. These were transfected with *Ascl1/RFP*- or *RFP*-encoding vectors and treated or untreated

effect on proliferation (Figure S4E). This effect is both transcription factor and cell type independent, as Fk also improved reprogramming efficiency of MEFs and pericytes (Figure S5) mediated by different transcription factors (i.e., *Ascl1*, *Neurog2*, *Sox2*) but did not induce neuronal conversion in absence of any neurogenic fate determinant (Figures S4F and S5C).

As expected, the proportion of Lip-Ox reporter-positive cells among *Ascl1*-transduced astrocytes was significantly reduced from about 60% to below 20% by Fk treatment (Figures 4F and 4G). Likewise, CellRox Green reagent (Molecular Probes; Figure 4H) showed high levels of nuclear green fluorescence in *Ascl1*-transduced astrocytes at 3DPT, when many cells succumb to cell death, which was reduced after Fk treatment (Figure 4H). As further proof of oxidation-dependent processes occurring during reprogramming, we monitored the oxidation of peroxiredoxin-2, a protein involved in oxidative stress detoxification (Prx2; Godoy et al., 2011), by western blot. Prx2 was predominantly detected in its dimeric (oxidized) form in astrocytes and MEFs 3 days after transduction with *Ascl1*, and dimerization was reduced by Fk treatment (Figure 4I). Thus, reducing

with Fk for 24 hr (1DPT) or co-transduced with *A(70)-Bcl-2-GFP* (Figure 5A). Upon Fk treatment, 507 probe sets were significantly regulated (p < 0.01, fold change  $\geq$  1.5 $\times$ , see Table S1; for genes regulated after *A(70)-Bcl-2* co-transduction, see Table S2). Heat maps show the 60 strongest upregulated genes upon Fk treatment of *Ascl1*-transduced cells (Figure 5B, left) and the subset of transcriptional regulators (right). The reliability of the transcriptome analysis was confirmed by quantitative real-time PCR analysis (Figure 5C). As expected from the known role of Fk, we found increased expression of genes involved in the cAMP signaling pathway (Table S3) and many targets of Creb, including those regulating neurite outgrowth and cAMP-signaling mediators (Tables S1 and S3), as well as genes promoting neuronal differentiation (e.g., *Prox1*, *Eya2*, *Sox11*; Figure 5B). In addition, we found enrichment of several signaling pathways (e.g., IL-10 and IL-1; Wnt, Bmp) and nuclear receptors (Figure 5B; Table S3). Interestingly, some of these genes, including *Nrf-2* effectors and *JAK/STAT* (Tables S1 and S3), are known to regulate metabolism and the oxidative stress response (Nguyen et al., 2009; Park et al., 2012). Gene Ontology (GO) term analysis further supported anti-oxidative

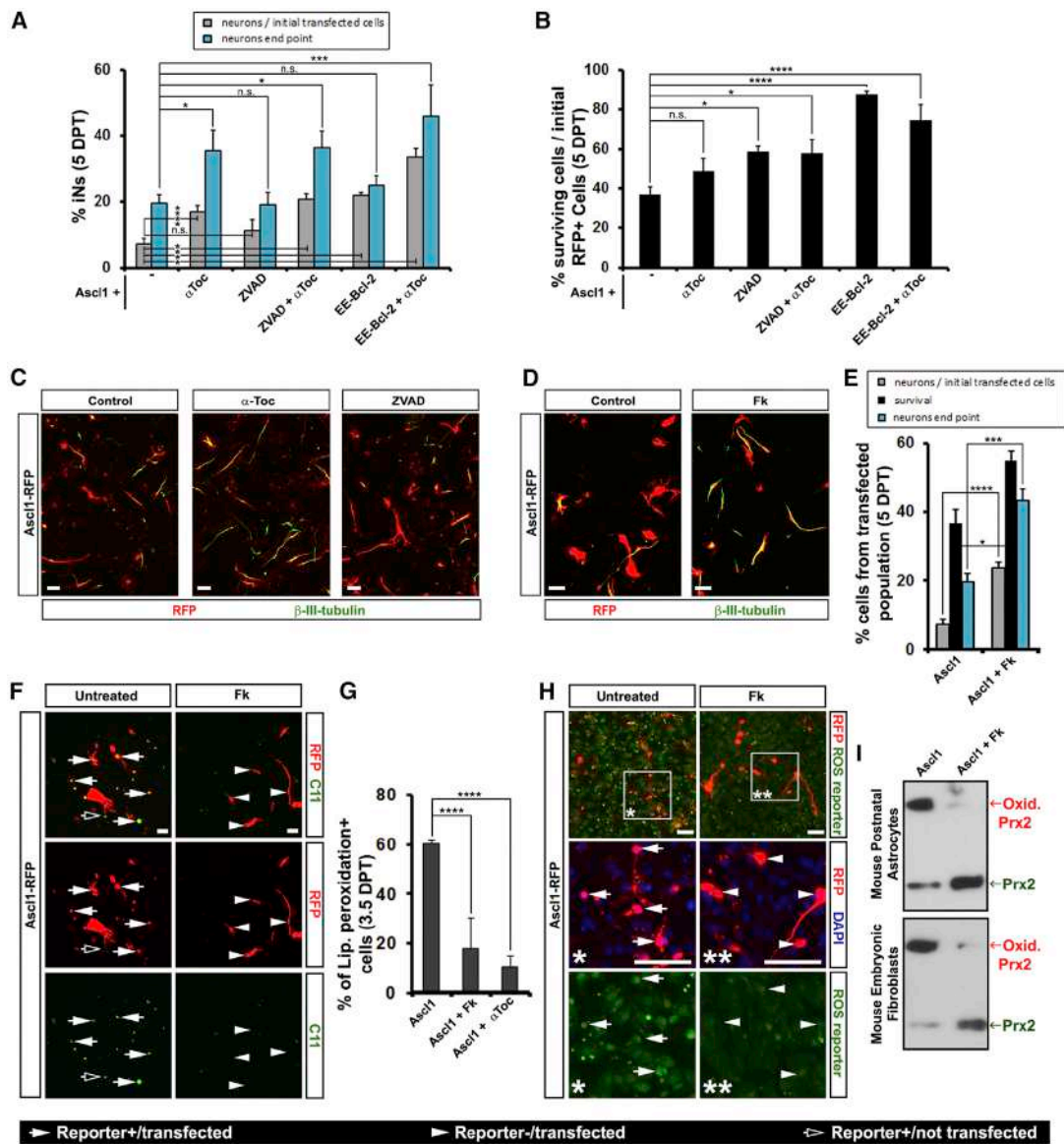


**Figure 4. Increased Reprogramming Mediated by a Reduction of Lipid Peroxidation Levels Is Reproduced by Treatment with Forskolin** (A–C) Histograms show iNs ( $\beta$ -III-tubulin+; green in micrographs in C) and survival rate at 5 DPT from astroglial cells transfected and treated as detailed in Figure 3 (n = 3; cells = 1,500–2,000).

(D and E) Micrographs (D) and histogram (E, n = 3; cells = 110–200) of survival rate/neuronal conversion of astroglia transfected with *Ascl1/RFP* (red cells) and cultured 5 days in absence/presence of 10  $\mu$ M Fk. Neuronal conversion was monitored by  $\beta$ -III-tubulin (green).

(F and H) Micrographs showing examples of the C11-Bodipy reporter (F) or CellROX reporter (green in H) in astrocyte cultures transfected and treated as indicated at 3.5 DPT. Arrows depict transfected cells (red) with increased levels of ROS (green); empty arrows depict untransfected cells; arrowheads show transfected cells with low ROS signal.

(G) Quantification of cells depicted in (F). The result with  $\alpha$ Toc treatment has been included to compare with the effect of Fk (n = 3 for Ascl1 +  $\alpha$ Toc; n = 4 for Ascl1 and Ascl1+Fk; cells = 80–250).

(I) Immunoblots showing that 24-hr treatment with Fk reduces the levels of oxidized Prx2 (dimer, upper band) in both astroglial (upper) and MEF (lower) cultures infected with *Ascl1/RFP*-encoding vectors.

Error bars indicate  $\pm$  SD. \*p < 0.05, \*\*p < 0.01, \*\*\*p < 0.001; ANOVA with Dunnett's post hoc test in (A), (B), and (E); ANOVA with Tukey's post hoc test in (G). Scale bars represent 40  $\mu$ m in (C) and (D), 20  $\mu$ m in (F), and 80  $\mu$ m in (H). See also Figure S4 and Movie S3.

pathways activated by Fk, with Nrf2-mediated pathway at the top (Table S3). Indeed, we confirmed increased Nrf2-responsive luciferase activity 15 hr after Fk addition (Figure 5D). Interestingly, Nrf2-mediated pathway was found activated by

both Fk treatment and A(70)-Bcl-2 co-expression (Table S4). These data support the notion of excessive oxidation occurring during reprogramming and Fk as well as A(70)-Bcl-2 alleviating this.

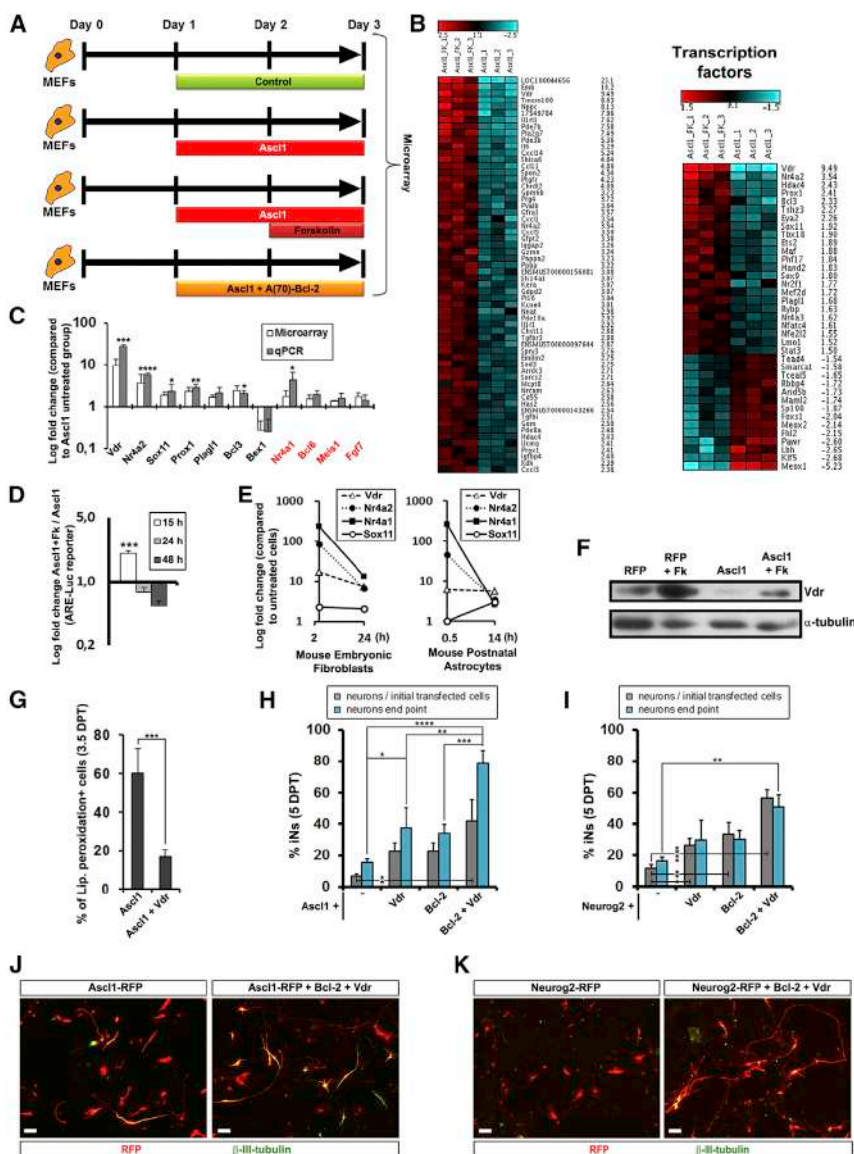


**Figure 5. Transcriptome and Functional Analysis of Genes Activated by Fk and Bcl-2**

(A) Schematic drawing of the experimental protocol.

(B) Heatmaps of linear fold changes with the top 60 upregulated genes (left) or transcriptional regulators (right) in microarrays of *Ascl1*+Fk versus *Ascl1* only transfected MEFs;  $p < 0.01$ , fold-change  $\geq 1.5$ .

(C) Histogram showing qRT-PCR for genes predicted to be regulated by the microarray analysis (ratio paired t test,  $p < 0.01$ ; FC  $\geq 1.5$ ). Genes with lower significance were also validated ( $p < 0.07$ ; shown in red).

(D) Bars represent fold change of luciferase levels from a Nrf2-responsive construct co-transfected with *Ascl1* in astroglial cultures induced by Fk (15, 24, and 48 hr) compared with untreated cells.

(E) qRT-PCR analysis of mRNA levels from four representative targets induced by Fk in MEFs and astrocytes.

(F) Western blot depicting levels of Vdr protein after 24-hr treatment with Fk in astroglial cultures infected with RFP- or *Ascl1*/RFP-encoding retroviral vectors.

(G) Percentage of astrocytes positive for the lipid reporter based on linoleic acid (Life Technologies) among the *Ascl1*- or *Ascl1*+*Vdr*-transfected population at 3.5 DPT.  $n = 3$ .

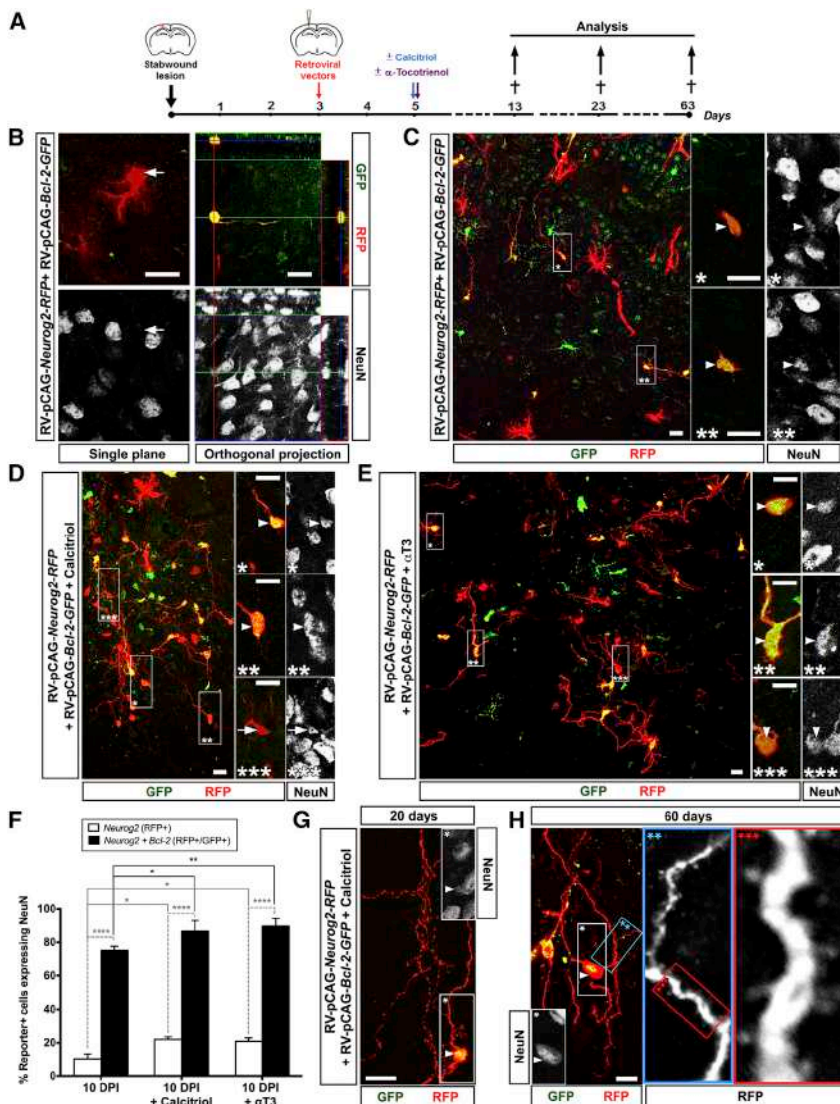
(H–K) Histograms and corresponding micrographs (J and K) depicting the neuronal conversion efficiency of astroglial cultures transfected with constructs indicated on x axis at 5 DPT ( $n = 3$ ; cells = 80–250).

\* $p < 0.05$ , \*\* $p < 0.01$ , \*\*\* $p < 0.001$ , \*\*\*\* $p < 0.0001$ ; ratio paired t test in (C); two-way ANOVA with Sidak's post hoc test in (D); t test in (G); ANOVA with Tukey's post hoc test in (G) and (H); ANOVA with Dunnett's comparison test in (I). Scale bars represent 45  $\mu\text{m}$ . See also Figure S5 and Tables S1, S2, S3, and S4.

As vitamin D receptor (*Vdr*) was already implicated in the anti-oxidative stress response (Bao et al., 2008; Dong et al., 2012), we validated its upregulation at mRNA level in MEFs and astrocytes (Figure 5E; see also confirmation of other nuclear receptors) and protein level in astrocytes (Figure 5F). We then tested its effect on Lip-Ox in astrocytes and found that co-expression of *Vdr* reduced the percentage of cells positive for LAA-based reporter to less than one-third in *Ascl1*-transfected astrocytes at 3.5 DPT (Figure 5G). Accordingly, co-transfection with *Vdr* improved neuronal reprogramming by *Ascl1* or *Neurog2* to a similar extent as Fk (data not shown) or *Bcl-2* co-transfection (Figures 5H–5K). Co-transduction of *Bcl-2* and *Vdr* further increased reprogramming (Figures 5H–5K) reaching up to 80% neurons among *Ascl1*-transduced astrocytes (Figures 5H and 5J). Taken together, genome-wide expression analysis confirmed the key role of oxidative stress response in regulating reprogramming, with *Vdr* as the top transcriptional regulator.

### The Role of Bcl-2 and Anti-oxidants in Neuronal Reprogramming In Vivo

We next examined the relevance of the above-identified pathways after brain injury in vivo. Such lesions induce a highly inflammatory environment (Abdul-Muneer et al., 2015) that may impose oxidative stress and other metabolic constraints to the generation and survival of iNs. Indeed, in the intact striatum and cerebral cortex, neuronal reprogramming was more efficient (Guo et al., 2014; Niu et al., 2013; Torper et al., 2013) than after large invasive brain injury (Buffo et al., 2005; Grande et al., 2013; Heinrich et al., 2014). Among the previously tested factors, we chose *Neurog2*, as it instructs glutamatergic neurons in the developing cerebral cortex (Imayoshi and Kagiyama, 2014) and from astrocytes in vitro (Berninger et al., 2007; Heinrich et al., 2010; Masserdotti et al., 2015), but exhibits a limited efficiency in neuronal conversion after brain injury in vivo (Grande et al., 2013).



Retroviral vectors encoding *Neurog2*-IRES-*RFP* alone or in combination with *Bcl-2*-IRES-*GFP* were injected close to the stab-wound injury site 3 days later (Figure 6A), as previously described (Buffo et al., 2005; Heinrich et al., 2014), and immunohistochemistry was performed at 10 days post-injection (DPI). *GFP* or *Bcl-2* single (*GFP+*) infected cells were NG2+ glia or S100β/GFAP+ astrocytes (Figures 6C and S6C). Similarly, most of the cells transduced with *Neurog-2* (*RFP+* only) were glia and only rarely acquired the neuronal marker NeuN (Figures 6B, 6C, and 6F; 2% in only *Neurog2*-infected brains, Figure S6D). Conversely, many co-transduced cells (*GFP+/RFP+*) exhibited elongated neuronal-like morphology and were immunoreactive for DCX or NeuN (Figures 6C and S6E). Indeed, around 75% of co-transduced cells had turned into NeuN+ neurons with a clear neuronal morphology at 10 DPI (Figure 6F). Taken together, the addition of *Bcl-2* not only increased the number of NeuN+ iNs but also accelerated neuronal maturation, as appearance of NeuN typically takes about 14–21 DPI (Grande et al., 2013). Thus, as in vitro,

ingly, a single calcitriol administration at 2 DPI more than doubled the proportion of NeuN+ iNs in *Neurog2*-transduced cells (Figures 6D and 6F; 3.5-fold increase in only *Neurog2*-infected brains, see Figure S6D). Most importantly, calcitriol treatment resulted in almost 90% conversion of all *Neurog2/Bcl-2* co-transduced cells (*GFP+/RFP+*; Figures 6D and 6F), dramatically increased levels of NeuN (see Figures S6F and S6G) and improved morphology and complexity of iNs, resulting in the formation of long neuronal processes (Figures 6G and S6G). Moreover, long-term analysis of iNs after calcitriol treatment often revealed very elaborate neurites with bouton-like (20 DPI; Figure 6G) and/or spine-like structures (60 DPI; Figure 6H). Taken together, these data demonstrate that calcitriol has a beneficial effect on the reprogramming efficiency but more importantly on the maturation of iNs.

To confirm that the oxidative state directly affects reprogramming in vivo, we administered  $\alpha$ -Tocotrienol ( $\alpha$ T3; Figure 6A), the vitamin E analog described above. Similarly to calcitriol,  $\alpha$ T3 administration improved the conversion efficiency and

### Figure 6. Conversion of Reactive Glia into Neurons Is Improved by *Bcl-2*, Calcitriol, and $\alpha$ -Tocotrienol In Vivo

(A) Scheme of the protocol used for stab-wound injury and subsequent infection with retroviral vectors for *Neurog2*-IRES-*RFP* and *Bcl-2*-IRES-*GFP*, the respective treatments and analysis time points. (B) High-power micrograph of cells infected by *Neurog2*-IRES-*RFP* alone or with *Bcl-2*-IRES-*GFP* stained for NeuN at 10 DPI, with orthogonal projections of the confocal stack. The *RFP+* cell maintains an astroglial morphology and is NeuN-immunonegative (arrows, left), whereas the co-infected cell displays a distinct neuronal-like morphology and NeuN signal (right). (C–E) Confocal micrographs of the injection site at 10 DPI upon the treatments indicated (C, none; D, Calcitriol; E,  $\alpha$ T3) stained for NeuN. Co-infected cells immunopositive for NeuN (arrowheads) are shown at higher magnification in single optical sections (\*, \*\*, \*\*\*, right). (F) Histogram with the proportion of induced, NeuN+ neurons among *RFP+* and *RFP+/GFP+* cells at 10 DPI, without ( $n = 3$ ) or with treatments (calcitriol,  $n = 3$ ;  $\alpha$ T3,  $n = 4$ ; 390–575 cells per condition). (G and H) Micrographs of maximum intensity projections of neuronal examples as indicated. Inserts show single optical section of the NeuN+ nucleus (\*; white arrow). The blue and red boxes in H (\*\*, \*\*\*) display higher magnifications of a process with spine-like structures. Error bars indicate  $\pm$  SD. \* $p < 0.05$ , \*\* $p < 0.01$ , \*\*\*\* $p < 0.0001$ ; two-way ANOVA with Tukey's post hoc test in (F). Scale bars represent 10  $\mu$ m, except 20  $\mu$ m in (B). See also Figure S6.

*Bcl-2* potently improves reprogramming speed and efficiency in vivo.

We next examined whether activating the *Vdr* pathway by the ligand calcitriol after *Neurog2/RFP* transduction with/without *Bcl-2/GFP* would elicit a further improvement in reprogramming. Strik-

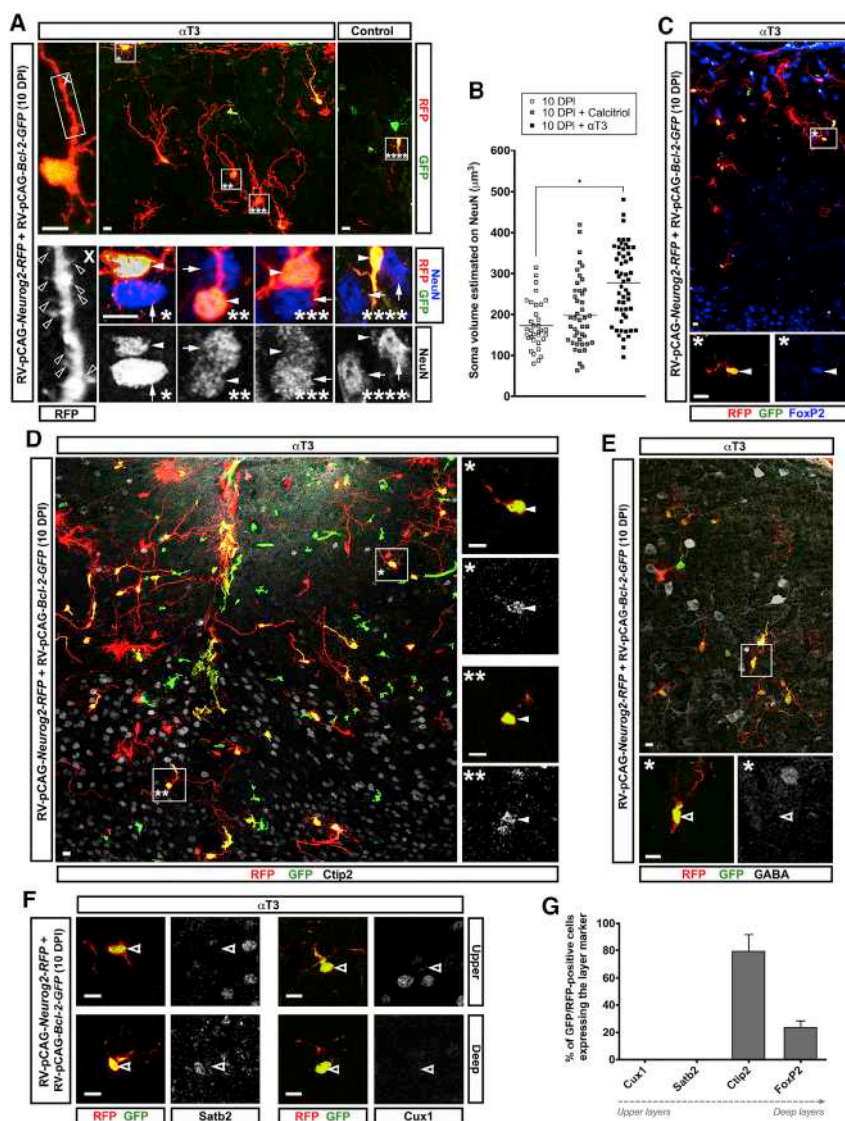


**Figure 7. Subtype Identity of iNs after Stab-Wound Injury**

(A and B) Confocal micrographs (maximum intensity projection, A) and histogram of soma size (B) of cells at 10 DPI by *Neurog2/RFP* and *Bcl-2/GFP* retroviral vectors after stab-wound injury and  $\alpha$ T3 treatment (see Figure 6A) with thick processes and spine-like structures (box X, left). The soma size of these cells (NeuN staining, magnified in boxes \*, \*\*, \*\*\*; arrowheads) is similar to the size of nearby endogenous neurons (arrows), unlike for mice that did not receive  $\alpha$ T3 (right, magnified in \*\*\*\*).

(C–F) Confocal micrographs showing neuronal subtype markers FoxP2 (C), Ctip2 (D), GABA (E), Satb2, and Cux1 (F) at 10 DPI. Filled arrowheads indicate immunopositive, empty arrowheads immunonegative cells in the squared box (\*, \*\*). Specific examples of cells located in upper or deep layers are depicted in (F).

(G) Histogram of double infected cells expressing the indicated markers.

Horizontal lines in (B) indicate the mean.  $n = 4$  in A and B ( $\alpha$ T3);  $n = 3$  in B (no treatment and calcitriol, 40–60 cells per condition), (C), (D), and (G) for Ctip2 and FoxP2 (80–180 cells per condition);  $n = 2$  in (E), (F), and (G) for Cux1 and Satb2 (40–60 cells per condition). \* $p < 0.05$ ; one-way ANOVA with Tukey's post hoc test in (B). Scale bars represent 10  $\mu\text{m}$ . See also Figure S7.

marker FoxP2, albeit with lower intensity than endogenous neurons (Figures 7C and 7G; Molyneaux et al., 2007). Consistent with a V pyramidal neuron identity, iNs were negative for the upper layer markers Satb2 (Figures 7F, left, and 7G; Britanova et al., 2008) or Cux1 (Figures 7F, right, and 7G; Molyneaux et al., 2007) and the interneuron transmitter GABA (Figure 7E). Therefore, we confirmed the identity of reprogrammed cells as deep layer glutamatergic pyramidal neurons, consistent with

the levels of NeuN (Figures 6E and 6F). Strikingly, cells co-transduced with *Neurog2/Bcl-2* displayed a very complex neuronal morphology in animals treated with  $\alpha$ T3 already at 10 DPI (Figures 6E and 7A) and had a soma size comparable to the endogenous neurons in the same area (Figures 7A and 7B). Notably, iNs also reached this soma size after calcitriol administration, but at a much later time points (60 DPI; see Figures 7A and S6H). Likewise, upon  $\alpha$ T3 treatment, iNs exhibited the first spine-like protrusions already at 10 DPI (Figure 7A, left), further corroborating the faster iN differentiation and maturation elicited by this anti-oxidant.

As *Neurog2/Bcl-2* overexpression and  $\alpha$ T3 administration resulted in most developed iNs, we used this paradigm to determine their subtype identity. Regardless of the localization of the co-transduced cells, about 80% were immunopositive for Ctip2 (Figures 7D and 7G), a marker for layer V subcortical neurons (Arlotta et al., 2005; Molyneaux et al., 2007). Most of the remainder (20%) was positive for the deep layer

the role of *Neurog2* in cortical development (Schuurmans et al., 2004).

## DISCUSSION

Here we used continuous live imaging to unravel critical hurdles in direct neuronal reprogramming. Neuronal conversion became detectable around 2–4 days after transduction by live neuronal (*DCX-GFP*) reporters, post-imaging immunostaining ( $\beta$ -III-tubulin, MAP2, NeuN), and morphological analysis (small cell soma and thin processes). At around the same time, most transduced astrocytes succumbed to cell death, while fewer of the successfully converted cells died, suggesting that high levels of *Ascl1* may be incompatible with astrocyte survival under these conditions. Importantly, few astrocytes proliferated—neither prior to cell death nor prior to fate conversion. Thus, a major limitation in reprogramming efficiency is cell death around the time of fate conversion.

### Different Modes of Cell Death and Oxidative Stress Limit Neuronal Reprogramming

While blocking apoptosis by caspase inhibitors and necroptosis by RIPK1 inhibitors significantly increased cell survival, these cell death pathways did not affect the proportion of iNs. This revealed an additional block for neuronal conversion that could be consistently relieved by ferroptosis inhibitors (Liproxstatin-1 or vitamin E). Ferroptosis is typically induced by ROS, resulting in peroxidation of lipids due to impaired cysteine availability, glutathione depletion and GPX4 inhibition (Dixon et al., 2012; Friedmann Angeli et al., 2014; Yang et al., 2014). Hence, excessive ROS may be generated as a consequence of instructing reprogramming per se or specifically into neurons that use oxidative phosphorylation. In favor of the former possibility are the findings of an oxidative burst with deleterious consequences during the generation of mouse iPSCs (Kida et al., 2015; Qi et al., 2015), initiated when cells are instructed to divide fast during reprogramming (Kida et al., 2015). This is notably different from direct neuronal reprogramming, where few cells divide and yet increased ROS and Lip-Ox occur. We therefore favor the hypothesis that this effect is due to transitioning too hastily to the neuronal oxidative metabolism during reprogramming (see also below).

Consistent with high oxidation levels limiting neuronal reprogramming efficiency, we show here that treatments beneficial for reprogramming, such as Fk or A(70)-Bcl-2, reduce Lip-Ox and mount an anti-oxidative response mediated by Nrf2 among others. Various agents attenuating Lip-Ox, such as  $\alpha$ Toc,  $\alpha$ T3, or Calcitriol, also improve neuronal reprogramming. This is not only of crucial importance to better understand the conversion process into iNs but also for the widespread application of generating neurons from different cell types (astrocytes, MEFs, pericytes, etc.) with various neurogenic transcription factors (Ascl1, NeuroD4, Neurog2, Sox2, etc.) at much increased efficiency.

### An Unexpected Role for Bcl-2 In Direct Neuronal Reprogramming

Interestingly, Bcl-2 affected both reprogramming efficiency and speed of neuronal conversion in a manner uncoupled from its function in apoptosis. The Bcl-2 mutant with increased affinity for Bax/Bak and therefore improved anti-apoptotic function (EE-Bcl-2) neither improved neuronal reprogramming nor reduced Lip-Ox. In contrast, A(145)- and A(70)-Bcl-2 mutants, unable to bind Bax/Bak and with reduced anti-apoptotic function (Deng et al., 2006; Yin et al., 1994), improved neuronal reprogramming, with the latter being the most effective in reducing Lip-Ox and, consequently, enhancing reprogramming efficiency. While this is the first time that specific Bcl-2 mutants have been used to assess selective effects on Lip-Ox, Bcl-2 has formerly been implicated in the regulation of both metabolic transition and oxidative stress pathways by reducing oxidation in mitochondria (Krishna et al., 2011) or improving metabolic conversion via interaction with, e.g., p53 or Myc (Deng et al., 2006; Jin et al., 2006). As EE-Bcl-2 interacts strongly with Bax, its lack of effect on reprogramming could be due to its reduced availability for molecular partners acting in the nucleus. Conversely, A(70)-Bcl-2 may be more efficient in improving neuronal reprogramming as more of this protein may be available in the nucleus for interaction with relevant partners.

Notably, we show that Fk and A(70)-Bcl-2 lead to common transcriptional changes in pathways (e.g., LXR) that have been previously implicated in neurogenesis (Theofilopoulos et al., 2013), suggesting that nuclear interactions of Bcl-2 may explain the particular efficiency of the A(70)-Bcl-2 mutant in direct neuronal reprogramming. Although not precluding additional roles of Bcl-2 at the mitochondria or other mechanisms, our data demonstrate that the effect of Bcl-2 in reprogramming is independent of its well-known anti-apoptotic function.

### Metabolic Conversion as Critical Factor in Direct Neuronal Reprogramming

Importantly, factors alleviating Lip-Ox also accelerate fate transition. We observed this in vivo and by continuous single-cell tracking analysis in vitro, both upon Fk treatment and in cells co-expressing Bcl-2 (Figures 1 and S3). Fk treatment regulates several genes affecting the cellular redox potential, e.g., *Nor-1* that promotes the endurance phenotype in oxidative muscle fibers (Pearen et al., 2012) and *Vdr* that alleviates oxidative stress in various organs (Dong et al., 2012; George et al., 2012). It has been previously shown that ROS and redox-signaling mechanisms play a key role in cell fate decisions, including neurogenesis (Maryanovich and Gross, 2013; Prozorovski et al., 2015), although the molecular mechanisms mediating these effects are not yet fully understood. In iPSC reprogramming, changes to a more glycolytic metabolism have been shown to govern fate conversion (Liu et al., 2013b), despite the initial oxidative burst mentioned above (Kida et al., 2015). The faster neuronal conversion when excessive oxidation products are successfully controlled is consistent with (1) ROS affecting gene expression, e.g., by altering SIRT activity, a key regulator of neurogenesis, and (2) interfering with metabolic pathways acting upstream of other aspects of fate conversion. If the metabolic transition is a prerequisite for the conversion in cell fate, redox homeostasis failure may ultimately reduce efficiency or speed of conversion.

Confirming this hypothesis, we observed that cells cultured in a medium with oligomycin A, allowing anaerobic glycolysis as the only metabolic pathway to generate ATP (see Supplemental Information), preserved astroglial features and interfered with the conversion to a neuronal fate (Figures S7A–S7C, S7E, and S7F). As the total cell number did not decrease much (Figures S7A and S7F), fate conversion seems to be blocked when oxidative phosphorylation is hampered. Notably, cells grown in anaerobic glycolysis-only medium were also protected from Lip-Ox (Figures S7C and S7D), demonstrating that the metabolic change during neuronal reprogramming causes oxidative stress. Conversely, boosting the metabolic shift with a medium containing 2-deoxy-glucose, which can only be metabolized at mitochondria (see Supplemental Information), caused extraordinarily high levels of Lip-Ox (Figure S7C) in astrocytes and resulted in cell death (Figures S7A and S7F). Overall, these experiments demonstrate that the metabolic shift is not only necessary to allow survival of the neurons during reprogramming but also constitutes a prerequisite for cell fate transition.

### Potent Improvement of Direct Reprogramming in the Injured Brain In Vivo

Importantly,  $\alpha$ T3 supplementation or activation of anti-oxidant pathways by calcitriol was remarkably powerful in improving iN

maturation from reactive glia after traumatic brain injury in vivo. Interestingly, calcitriol treatment has been shown to reduce glutamate-induced neuronal death in vitro and attenuate hypoxic brain damage in vivo (Gianforcaro and Hamadeh, 2014), as well as the fibrotic reaction upon injury in other organs (Ding et al., 2013; Sherman et al., 2014). These data thus suggest that calcitriol alleviates several negative effects after injury. While both calcitriol and  $\alpha$ T3 also improve efficiency of reprogramming but predominantly affect maturation and neurite growth, *Bcl-2* co-expression was the most efficient in increasing iNs. The combined action of *Bcl-2* and Calcitriol or  $\alpha$ T3 allowed us for the first time to achieve an in vivo reprogramming efficiency of more than 90% after stab wound injury. The neurons survived for several months and acquired a remarkably advanced state of maturation. These data demonstrate that the number of neurogenic fate determinants was not the limiting factor in neuronal reprogramming after injury in vivo, as believed so far. In fact, while applying various combinations of neurogenic transcription factors only marginally improved reprogramming in the same paradigm (Buffo et al., 2005; Grande et al., 2013; Heinrich et al., 2014; Kronenberg et al., 2010), co-expressing *Bcl-2* and alleviating excessive ROS had an astounding effect. Indeed, our protocol allowed iNs to proceed largely to a specific neuronal subtype, namely Ctip2+ pyramidal neurons even when they were located at more superficial positions and surrounded by Cux1+ upper layer neurons. Interestingly, *Ctip2* is not a direct target of *Neurog2* (Masserdotti et al., 2015; Schuurmans et al., 2004) and acts as the key effector of subcortical deep layer neuron fate (Amamoto and Arlotta, 2014). Moreover, *Neurog2* knockout mice have selective defects in deep layer, but not upper-layer neurons of the developing cerebral cortex (Fode et al., 2000), supporting the concept that *Neurog2* is largely involved in specifying deep-layer neuron fate in this region.

Taken together, our data on the mechanisms facilitating the metabolic transition and redox homeostasis in neuronal reprogramming have not only widespread relevance for brain injury and repair, but also highlight the urgency of improving the timely and coordinated metabolic conversion as well as protection from ferroptosis in aiming at neuronal repair.

## EXPERIMENTAL PROCEDURES

### Primary Cell Cultures

Astrocytes were cultured and transduced as described in Heinrich et al. (2010) and MEFs as described in Vierbuchen et al. (2010).

### Live-Imaging Microscopy

Time-lapse video microscopy was performed with a cell observer (Zeiss) at a constant temperature of 37°C and 8% CO<sub>2</sub>. Phase-contrast images were acquired every 5 min and fluorescence pictures every 4–6 hr for 6.5–7.5 days using a 10× phase contrast objective (Zeiss) and an AxioCam HRm camera with a self-written VBA module remote controlling Zeiss AxioVision 4.7 software. Movies were assembled and analyzed using ImageJ (NIH) software. For description of the analysis, see Supplemental Information.

### Analysis of Lipid Peroxidation

For the detection of lipid peroxidation, we used either the reagent Click-iT lipid peroxidation kit based on linoleamide alkyne (LAA) reagent (Life Technologies) or BODIPY 581/591 C11 (C11-Bodipy, Molecular Probes; Drummen et al., 2002). Astroglial cells were first cultured and transfected as previously described (Heinrich et al., 2010; see also Supplemental Information).

At 3.5 days later, the cells were labeled according to the specifications described in the product data sheet and fixed with 4% paraformaldehyde (PFA) for 5 min. Finally, the direct fluorescence of the reporters was detected by epi-fluorescent microscopy.

### Animal Surgery

Operations were performed in accordance with the policies of the state of Bavaria under license number 55.2-1-54-2532-171-2011. Three days after performing a stab-wound injury, 0.5–1.0  $\mu$ l of retroviral suspension (*Neurog2*-IRES-*RFP* alone or 1:1 with *Bcl-2*-IRES-*GFP*) was injected into the site of the lesion as described by Heinrich et al. (2014). When indicated in the text, 200  $\mu$ l of Calcitriol (1 ng/ $\mu$ l, Tocris) or  $\alpha$ T3 (100 mg/kg body weight; Sigma Aldrich) diluted in corn oil was administered through oral gavage at 2 DPI. The dosage was determined according with previous publications.

### ACCESSION NUMBERS

Array data have been submitted to GEO under the accession number GEO: GSE70921.

### SUPPLEMENTAL INFORMATION

Supplemental Information includes Supplemental Experimental Procedures, seven figures, four tables, and three movies and can be found with this article online at <http://dx.doi.org/10.1016/j.stem.2015.12.003>.

### AUTHOR CONTRIBUTIONS

S.G. and M.G. conceived and designed the experiments; S.G., E.M., and M.G. designed in vivo experiments; E.M. performed in vivo experiments; S.G., F.O., A.D., G.L.R., and M.K. performed in vitro experiments; D.P. performed electrophysiological recordings; M.I., S.G., M.G., and G.M. performed genome-wide experiments and analysis; S.G., E.M., G.M., F.O., A.D., and G.L.R. analyzed data; G.M., M.I., J.B., J.P.F.A., M.C., C.B., T.S., and S.R. contributed reagents/materials/analysis tools; and M.G., S.G., E.M., and B.B. wrote the paper. All authors discussed the manuscript.

### ACKNOWLEDGMENTS

We thank Tatjana Ebert, Carmen Meyer, Detlef Franzen, and Anke Pettenbrock for excellent technical assistance and Alex Lepier for advice with viral vector design. We are very grateful to Stefan Stricker, Leda Dimou, and Sofia Grade for excellent comments on the manuscript. Anti-Prx-AK was a kind gift of C.H. Lillig (Ernst-Moritz-Arndt-University, Greifswald, Germany). This work was supported by the German Research Foundation (M.G., GO 640/8-1, 10-1), the Helmholtz Portfolio Theme “Metabolic Dysfunction and Common Disease” (J.B.) and the Helmholtz Alliance “ICEMED” (J.B. and M.G.), the SFB 870 and the advanced ERC grant ChroNeuroRepair (M.G.), the grant “NewNeurons” (B.B. and M.G.) financed by the Ministry of Science and Education, and German Research Foundation Priority Program “Pluripotency and Reprogramming” (BE 4182/2-2 and GO 640/9-2).

Received: July 30, 2015

Revised: November 7, 2015

Accepted: December 10, 2015

Published: December 31, 2015

### REFERENCES

- Abdul-Muneer, P.M., Chandra, N., and Haorah, J. (2015). Interactions of oxidative stress and neurovascular inflammation in the pathogenesis of traumatic brain injury. *Mol. Neurobiol.* 51, 966–979.
- Amamoto, R., and Arlotta, P. (2014). Development-inspired reprogramming of the mammalian central nervous system. *Science* 343, 1239882.
- Andervová, M., Antonova, T., Petřík, D., Neprasová, H., Chvátal, A., and Syková, E. (2004). Voltage-dependent potassium currents in hypertrophied rat astrocytes after a cortical stab wound. *Glia* 48, 311–326.

- Arlotta, P., Molyneaux, B.J., Chen, J., Inoue, J., Kominami, R., and Macklis, J.D. (2005). Neuronal subtype-specific genes that control corticospinal motor neuron development in vivo. *Neuron* *45*, 207–221.
- Bao, B.Y., Ting, H.J., Hsu, J.W., and Lee, Y.F. (2008). Protective role of 1 alpha, 25-dihydroxyvitamin D3 against oxidative stress in nonmalignant human prostate epithelial cells. *Int. J. Cancer* *122*, 2699–2706.
- Berninger, B., Costa, M.R., Koch, U., Schroeder, T., Sutor, B., Grothe, B., and Götz, M. (2007). Functional properties of neurons derived from in vitro reprogrammed postnatal astroglia. *J. Neurosci.* *27*, 8654–8664.
- Blum, R., Heinrich, C., Sánchez, R., Lepier, A., Gundelfinger, E.D., Berninger, B., and Götz, M. (2011). Neuronal network formation from reprogrammed early postnatal rat cortical glial cells. *Cereb. Cortex* *21*, 413–424.
- Britanova, O., de Juan Romero, C., Cheung, A., Kwan, K.Y., Schwark, M., Gyorgy, A., Vogel, T., Akopov, S., Mitkovski, M., Agoston, D., et al. (2008). *Satb2* is a postmitotic determinant for upper-layer neuron specification in the neocortex. *Neuron* *57*, 378–392.
- Buettner, G.R. (1993). The pecking order of free radicals and antioxidants: lipid peroxidation, alpha-tocopherol, and ascorbate. *Arch. Biochem. Biophys.* *300*, 535–543.
- Buffo, A., Vosko, M.R., Ertürk, D., Hamann, G.F., Jucker, M., Rowitch, D., and Götz, M. (2005). Expression pattern of the transcription factor *Olig2* in response to brain injuries: implications for neuronal repair. *Proc. Natl. Acad. Sci. USA* *102*, 18183–18188.
- Chanda, S., Ang, C.E., Davila, J., Pak, C., Mall, M., Lee, Q.Y., Ahlenius, H., Jung, S.W., Südhof, T.C., and Wernig, M. (2014). Generation of induced neuronal cells by the single reprogramming factor *ASCL1*. *Stem Cell Reports* *3*, 282–296.
- Degterev, A., Huang, Z., Boyce, M., Li, Y., Jagtap, P., Mizushima, N., Cuny, G.D., Mitchison, T.J., Moskowitz, M.A., and Yuan, J. (2005). Chemical inhibitor of nonapoptotic cell death with therapeutic potential for ischemic brain injury. *Nat. Chem. Biol.* *1*, 112–119.
- Deng, X., Gao, F., Flagg, T., Anderson, J., and May, W.S. (2006). *Bcl2*'s flexible loop domain regulates p53 binding and survival. *Mol. Cell. Biol.* *26*, 4421–4434.
- Ding, N., Yu, R.T., Subramaniam, N., Sherman, M.H., Wilson, C., Rao, R., Leblanc, M., Coulter, S., He, M., Scott, C., et al. (2013). A vitamin D receptor/SMAD genomic circuit gates hepatic fibrotic response. *Cell* *153*, 601–613.
- Dixon, S.J., Lemberg, K.M., Lamprecht, M.R., Skouta, R., Zaitsev, E.M., Gleason, C.E., Patel, D.N., Bauer, A.J., Cantley, A.M., Yang, W.S., et al. (2012). Ferroptosis: an iron-dependent form of nonapoptotic cell death. *Cell* *149*, 1060–1072.
- Dong, J., Wong, S.L., Lau, C.W., Lee, H.K., Ng, C.F., Zhang, L., Yao, X., Chen, Z.Y., Vanhoutte, P.M., and Huang, Y. (2012). Calcitriol protects renovascular function in hypertension by down-regulating angiotensin II type 1 receptors and reducing oxidative stress. *Eur. Heart J.* *33*, 2980–2990.
- Drummen, G.P., van Liebergen, L.C., Op den Kamp, J.A., and Post, J.A. (2002). C11-BODIPY(581/591), an oxidation-sensitive fluorescent lipid peroxidation probe: (micro)spectroscopic characterization and validation of methodology. *Free Radic. Biol. Med.* *33*, 473–490.
- Fode, C., Ma, Q., Casarosa, S., Ang, S.L., Anderson, D.J., and Guillemot, F. (2000). A role for neural determination genes in specifying the dorsoventral identity of telencephalic neurons. *Genes Dev.* *14*, 67–80.
- Friedmann Angeli, J.P., Schneider, M., Proneth, B., Tyurina, Y.Y., Tyurin, V.A., Hammond, V.J., Herbach, N., Aichler, M., Walch, A., Eggenhofer, E., et al. (2014). Inactivation of the ferroptosis regulator *Gpx4* triggers acute renal failure in mice. *Nat. Cell Biol.* *16*, 1180–1191.
- George, N., Kumar, T.P., Antony, S., Jayanarayanan, S., and Paulose, C.S. (2012). Effect of vitamin D3 in reducing metabolic and oxidative stress in the liver of streptozotocin-induced diabetic rats. *Br. J. Nutr.* *108*, 1410–1418.
- Gianforcaro, A., and Hamadeh, M.J. (2014). Vitamin D as a potential therapy in amyotrophic lateral sclerosis. *CNS Neurosci. Ther.* *20*, 101–111.
- Godoy, J.R., Oesteritz, S., Hanschmann, E.M., Ockenga, W., Ackermann, W., and Lillig, C.H. (2011). Segment-specific overexpression of redoxins after renal ischemia and reperfusion: protective roles of glutaredoxin 2, peroxiredoxin 3, and peroxiredoxin 6. *Free Radic. Biol. Med.* *51*, 552–561.
- Grande, A., Sumiyoshi, K., López-Juárez, A., Howard, J., Sakthivel, B., Aronow, B., Campbell, K., and Nakafuku, M. (2013). Environmental impact on direct neuronal reprogramming in vivo in the adult brain. *Nat. Commun.* *4*, 2373.
- Guo, Z., Zhang, L., Wu, Z., Chen, Y., Wang, F., and Chen, G. (2014). In vivo direct reprogramming of reactive glial cells into functional neurons after brain injury and in an Alzheimer's disease model. *Cell Stem Cell* *14*, 188–202.
- Halley-Stott, R.P., Jullien, J., Pasque, V., and Gurdon, J. (2014). Mitosis gives a brief window of opportunity for a change in gene transcription. *PLoS Biol.* *12*, e1001914.
- Heinrich, C., Blum, R., Gascón, S., Masserdotti, G., Tripathi, P., Sánchez, R., Tiedt, S., Schroeder, T., Götz, M., and Berninger, B. (2010). Directing astroglia from the cerebral cortex into subtype specific functional neurons. *PLoS Biol.* *8*, e1000373.
- Heinrich, C., Bergami, M., Gascón, S., Lepier, A., Viganò, F., Dimou, L., Sutor, B., Berninger, B., and Götz, M. (2014). Sox2-mediated conversion of NG2 glia into induced neurons in the injured adult cerebral cortex. *Stem Cell Reports* *3*, 1000–1014.
- Imayoshi, I., and Kageyama, R. (2014). bHLH factors in self-renewal, multipotency, and fate choice of neural progenitor cells. *Neuron* *82*, 9–23.
- Jin, Z., May, W.S., Gao, F., Flagg, T., and Deng, X. (2006). *Bcl2* suppresses DNA repair by enhancing c-Myc transcriptional activity. *J. Biol. Chem.* *281*, 14446–14456.
- Kawamura, T., Suzuki, J., Wang, Y.V., Menendez, S., Morera, L.B., Raya, A., Wahl, G.M., and Izpisua Belmonte, J.C. (2009). Linking the p53 tumour suppressor pathway to somatic cell reprogramming. *Nature* *460*, 1140–1144.
- Kida, Y.S., Kawamura, T., Wei, Z., Sogo, T., Jacinto, S., Shigeno, A., Kushige, H., Yoshihara, E., Liddle, C., Ecker, J.R., et al. (2015). ERRs Mediate a Metabolic Switch Required for Somatic Cell Reprogramming to Pluripotency. *Cell Stem Cell* *16*, 547–555.
- Krishna, S., Low, I.C., and Pervaiz, S. (2011). Regulation of mitochondrial metabolism: yet another facet in the biology of the oncoprotein *Bcl-2*. *Biochem. J.* *435*, 545–551.
- Kronenberg, G., Gertz, K., Cheung, G., Buffo, A., Kettenmann, H., Götz, M., and Endres, M. (2010). Modulation of fate determinants *Olig2* and *Pax6* in resident glia evokes spiking neuroblasts in a model of mild brain ischemia. *Stroke* *41*, 2944–2949.
- Liu, M.L., Zang, T., Zou, Y., Chang, J.C., Gibson, J.R., Huber, K.M., and Zhang, C.L. (2013a). Small molecules enable neurogenin 2 to efficiently convert human fibroblasts into cholinergic neurons. *Nat. Commun.* *4*, 2183.
- Liu, W., Long, Q., Chen, K., Li, S., Xiang, G., Chen, S., Liu, X., Li, Y., Yang, L., Dong, D., et al. (2013b). Mitochondrial metabolism transition cooperates with nuclear reprogramming during induced pluripotent stem cell generation. *Biochem. Biophys. Res. Commun.* *437*, 767–771.
- Maryanovich, M., and Gross, A. (2013). A ROS rheostat for cell fate regulation. *Trends Cell Biol.* *23*, 129–134.
- Masserdotti, G., Gillotin, S., Sutor, B., Drechsel, D., Imler, M., Jørgensen, H.F., Sass, S., Theis, F.J., Beckers, J., Berninger, B., et al. (2015). Transcriptional Mechanisms of Proneural Factors and REST in Regulating Neuronal Reprogramming of Astrocytes. *Cell Stem Cell* *17*, 74–88.
- McKay, N.D., Robinson, B., Brodie, R., and Rooke-Allen, N. (1983). Glucose transport and metabolism in cultured human skin fibroblasts. *Biochim. Biophys. Acta* *762*, 198–204.
- Molyneaux, B.J., Arlotta, P., Menezes, J.R., and Macklis, J.D. (2007). Neuronal subtype specification in the cerebral cortex. *Nat. Rev. Neurosci.* *8*, 427–437.
- Nguyen, T., Nioi, P., and Pickett, C.B. (2009). The Nrf2-antioxidant response element signaling pathway and its activation by oxidative stress. *J. Biol. Chem.* *284*, 13291–13295.
- Ninkovic, J., Steiner-Mezzadri, A., Jawerka, M., Akinci, U., Masserdotti, G., Petricca, S., Fischer, J., von Holst, A., Beckers, J., Lie, C.D., et al. (2013). The BAF complex interacts with *Pax6* in adult neural progenitors to establish

- a neurogenic cross-regulatory transcriptional network. *Cell Stem Cell* **13**, 403–418.
- Niu, W., Zang, T., Zou, Y., Fang, S., Smith, D.K., Bachoo, R., and Zhang, C.L. (2013). In vivo reprogramming of astrocytes to neuroblasts in the adult brain. *Nat. Cell Biol.* **15**, 1164–1175.
- Park, S.K., Dahmer, M.K., and Quasney, M.W. (2012). MAPK and JAK-STAT signaling pathways are involved in the oxidative stress-induced decrease in expression of surfactant protein genes. *Cell. Physiol. Biochem.* **30**, 334–346.
- Pearen, M.A., Eriksson, N.A., Fitzsimmons, R.L., Goode, J.M., Martel, N., Andrikopoulos, S., and Muscat, G.E. (2012). The nuclear receptor, Nor-1, markedly increases type II oxidative muscle fibers and resistance to fatigue. *Mol. Endocrinol.* **26**, 372–384.
- Pedroni, A., Minh, D., Mallamaci, A., and Cherubini, E. (2014). Electrophysiological characterization of granule cells in the dentate gyrus immediately after birth. *Front. Cell. Neurosci.* **8**, 44.
- Prozorovski, T., Schneider, R., Berndt, C., Hartung, H.P., and Aktas, O. (2015). Redox-regulated fate of neural stem progenitor cells. *Biochim. Biophys. Acta* **1850**, 1543–1554.
- Qi, S., Fang, Z., Wang, D., Menendez, P., Yao, K., and Ji, J. (2015). Concise review: induced pluripotency by defined factors: prey of oxidative stress. *Stem Cells* **33**, 1371–1376.
- Ruiz, S., Panopoulos, A.D., Herrerías, A., Bissig, K.D., Lutz, M., Berggren, W.T., Verma, I.M., and Izpisua Belmonte, J.C. (2011). A high proliferation rate is required for cell reprogramming and maintenance of human embryonic stem cell identity. *Curr. Biol.* **21**, 45–52.
- Schuurmans, C., Armant, O., Nieto, M., Stenman, J.M., Britz, O., Klenin, N., Brown, C., Langevin, L.M., Seibt, J., Tang, H., et al. (2004). Sequential phases of cortical specification involve Neurogenin-dependent and -independent pathways. *EMBO J.* **23**, 2892–2902.
- Sherman, M.H., Yu, R.T., Engle, D.D., Ding, N., Atkins, A.R., Tiriác, H., Collisson, E.A., Connor, F., Van Dyke, T., Kozlov, S., et al. (2014). Vitamin D receptor-mediated stromal reprogramming suppresses pancreatitis and enhances pancreatic cancer therapy. *Cell* **159**, 80–93.
- Theofilopoulos, S., Wang, Y., Kitambi, S.S., Sacchetti, P., Sousa, K.M., Bodin, K., Kirk, J., Saltó, C., Gustafsson, M., Toledo, E.M., et al. (2013). Brain endogenous liver X receptor ligands selectively promote midbrain neurogenesis. *Nat. Chem. Biol.* **9**, 126–133.
- Torper, O., Pfisterer, U., Wolf, D.A., Pereira, M., Lau, S., Jakobsson, J., Björklund, A., Grealish, S., and Parmar, M. (2013). Generation of induced neurons via direct conversion in vivo. *Proc. Natl. Acad. Sci. USA* **110**, 7038–7043.
- Tsacopoulos, M., and Magistretti, P.J. (1996). Metabolic coupling between glia and neurons. *J. Neurosci.* **16**, 877–885.
- Vierbuchen, T., Ostermeier, A., Pang, Z.P., Kokubu, Y., Sudhof, T.C., and Wernig, M. (2010). Direct conversion of fibroblasts to functional neurons by defined factors. *Nature* **463**, 1035–1041.
- Wapinski, O.L., Vierbuchen, T., Qu, K., Lee, Q.Y., Chanda, S., Fuentes, D.R., Giresi, P.G., Ng, Y.H., Marro, S., Neff, N.F., et al. (2013). Hierarchical mechanisms for direct reprogramming of fibroblasts to neurons. *Cell* **155**, 621–635.
- Yang, W.S., SriRamaratnam, R., Welsch, M.E., Shimada, K., Skouta, R., Viswanathan, V.S., Cheah, J.H., Clemons, P.A., Shamji, A.F., Clish, C.B., et al. (2014). Regulation of ferroptotic cancer cell death by GPX4. *Cell* **156**, 317–331.
- Yin, X.M., Oltvai, Z.N., and Korsmeyer, S.J. (1994). BH1 and BH2 domains of Bcl-2 are required for inhibition of apoptosis and heterodimerization with Bax. *Nature* **369**, 321–323.
- Zhang, J., Nuebel, E., Daley, G.Q., Koehler, C.M., and Teitell, M.A. (2012). Metabolic regulation in pluripotent stem cells during reprogramming and self-renewal. *Cell Stem Cell* **11**, 589–595.

**Cell Stem Cell, Volume 18**

## **Supplemental Information**

### **Identification and Successful Negotiation of a Metabolic Checkpoint in Direct Neuronal Reprogramming**

**Sergio Gascón, Elisa Murenu, Giacomo Masserdotti, Felipe Ortega, Gianluca L. Russo, David Petrik, Aditi Deshpande, Christophe Heinrich, Marisa Karow, Stephen P. Robertson, Timm Schroeder, Johannes Beckers, Martin Irmeler, Carsten Berndt, José P. Friedmann Angeli, Marcus Conrad, Benedikt Berninger, and Magdalena Götz**

## Supplemental Figures and Legends

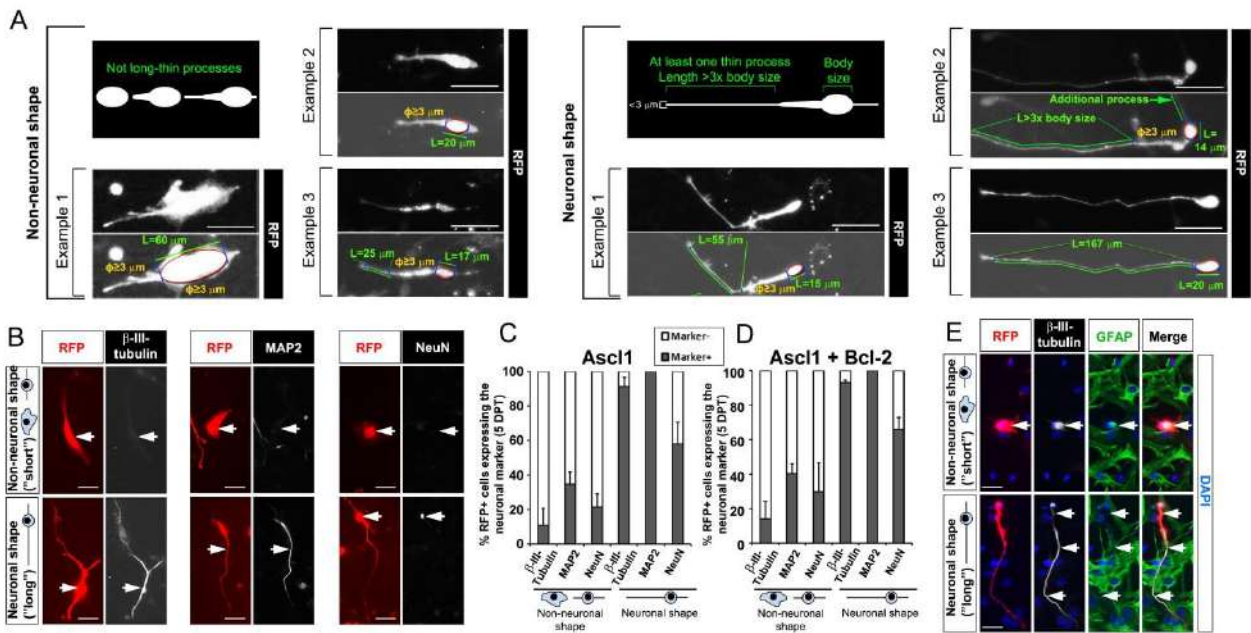


**Figure S1. Related to Figure 1**

### Validation of the Morphological Criteria.

(A) Description of the morphological criteria used to classify cells as “non-neuronal/astroglial” or “neuronal” in the time-lapse movies. Cells with at least one thin process ( $\phi < 3\ \mu\text{m}$ )  $3\times$  longer than the soma were classified as “neuronal”. The cell soma was designated as an ellipsoid located at the most prominent swelling part of the cell, at the level where the nucleus is located (visible by accumulation of RFP fluorescence). The largest diameter of the ellipsoid was measured and compared to the length of the longest thin process (see examples). For the morphometric analysis and the video tracking of single cells we used the software ImageJ (FIJI version).

(B) Examples of astrocytes transfected with *Asc11* and RFP-encoding plasmid at 5 DPT classified according to morphological criteria. Cells classified as neurons (lower panels) are immune-reactive for the neuronal markers  $\beta$ -III-tubulin, MAP2 and NeuN, contrary to cells with an astrocyte morphology (upper panels).

(C, D) Histograms show quantifications of the analysis from B in cultures transfected with *Asc11/RFP* alone (C) or in combination with *Bcl-2* (D).

(E) Immunocytochemistry showing that some “non-neuronal/astroglial” cells (upper panels) transduced with *Asc11* co-express both neuronal ( $\beta$ -III-tubulin, white) and astroglial (GFAP, green) markers at 5 DPT. Contrarily, cells with neuronal morphology (lower panels) only express neuronal markers ( $\beta$ -III-tubulin).

Error bars indicate  $\pm$ SD. Scale bars:  $20\ \mu\text{m}$  in (B, E) and  $40\ \mu\text{m}$  in (A).

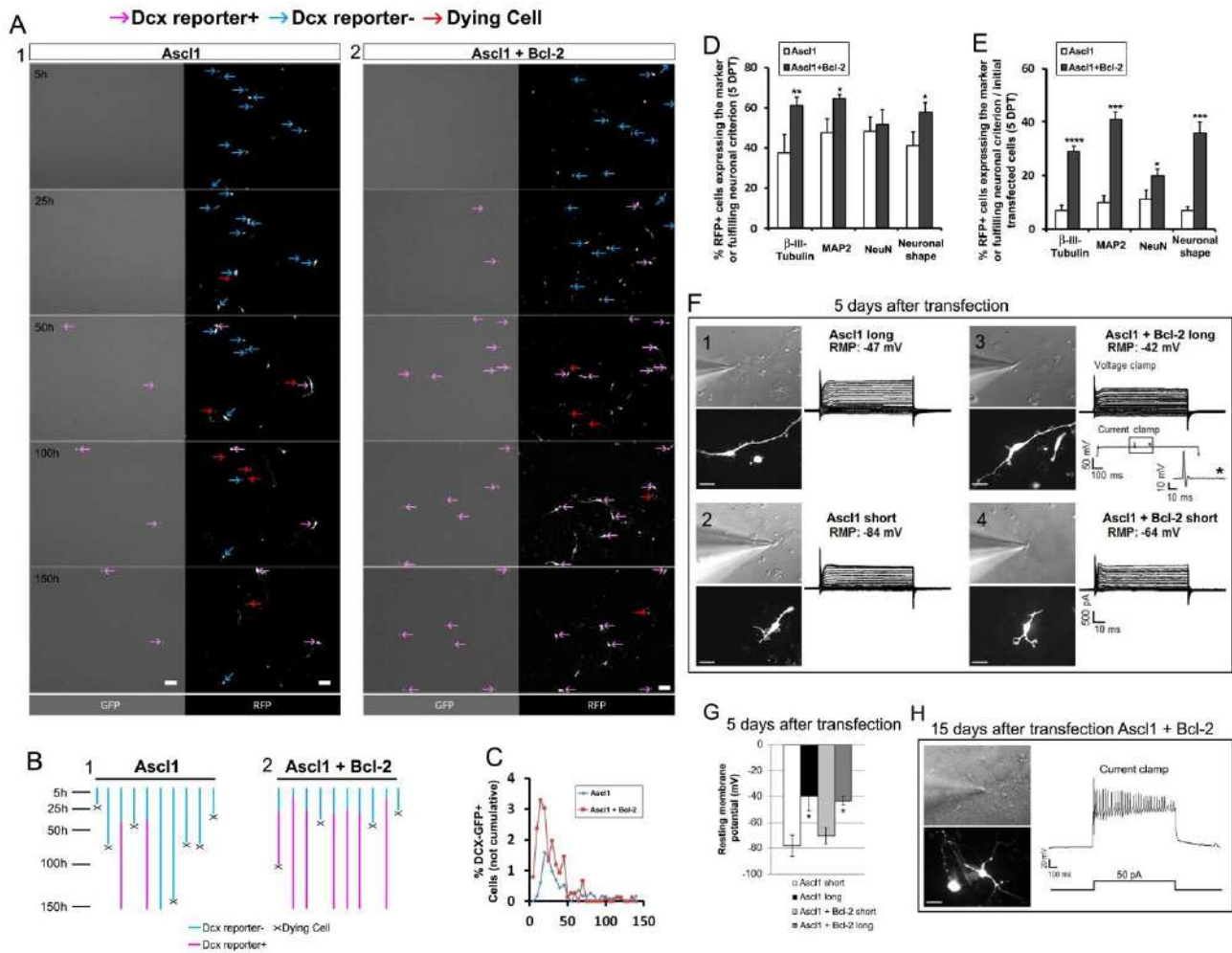


**Figure S2. Related to Figure 2**

**Analysis of Neuronal Conversion by DCX-GFP, Expression of Neuronal Markers and Electrophysiology.**

(A) Still images from time-lapse movies (Figure 1A and Movie S2) show astroglial cells (blue arrows), DCX-GFP+ neurons (purple arrows, GFP reporter column) and dying cells (red arrows) at different time points in cultures co-transfected with only DCX-GFP and *Ascl1* (left panels) or in combination with *Bcl-2* (right panels).

(B) Progeny-trees of single cells tracked from the examples in A showing that cells rarely proliferate during reprogramming. Most astroglial cells (blue lines) do not turn directly into DCX-GFP neurons (purple lines) and die (depicted with “x”) before converting.

(C) Percent of transfected cells that newly acquire DCX-GFP signal at different time-points in the movies from A. 1095 and 220 cells were counted in *Ascl1* and *Ascl1+Bcl-2*, respectively.

(D, E) Histograms showing the percent of cells immune-reactive for neuronal markers or having a neuronal shape, as indicated, among the transfected (RFP+) cells at 5 DPT (N=3).

(F) Patch-clamp recordings from the cells transfected with only *Ascl1/RFP* (1-2) or in combination with *Bcl-2* (3, 4) at 5 DPT. The left panels show brightfield with a patch electrode attached (up) and red-fluorescence (down). On the right, the resting membrane potential and voltage-clamp is shown for all the examples. In the example 3, a current-clamp displays very immature action potential-like features elicited by co-transfection with *Ascl1/RFP* and *Bcl-2*.

(G) Histogram shows quantification of resting membrane potential (RMP) in short/long cells transfected with only *Ascl1* or in combination with *Bcl-2*. N=6 cells in *Ascl1/long-short* cells; N=10 cells in *Ascl1+Bcl-2/long* cells; N=8

cells in *Ascl1*+*Bcl-2*/short cells. Note that a higher number of cells has a neuronal morphology upon *Bcl-2* co-transduction (E) and hence a higher number of cells has a more positive RMP.

(H) Recordings from a cell transfected with *Ascl1* and *Bcl-2* at 15 DPT show a current-clamp trace elicited by 50 pA current injection with notable mature action potentials.

Error bars indicate  $\pm$ SD. \*p 0.05, \*\*p<0.01, \*\*\*p<0.001, \*\*\*\*p<0.0001; unpaired t test in D, E, G. Scale bars 50  $\mu$ m in A, 40  $\mu$ m in F, H.

See also Movie S2.

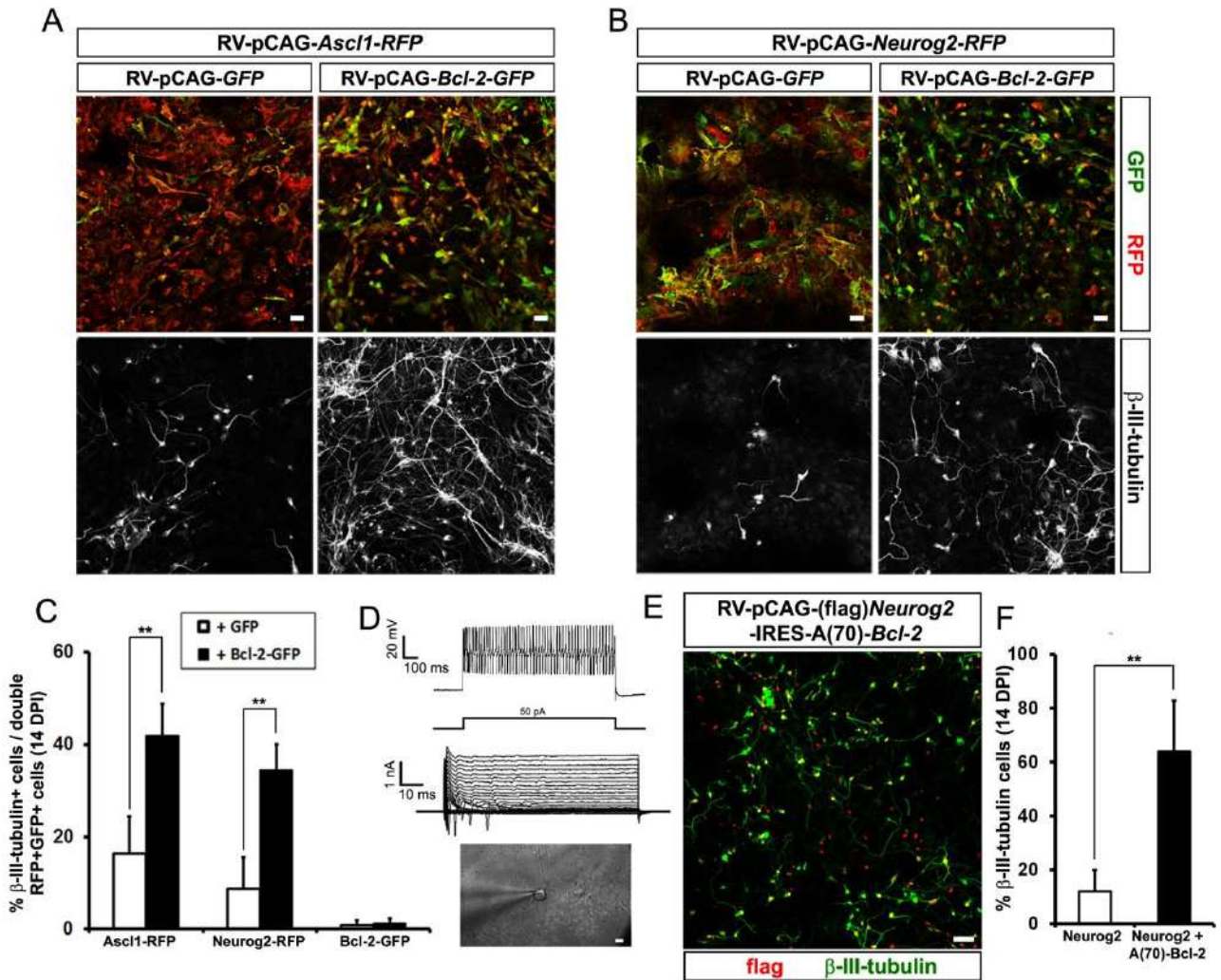


**Figure S3. Related to Figure 3**

***Bcl-2* and A(70)-*Bcl-2* Enhance Neuronal Conversion of MEFs.**

(A, B) Epifluorescence images of MEF cultures co-infected with *Ascl1/RFP*- (A) or *Neurog2/RFP*- (B) encoding viral vectors in combination with the *GFP* control or *Bcl-2/GFP*-encoding viral vectors. Note that *Bcl-2* increases the number of neurons immunoreactive for  $\beta$ -III-tubulin obtained at 14 DPI (lower panels; white cells).

(C) Histogram showing the quantifications of experiments from A and B (N=4).

(D) Electrophysiological recordings from the cell infected with *Ascl1* and *Bcl-2* and shown in brightfield in the lowest panel with a patch electrode attached. On the top panel, a current-clamp trace elicited by 50 pA current injection is shown revealing a train of action potentials, while the middle panel shows voltage-clamp traces with notable fast-inactivating inward currents.

(E) Epifluorescence images of MEF cultures transduced with the retroviral vector *Neurog2*-IRES-A(70)-*Bcl-2*. Note the high proportion of neurons immunoreactive for  $\beta$ -III-tubulin (green) among the transduced population (flag+; red).

(F) Histogram showing the high increase in the conversion efficiency mediated by *Neurog2*- and A(70)-*Bcl-2*-co-expression compared to the *Neurog2*-only transduced controls (N=3).

Error bars indicate  $\pm$ SD. \*\* $p < 0.01$ ; unpaired t test in C, F. Scale bars: 40  $\mu$ m.

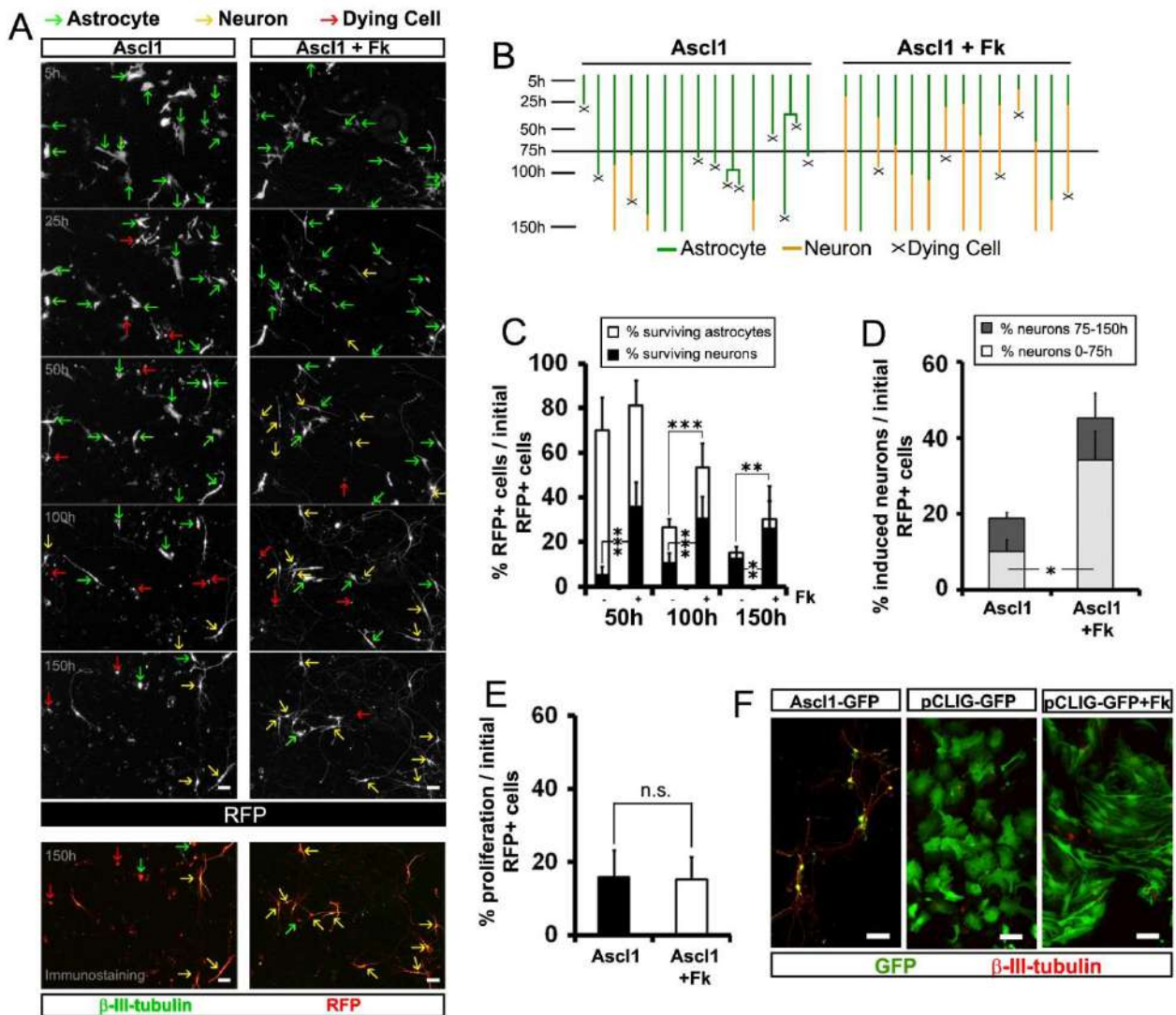


**Figure S4. Related to Figure 4**

**Analysis of Astrocyte-to-Neuron Conversion upon Forskolin Treatment by Live Imaging.**

(A) Examples of still images from time-lapse movies (see Movie S3) show astroglial cells (green arrows), neurons (yellow arrows) and dying cells (red arrows) at different time points, in the presence or absence of Fk. Last image shows immunostaining of fixed cells confirming that all RFP+ cells are neurons (yellow arrows) expressing  $\beta$ -III-tubulin (green). Note that at the end of the movie, the number of neurons increased in Fk treated cultures (20  $\mu$ M).

(B) Progeny-trees of single cells tracked from example in A showing that cells rarely proliferate during reprogramming and most astroglial cells (green lines) die (dead cells depicted with “x”) before they could become neurons (yellow lines). Fk treatment (right diagram) resulted in faster acquisition of neuronal morphology, reduced cell death and increased reprogramming efficiency.

(C) Analysis of neuronal conversion and cell survival during the observation period, in Fk treated and untreated cultures. The total number of astrocytes/neurons (white and black bars, respectively) is normalized to the initial number of transfected cells analysed at 1 DPT.

(D) Histogram showing that neurons appear mostly in the first half of imaging time upon Fk treatment.

(E) Histogram of the proportion of *Ascl1*-transfected cells proliferating during 150 h of observation with or without Fk treatment. Note that this value is low and not significantly increased upon Fk treatment.

(F) Micrograph showing that Fk does not induce neuronal conversion of astrocytes ( $\beta$ -III-tubulin, Red) without the expression of neuronal fate determinants.

N=5 in the control condition (339 initial tracked cells); N=4 in Fk treated condition (195 cells).

Error bars indicate  $\pm$ SD. \* $p < 0.05$ , \*\* $p < 0.01$ , \*\*\* $p < 0.001$ ,  $p \geq 0.05$  no statistically significant difference (n.s.); ANOVA with Tukey's post-hoc test in C; unpaired t test in D, E. Scale bars: 40  $\mu$ m.

See also Movie S3.

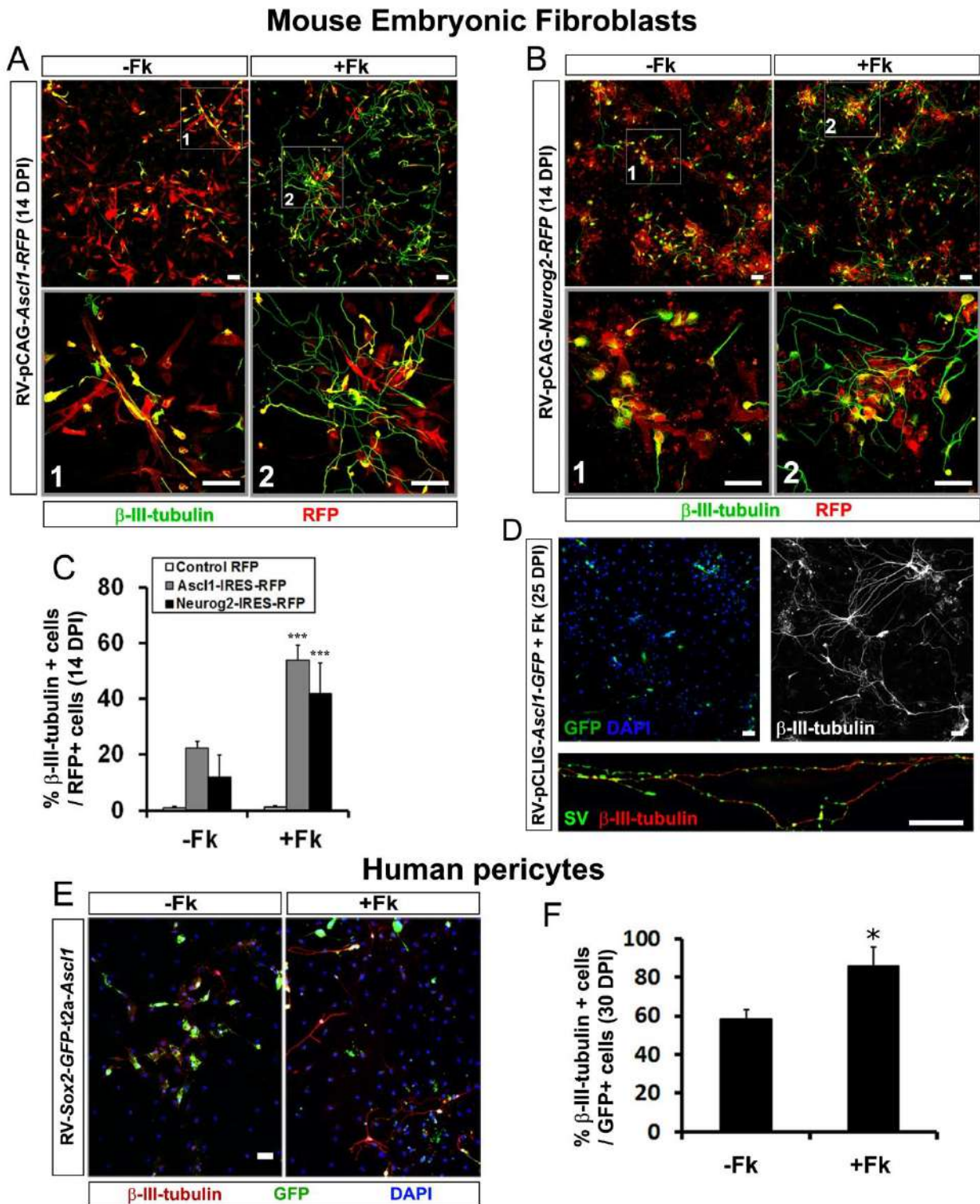


Figure S5. Related to Figure 5

#### Widespread Effect of Forskolin in Enhancing Neuronal Reprogramming

(A, B) Micrographs showing *Ascl1*- or *Neurog2*-transduced MEFs analysed for  $\beta$ -III-tubulin immunoreactivity (green) 14 days after retroviral infection. MEF-derived neurons exhibit longer and more complex processes upon Fk treatment (boxed areas 1 and 2 magnified in the lower panels).

(C) Histogram showing the proportion of  $\beta$ -III-tubulin+ neurons amongst control (white bars), *Ascl1* (grey bars) or *Neurog2* (black bars) transduced (RFP+) MEFs upon Fk treatment (N=3).

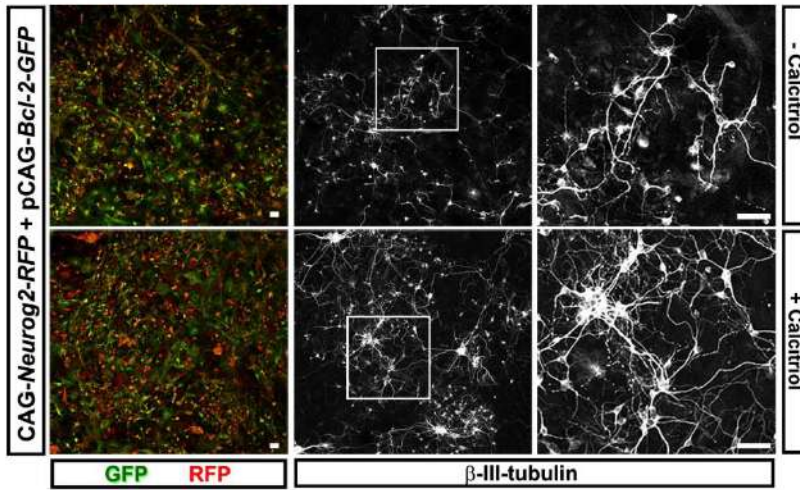
(D) Micrograph showing highly complex  $\beta$ -III-tubulin+ processes (upper right panel) of *Ascl1*-infected MEFs (upper left panel, green cells) upon Fk addition at 25 DPI. Lower panel shows high magnification view of  $\beta$ -III-tubulin+ (red) neurites with high density of synaptobrevin (SV) puncta (green) indicating synaptic contacts.

(E) Epifluorescence images of human pericyte-derived neurons showing  $\beta$ -III-tubulin-immunoreactivity (red) 4 weeks after infection with a viral vector co-expressing *Ascl1*, *Sox2* and *GFP* (green) in cultures with (right panels) or without Fk addition. After Fk treatment neurons show more mature morphology, with more complex and extended neurites.

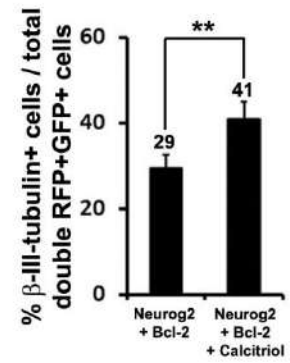
(F) Histogram depicting the proportion of  $\beta$ -III-tubulin-immunoreactive cells from (E) amongst all GFP+ transduced cells (N=3).

Error bars indicate  $\pm$ SD. Statistical tests performed on treated and untreated cells transduced with the same transcription factor (Control, *Ascl1*, *Neurog2*, *Dlx2*). \* $p < 0.05$ , \*\* $p < 0.01$ , \*\*\* $p < 0.001$ ; unpaired t test. Scale bars: 40  $\mu$ m.

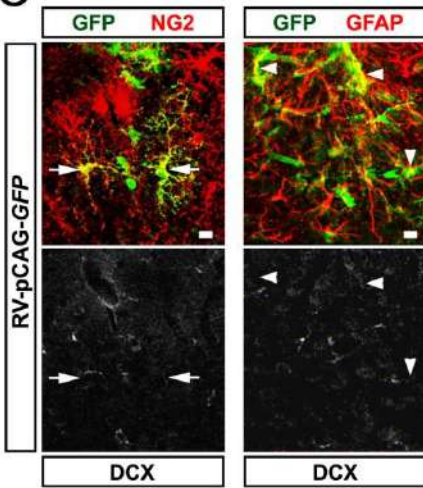
**A**



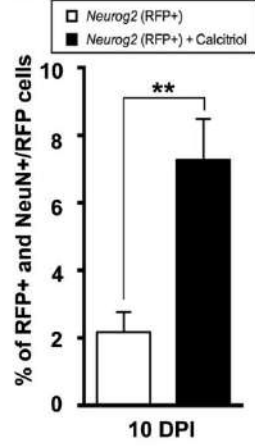
**B**



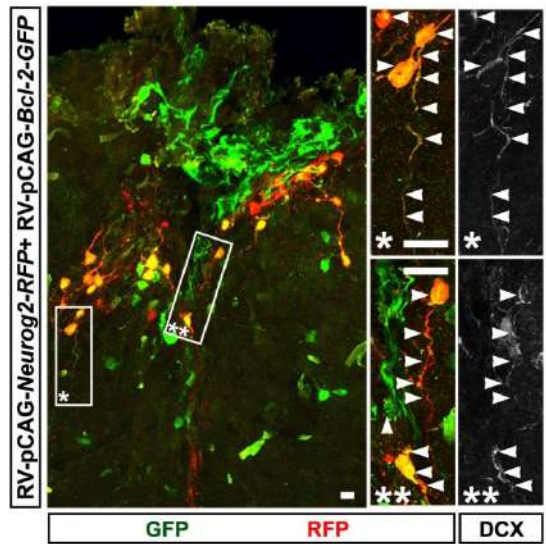
**C**



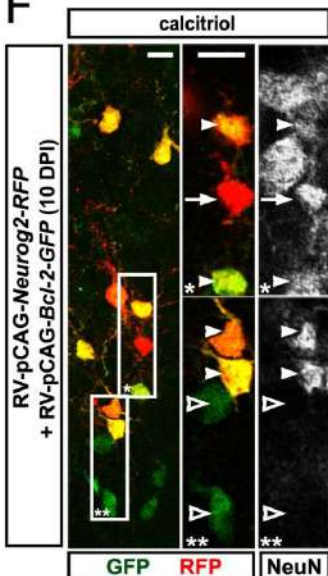
**D**



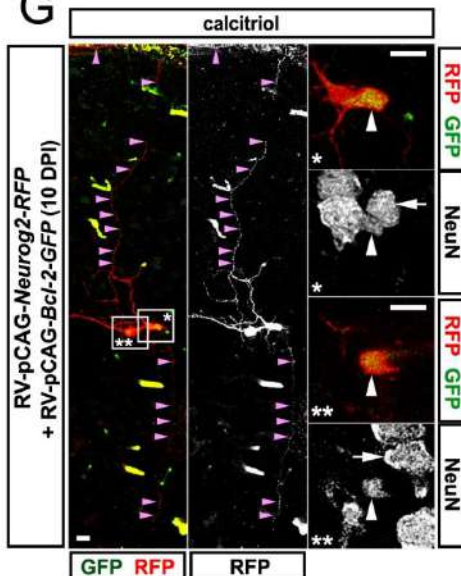
**E**



**F**



**G**



**H**

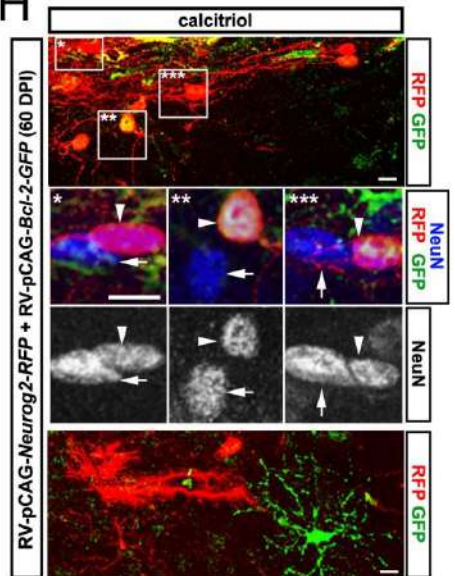


## Figure S6. Related to Figure 6

### Calcitriol Enhances Neurog2-Mediated Reprogramming of MEFs *In Vitro* and Glial Cells After stab wound Injury *In Vivo*.

(A) Epifluorescence micrographs of MEF cultures 10 days after co-transduction with *Neurog2/RFP* and *Bcl-2/GFP* in the absence (upper row) or presence (lower row) of calcitriol. Higher magnification (right column) of the insets shows the beneficial effects of calcitriol.

(B) Histogram depicting the proportion of  $\beta$ -III-tubulin-immunoreactive cells amongst the MEFs co-infected with *Neurog2/RFP* and *Bcl-2/GFP* with or without calcitriol, at 10 days after retroviral transduction.

(C) Confocal micrographs (maximum intensity projection) of cells infected by the retroviral vector encoding for *GFP in vivo* after stab-wound injury and immunostained for NG2, GFAP and Doublecortin (DCX) at 7 days post-injection (DPI). GFP+ cells are NG2+ (left panel, arrow) or GFAP+ (right panels, arrowheads). No DCX+ cells were detected around the lesion site.

(D) Quantifications of NeuN/RFP double-positive cells after stab-wound injury and subsequent injection with *Neurog2/RFP in vivo*. Mice were treated or not with calcitriol and analysed at 10 DPI as depicted in Figure 6A.

(E) Confocal micrographs of the injection site (10 DPI, maximum intensity projection) and immunohistochemistry for DCX. The cells in the insets (\*,\*\*) are shown at higher magnification, with white arrowheads indicating the colocalization of the processes with DCX.

(F) Cells infected by *Neurog2/RFP* alone or with *Bcl-2/GFP* after stab-wound injury *in vivo*, analyzed at 10 DPI after treatment with calcitriol (Figure 6A), with magnified single optical sections (\*,\*\*) shown on the right. Some RFP+ cells (transduced with *Neurog2* only) are NeuN-immunopositive (arrow), whereas GFP+ cells (transduced only with *Bcl-2*) never do (empty arrowheads). Co-infected cells are frequently NeuN+ (filled arrowheads).

(G) Confocal micrographs (maximum intensity projection) showing neurons co-transduced *in vivo* (10 DPI) after treatment with calcitriol. Purple arrowheads indicate neurites emerging from adjacent neurons and growing towards the pial surface (above) and the white matter (below). High magnification panels on the right (\*,\*\*) show that both neurons have high levels of NeuN (white arrowheads), comparable to those found in native neurons around the same area (white arrows).

(H) Confocal micrographs (maximum intensity projection) of cells co-infected by *Neurog2/RFP* and *Bcl-2/GFP* (magnified in boxes \*, \*\* and \*\*\*, arrowheads) after treatment with calcitriol are immunoreactive for NeuN at 60 DPI. Note that their soma size is comparable to the one displayed by surrounding endogenous neurons (arrows). The picture at the bottom shows single infected cells (RFP+ or GFP+) still viable after 60 DPI and maintaining their glial nature. Error bars indicate  $\pm$ SD. N=1 in C, E, H; N=3 in A, B, D, F, G \*\*p<0.01; unpaired t test in B, D. Scale bars: 40  $\mu$ m in A and 10  $\mu$ m in C, E, F-H.

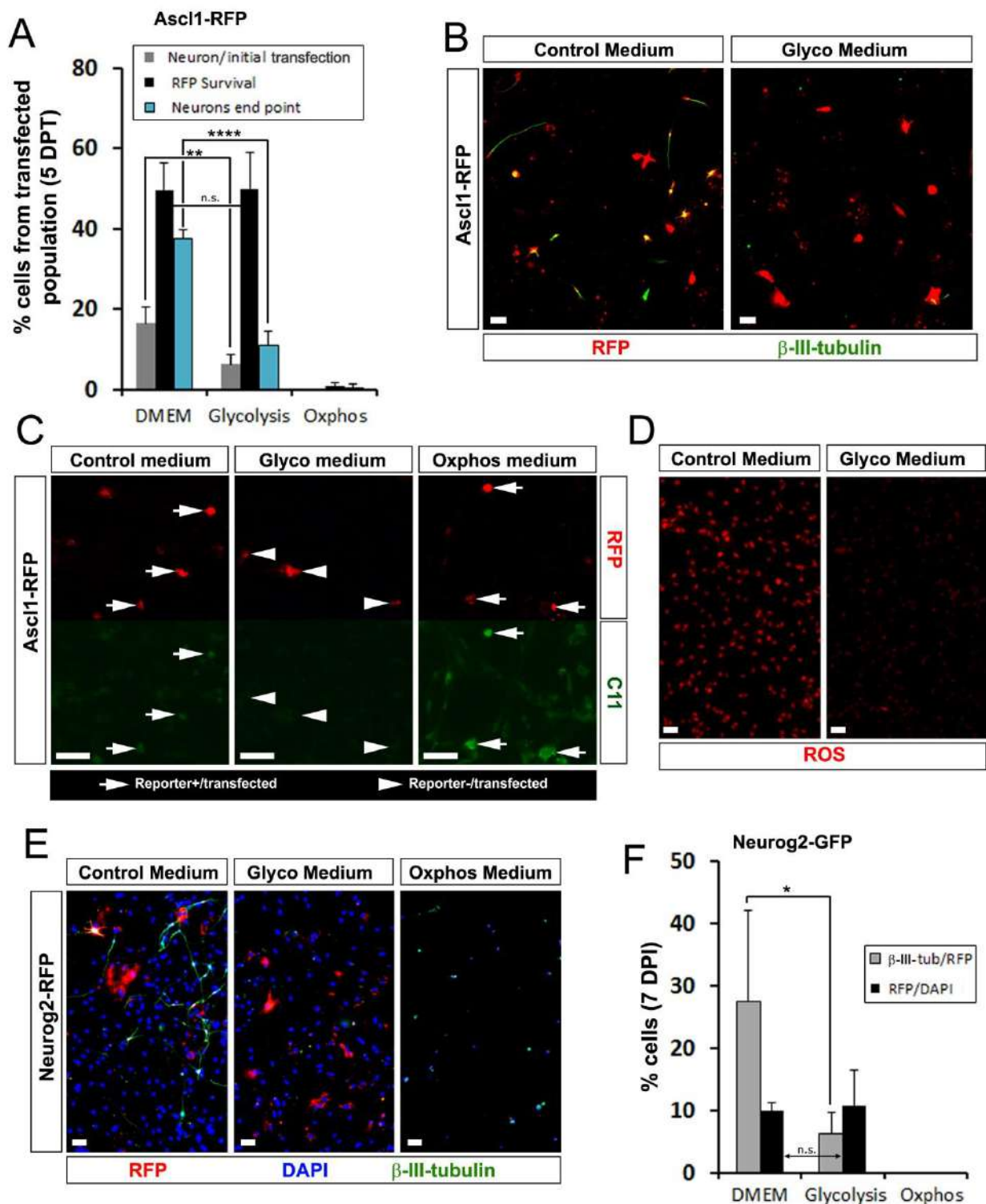


Figure S7. Related to Figure 7

**Maintaining Glycolysis in Astroglial Cells Reduces Oxidative Stress but Blocks Reprogramming Into Neurons.**

(A) Quantification of experiments with examples of cells shown in B depicting the % of neuronal conversion normalized to the initial number of transfected cells (1 DPT; grey bars), at the end point (5 DPT; blue bars) and % of surviving cells (black bars) grown in anaerobic glycolysis-only, OxPhos-only or control medium. Note that all cells grown in OxPhos medium die, while cells grown in anaerobic glycolysis medium survive but fail to convert into neurons.

(B) Micrographs of astroglial cultures transfected with *Asc11/RFP* and maintained in culture for 5 days in normal differentiation medium (control medium) or anaerobic glycolysis medium. As previously, neuronal conversion was monitored by  $\beta$ -III-tubulin immunoreactivity (green) among the transfected population (RFP+, red). Note that cells in glycolysis only medium do not acquire  $\beta$ -III-tubulin.

(C) Micrographs showing representative examples of Lip-Ox evaluated by C11-Bodipy reaction (green channel), of *Asc11/RFP* transfected cells (RFP+, red) 24 hours after change with medium capable of inducing selective metabolisms (control medium, anaerobic glycolysis-only medium, OxPhos-only medium). Arrows indicate transfected cells (red) with increased levels of Lip-Ox (green); arrowheads transfected cells without green signal. Note that anaerobic glycolysis medium reduces Lip-Ox in transfected cells, while OxPhos medium potentially increases it compared to Control medium.

(D) Micrographs of astroglial culture at 24h in the anaerobic glycolysis-only medium already shows much reduced ROS signal detected by the superoxide indicator dye Dihydroethidium (DHE, 5 $\mu$ M, Life Technologies), which shifts from a blue fluorescence in the cytosol to a red fluorescence in the nucleus when oxidized.

(E) Micrographs of astroglial cultures transduced with *Neurog2/RFP* and maintained 7 days in normal differentiation medium (control Medium, left), anaerobic glycolysis-only medium (middle) or OxPhos-only medium (right). Neuronal conversion was monitored by  $\beta$ -III-tubulin immunoreactivity (green) among the transfected cells (RFP+, red). Note that also *Neurog2*-induced reprogramming is impaired in anaerobic glycolysis medium, while cells do not survive in OxPhos-only metabolism.

(F) Quantification of the experiment in E showing that the % of neuronal conversion normalized to the final number of transduced cells ( $\beta$ -III-tubulin/RFP at 7 DPI; grey bars) is drastically reduced when cells are grown in anaerobic glycolysis medium, while % of surviving cells (RFP/total DAPI at 7 DPI; black bars) is unaffected.

Error bars indicate  $\pm$ SD. \* $p$ <0.05, \*\* $p$ <0.01; \*\*\*\* $p$ <0.0001; ANOVA with Tukey's post-hoc test in A; ANOVA with Holm-Sidak's post-hoc test in F. Scale bars: 40  $\mu$ m.

## Supplemental tables

### Table S1 as Excel file. Related to Figure 5

**Genes Regulated by Forskolin.** Microarray analysis of MEF cultures treated or not with Fk. All cells were transduced with an Ascl1/RFP- encoding vector. Shown are 507 probe sets regulated in Ascl1+Fk vs Ascl1 as defined by  $p < 0.01$ , fold change  $\geq 1.5x$ , and average expression in at least one group in the dataset  $> 20$  arbitrary units. See Excel file.

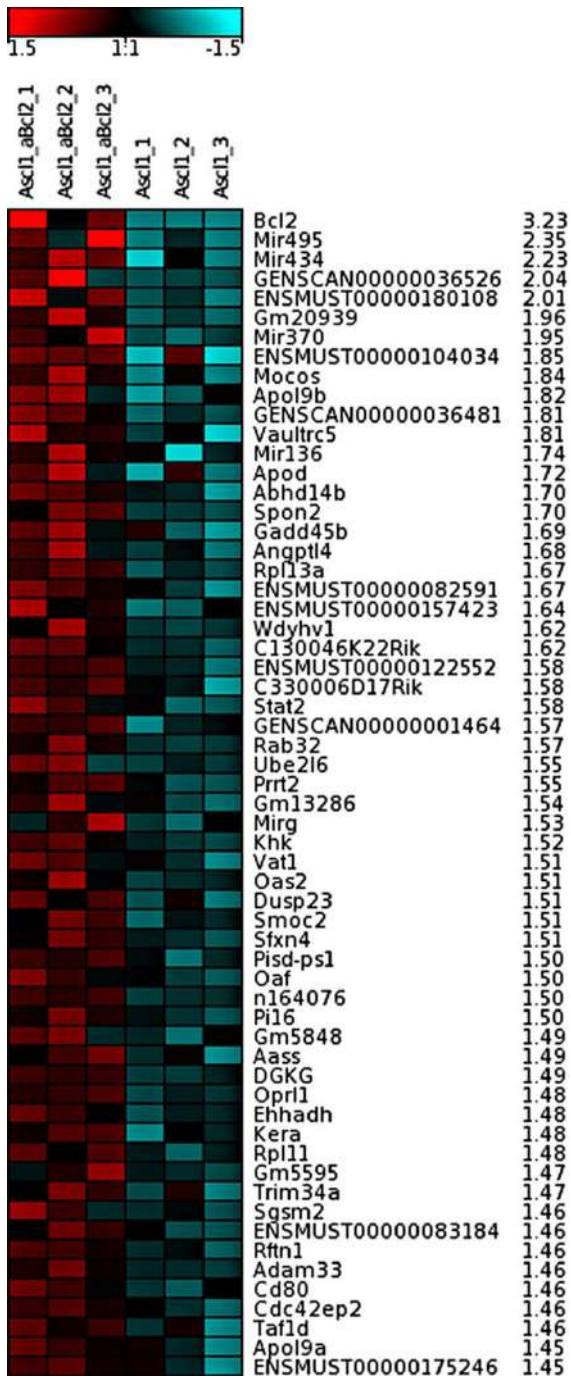


**Table S2. Related to Figure 5**

**Genes Regulated by A(70)-Bcl-2.** Table shows heatmaps of the top 60 up-regulated genes based on microarray analysis (Asc11+A(70)-Bcl-2 vs Asc11;  $p < 0.01$ , fold-change  $\geq 1.45$ ). Linear fold-changes are indicated.

Ingenuity Canonical Pathways associated with up-regulated genes	-log(p-value)	Molecules
Axonal Guidance Signaling	5.76	SLIT3, ENPEP, PAPP2, FZD3, BMP2, CXCL12, EPHA4, PLXNA2, GNA14, FZD1, ADAMTS2, SEMA4C, PRKAG1, TUBB2B, SRGAP1, WNT4, PRKD1, PRKCA, BMP1, GNG4, PAPP, TUBB3, SEMA5A, CHP1, TUBA4A, FZD9, NFATC4, BMP5, NTRK2, ADAM12, EPHA6, BMP7
cAMP-mediated signaling	5.69	GRK4, ADCY2, PDE7A, VIPR2, PDE10A, CNR1, PDE3A, STAT3, PDE4B, PDE1A, PDE1C, PDE8A, S1PR3, ADCY9, LPAR1, PDE7B, PDE3B, ADCY5, PDE8B, AGTR2, AGTR1
PPAR $\alpha$ /RXR $\alpha$ Activation	6.89	ADCY2, IL1RL1, TGFB3, BCL3, IL6, GNA14, IL1R1, NFKB2, ABCA1, PRKAG1, ACVR1B, IL1R2, NR2F1, TGFB2, ADCY9, JUN, IL1RL2, ADCY5, GPD2, PRKCA
IL-10 Signaling	6.30	IL33, IL1R2, SOCS3, IL4R, JUN, IL1RL2, IL1RL1, STAT3, IL1R1, LBP, NFKB2, IL6
PPAR Signaling	4.11	IL33, PPARG, IL1R2, NR2F1, JUN, IL1RL2, IL1RL1, PDGFRA, IL1R1, PTGS2, NFKB2
LXR/RXR Activation	3.36	IL33, IL1R2, IL1RL2, IL1RL1, LBP, PTGS2, NFKB2, IL6, PON3, ABCA1
LPS/IL-1 Mediated Inhibition of RXR Function	3.01	MGST1, CPT1A, IL1RL1, IL1R1, SOD3, ABCA1, IL33, IL1R2, JUN, IL1RL2, CHST11, ACSL4, HS3ST1, LBP, ACSL1
Wnt/ $\beta$ -catenin Signaling	2.85	FZD3, TGFB3, LRP6, FZD9, KREMEN1, FZD1, SOX11, ACVR1B, TGFB2, JUN, WNT4, SOX9, SFRP1
BMP signaling pathway	2.83	SOSTDC1, JUN, BMP2, BMP7, NFKB2, BMP5, PRKAG1, BMP1
IL-9 Signaling	2.47	SOCS3, IRS2, BCL3, STAT3, NFKB2
NF- $\kappa$ B Signaling	2.45	IL33, IL1R2, TGFB2, TNFSF11, NTRK2, TGFB3, BMP2, PDGFRA, FGFR2, IL1R1, NFKB2, IRAK3
IL-17 Signaling	2.42	JUN, TIMP1, CEBPB, PTGS2, IL6, IL17RA, CCL11
STAT3 Pathway	2.18	TGFB2, SOCS3, NTRK2, TGFB3, PDGFRA, FGFR2, STAT3
VDR/RXR Activation	2.03	TNFSF11, IL1RL1, CEBPB, VDR, S100G, PRKD1, PRKCA
HGF Signaling	1.91	JUN, ETS2, HGF, STAT3, PTGS2, IL6, PRKD1, PRKCA
NRF2-mediated Oxidative Stress Response	1.86	MGST1, SOD2, JUN, MAF, JUND, GCLM, NFE2L2, TXNRD1, SOD3, PRKD1, PRKCA
FGF Signaling	1.83	FGF21, FGF10, HGF, FGFR2, STAT3, FGF7, PRKCA
TGF- $\beta$ Signaling	1.83	TGFB2, JUN, BMP2, BMP7, VDR, INHBB, ACVR1B
CXCR4 Signaling	1.83	GNG4, ADCY9, ADCY2, JUN, ADCY5, CXCL12, RHOU, GNA14, PRKD1, PRKCA
JAK/Stat Signaling	1.66	SOCS3, JUN, STAT3, CEBPB, NFKB2, IL6
Ingenuity Canonical Pathways associated with down-regulated genes	-log(p-value)	Molecules
Axonal Guidance Signaling	1.32	BMP4, ADAMTS1, PDGFA, BMP3, GNA11, VEGFC, ABLIM1, FZD8, SEMA3A, RRAS2, PRKAR2B, SEMA3D, PAK3, ARHGEF6, ADAM23, FIGF, ROBO2, ADAMTS5, ITGA4
VEGF Signaling	2.32	RRAS2, PTK2B, ACTA2, FLT1, VEGFC, FIGF, VCL, BCL2
Death Receptor Signaling	1.32	GAS2, ACTA2, HSPB2, PARP14, HSPB1, BCL2

**Table S3. Related to Figure 5**

**Analysis of Pathways Regulated by Forskolin.** Enrichment analysis of canonical pathways based on the set of 1321 probe sets differentially regulated between MEF cultures treated or not with Fk (fold change > 1.3x,  $p < 0.05$ ,  $A_v > 20$ ). All cells were transduced with an Ascl1/RFP- encoding vector. Analysis was done separately for up- and down-regulated probes using Ingenuity Pathway Analysis software and selected significantly enriched terms ( $p < 0.05$ ) are shown.

Ingenuity Canonical Pathways associated with up-regulated genes	-log(p-value)	Molecules
NRF2-mediated Oxidative Stress Response	5.74	MGST1, MAF, HSPB8, DNAJC15, JUNB, CLPP, GSTO1, GSR, DNAJC4, CAT, DNAJA3, JUND, GCLM, NFE2L2, GSTP1, MGST3, GSTK1
Granulocyte Adhesion and Diapedesis	5.09	HRH2, VCAM1, IL1RL1, PF4, IL1R1, CCL5, CCL11, CXCL6, IL33, IL1RL2, CCL7, Ccl2, PPBP, CXCL2, MMP19
Glutathione-mediated Detoxification	4.85	MGST1, ANPEP, GSTP1, GSTO1, MGST3, GSTK1
Role of Macrophages, Fibroblasts and Endothelial Cells in Rheumatoid Arthritis	4.36	SOCS3, VCAM1, FRZB, IL1RL1, CHP1, WNT2B, IRAK3, STAT3, IL1R1, CCL5, IL17RA, PRSS3, TLR2, IL33, FZD4, IL1RL2, LTBR, SFRP1, WNT5A, CAMK2G
LXR/RXR Activation	3.97	IL33, FDF1, IL1RL2, CCL7, IL1RL1, LPL, SERPINA1, IL1R1, PTGS2, NFKB2, RXRA
IL-10 Signaling	3.62	IL33, SOCS3, IL4R, IL1RL2, IL1R1, STAT3, IL1R1, NFKB2
Agranulocyte Adhesion and Diapedesis	3.55	IL33, VCAM1, CCL7, Ccl2, PF4, PPBP, CCL5, IL1R1, CXCL2, CCL11, CD34, CXCL6, MMP19
Glutathione Redox Reactions I	3.34	GSR, MGST1, MGST3, GSTK1
Hepatic Fibrosis / Hepatic Stellate Cell Activation	3.14	IGFBP4, IL4R, VCAM1, IL1RL2, TIMP1, IL1RL1, PDGFRA, IL1R1, CCL5, NFKB2, AGTR1
IL-9 Signaling	2.80	SOCS3, IRS2, BCL3, STAT3, NFKB2
LPS/IL-1 Mediated Inhibition of RXR Function	2.74	IL33, MGST1, IL1RL2, CYP3A5, IL1RL1, CAT, IL1R1, RXRA, MGST3, GSTP1, GSTO1, SULT2A1, GSTK1
PPAR Signaling	2.71	IL33, IL1RL2, IL1RL1, PDGFRA, IL1R1, PTGS2, NFKB2, RXRA
Role of IL-17A in Arthritis	2.70	CCL7, CCL5, PTGS2, NFKB2, IL17RA, CXCL6
Xenobiotic Metabolism Signaling	2.47	MGST1, MAP3K6, MAF, NFKB2, SULT2A1, GSTO1, CYP3A5, CAT, RXRA, NFE2L2, GSTP1, MGST3, CAMK2G, GSTK1
Geranylgeranyldiphosphate Biosynthesis	2.42	COX10, GGPS1
Hepatic Cholestasis	2.21	IL33, IL1RL2, IL1RL1, IL1R1, NFKB2, IRAK3, RXRA, PRKAG1, ATP8B1
Mitochondrial Dysfunction	2.19	GSR, NDUFS5, COX10, CAT, NDUFA7, SDHD, CYB5A, BACE2, UQCRCQ, PSEN1
Acute Phase Response Signaling	2.09	IL33, C1R, SOCS3, SERPINA3, OSMR, SERPINA1, STAT3, IL1R1, NFKB2, RBP1
Gai Signaling	2.01	S1PR3, CNR1, GNG5, STAT3, AGTR2, AGTR1, PRKAG1, OPRL1
IL-17A Signaling in Fibroblasts	1.98	CCL7, LCN2, NFKB2, IL17RA
Role of IL-17F in Allergic Inflammatory Airway Diseases	1.77	CCL7, NFKB2, IL17RA, CXCL6
Aryl Hydrocarbon Receptor Signaling	1.74	MGST1, NFKB2, RXRA, NFE2L2, GSTP1, GSTO1, MGST3, GSTK1
cAMP-mediated signaling	1.72	PDE8A, AKAP12, S1PR3, HRH2, PDE7B, CNR1, STAT3, AGTR2, AGTR1, CAMK2G, OPRL1
IL-17A Signaling in Airway Cells	1.71	STAT3, NFKB2, IL17RA, CCL11, CXCL6
Role of IL-17A in Psoriasis	1.68	IL17RA, CXCL6
Prostanoid Biosynthesis	1.68	PTGS1, PTGS2
Role of Osteoblasts, Osteoclasts and Chondrocytes in Rheumatoid Arthritis	1.68	IL33, FZD4, IL1RL2, FRZB, IL1RL1, WNT2B, CHP1, IL1R1, SFRP1, WNT5A, BMP1
Protein Kinase A Signaling	1.67	AKAP12, PTPN13, PPP1R3C, CHP1, NFKB2, PRKAG1, PDE8A, PHKB, ADD3, PPP1R10, PDE7B, DUSP10, GNG5, PTGS2, CAMK2G, MTMR3
Atherosclerosis Signaling	1.67	IL33, VCAM1, LPL, SERPINA1, NFKB2, CCL11, F3
Remodeling of Epithelial Adherens Junctions	1.63	DNM1, TUBA1A, ARPC1B, DNMT3, TUBA1B
PPAR $\alpha$ /RXR $\alpha$ Activation	1.60	IL1RL2, IL1RL1, TGFB3, LPL, BCL3, IL1R1, NFKB2, RXRA, PRKAG1
Role of JAK family kinases in IL-6-type Cytokine Signaling	1.60	SOCS3, OSMR, STAT3
Nur77 Signaling in T Lymphocytes	1.59	HLA-DMA, CHP1, NR4A1, RXRA
IL-6 Signaling	1.59	IL33, SOCS3, IL1RL2, IL1RL1, STAT3, IL1R1, NFKB2
G-Protein Coupled Receptor Signaling	1.58	PDE8A, S1PR3, HRH2, PDE7B, CNR1, STAT3, NFKB2, AGTR2, AGTR1, PRKAG1, CAMK2G, OPRL1
Superpathway of Cholesterol Biosynthesis	1.51	FDF1, TM7SF2, GGPS1
Hematopoiesis from Multipotent Stem Cells	1.51	KITLG, THPO
Oleate Biosynthesis II (Animals)	1.51	CYB5A, FADS1
$\gamma$ -glutamyl Cycle	1.51	GCLM, ANPEP
Clathrin-mediated Endocytosis Signaling	1.45	DNM1, FGF21, ARPC1B, PIP5K1C, CHP1, DNMT3, SERPINA1, FGF7, RAB4B
Amyloid Processing	1.44	CAPN1, BACE2, PRKAG1, PSEN1
Cardiac $\beta$ -adrenergic Signaling	1.39	PDE8A, AKAP12, PPP1R10, PDE7B, PPP1R3C, GNG5, PRKAG1
Cholesterol Biosynthesis I	1.38	FDF1, TM7SF2
Cholesterol Biosynthesis II (via 24,25-dihydrolanosterol)	1.38	FDF1, TM7SF2
Cholesterol Biosynthesis III (via Desmosterol)	1.38	FDF1, TM7SF2
Insulin Receptor Signaling	1.37	SOCS3, PPP1R10, SGK1, PPP1R3C, IRS2, NCK1, PRKAG1
Oxidative Phosphorylation	1.37	NDUFS5, COX10, NDUFA7, SDHD, CYB5A, UQCRCQ
Triacylglycerol Biosynthesis	1.36	PPAPDC1B, PPAP2B, AGPAT1
TREM1 Signaling	1.34	TLR2, CCL7, STAT3, NFKB2
VDR/RXR Activation	1.33	IL1RL1, VDR, CCL5, RXRA, SULT2A1
Role of JAK2 in Hormone-like Cytokine Signaling	1.32	SOCS3, IRS2, STAT3
Vitamin-C Transport	1.32	SLC2A1, GSTO1
Human Embryonic Stem Cell Pluripotency	1.31	S1PR3, FZD4, KLK3, WNT2B, PDGFRA, WNT5A, BMP1

**Table S4. Related to Figure 5**

**Analysis of Pathways Regulated by Forskolin and A(70)-Bcl-2.** Enrichment analysis of canonical pathways based on a set of 205 probe sets upregulated in both, MEF cultures treated with forskolin and MEF cultures expressing A(70)-Bcl-2 (each versus control cells, paired Limma test  $p < 0.05$ ). All cells were transduced with an *Ascl1/RFP*- encoding vector. Analysis was done using Ingenuity Pathway Analysis software and significantly enriched terms ( $p < 0.05$ ) are shown.

## Supplemental Movies Legends

### Movie S1. Related to Figure 1

#### Time-Lapse of the Effect of Bcl-2 During Neuronal Reprogramming

Video example showing 150 h of astroglia-to-neuron conversion of cultures transfected with plasmids encoding *Ascl1/RFP* (cells in white, left) or *Ascl1/RFP+Bcl-2* (cells in white, right; see Figure 1A and 2F for more details).

### Movie S2. Related to Figure 1

#### DCX-GFP Reporter Expression in *Ascl1*- and *Ascl1/Bcl-2*-Mediated Reprogramming.

Video example showing 150 h of astroglia-to-neuron conversion of cultures co-transfected with the *Ascl1/RFP*- or *Ascl1/RFP+Bcl-2*-encoding plasmids (RFP is shown in white, right panels) and *DCX-GFP* (expression of GFP is shown in white, left panels).

### Movie S3. Related to Figure 4

#### Time-Lapse of the Effect of Fk During Neuronal Reprogramming.

Video example showing neuronal conversion of astroglial cultures transfected with the plasmid encoding for *Ascl1/RFP* (cells in white) and tracked for 150 h. On the right, cells were additionally treated with Fk (20  $\mu$ M) 5 h before the tracking time started (See Figure 1A for more details). The last frames of the movie show immunostaining for RFP (red) and  $\beta$ -III-tubulin (green).

## **Supplemental Experimental Procedures**

### **Transfection of Mouse Postnatal Astroglia Cultures**

For transfection DNA-liposome complexes were prepared in Optimem medium (Invitrogen) using the retroviral plasmids described below and Lipofectamine 2000 (Invitrogen). Astrocyte cultures were exposed to DNA-liposome complexes at a concentration of 0.5 µg DNA per 400 µl of Optimem medium for 4 hours and cultured after that in the differentiation medium as above. See (Heinrich et al., 2011)

For survival analysis of transfected cells after immunostaining we counted the total number of RFP+ cells at 5 DPT and normalized by the total number of RFP+ cells counted at day 1. To quantify the ratio of neurons/initial transfected cells we counted the proportion of RFP+/β-III-tubulin+ cells at 5 DPT and normalized by the whole population of RFP+ cells at 1 DPT.

### **Cell Cultures of Pericyte-Like Cells from Adult Human Cerebral Cortex**

After removal of the meninges, tissue was dissected and dissociated mechanically. Subsequently, cells were centrifuged for 5 min at 1000 rpm, re-suspended, and plated in a medium consisting of DMEM high glucose with GlutaMAX (Gibco), 20% fetal calf serum (Gibco), penicillin/streptomycin (Gibco). For reprogramming experiments cells were harvested and replated as described above after 2-3 weeks of expansion. See also (Karow et al., 2012)

### **Cell Cultures of Mouse Embryonic Fibroblasts (MEFs)**

MEFs were obtained from mouse embryos at day 14 gestation. Head, spine and viscera were removed and discarded (Vierbuchen et al., 2010). The remaining tissue was dissociated with 0.15% of trypsin, centrifuged for 5 min at 1300 rpm, re-suspended, and plated in a medium consisting of DMEM high glucose (3.5mM) with GlutaMAX (Gibco), 10% fetal calf serum (Gibco) and penicillin/streptomycin (Gibco) in 5% CO<sub>2</sub> and normoxygenated conditions. Fibroblasts were used for experiments after minimum 3 passages. For reprogramming experiments cells were harvested and replated as described above for astrocytes.

### **Glycolytic and Oxidative Media**

To force different metabolism during neuronal reprogramming, astrocytes were prepared and plated as previously described. At 24 hours after plating cells were either transfected with plasmid or infected with retroviral vectors and after further 24 hours medium was replaced with one of the following. (1) Control medium, composed of DMEM without sodium pyruvate or glucose (Gibco), supplemented with penicillin/streptomycin, B27 supplement (Gibco), glucose (4,5gr/l), sodium pyruvate (110mg/l); (2) Glycolysis-only (Glyco) medium, composed of DMEM without sodium pyruvate or glucose (Gibco), supplemented with penicillin/streptomycin, B27 supplement (Gibco), glucose (4,5gr/l), Oligomycin A (1µg/ml) (Gajewski et al., 2003). (3) Oxidative Phosphorylation-only (OxPhos) medium, composed of DMEM without sodium pyruvate or glucose (Gibco), supplemented with penicillin/streptomycin, B27 supplement (Gibco), sodium pyruvate (110mg/l), 2-Deoxy-D-glucose (5mM) (Candelario et al., 2013; Gajewski et al., 2003) .

### **Analysis of Redox State**

To evaluate general ROS we used the CellRox Green reagent from Molecular probes that acquires green fluorescence and nuclear localization via DNA binding upon oxidation. The procedure was accordingly with the manufacturer's specifications and the green reporter was finally detected by microscopy of living cells stained with DAPI.

To detect ROS production from astrocytes in the different metabolic conditions, cells were loaded with the Dihydroethidium dye (DHE, life tech), a superoxide indicator that when oxidized intercalates within the cell's DNA, staining its nucleus a bright fluorescent red. After 24 hours in the metabolic medium, cells were incubated for 15 minutes with DHE (30µM) at 37°C, then washed 3 times in 1x phosphate-buffered saline (PBS), fixed with 4% PFA for 5 minutes and fluoresce was detected by microscopy (see below).

For *in vitro* experiments the antioxidants  $\alpha$ Toc, Fk (Sigma) and/or calcitriol (Tocris) were supplemented once with the differentiation medium at 2 DPT/DPI in a final concentration of 0.5  $\mu$ M, 20  $\mu$ M and 70  $\mu$ g/ $\mu$ l, respectively.

### Plasmids and DNA Constructs

For the expression of neurogenic transcription factors we used self-inactivating retroviral vectors containing the actin promoter with the cytomegalovirus early enhancer element and the splice acceptor of the rabbit beta-globin gene (pCAG) driving the expression of the gene of interest (flag/myc-*Ascl1*, flag-*Neurog2*, *Bcl-2* or *Dlx-2*) linked to a fluorescent reporter by internal ribosomal entry site (IRES) as previously described (Heinrich et al., 2011). To follow the conversion process of astrocytes into neurons, we used a neuronal reporter plasmid with GFP driven by the doublecortin promoter (*DCX-GFP*) previously described (Franco et al., 2011). The mouse version of *Bcl-2* cDNA was obtained from Source BioScience (IRAVp968H01145D; pCMV-SPORT6.1-*Bcl-2*) and the human cDNA version (h-*Bcl-2*) from addgene (Plasmid number 8793; pMIG-*Bcl-2*-IRES-GFP) to generate RV-pCAG-flag/myc-*Ascl1*-IRES-*Bcl-2*, RV-pCAG-flag-*Neurog2*-IRES-*Bcl-2* or RV-pCAG-*Bcl-2*-IRES-GFP, which encodes for both *Bcl-2* and the reporter GFP. The *Bcl-2* mutants A-*Bcl-2* and EE-*Bcl-2* were produced by directed mutagenesis with the oligos 5'-ggctgccaggacggctcctcaggccctcgttg-3' (and complementary) and 5'-gggacatggctgccagggaggagcctcaggccctcgttgcc-3' (and complementary) respectively, to generate the vectors pCMV-SPORT6.1-A-*Bcl-2*, RV-pCAG-*Ascl1*-IRES-A-*Bcl-2* and RV-pCAG-*Neurog2*-IRES-A-*Bcl-2* and the corresponding EE-*Bcl-2* versions. Mutations were verified by sequencing. The murine *Vdr* was obtained from Sino Biological (MG51106-G, Vector pGEM-T) and sub-cloned in the retroviral vector to generate RV-pCAG-*Vdr*-IRES-GFP.

Viral vectors were produced with a vesicular stomatitis virus pseudotyping at titers of  $10^{6-9}$  and cells were infected about 24 hours after splitting as described above. Cells were allowed to differentiate in 16% O<sub>2</sub> and 9% CO<sub>2</sub>.

### Immunoblot Analysis

The cultures were lysed in RIPA buffer (10 mM Na<sub>2</sub>HPO<sub>4</sub>, pH 7.2, 150 mM NaCl, 1% sodium deoxicolate, 1% Nonidet P-40, 0.1% SDS) containing protease (Complete EDTA-free, Roche). Protein concentrations were determined with the BCA reagent from Interchim. Equal amounts of protein (50  $\mu$ g) were diluted in Laemmli Sample buffer containing  $\beta$ -mercaptoethanol (BioRad, 161-0747) and separated by polyacrylamide gel electrophoresis and transferred to polyvinylidene difluoride membranes (Pall; Life Sciences).

For the detection of *Prx1* the cells were previously incubated 15 min with PBS containing 100 mM N-ethylmaleimide (NEM, Sigma, E3876-5G) and collected in RIPA buffer also containing 100 mM NEM. In this case, samples were diluted in sample buffer without  $\beta$ -mercaptoethanol (Pierce, 84788).

Immunodetection of proteins was performed by standard procedures (ECL Prime Western Blotting Detection Reagent, Amersham).

### Immunocytochemistry

Cells were fixed in 4 % PFA in PBS for 10 min at room temperature (RT), washed in PBS and pretreated in 0.5% Triton X-100 in PBS for 30 min, followed by incubation in 2% BSA and 0.5% Triton X-100 in PBS for 30 min. Primary antibodies were incubated on specimen overnight at 4°C in 2% BSA, 0.5% Triton X-100 in PBS. The following primary antibodies were used: polyclonal anti-Green Fluorescent Protein (GFP, chicken, 1:1000, Aves Labs, *GFP-1020*), polyclonal anti-Glial Fibrillary Acidic Protein (GFAP, rabbit, 1:4000, DakoCytomation, *Z0334*), polyclonal anti-Red Fluorescent Protein (RFP, rabbit, 1:500, Chemicon, *AB3216*, or 1:2000, Rockland *600-401-379*), monoclonal anti  $\beta$ -III-tubulin (mouse IgG2b, 1:500, Sigma, T8660), monoclonal anti *Map2* (mouse IgG1, 1:500, Sigma, M4403), monoclonal anti NeuN (mouse IgG, 1:300, Millipore, MAB377), polyclonal anti V-Glut1 (rabbit, 1:500, SYSY, 135302), polyclonal anti synaptobrevin (SV, rabbit, 1:1000, SYSY). After washing in PBS, cells were incubated with appropriate species- or subclass-specific secondary antibodies conjugated to Cy<sup>TM</sup>2, Cy<sup>TM</sup>3, Cy<sup>TM</sup>5 (1:500, Jackson ImmunoResearch), Alexa Fluor 488 (1:500, Invitrogen), FITC (fluorescein isothiocyanate, 1:500, Jackson ImmunoResearch), TRITC (tetramethyl rhodamine isothiocyanate, 1:500, Jackson ImmunoResearch) or biotin (1:500, Jackson ImmunoResearch or Vector Laboratories) for 2h in the dark at room temperature, followed by extensive washing in PBS. Following treatment with secondary antibodies conjugated to biotin, cells were subsequently incubated for 2h at room temperature with DAPI (1:1000, Sigma) and AMCA streptavidin (1:200, Vector Laboratories) or Alexa Fluor 647 streptavidin (1:500, Sigma, D9542) and mounted with Aqua Poly/Mount (Polysciences, Warrington, PA).

## Luciferase assay

To test the activity of the Nrf2 pathway, we used a Nrf2-responsive luciferase construct obtained from Qiagen (kit CCS-5020). Accordingly with the described protocol, levels of Luciferase were normalized by the expression levels of a non-responsive construct encoding Renilla.

## Immunohistochemistry

Animals were anesthetized and transcardially perfused with PBS, followed by 4% PFA in PBS. Brains were post-fixed overnight, washed twice with PBS and embedded in 4% agarose/water. Finally, 60µm-thick coronal sections were cut using a vibrating microtome (Leica).

For immunohistology, sections were pre-incubated for 30 min in blocking solution (2% bovine serum albumin, 0.5% Triton X-100 in PBS). The following primary antibodies were diluted in blocking solution and incubated with the sections for 48 hours at 4°C: chick anti-GFP (1:500, Aves Labs, GFP-1020), rabbit anti-RFP (1:500, Rockland, 600-401-379) or goat mCherry (1:250, Acris, AB0081-200), mouse anti-NeuN (1:250, Chemicon, MAB377), rat Ctip2 (1:250, Abcam, Ab18465), rabbit Cux1 (1:250, Santa Cruz, sc-13024), mouse Satb2 (1:250, Abcam, 51502), goat FoxP2 (1:250, Santa Cruz, sc-81069). After washing in PBS, secondary antibodies were diluted in blocking solution and incubated at room temperature for 2 hours. Such antibodies were chosen according to the primary ones and were coupled to Alexa Fluor 488 or FITC, Cy3, Alexa Fluor 647 (Dianova). Sections were eventually counterstained with DAPI (1:500, Sigma) prior to mounting.

## RNA Extraction and Real Time Quantitative PCR (qRT-PCR)

RNA was extracted using RNeasy Plus Micro Kit (Qiagen) according to manufacturer's instructions, including removal of genomic DNA. RNA was retro-transcribed using SuperScriptIII Reverse Transcriptase and Random Primers (Roche). Each cDNA sample was diluted one to 5 and 1µl was used for each quantitative real time reaction. Real Time quantitative PCR (qPCR) was performed on a LightCycler480 instrument (Roche) using LightCycler Probe Master kit (Roche) and Monocolor Hydrolysis Probe (UPL) Probe (Roche) according to manufacturer's instructions (20µl final volume). The expression of each gene was analyzed in triplicate. Data were processed with the  $\Delta\Delta C_t$  method (Livak and Schmittgen, 2001). Quantification was performed on 3 independent biological samples.

## Microarray Analysis Procedure.

Total RNA (30 ng) was amplified using the Ovation Pico WTA System V2 in combination with the Encore Biotin Module (Nugen). Amplified cDNA was hybridized on Affymetrix Mouse Gene 2.0 ST arrays. Staining and scanning was done according to the Affymetrix expression protocol including minor modifications as suggested in the Encore Biotin protocol. Expression console was used for quality control and to obtain normalized RMA gene-level data. Statistical analyses were performed by utilizing the statistical programming environment R (Team, R. D. C., R: A language and environment for statistical computing. 2005) implemented in CARMAweb (Rainer et al., 2006). Genewise testing for differential expression was done employing the limma t-test. Sets of regulated genes were defined by  $p < 0.01$  (507 probe sets) or  $p < 0.05$  (1321 probe sets), including filters for fold change  $\geq 1.5x$  and average expression in at least one group in the dataset  $> 20$  arbitrary units. Heatmaps were generated with CARMAweb and pathway enrichment analyses were generated through the use of IPA (Ingenuity® Systems, [www.ingenuity.com](http://www.ingenuity.com)).

Array data has been submitted to GEO under the accession number GEO: GSE70921

## Microscopy

Immunostainings were analyzed with a LSM710 laser-scanning confocal or Axio Observer Z1 epifluorescence microscope (Carl Zeiss). Digital images were captured using the ZEN software (Carl Zeiss) and cell counts of all RFP/GFP immunoreactive cells performed with a 10X objective.

## Live Imaging Microscopy Analysis

For quantifications, cells were tracked in every frame and proliferation, neuronal conversion or cell death was analyzed for every single cell in each movie. For quantification of proportion of dead neurons or astrocytes we counted cells dying as positive events and classified them as neurons or astrocytes according to their morphology described in Figure 1. Next we add to this value the number of surviving cells (astrocytes or neurons in each group) at the end of the tracking period. This result is the total population for each lineage (dead + surviving astrocytes or neurons). Finally we normalized the proportion of dead neurons (counted as described) to the total population of neurons (calculated as described) and the same process was done for astrocytes.

## Patch-Clamp Method

Transfected GFP<sup>+</sup> or RFP<sup>+</sup> cells were recorded using the patch-clamp technique in the perforated-patch or whole-cell configurations. For the perforated-patch, fire-polished patch pipettes with 4-6 M $\Omega$  resistance were front-filled with intracellular solution containing Amphotericin B (0.33  $\mu$ g /ul) and backfilled with Amphotericin-free intracellular solution (in mM: 4 KCl, 2 NaCl, 0.2 EGTA, 135 K-Gluc, 10 HEPES, 4 ATP, 0.5 Na-GTP; pH = 7.3, 290 mOsm). Experiments were performed at room temperature with constant flow (2 ml/min) of the extracellular solution (in mM: 3 KCl, 140 NaCl, 2 CaCl<sub>2</sub>, 2 MgCl<sub>2</sub>, 10 HEPES, 5 Glucose; pH = 7.4, 305 mOsm). For the whole-cell configuration, the cells were kept in following extracellular solution (in mM: 125 NaCl, 3 KCl, 1.25 NaH<sub>2</sub>PO<sub>4</sub>, 25 NaHCO<sub>3</sub>, 25 D-Glucose, 0.4 Ascorbic acid, 2 CaCl<sub>2</sub>, 2 MgCl<sub>2</sub>; pH = 7.4, 310-330 mOsm) oxygenated by 95% O<sub>2</sub>/5% CO<sub>2</sub> with constant fluid flow (2ml/min) at room temperature. The cells were recorded at 5 days post-transfection in the whole-cell configuration (4-6 M $\Omega$  electrodes) with the following intracellular solution (in mM: 135 K-Gluconat, 4 KCl, 2 NaCl, 10 HEPES, 0.2 EGTA, 4 ATP, 0.5 NaGTP, 10 Phospho-Kreatin; pH = 7.3, 290-300 mOsm). The passive membrane properties were recorded using the membrane test paradigm of the pClamp software (Molecular Devices, Sunnyvale, CA, USA). In the voltage-clamp mode, a series of 10 mV rectangular pulse increments (50 ms long) ranging from -120 mV to +100 mV was used. Data were sampled at 10-30- $\mu$ s intervals and low-pass filtered at 2 kHz using the Axopatch 200B 4-pole Bessel filter (Molecular Devices). Leak currents were subtracted after the test pulse using five repeated 10 mV negative pulses from a holding potential of -120 mV. The current-voltage relation expressed the steady-state whole-cell current (at 40 ms of the rectangular pulse) as a function of the voltage command. In the current clamp, 1 second current injections of 10 pA increments were applied from 0 to 150 pA. All recorded cells were photographed both in the brightfield and the fluorescence using a CCD digital camera (Orca-D2, Hamamatsu, Herrsching, Germany).

## Quantifications and statistics

All error bars in this work indicate  $\pm$ SD. Statistical analyses were performed with GraphPad Prism 4 software by using t test or ANOVA with different post-hoc tests (Tukey's, Holm-Sidak's or Dunnett's). All the transfected cells from 3 coverslips were counted for each experiment with at least 3 independent experimental batches. Retroviral vector-transduced cells were quantified from five randomly chosen 10x fields in 3 different wells for each experiment in at least 3 independent experiments.

For *in vivo* experiments, pictures of the injected area were acquired with a confocal microscope (Zeiss) using 40x magnification. Cells infected by either one virus or both were quantified according to NeuN immunoreactivity, in animals treated and untreated with calcitriol or  $\alpha$ -Tocotrienol, with the open-source software Fiji (<http://fiji.sc/Fiji>). For the volume estimation, we applied the plugin Volumest on NeuN immunostaining of co-infected cells. The data were tested for significance using t test and one- or two-way ANOVA analysis (no repeated measurements) with Tukey's correction for multiple comparisons (Prism 6, GraphPad). Asterisks in the plot represent multiplicity adjusted P-values.

## Supplemental References

Candelario, K.M., Shuttleworth, C.W., and Cunningham, L.A. (2013). Neural stem/progenitor cells display a low requirement for oxidative metabolism independent of hypoxia inducible factor-1alpha expression. *J Neurochem* 125, 420-429.

- Franco, S.J., Martinez-Garay, I., Gil-Sanz, C., Harkins-Perry, S.R., and Muller, U. (2011). Reelin regulates cadherin function via Dab1/Rap1 to control neuronal migration and lamination in the neocortex. *Neuron* 69, 482-497.
- Gajewski, C.D., Yang, L., Schon, E.A., and Manfredi, G. (2003). New insights into the bioenergetics of mitochondrial disorders using intracellular ATP reporters. *Mol Biol Cell* 14, 3628-3635.
- Heinrich, C., Gascon, S., Masserdotti, G., Lepier, A., Sanchez, R., Simon-Ebert, T., Schroeder, T., Gotz, M., and Berninger, B. (2011). Generation of subtype-specific neurons from postnatal astroglia of the mouse cerebral cortex. *Nat Protoc* 6, 214-228.
- Karow, M., Sanchez, R., Schichor, C., Masserdotti, G., Ortega, F., Heinrich, C., Gascon, S., Khan, M.A., Lie, D.C., Dellavalle, A., *et al.* (2012). Reprogramming of pericyte-derived cells of the adult human brain into induced neuronal cells. *Cell Stem Cell* 11, 471-476.
- Rainer, J., Sanchez-Cabo, F., Stocker, G., Sturn, A., and Trajanoski, Z. (2006). CARMAweb: comprehensive R- and bioconductor-based web service for microarray data analysis. *Nucleic Acids Res* 34, W498-503.
- Vierbuchen, T., Ostermeier, A., Pang, Z.P., Kokubu, Y., Sudhof, T.C., and Wernig, M. (2010). Direct conversion of fibroblasts to functional neurons by defined factors. *Nature* 463, 1035-1041.

## **Aim of the study III**

The aim of the study is to investigate:

1. How astrocytes and neurons differ in term of metabolic properties and mitochondria composition, evaluating if mitochondria reorganization occurs during direct neuronal reprogramming and how manipulating mitochondrial proteome can affect neuronal conversion.

## **Mitochondrial reprogramming using dCas9 boosts glia-to-neuron conversion**

*Gianluca Luigi Russo*, Giovanna Sonsalla, Christopher Thomas Breunig, Juliane Merl-Pham, Sabine Schmitt, Martin Jastroch, Hans Zischka, Stefan Stricker, Stefanie M. Hauck, Giacomo Masserdotti and Magdalena Götz

For this paper I performed most of the experiments and analysed all the data, with the exception of the proteomic analysis done by Merl-Pham Juliane and Hauck M. Stephanie. I wrote and revised the first draft of the manuscript with Magdalena Götz, which was further reviewed and edited by us and all other authors.

*The project is finalized in a manuscript that will be submitted in the next month to Cell Stem Cell.*

*Note that due to elevated number of pages Table 1, Supplementary Table 1 and Supplementary Table 2 are not included in the PDF version of the thesis, but are available as separated excel files.*

## Mitochondrial reprogramming using dCas9 boosts glia-to-neuron conversion

Gianluca Luigi Russo<sup>1,2,3</sup>, Giovanna Sonsalla<sup>1,2,3</sup>, Christopher Thomas Breunig<sup>4,5</sup>, Juliane Merl-Pham<sup>6</sup>, Sabine Schmitt<sup>7</sup>, Martin Jastroch<sup>9,+</sup>, Hans Zischka<sup>7,8</sup>, Stefan Stricker<sup>4,5</sup>, Stefanie M. Hauck<sup>6,#</sup>, Giacomo Masserdotti<sup>1,2</sup> and Magdalena Götz<sup>1,2,10,#,\*</sup>

<sup>1</sup> Physiological Genomics, Biomedical Center, Ludwig Maximilians Universitaet Munich, Germany.

<sup>2</sup> Institute for Stem Cell Research, Helmholtz Center Munich, Neuherberg, Germany.

<sup>3</sup> Graduate School of Systemic Neurosciences, Biomedical Center, Ludwig Maximilians Universitaet Munich, Germany.

<sup>4</sup> MCN Junior Research Group, Munich Center for Neurosciences, Biomedical Center, Ludwig Maximilians Universitaet Munich, Germany.

<sup>5</sup> Epigenetic Engineering, Institute of Stem Cell Research, Helmholtz Zentrum, German Research Center for Environmental Health, Planegg-Martinsried, Germany.

<sup>6</sup> Research Unit Protein Science, Helmholtz Zentrum Munich, German Research Center for Environmental Health (GmbH), Munich, Germany.

<sup>7</sup> Institute of Molecular Toxicology and Pharmacology, Helmholtz Center Munich, Neuherberg; Institute of Toxicology and Environmental Hygiene, Technical University Munich, Munich, Germany.

<sup>7</sup> Institute of Toxicology and Environmental Hygiene, Technical University Munich, School of Medicine, 80802 Munich, Germany.

<sup>8</sup> Institute of Molecular Toxicology and Pharmacology, Helmholtz Center Munich, German Research Center for Environmental Health, 85764 Neuherberg, Germany.

<sup>9</sup> Helmholtz Diabetes Center & German Diabetes Center (DZD), Helmholtz Center Munich, Neuherberg; Division of Metabolic Diseases, Technical University, Munich, Germany.

<sup>10</sup> Excellence Cluster of Systems Neurology (SYNERGY), Munich, Germany.

<sup>+</sup>Present address: Department of Molecular Biosciences, The Wenner-Gren Institute, The Arrhenius Laboratories F3, Stockholm University, SE-106 91 Stockholm, Sweden.

<sup>#</sup> Co-Last authors

\*Corresponding author: [Magdalena.goetz@helmholtz-muenchen.de](mailto:Magdalena.goetz@helmholtz-muenchen.de)

### Abstract

Astrocyte to neuron conversion has developed into a promising avenue for neuronal replacement therapy. However, during the reprogramming process excessive ROS production causes death by ferroptosis. To ease the metabolic conversion process, we set out to determine the differences in the mitochondrial proteome of cortical neurons and astrocytes to then ask if inducing the expression of neuron-specific mitochondrial proteins may help the conversion. Proteome analysis of isolated intact and functional mitochondria revealed profound differences in the mitochondrial proteome of cortical astrocytes and neurons. During Neurogenin2- or Ascl1-induced reprogramming, neuron-specific mitochondrial proteins are typically induced 5-7 days post transduction, while astrocyte-specific mitochondrial proteins are only partly down-regulated at this stage. Thus, conversion of the mitochondrial proteome is incomplete and occurs late during the process. To improve the acquisition of neuron-specific mitochondrial hallmarks, we used dCas9 technology to induce e.g. Prdx2 and Sod1, enriched in neuronal mitochondria. This resulted not only in seven fold increased conversion into neurons, but also speeded up the process, as shown by continuous live imaging *in vitro*. Taken together, reprogramming mitochondria in a cell type-specific manner has powerful effects on astrocyte to neuron conversion, suggesting mitochondria to be a driving force for this conversion process.

## Introduction

The ability to regenerate lost neurons, after an injury or degenerative disease, is still a key challenge in the field of regenerative medicine. Several approaches to replace degenerated neurons are pursued, ranging from recruitment of endogenous cells or transplantation of neurons to the use of direct conversion of local glial cells for neuronal replacement (Barker et al., 2018; Grade and Götz, 2017). Indeed, direct glia-to-neuron reprogramming, first demonstrated after traumatic brain injury (Buffo et al., 2005), has become a viable option to replace functional neurons in different brain regions (Gascón et al., 2017; Heinrich et al., 2015; Li and Chen, 2016). However, the long-term survival of the induced neurons is still a major obstacle, and little is known about how adequate their metabolic conversion actually is. We have previously described the increased production of reactive oxygen species (ROS) during the conversion process reduces the efficiency of neuronal generation *in vitro* and *in vivo* (Gascón et al., 2016). The co-expression of Bcl2, or pharmacological application of ROS scavengers drastically improved the conversion and survival of induced neurons, but long-term survival of these neurons was still compromised.

Reactive oxygen species (ROS), highly reactive reduced forms of molecular oxygen, are physiological byproducts of the mitochondrial electron transport chain (ETC), possessing important signaling function but also harmful effects (Ito and Suda, 2014). For this reason, cells with strong reliance on oxidative phosphorylation (OxPhos), such as neurons (Harris et al., 2012), are likely to produce a higher amount of ROS, and hence require antioxidant scavengers to prevent excessive ROS-mediated damage. Surprisingly, neurons are extremely sensitive to oxidative stress, expressing antioxidative proteins at lower concentration and activity than astrocytes (Wang and Michaelis, 2010). The tight interplay of neurons with the surrounding astrocytes, which mostly rely on glycolysis, fatty acid oxidation and gluconeogenesis for cellular energy production (Bélanger et al., 2011; Panov et al., 2014), provides them with the substrates to survive in situations of intense metabolic activity (Fernandez-Fernandez et al., 2012). As such, in situation of stress, neurons are the first cells to die, while metabolically versatile astrocytes provide a first barrier to oxidative-damage (Burda and Sofroniew, 2014; Chen et al., 2009).

In direct neuronal reprogramming neurons are generated from different somatic cells. This involves for most cells a transition to higher ATP demand, thus an increase in Oxphos and mitochondrial activity, with the potential side effect of increased oxidative stress, previously observed during the process (Gascón et al., 2016). However, beyond regulating ROS levels and redox homeostasis, mitochondria perform a plethora of functions within the cell. As primary hub for metabolic regulation, mitochondria catabolize nutrients for energy production, generate precursors for macromolecule biosynthesis and manage metabolic waste (Spinelli and Haigis, 2018). All these functions have great impact on cell fate regulation. For example, amino acid metabolism and mitochondria-derived co-factors, or intermediates, such as NAD<sup>+</sup> and acetyl-CoA, together with redox-mediated signaling cascades, act as master regulators of transcriptional and epigenetic regulation of gene expression (Gascón et al., 2017; Janke et al., 2015; Lu and Thompson, 2012; Ryall et al., 2015). As metabolic functions differ amongst cell types (Folmes et al., 2012), specific mitochondrial proteins are likely to implement some of these cell type-specific functions (Calvo and Mootha, 2010; Pagliarini et al., 2008). It is thus surprising that the mitochondrial protein composition has hardly been explored at comprehensive level in different CNS cell types (Graham et al., 2017; Völgyi et al., 2015), with no mitochondrial proteome of astrocytes or any information about changes in mitochondrial proteins in direct neuronal reprogramming. While interesting results have been achieved by determining the mitochondrial proteome of different muscle cells (Murgia et al., 2015), most often mitochondria are examined in whole tissue or a mixture of cell types (Forner et al., 2006). Thus, the proteome of

mitochondria from cortical astrocytes and neurons has not yet been examined by unbiased, comprehensive proteome analysis.

Therefore, we set out here to determine the mitochondrial proteome of cortical neurons and astrocytes *in vitro*, to then explore the extent to which activating neuron-specific mitochondrial proteins may help the conversion process. This is achieved by employing dCas9-mediated transcriptional engineering, which allow targeting and regulating several genes simultaneously (Breunig et al., 2018a; Zhou et al., 2018).

## Results

### *Changes in mitochondria morphology in astrocyte to neuron reprogramming in vitro*

To better understand if astrocytes undergoing neuronal conversion not only change morphological, electrophysiological and transcriptional features, as previously described (Heinrich et al., 2010; Masserdotti et al., 2015), but also adapt their mitochondria and metabolism, we first monitored morphological changes of mitochondria during astrocyte-to-neuron reprogramming. Astrocytes isolated from postnatal day 5 murine cerebral cortex (Heinrich et al., 2011) were transduced with retroviral vectors containing the proneural factors *Ascl1* or *Neurog2* cDNA (Heinrich et al., 2010) and GFP targeted to mitochondria (*Ascl1*-IRES- mitoGFP, **Figure 1A**). Interestingly, the conversion from astrocytes to neurons was associated with profound remodeling of mitochondria. Astrocytes that fail to convert maintain their mitochondria in a tubular morphology, forming an elongated and ramified mitochondrial network (**Figure 1A, left**), indicative of higher rates of mitochondrial fusion, as also seen in astrocytes *in vivo* under physiological conditions (Motori et al., 2013). On the contrary, when astrocytes successfully convert into neurons, as indicated by morphological changes, acquisition of neuron-specific  $\beta$ -III-tubulin-immunoreactivity and downregulation of the astroglial protein gliafibrillary acidic protein (GFAP), the size of mitochondria notably decreased assuming mostly short and round morphology (**Figure 1A, right**). This is in line with *in vivo* data, showing smaller mitochondria and dynamic properties of higher fission in neurons, allowing them to reach and support the distant neuronal processes (Misgeld and Schwarz, 2017; Plucińska and Misgeld, 2016). Thus, direct neuronal reprogramming is accompanied by profound changes in mitochondrial morphology, most likely accompanying also profound functional changes (Gascón et al., 2016), prompting us to examine the mitochondrial proteome of astrocytes and neurons in an unbiased manner.

### *Cultured astrocytes and neurons from cerebral cortex differ in mitochondrial structure and function*

To determine the mitochondrial proteome of neurons and astrocytes, we used high purity neuron cultures derived from embryonic day (E) 14 cerebral cortex, cultured for 7 days (Walcher et al., 2013) and primary astrocyte cultures, obtained from postnatal P5 cerebral cortex, the same starting population used in our direct neuronal reprogramming protocol. First, we measured the Oxygen Consumption Rate (OCR) and the extracellular acidification, converted to Proton Production Rate (PPR), as measure for OxPhos and indicator for glycolytic rates respectively, in both cell types. As expected, we found profound differences between primary astrocytes and primary neurons, as highlighted by the different metabolic responses to stimuli in real-time, in both OCR and PPR (**Figure 1B**). Focusing on the basal metabolic rates, astrocytes showed higher basal OCR and PPR rates compared to neurons (**Figure 1C, 1D**). Of note, astrocytes can promptly compensate with glycolysis when mitochondrial ATP synthesis is blocked by oligomycin, while neuronal glycolytic capacity appears limited (**Figure 1E**). This conclusion is further corroborated by PPR rates when completely

blocking the ETC with rotenone and antimycin A, thus blocking TCA cycle acidification (**Figure 1F**). The OCR/PPR ratio reflects that neurons rely predominantly on OCR rather than on PPR for energy production, compared to astrocytes (**Figure 1G**).

Having confirmed the metabolic differences of cultured cortical astrocytes and neurons, we isolated functional mitochondria for proteome analysis through a cell fractionation-based method, as previously described (Schmitt et al., 2013, 2015) (**Figure S1A**). Mitochondria enrichment in the fraction of interest (**Figure 1H**, 9000g) was confirmed by Western Blot for mitochondrial proteins (*Complex I, II, III, IV, V, ANT*, residing in the inner mitochondrial membrane; *VDAC*, residing in the outer mitochondrial membrane; *CS*, residing in the mitochondrial matrix). Analysis of cytosolic (*GAPDH*, *tubulin*), nuclear (*H3*), lysosomal (*Lamp2*), endoplasmic reticulum (*Bip*) or peroxisomal (*Pmp70*) proteins showed their enrichment in the first two fractions (**Figure S1B**, 800g and S.N.). To verify that isolated mitochondria were functional and not damaged, we used Rhodamine 123, a cell-permeant, cationic green fluorescent dye that is sequestered in quench-mode by functional mitochondria. Indeed, the membrane potential of the mitochondria isolated from both neurons and astrocytes remained constant for at least 1 hour after the isolation (**Figure S1C**) and similar to previous data (Schmitt et al., 2013). Also the swelling parameter, measured by the absorbance at 540nm, showed a linear trend over time, indicative of intact/functional mitochondria (**Figure S1C**). Finally, ultrastructural analysis of the isolates by electron microscopy (EM) also showed largely intact mitochondria (**Figure 1I**). Mitochondrial isolates showed a higher purity when obtained from astrocytes compared to neurons, with some other organelles and debris present in neuronal samples (**Figure 1I**). This is most likely due to the complexity of isolating smaller mitochondria, tightly joined to cytoskeleton molecules, inside the thin neuronal processes. However, EM analysis confirmed that mitochondria from astrocytes are longer than the small and roundish neuronal mitochondria, as we also observed by immunofluorescent staining in the reprogrammed neurons (**Figure 1A**). Interestingly, mitochondrial complexity, in terms of *crisetae* and membrane invagination, was comparable between the two cell types, supporting our functional data on mitochondria activity (**Figure 1B**), indicative of their differentiated and mature phenotype.

### ***Astrocytes and neurons exhibit profound differences in the mitochondria proteome***

To determine the mitochondrial proteome we used liquid chromatography-tandem mass spectrometry (LC-MS/MS) of the isolates from 3 independent biological replicates (**Table S1**). This allowed the quantification of 798 of the 1158 proteins classified as mitochondrial by MitoCarta 2.0 (Calvo et al., 2016). Of these, 294 proteins were more abundant in astrocytes and 60 more abundant in neurons (p-value<0.05 and a two-fold enrichment, **Figure 2B**). The PCA analysis and the heatmap cluster analysis of the differentially enriched mitochondrial proteins show a high degree of similarity for the biological replicates (**Figure 2A, 2C**).

Gene Ontology (GO) term analysis (Genomatix Generanker) of the mitochondrial proteins significantly enriched in one of the cell types (**Figure 2D, S1D** for top 35 GO terms from biological processes and molecular functions, **Table S2** for complete list), revealed that the astrocyte-enriched mitochondrial proteome contains more proteins involved in *fatty acid catabolic process*, *fatty acid  $\beta$ -oxidation* and *lipid metabolic process*, which are relevant pathways for astrocytes also *in vivo* (van Deijk et al., 2017). Indeed, some of the top proteins specifically enriched in astrocyte-isolated mitochondria were *Acads* (Astrocytes versus Neurons (A/N) ratio=14,97, p-value=0,0008), *Cpt1a*, (A/N Ratio=13,63, p-value=0,0000), *Cpt2* (A/N Ratio =11,27, p-value=0,0002), *Acsf2* (A/N Ratio =9,39, p-value=0,0004); key regulators of lipid metabolism and fatty acid  $\beta$ -oxidation (**Table 1**). Furthermore, GO terms significantly enriched for astrocyte mitochondrial proteins comprise *cellular*

*respiration, mitochondrion organization and respiratory electron transport chain*, consistent with their higher energetic demand and metabolic rate *in vitro* (see also above).

Mitochondrial proteins enriched in neurons shared most of the GO terms with astrocytes, such as *small molecule metabolic process, carboxylic acid metabolic process* and *small molecules biosynthetic process*, indicative of functional and active mitochondria in both cell types. Interestingly *cholesterol biosynthetic process* was mostly characteristic for neuronal mitochondria. Important proteins highly abundant in neuronal mitochondria were glutaminase (Gls, A/N Ratio =0,04, p-value=0,0000), the primary enzyme for the production of glutamate from hydrolysis of glutamine and ammonia, as well as Acly (A/N Ratio =0,41, p-value=0,0003), involved in the production of cytosolic acetyl-CoA with a central role in regulating cell metabolism, signaling and epigenetic marks. These results support the different metabolic reliance of astrocytes and neurons, as also shown above by Seahorse analysis. The “molecular function” GO terms mirrored and explained the metabolic pathways of both cell types represented in the selectively enriched mitochondrial proteome (**Figure S1D**).

Supporting our observation that astrocytes have elongated mitochondria compared to reprogrammed neurons (**Figure 1A**), the mitochondria fusion protein Mitofusin 1 (MFN1) was enriched in astrocytes (A/N Ratio =5,97, p-value=0,0123). Conversely, neurons are enriched for the fission master regulator Dynamin related protein Dnm1l (Drp1, A/N ratio=0,12, p-value=0,0000; see **Table 1**). Notably, the GO terms *cellular oxidant detoxification, oxidation-reduction process and oxidoreductase activity* are among the most commonly represented in the mitochondrial proteome of both cell types (**Table S2**). This highlights that astrocytes and neurons use different proteins to respond to exogenous and endogenous oxidative stress, whose molecular function does not necessarily overlap. For example, some of the top enriched anti-oxidant molecules in astrocytes are Gpx1 (A/N ratio=9,37, p-value=0,0205) and Gpx4 (A/N ratio=3,23, p-value=0,0032), while neurons have much more Prdx2 (A/N ratio=0,35, p-value=0,0021) and Sod1 (A/N ratio=0,38 p-value=0,0313; see **Table 1**).

This raises the intriguing question whether the neuron-specific antioxidant proteins may be specifically required during the direct conversion process, as antioxidant defense has been identified as critical in direct neuronal reprogramming *in vitro* and *in vivo* (Gascón et al., 2016).

### ***Mitochondrial protein changes during astrocyte-to-neuron reprogramming***

As mitochondrial proteins have so far not been examined in direct neuronal reprogramming, we aimed to determine whether astrocytes down-regulate their characteristic mitochondrial proteins and induce the expression of neuron-specific ones during the process of fate conversion. We chose mitochondrial proteins that can be reliably detected by immunostaining and/or play crucial functional roles (**Table 1**).

For example, Sfxn5 is a mitochondrial transporter of citrate (Miyake et al., 2002), an essential intermediate of the TCA cycle derived from condensation of oxaloacetate and acetyl-CoA, and is enriched in mitochondria isolated from astrocytes. Accordingly, it was detected by immunocytochemistry in mitochondria of GFAP<sup>+</sup> astrocytes that were not transduced or were still GFAP<sup>+</sup> at 3 days post infection (DPI) with the proneural factor Neurogenin 2 (hereafter Neurog2, **Figure 3A**, arrowhead). Astrocytes that acquire neuronal  $\beta$ -III-tubulin and lose GFAP-immunoreactivity instead show decreased Sfxn5-immunostaining over time (**Figure 3A**, arrow, 5 DPI, 7 DPI). However, 60% of these converting astrocytes still retain Sfxn5 protein (**Figure S4A, S4B**), even though at lower levels than surrounding astrocytes (**Figure 3A**, arrow). Thus, down-regulation of Sfxn5 is incomplete, at least within 7 DPI, and reprogrammed neurons show some degree of heterogeneity in switching to the neuronal mitochondrial proteins.

Conversely, immunoreactivity for the astrocyte-enriched protein Cpx was down-regulated faster and more efficiently during the reprogramming process, as it was detectable only in 30% of GFAP-negative cells (arrow) at 5 DPI (**Figure S2A, S4C**), and almost undetectable in converted neurons at 7 DPI (**Figure S2A, arrow; Figure S4C**). Notably, also astrocytes that fail to convert to neurons, but still overexpress the transcription factor, largely lose expression of the astrocyte-specific Cpx protein (**Figure S4C**), while surrounding astrocytes do not (**Figure S2A, arrowhead**). Thus, astrocytes failing to reprogram appear to be in an intermediate metabolic state retaining some mitochondrial hallmarks of their original identity. Notwithstanding, these non-reprogrammed astrocytes do not up-regulate any of the neuronal mitochondrial marker proteins analyzed (**Figure S4D, S4E, S4F**).

We also investigated if and when reprogrammed neurons express neuron-specific mitochondrial proteins. To this end, we analyzed the expression of Prdx2 and Gls. Prdx2, which catalyzes the reduction of peroxides and hence protects from oxidative stress (Boulos et al., 2007), was not expressed at detectable levels until 5 DPI in Neurog2-expressing cells undergoing reprogramming (**Figure S2B, arrow**). However, by 7 DPI up of 80% of reprogrammed neurons had acquired Prdx2 immunoreactivity (**Figure S4F**).

Instead glutaminase, the enzyme regulating glutamine metabolism and glutamate neurotransmitter levels (Márquez et al., 2009), was up-regulated at earlier stages in converting neurons. It was detectable already at 3 DPI (**Figure 3B, arrow**) in neurons induced either by Ascl1 or Neurog2 induced cells (**Figure 3B, S3B, S4D, S4E**), and was present in virtually all transduced neurons by 7 DPI (**Figure S4D, S4E**). Gls and Prdx2 were instead virtually absent in astrocytes that failed to reprogram, at all time-points analyzed (**Figure S2B, arrowhead, Figure S4D, S4E, S4F**).

Notably, the down-regulation of Sfxn5 and up-regulation of Gls follow similar dynamics in the conversion process (starting at 3 DPI and further progressing at 5 DPI) independently on the neurogenic reprogramming factor used (Neurog2 or Ascl1, **Figure 3, Figure S3, Figure S4**). This is interesting as our proteome was performed with cortical neurons i.e. largely with glutamatergic neurons, but also induction of GABAergic neurons with Ascl1 (Masserdotti et al., 2015) shows increase in Gls. We further noticed that neuron-specific mitochondrial proteins are higher in reprogrammed neurons with more mature morphologies (**Figure 3B, Figure S2B**), suggesting that the acquisition of a proper neuronal mitochondrial proteome may continue with prolonged maturation (e.g. further down-regulation of astrocyte-specific proteins, such as Cpx or Sfxn5, **Figure S4A, S4B, S4C**). Importantly, however, our data show that changes in mitochondrial proteins occur in a relatively uncoordinated manner (astrocyte-specific often fail to be down-regulated despite up-regulation of neuron-specific ones) and at a late stage during the conversion process (5-7 DPI). Moreover, our data suggest that astrocytes undergoing conversion to neurons pass through an intermediate stage (around 3-5 DPI), when some astrocyte-specific mitochondrial proteins are already down-regulated (Cpx), while neuron-specific mitochondrial proteins have not yet increased much (like Prdx2). This prompted us to examine whether inducing neuron-specific mitochondrial proteins along with the proneural factors, e.g. providing them from the beginning of the reprogramming process, may improve the conversion speed or efficiency.

### ***dCas9-mediated induction of neuron-specific mitochondrial proteins potently improves speed and efficiency of direct neuronal reprogramming***

To examine if the early expression of specific neuronal mitochondrial proteins in astrocytes undergoing reprogramming would improve the process, we took advantage of the recently developed STAgR technique that allows expressing a series of gRNAs targeting different genes in one vector (Breunig et al., 2018b). This approach combines deactivated Cas9 (dCas9) with the VPR

transcriptional activator, which targets promoter regions of selected genes through gRNAs sequences, to induce endogenous expression (Chavez et al., 2015). As astrocytes and neurons possess cell-specific mitochondrial proteins to respond to oxidative stress and coping with oxidative stress is a key factor in the neuronal reprogramming (Gascón et al., 2016), we first focused on neuron-specific antioxidant proteins as potential candidates to improve reprogramming. We therefore selected the neuronal specific proteins Sod1 and Prdx2, important regulators of oxidative stress in physiological and pathological conditions (Boulos et al., 2007) and most abundant anti-oxidant proteins in neuronal mitochondria (**Table 1**). We chose gRNAs targeting the promoter of these genes as previously described (Breunig et al., 2018a) and cloned the respective gRNAs in a newly developed construct with a GFP reporter, which is only activated in the presence of both the self-transcribed gRNAs (e.g. for Sod1) and dCas9-VPR, i.e. when cells are co-transduced (**Figure 4A**). The specificity of the reporter is based on a minimal CMV promoter and the target sequences of one of the gRNAs included in the vector (here Sod1 or scrambled gRNA target for control)(**Figure 4A**).

We first examined the extent of Sod1 and Prdx2 mRNA induction after co-transfection of cortical astrocytes with dCas9-VPR and the respective gRNAs or control (scrambled gRNAs combined with inducible GFP). Sod1 and Prdx2 mRNA levels were increased 15x and 11x respectively compared to the control in astrocytes sorted by FACS for GFP, 48 hours after transfection (**Figure 4B**). Subsequently, we transfected dCas9-VPR and the inducible GFP construct carrying the gRNAs targeting Sod1 and Prdx2 promoters (STAgR P-S), or alternatively control gRNAs (STAgR Cntrl), together with the reprogramming vector Ascl1-RFP, and examined neuronal conversion 6 days after transfection (**Figure 4C**). Strikingly, we observed a seven-fold increase in the proportion of induced neurons; from 5% with only Ascl1-RFP and control gRNAs to over 35%, when Ascl1-RFP was combined with STAgR P-S (**Figure 4C, 4E**). These data suggest that neuron-specific anti-oxidant mitochondrial proteins are needed during the neuronal conversion process and their earlier and/or higher expression strongly improves reprogramming.

This prompted the question whether neuronal conversion occurs faster or simply at the same speed but with more cells converting or more converted cells surviving (see Gascón et al., 2016). To test these possibilities, we took advantage on continuous single cell live imaging following the conversion process, as previously described (Costa et al., 2011). Images were taken in bright field every 10 minutes, and in GFP/RFP every 3 hours, over a period of 6 days. Transfected cells acquiring a neuronal morphology (criteria as in Gascón et al., 2016: processes longer than 3x cell soma) could be observed around 60 hours after transduction (**Figure 4D**). However, astrocytes co-transfected with Ascl1-RFP and STAgR P-S speeded up the neuronal differentiation with significantly more neuronal cells present at 90 hours after transduction (**Figure 4D**). Examples illustrating the hugely different level of neuronal maturation in the two conditions are depicted in **Figure 4E**. Importantly, while the cells with upregulated neuron-specific anti-oxidant proteins linearly increased neuronal generation up to 110 hours, Ascl1-RFP control cells turning into neurons reached a *plateau* fast and often died shortly after (**Figure 4D**). Thus, the early expression of neuron-specific anti-oxidant mitochondrial proteins promotes the speed of astrocyte-to-neuron conversion and improves their survival, thereby significantly improving the conversion efficiency. Taken together, reprogramming the mitochondrial proteome along with respective fate determinants potently improves fate conversion.

## Discussion

Mitochondrial performance is key for neuronal survival and function, as also evident from neurodegenerative disease often caused by mitochondrial defects (Fernandez-Fernandez et al., 2012; Willems et al., 2015). Furthermore, mitochondrial function affects epigenetic, transcriptional and

signaling cascades (Janke et al., 2015; Spinelli and Haigis, 2018), highlighting the importance of a investigating the cell-type-specific mitochondrial proteome (Johnson et al., 2007). Given the importance of mitochondria function, it is surprising how little is known about cell-type-specific mitochondrial composition and its changes in direct neuronal reprogramming. Our data demonstrate profound differences in the mito-proteome of cortical neurons and astrocytes and their uncoordinated and partial regulation during reprogramming. This is clearly different from gradual timely-regulated metabolic changes from neural stem cells via transit-amplifying progenitors to neurons in normal neurogenesis during development and in adulthood (Khacho et al., 2016). Accordingly, the use of dCas9-mediated transcriptional engineering to promote neuron-specific mitochondrial protein acquisition potentially improved the conversion process.

*Cell-type-specific mitochondrial proteome reveals profound differences between astrocytes and neurons related to specific metabolic pathways*

Cultured astrocytes showed flexible metabolic profile, as they rely on OxPhos but are able to compensate with high glycolytic capacity when required, as also observed *in vivo* (Panov et al., 2014; Supplie et al., 2017). Conversely, neurons did not demonstrate this potential, but mostly relied on OxPhos for energy production, as observed evaluating the OCR/PPR ratio (**Figure 1G**). Supporting this, neurons express key enzymes necessary to activate glycolysis at lower levels (Herrero-mendez et al., 2009; Zheng et al., 2016), while astrocytes respond better to energy deprivation (Lovatt et al., 2007). Notably, extracellular flux analysis using the Seahorse device revealed that both cultured cell types were close to the maximal rate of their metabolism under basal conditions, limiting spare respiratory capacity (**Figure 1B**). For astrocytes, this may be explained at least partially by proliferation (Heins et al., 2002), which is linked to energetically demanding catabolic and anabolic reactions, enhancing metabolic requirements (Ito and Suda, 2014; Lunt and Vander Heiden, 2011). In the case of the neurons, this could be attributed to the fact that they are cultured in the absence of other glial cells, especially astrocytes, that metabolically support neurons *in vivo* (Bélanger et al., 2011; Chen et al., 2009; Diaz et al., 2012; Weber and Barros, 2015) and assist to respond to higher oxidative stress (Schreiner et al., 2015). For our purpose this was useful, as it allowed to determine the proteome of mitochondria at full functional capacity with supposedly all proteins needed present.

Indeed, the mitochondrial proteome of the cultured neurons and astrocytes revealed profound differences in several cell-type-specific pathways (see **Table S2**). For example, some of the top GO terms enriched in the mitochondrial proteome of cortical astrocytes are *lipid metabolism* and *fatty acid  $\beta$ -oxidation*, demonstrating distinct specialization of astrocytic mitochondria. Indeed, this is also consistent with expression analysis at the RNA level in adult astrocytes (van Deijk et al., 2017; Hofmann et al., 2017). Despite controversial reports, this pathway seems to provide astrocytes with higher amount of ATP and co-factors, when sustained oxygen availability occurs, compared to glycolysis (Panov et al., 2014; Perevoshchikova et al., 2013; Schönfeld and Reiser, 2013; Souza et al., 2019). Yet, astrocytes seemingly derive 20% of brain energy supply by  $\beta$ -oxidation (Panov et al., 2014) and our *in vitro* data suggest a contribution of 30% when blocking this pathway by  $\beta$ -etomoxir (*data not shown*). This raises the interesting question if it would be beneficial for derived neurons, e.g. in direct reprogramming, to maintain a high capacity of this pathway, even though they clearly need to activate other pathways for fast and efficient ATP generation.

During endogenous neurogenesis key enzymes of the fatty acid metabolism, such as carnitine palmitoyltransferase 1a (Cpt1a), are not only highly expressed in astrocytes (**Table 1**) (Zhang et al., 2014), but also in adult neural stem cells (NSCs) where they regulate quiescence (Knobloch et al., 2017), and are down-regulated when neurons are generated. Thus, the conversion of the metabolism is

regulated gradually during neurogenesis, while it is largely unknown how these enzymes are regulated during transcription factor induced astrocyte to neuron reprogramming. For example, Cpt1a is not yet down-regulated by 48 hours in astrocytes converting into neurons (Gascón et al., 2016; Masserdotti et al., 2015, Masserdotti et al., *unpublished data*), suggesting a relatively slow metabolic conversion.

Interestingly, however, the mitochondrial proteome isolated from astrocytes is also enriched in proteins linked to *cellular respiration*, *mitochondrion organization* and *respiratory electron transport chain* compared to neurons. This fits to the recent observation that reactive astrocytes require OxPhos and complex I-V (Fiebig et al., 2019), and *in vitro* cultured astrocytes resemble reactive astrocytes (Götz et al., 2015). In comparison to neurons that mostly rely only on OxPhos (Bélanger et al., 2011; Kasischke et al., 2004) (*present data*), this enrichment in astrocytes seems surprising. However, astrocytes, as feeder cells for neurons, require higher energy metabolism to function (Bélanger et al., 2011; Bouzier-Sore and Pellerin, 2013; Chuquet et al., 2010), while neurons also express proteins reducing glycolysis in other conditions which further restrict their energetic sustainability (Herrero-mendez et al., 2009; Khacho et al., 2016).

Importantly, however, most of these differences are quantitative, meaning that e.g. the proteins involved in the ETC are more abundant in astrocytes, but also present in neurons (see **Table 1**). Indeed, when comparing the mitochondrial proteome composition of different cell types, between 50% and 70% of the mitochondrial proteins are common (51% of mitochondrial proteins within a 2-fold change between astrocytes and neurons in our analysis, see **Table S1**) and expressed at similar levels (Mootha et al., 2003; Pagliarini et al., 2008), with ETC subunits among the less variable proteins (Calvo and Mootha, 2010). However, also subtle differences in ETC subunit assembly, beyond their relative abundance, differentiate astrocytes and neurons functionally (Lopez-Fabuel et al., 2016). Most importantly, direct neuronal reprogramming provides a read-out to determine which of these differences matter.

### Promoting neuronal fate conversion by early reprogramming of the mitochondrial proteome

When monitoring individual mitochondrial proteins that were differentially enriched in astrocytes versus neurons, we observed only partial down-regulation of astrocyte-enriched and relatively late up-regulation of neuron-enriched proteins. One of the markers tested was glutaminase, which is also functionally relevant, as it catalyzes the hydrolysis of glutamine to glutamate and ammonia and is involved in generating neurotransmitters in neurons (Albrecht et al., 2010). Thus, the expression of this enzyme represents a further step towards the acquisition of specific neuronal metabolic function in induced neurons. Interestingly, these changes in metabolic and mitochondrial enzymes were only detected in astrocytes that actually convert to neurons, but not in those that fail to do so. This is also the reason why a comprehensive mitochondrial proteome analysis of reprogrammed cells is difficult to determine – not only due to the limited number of cells, but also due to the heterogeneity in reprogramming outcome. This heterogeneous response can also be observed in the transduced astrocytes that fail to convert, as some of them down-regulate astrocyte-specific mitochondrial proteins, while others maintain them. As they do not acquire neuronal mitochondrial markers, many are in a confused metabolic state that may hinder reprogramming. This could explain, why our converse strategy, i.e. the up-regulation of neuron-specific mitochondrial proteins, is more successful in neuron induction, thereby overcoming unsuccessful reprogramming.

We analyzed the expression of cell-specific mitochondrial proteins (Sfxn-5, CpoX, Prdx2, Gls) and found that differences emerged earliest at 3 DPI with most neuron-specific mitochondrial proteins

being induced only at 5 DPI (**Figure S4**). Given the fast induction of neuronal genes within a few hours (Masserdotti et al., 2015) and the change to neuronal morphology and neuronal proteins already by 2-3 days, neuron-specific mitochondrial proteins appear to lag behind. For instance, Prdx2 is detectable in converting neurons only starting from 5 DPI. However, as Prdx2 is a neuron-specific anti-oxidant protein protecting neurons from oxidative stress (Boulos et al., 2007), its late expression may be one reason why increased ROS levels cause cell death during direct neuronal reprogramming (Gascón et al., 2016).

As *oxidation-reduction process* and *cellular oxidant detoxification* are also highly significant GO terms in the cell-type-specific mitochondrial proteome analysis of neurons and astrocytes, we examined the effects of the early co-expression of neuronal mitochondrial proteins, with known antioxidant functions, in the reprogramming process. To achieve this, we exploited the recently developed STAgR and dCas9 technology (Chavez et al., 2015), allowing synchronous overexpression of multiple endogenous targets. We selected two known antioxidant neuronal proteins, Sod1 and Prdx2, mostly involved in detoxification of superoxide and hydrogen peroxide, that when mutated lead to severe neurodegenerative diseases (Bunton-Stasyshyn et al., 2015; Hu et al., 2011).

Interestingly we could prove, through time-lapse experiments, that selective overexpression of these two proteins in astrocytes turning into neurons could greatly help the reprogramming process, most likely acting both on cell survival and neuronal maturation. This implies that modification of the mitochondrial proteome of astrocytes converting into neurons might not only be a phenotypic consequence of a cellular change, but directly a driving force for the conversion process. Cas9 technology offers great advantages for direct neuronal reprogramming, as recently demonstrated by *in vivo* (Zhou et al., 2018) and *in vitro* (Black et al., 2016) studies. It will be important to understand whether the powerful increase in reprogramming speed and efficiency achieved here by activating only 2 neuron-specific mitochondrial proteins is specific or also true for others. Genome-wide screening of mitochondrial proteins via CRISPR technology, as demonstrated for the OxPhos genes (Arroyo et al., 2016), could help answering this question and determining the mitochondrial proteins that are most relevant for this fate conversion.

Excitingly, our data further corroborate the concept that the metabolic conversion is a key driver, not only a consequence, of fate conversion. This is supported by the much faster conversion to a neuronal morphology when Sod1 and Prdx2 were up-regulated from the onset of proneural gene expression. Thus, when these neuron-specific antioxidant proteins are not yet up-regulated the conversion process stalls and possibly aborts, despite the expression of a multitude of anti-oxidant proteins in astrocytes. It will be fascinating to determine how Sod1 and Prdx2 may speed up the acquisition of neuronal morphology at a mechanistic level, but most important for now, they hugely improve the conversion process.

## **Acknowledgements**

We are very grateful to the excellent technical assistance of Tatiana Simon-Ebert and Andrea Steiner-Mezzadri (BMC, Munich) and to Daniel Brandt (Helmholtz Zentrum, Munich) for his great technical support with the Seahorse analyzer. We thank Uli Ohmayer (Helmholtz Zentrum, Munich) for initial support with the proteomic analysis. We are especially grateful to Thomas Misgeld and Caroline Fecher (Technical University of Munich) for providing the antibodies against Sfxn5 and Glis. We thank Nicola Mattugini for precious inputs on manuscript. This work was funded by the German Research Foundation SFB 870, SPP1757 (to M.G.), the advanced ERC ChroNeuroRepair (to M.G.), and ERAnet (to M.G.).

## **Author Contributions**

M.G. conceived and designed the project. G.L.R. shaped the project and performed most of the experiments and analysis. G.S. contributed to some immunostainings. C.B. and S.S. provided the CRISPR Cas expertise, developed and designed the STAgR approach, and C.B. helped with cloning of the constructs. J.M-P. and S.M.H. provided the proteomic expertise, experiments and analysis. S.S. and H.Z. performed the mitochondrial isolation and electron microscopy. M.J. provided expertise in metabolism and Seahorse analysis. G.M. provided expertise and training of G.L.R. in reprogramming and was also involved in directing the project together with M.G. G.L.R. and M.G. wrote the manuscript and all authors contributed corrections and comments.

## **Declaration of interests**

The authors declare no conflict of interests.

## **Materials and Method**

### **Primary Astrocytes cultures and neuronal reprogramming**

Astrocytes were isolated and cultured as described previously (Heins et al., 2002). After removal of the meninges, grey matter tissue from P5–P7 cerebral cortex of C57BL/6J mice was dissected and dissociated mechanically. Subsequently, cells were centrifuged for 5 min at 1,300 rpm, re-suspended, and plated in a T25 flask in medium consisting of DMEM/F12 (Gibco), 10% fetal bovine serum (Gibco), penicillin/streptomycin (Gibco), and supplemented with B27 (Gibco), 10 ng/mL epidermal growth factor (EGF, Roche), 10 ng/mL fibroblast growth factor 2 (FGF2, Roche). Cells were passaged when confluence was reached after 7-10 days using trypsin/EDTA (Gibco) and plated on poly-D-lysine (Sigma-Aldrich, Munich, Germany) coated glass coverslips at a density of 80,000 cells per coverslip (in 24-well plates; BD Biosciences,) in the same medium. The vast majority of the cells (>90%) in these cultures were positive for glial fibrillary acidic protein (GFAP) as previously described. One day after transduction or transfection (see below), the medium was replaced with neuronal differentiation medium, containing B27, but lacking FBS, EGF and FGF. At 6 or 7 days after transfection or transduction cells were fixed and immunostained.

### **Primary neuronal cultures**

Cerebral cortices were dissected from embryonic day (E) 14 mice as described before (Hartfuss et al., 2001). Cortices were isolated, meninges removed and the samples mechanically dissociated in HBSS medium containing 10mM Hepes, on ice. Subsequently cells were digested for 15 min in trypsin-EDTA (0,05%), and subsequently centrifuged for 5 min at 1,000 rpm. The pellet was further mechanically dissociated and resuspended in Neurobasal Medium (Gibco, 21103-049), supplemented with Glutamax (100x), penicillin/streptomycin (Gibco), and B27 (Gibco). Cells were counted and plated at a density of 600,000 cells in 6-well plated (BD Biosciences) pre-coated with poly-D-lysine (Sigma-Aldrich). After one week in culture, cells had differentiated mostly into mature neurons, with high purity and little contamination by other cell types (data not shown).

### **Transfection and Transduction**

For transfection DNA-liposome complexes were prepared in Optimem medium (Invitrogen) using the retroviral plasmids described below and Lipofectamine 2000 (Invitrogen). Astrocytes culture were exposed to DNA-liposome complexes at a concentration of 0.6 µg DNA per 400 µl of Optimem medium for 3 hours and cultured in differentiation medium, as described above. For STAGR experiments a ratio of 2 : 1 : 1 was used respectively for dCas9-VPR : STAGr (Cntrl or P-S): Asc11 (or dsRed). For transduction of astrocytes, seeded astrocytes were infected with 1ul of virus one day after plating, before changing with fresh differentiation medium 24 hours after.

### **Mitochondria isolation and characterization**

Mitochondria isolation from cultured astrocytes and neurons was performed as previously described (Schmitt et al., 2013) using the pump-controlled cell rupture method; a cell homogenizer (Isobiotec, Germany) combined with 1-ml Luer Lock Gas-Tight Syringes (4.608 mm i.d., SGE Supelco, USA) and a high-precision pump (Pump 11, Harvard Apparatus, USA). The homogenizer was precooled on ice to ensure cooling of the samples during the isolation, the tungsten carbide ball (6µm diameter) was inserted and the homogenizer was equilibrated with isolation buffer (300 mM sucrose, 5 mM TES, and 200 µM ethyleneglycoltetraacetic acid [EGTA], pH 7.2). The sample of dissociated astrocytes or neurons was added to 1 ml of isolation buffer and passed three (neurons) to six (astrocytes) times through the system at a constant rate (700 µl/min). To recover the homogenate, the system was rinsed once with 1 ml of isolation buffer. The sample preparation and the tunable parameters of the PCC, such as the clearance and the number of strokes, were optimized for each sample. Yield and

functionality (mitochondrial transmembrane potential,  $\Delta\psi_m$ ) of the isolated mitochondria were used to assess the optimal parameters. Around 1 million astrocytes and neurons respectively were used to obtain a sufficient amount of mitochondria for further processing. The pooled homogenate was cleared from cell debris and nuclei by centrifugation ( $800\times g$ , 5 min at 4 °C), and mitochondria were pelleted at  $9000\times g$  (10 min at 4 °C). After the isolation, the syringes were rinsed three or four times with double distilled water (ddH<sub>2</sub>O). The tungsten carbide ball and the cell homogenizer were cleaned with isopropanol followed by ddH<sub>2</sub>O to allow processing of the next sample without contamination.

### Mitochondria characterization

The functional analysis of isolated mitochondria was performed by measuring Rhodamine 123 (Rh123) fluorescence quenching to determine  $\Delta\psi_m$  and measuring absorbance change at 540nm (Synergy 2, BioTek, USA) to determine mitochondrial swelling; as described previously (Schmitt et al., 2013). Protein concentrations were determined by the Bradford assay. For immunoblotting analysis, 10  $\mu$ g of protein was subjected to sodium dodecyl sulfate-polyacrylamide gel electrophoresis (SDS-PAGE), and separated proteins were transferred onto a polyvinylidene fluoride (PVDF) membrane. Equal protein loading and proper transfer were controlled by Ponceau red staining. Primary and secondary antibodies for Western Blot analysis are listed below.

Species	Primary Antibodies	Dilution	Company, Cat. Number	Mol. weight
Rabbit	Lamp2	1:2000	Invitrogen, 51-2200	100kDa
Rabbit	H3	1:1000	Cell Signaling, 96495	17kDa
Mouse	Bip	1:500	BD Pharmingen, 610978/9	78kDa
Rabbit	GAPDH	1:2000	Cell Signaling, 2118	42kDa
Mouse	$\alpha$ -tubulin	1:8000	Sigma–Aldrich, T5168	50kDa
Rabbit	Pmp70	1:500	Acris, SP5237P	70kDa
Rabbit	CS	1:5000	Novus Biologicals, NBP2-13878	50kDa
Rabbit	VDAC	1:1000	Cell Signaling, 4866	33kDa
Goat	ANT	1:250	Santa Cruz, sc.9299	30kDa
Mouse	Cytochrome I Complex	1:500	Abcam, ab110413	20kDa
Mouse	Cytochrome II Complex	1:500	Abcam, ab110413	30kDa
Mouse	Cytochrome III Complex	1:500	Abcam, ab110413	47kDa
Mouse	Cytochrome IV Complex	1:500	Abcam, ab110413	39kDa
Mouse	Cytochrome V Complex	1:500	Abcam, ab110413	53kDa
Species	Secondary Antibodies	Dilution	Company, Cat. Number	
Horse	Anti mouse, HRP linked	1:1000	Cell Signaling, 7076	
Goat	Anti rabbit, HRP linked	1:1000	Cell Signaling, 7074	
Donkey	Anti goat, HRP linked	1:1000	Santa Cruz, sc-2020	

Electron microscopy analysis of the isolated mitochondria was done as described previously (Zischka et al., 2007). ZE-FFE-separated mitochondrial fractions were immediately pelleted, fixed in 2.5% glutaraldehyde, post-fixed with 1% osmium tetroxide, dehydrated with ethanol and embedded in Epon. Ultrathin sections were negative stained with uranyl acetate and lead citrate and then analyzed on a Zeiss EM 10 CR electron microscope.

### Seahorse experiments

Primary cortical astrocytes or neurons were plated onto XF24 V3 PET cell culture microplates from Seahorse biosciences, pre-coated with PDL, and analyzed the day after plating. Cells were seeded at 20000, 30000, 50000 for neurons; and 15000, 25000 or 40000 for astrocytes. The final cell number was assessed by counting DAPI<sup>+</sup> nuclei and measuring DNA content to normalize the data to  $\mu$ g DNA or 1000 cells. Before measuring cellular respiration, cells were washed twice with assay medium (XF

DMEM + 25 mM glucose) and then incubated in 750  $\mu$ L of assay medium for 10 min in an air incubator without CO<sub>2</sub> at 37°C. The XF24 plate was then transferred to the XF24 Extracellular Flux analyzer (Seahorse Bioscience). Basal respiration was determined with 4-5 assay cycles (2 min mix, 2 min measuring), and for each of the parameters obtained after respective drug application. For the measurement of different mitochondrial respiration states, oligomycin (5  $\mu$ g/ml) was used to inhibit the ATP synthase, followed by FCCP (1  $\mu$ M) to induce *maximal substrate oxidation capacity*, and a cocktail containing rotenone (5  $\mu$ M) and antimycin A (2  $\mu$ M) to inhibit ETC activity and determine non-mitochondrial oxygen uptake. *Spare respiratory capacity* was determined by subtracting maximum from basal respiration values. Finally, 2-deoxyglucose (2-DG, 100mM) was added to block glycolysis. Extracellular acidification rate (ECAR) was converted to proton production rate (PPR) based on machine algorithms and buffer capacity of the medium. Basal PPR was measured averaging 3 to 5 values prior to oligomycin treatment. *Oligomycin-dependent PPR* determines the peak values of PPR during mitochondrial Oxphos inhibition.

### **Proteome analysis**

Per sample 10  $\mu$ g of isolated mitochondria were used. SDS was added to a final concentration of 2% for efficient solubilization, prior to tryptic protein digest using a modified FASP protocol (Wiśniewski et al., 2009). Proteomic measurements were performed on a Q-Exactive HF mass spectrometer (Thermo Scientific) online coupled to an Ultimate 3000 nano-RSLC (Dionex). Peptides were separated on a C18 nanoEase MZ HSS T3 column (100Å, 1.8  $\mu$ m, 75  $\mu$ m x 250 mm; Waters) in a 95 min non-linear acetonitrile gradient. Precursor (scan range 300 – 1500 m/z) and TOP10 fragment spectra of charges 2-7 were acquired in the orbitrap mass detector of the mass spectrometer, at resolutions of 60000 and 15000 respectively with each a maximum injection time of 50 ms and a dynamic exclusion of 30 s. The individual raw-files were loaded to the Proteome discoverer 2.2 software (Thermo scientific) allowing for peptide identification and label-free quantification using the Minora node. Searches were performed using Sequest HT as search engine in the Swissprot mouse database with the following search settings: 10 ppm precursor tolerance, 0.02 Da fragment tolerance, two missed cleavages allowed, carbamidomethyl on cysteine as fixed modification, deamidation of glutamine and asparagine allowed as variable modification, as well as oxidation of methionine and Met-loss combined with acetylation at the N-terminus of the protein. Proteins were quantified by summing up abundances of allocated unique and razor peptides; resulting protein abundances are given in supplementary table 1. Mitochondrial proteins were classified using the mitoCARTA 2.0 database (Calvo et al., 2016). Fold-change values were obtained from protein abundances across three independent biological replicates for each cell type, subsequently dividing astrocytes over neuronal values. Identified proteins were considered as enriched in neurons if fold-change value was < 0.5, and enriched in astrocytes if fold-change value was > 2. All selected proteins were considered as significantly different considering the three biological replicates showing a p-value <0.05 (unpaired t-test on individual proteins after imputation of missing values).

Principal components analysis was done in Perseus software (Tyanova et al., 2016) on the log<sub>2</sub> ratios of mitochondrial protein abundances in the individual samples to the median protein abundance across all samples. Heatmap analysis of the same ratios was performed using Cluster 3.0 software (Eisen et al., 1998). The distance matrix was calculated using the 'Euclidean distance' setting. Hierarchical clustering was completed using the 'complete linkage' algorithm. The resultant tree and heatmap were visualized with Java Treeview ([http://www.eisenlab.org/eisen/?page\\_id=42](http://www.eisenlab.org/eisen/?page_id=42)). Pathway enrichment analysis on significantly differentially abundant mitochondrial proteins per cell type was conducted applying GeneRanker (Genomatix). Significantly enriched molecular functions and biological processes (p<0.01) were exported and are given in supplementary table 2.

### **Immunocytochemistry**

Cells were fixed in 4% PFA in PBS for 10 min at room temperature (RT), washed in PBS twice for 5 minutes, and stored up to a month at 4°C before staining. Specimen were incubated in primary antibodies (at the concentration listed below) in PBS containing 2% Bovine Serum Albumine (BSA) and 0.5% Triton X-100 overnight at 4°C. After washing in PBS, cells were incubated with appropriate species- or subclass-specific secondary antibodies, with or without DAPI diluted 1:10.000, for 1h in the dark at room temperature. Optionally, after washing twice for 5 minutes with PBS, biotin-labeled secondary antibodies were used at a dilution of 1:200 for 1hour, followed by streptavidin coupled fluorophores (1:500). Coverslip were then mounted with Aqua Poly/Mount (Polysciences, Warrington, PA) and samples were imaged at the LSM710 laser-scanning confocal or Axio observer Z1 epifluorescence microscope (Carl Zeiss). Digital images were acquired using the ZEN software (Carl Zeiss) at 40X or 20x.

The following primary and secondary antibodies were used:

<b>Species</b>	<b>Primary Antibodies</b>	<b>Dilution</b>	<b>Company</b>	<b>Catalog Number</b>
Mouse IgG2b	β-III-Tubulin	1:100	Sigma	T8660
Rabbit	GFAP	1:400	Dako	Z0334
Mouse IgG1	GFAP	1:400	Sigma	G3893
Rat	RFP	1:300	Chromotek	5F8
Chicken	GFP	1:300	Aves Labs	GFP-1020
Rabbit	CPOX	1:200	Abcam	Ab169766
Rabbit	Prdx2	1:100	Provided by Sergio Gascon	
Rabbit	Gls	1:100	Proteintech	20170-1-AP
Rabbit	Sfxn5	1:200	Abcam	Ab172971
<b>Reactivity</b>	<b>Secondary Antibodies</b>	<b>Dilution</b>	<b>Company</b>	<b>Catalog Number</b>
Mouse IgG2b	Alexa Fluor 488	1:1000	Invitrogen	A21141
Chicken	Alexa Fluor 488	1:1000	ThermoFisher	SA5-10026
Rat	Cy3	1:1000	Dianova	112-165-167
Mouse IgG2b	A 633	1:1000	Invitrogen	A21146
Mouse IgG1	A647	1:1000	Invitrogen	A21240
Rabbit	Alexa Fluor 488	1:1000	Invitrogen	A21206
Mouse IgG1	Biotin	1:250	Biozol	1070-08
Streptavidin	A Fluor 405	1:500	Invitrogen	S32351

### **Fluorescence-activated cell sorting**

Astrocytes 48 hours after transfection with gRNAs and dCas9 were trypsinized and sorted for GFP positive cells, using the FACSaria III (BD Bioscience) system at high purity mode and a flow rate lower than 1200 cells per second. Forward and side scatter were adjusted to exclude cell debris and include only GFP positive cells, that were detected by 488nm laser-assisted excitation. 15.000 cells were sorted directly in RLT buffer (QIAGEN), to enhance RNA quality and efficiency, for subsequent extraction and qRT-PCR.

### **RNA Extraction and Real Time Quantitative PCR (qRT-PCR)**

RNA was extracted using RNeasy Plus Micro Kit (Qiagen) according to manufacturer's instructions, including removal of genomic DNA. RNA was retro-transcribed using SuperScriptIII Reverse Transcriptase and Random Primers (Roche). Each cDNA sample was diluted 1:5 and 1µl was used for each quantitative real time reaction. Real Time quantitative PCR (qPCR) was performed on a LightCycler480 instrument (Roche) using LightCycler Probe Master kit (Roche) and Monocolor

Hydrolysis Probe (UPL) Probe (Roche) according to manufacturer's instructions (20 $\mu$ l final volume). The expression of each gene was analyzed in triplicate. Data were processed with the  $\Delta\Delta$ Ct method (Livak and Schmittgen, 2001). Quantification was performed on 3 independent biological samples.

### **STAGr and gRNAs production**

gRNAs were designed to target in close proximity to the transcription start site of of Sod1 and Prdx2. All STAGr vectos were designed and produced as previously described (Breunig et al., 2018a).

### **Live-Imaging Microscopy**

Time-lapse video microscopy was performed with a cell observer (Zeiss) at a constant temperature of 37°C and 8% CO<sub>2</sub>. Phase-contrast images were acquired every 10 min and fluorescence pictures every 3 hrs for 6 days using a 10 $\times$  phase contrast objective (Zeiss) and an AxioCam HRm camera with a self-written VBA module remote controlling Zeiss AxioVision 4.7 software. Movies were assembled and analyzed using ImageJ (NIH) software.

### **Quantification and Statistics**

To analyze reprogramming efficiency with dCas9 experiments, the proportion of GFP<sup>+</sup>/RFP<sup>+</sup>/ $\beta$ -III-tubulin<sup>+</sup> cells was assessed at 6 DPT and normalized to the entire population of transduced GFP<sup>+</sup>/RFP<sup>+</sup> cells. For time lapse experiment quantification, cells were tracked in every frame of the movie. GFP<sup>+</sup>/RFP<sup>+</sup> cells acquiring neuronal morphology, considered as appearance of processes longer than 3x the cell soma, were quantified out of the total GFP<sup>+</sup>/RFP<sup>+</sup> cells, as previously published (Gascón et al., 2016). When virus was used to induce neuronal conversion, astrocytes were fixed at day1, day3, day5 and day7 after transduction, corresponding to different stages of neuronal maturation and glial dedifferentiation, to verify cell-specific mitochondrial markers appearance and disappearance.

Statistic analysis of data was performed using the GraphPad Prism 7.0 software. Data in Figure 1C, 2B, 4C are plotted as median  $\pm$  IQR; each dot represents one biological replicate. Data in Figure 1B, 4B, 4D are plotted as mean  $\pm$  SD as they are normally distribution according to the Shapiro-Wilk test. If not rejected, we performed unpaired two-tailed t-test analysis for group comparison. If normal distribution was rejected, significance between groups was analyzed using Kruskal Wallis test, followed by Mann-Whitney test. Significance is based on the P-value indicated on the figures as \* p $\leq$ 0.05, \*\* p $\leq$ 0.01, \*\*\*p $\leq$ 0.001.

### **References**

- Albrecht, J., Sidoryk-Węgrzynowicz, M., Zielińska, M., and Aschner, M. (2010). Roles of glutamine in neurotransmission. *Neuron Glia Biol.* 6, 263–276.
- Arroyo, J.D., Jourdain, A.A., Calvo, S.E., Ballarano, C.A., Doench, J.G., Root, D.E., and Mootha, V.K. (2016). A Genome-wide CRISPR Death Screen Identifies Genes Essential for Oxidative Phosphorylation. *Cell Metab.* 24, 875–885.
- Barker, R.A., Götz, M., and Parmar, M. (2018). New approaches for brain repair-from rescue to reprogramming. *Nature* 557, 329–334.
- Bélanger, M., Allaman, I., and Magistretti, P.J. (2011). Brain energy metabolism: Focus on Astrocyte-neuron metabolic cooperation. *Cell Metab.* 14, 724–738.
- Black, J.B., Adler, A.F., Wang, H.-G., D'Ippolito, A.M., Hutchinson, H.A., Reddy, T.E., Pitt, G.S., Leong, K.W., and Gersbach, C.A. (2016). Targeted Epigenetic Remodeling of Endogenous Loci by CRISPR/Cas9-Based Transcriptional Activators Directly Converts Fibroblasts to Neuronal Cells. *Cell Stem Cell* 19, 406–414.
- Boulos, S., Meloni, B.P., Arthur, P.G., Bojarski, C., and Knuckey, N.W. (2007). Peroxiredoxin 2 overexpression protects cortical neuronal cultures from ischemic and oxidative injury but not

glutamate excitotoxicity, whereas Cu/Zn superoxide dismutase 1 overexpression protects only against oxidative injury. *J. Neurosci. Res.* *85*, 3089–3097.

Bouzier-Sore, A.K., and Pellerin, L. (2013). Unraveling the complex metabolic nature of astrocytes. *Front Cell Neurosci* *7*, 179.

Breunig, C.T., Durovic, T., Neuner, A.M., Baumann, V., Wiesbeck, M.F., Köferle, A., Götz, M., Ninkovic, J., and Stricker, S.H. (2018a). One step generation of customizable gRNA vectors for multiplex CRISPR approaches through string assembly gRNA cloning (STAgR). *PLoS One* *10*–12.

Breunig, C.T., Neuner, A.M., Giehl-Schwab, J., Wurst, W., Götz, M., and Stricker, S.H. (2018b). A Customizable Protocol for String Assembly gRNA Cloning (STAgR). *JoVE* e58556.

Buffo, A., Vosko, M.R., Erturk, D., Hamann, G.F., Jucker, M., Rowitch, D., and Gotz, M. (2005). Expression pattern of the transcription factor Olig2 in response to brain injuries: Implications for neuronal repair. *Proc. Natl. Acad. Sci.* *102*, 18183–18188.

Bunton-Stasyshyn, R.K.A., Saccon, R.A., Fratta, P., and Fisher, E.M.C. (2015). SOD1 Function and Its Implications for Amyotrophic Lateral Sclerosis Pathology. *Neurosci.* *21*, 519–529.

Burda, J.E., and Sofroniew, M. V. (2014). Reactive gliosis and the multicellular response to CNS damage and disease. *Neuron* *81*, 229–248.

Calvo, S.E., and Mootha, V.K. (2010). The Mitochondrial Proteome and Human Disease. *Annu. Rev. Genomics Hum. Genet.* *11*, 25–44.

Calvo, S.E., Clauser, K.R., and Mootha, V.K. (2016). MitoCarta2.0: an updated inventory of mammalian mitochondrial proteins. *Nucleic Acids Res.* *44*, D1251–D1257.

Chavez, A., Scheiman, J., Vora, S., Pruitt, B.W., Tuttle, M., P R Iyer, E., Lin, S., Kiani, S., Guzman, C.D., Wiegand, D.J., et al. (2015). Highly efficient Cas9-mediated transcriptional programming. *Nat. Methods* *12*, 326–328.

Chen, P.-C., Vargas, M.R., Pani, A.K., Smeyne, R.J., Johnson, D.A., Kan, Y.W., and Johnson, J.A. (2009). Nrf2-mediated neuroprotection in the MPTP mouse model of Parkinson’s disease: Critical role for the astrocyte. *Proc. Natl. Acad. Sci.* *106*, 2933–2938.

Chuquet, J., Quilichini, P., Nimchinsky, E.A., and Buzsaki, G. (2010). Predominant Enhancement of Glucose Uptake in Astrocytes versus Neurons during Activation of the Somatosensory Cortex. *J. Neurosci.* *30*, 15298–15303.

Costa, M.R., Ortega, F., Brill, M.S., Beckervordersandforth, R., Petrone, C., Schroeder, T., Götz, M., and Berninger, B. (2011). Continuous live imaging of adult neural stem cell division and lineage progression in vitro. *1068*, 1057–1068.

van Deijk, A.-L.F., Camargo, N., Timmerman, J., Heistek, T., Brouwers, J.F., Mogavero, F., Mansvelter, H.D., Smit, A.B., and Verheijen, M.H.G. (2017). Astrocyte lipid metabolism is critical for synapse development and function in vivo. *Glia* *65*, 670–682.

Diaz, F., Garcia, S., Padgett, K.R., and Moraes, C.T. (2012). A defect in the mitochondrial complex III, but not complex IV, triggers early ROS-dependent damage in defined brain regions. *Hum. Mol. Genet.* *21*, 5066–5077.

Eisen, M.B., Spellman, P.T., Brown, P.O., and Botstein, D. (1998). Cluster analysis and display of genome-wide expression patterns. *Proc. Natl. Acad. Sci. U. S. A.* *95*, 14863–14868.

Fernandez-Fernandez, S., Almeida, A., and Bolaños, J.P. (2012). Antioxidant and bioenergetic coupling between neurons and astrocytes. *Biochem. J.* *443*, 3–11.

Fiebig, C., Keiner, S., Ebert, B., Schäffner, I., Jagasia, R., Lie, D.C., and Beckervordersandforth, R. (2019). Mitochondrial Dysfunction in Astrocytes Impairs the Generation of Reactive Astrocytes and Enhances Neuronal Cell Death in the Cortex Upon Photothrombotic Lesion. *Front. Mol. Neurosci.* *12*, 40.

Folmes, C.D.L., Dzeja, P.P., Nelson, T.J., and Terzic, A. (2012). Metabolic Plasticity in Stem Cell Homeostasis and Differentiation. *Cell Stem Cell* *11*, 596–606.

Fornier, F., Foster, L.J., Campanaro, S., Valle, G., and Mann, M. (2006). Quantitative proteomic comparison of rat mitochondria from muscle, heart, and liver. *Mol. Cell. Proteomics* *5*, 608–619.

Gascón, S., Murenu, E., Masserdotti, G., Ortega, F., Russo, G.L., Petrik, D., Deshpande, A., Heinrich, C., Karow, M., Robertson, S.P., et al. (2016). Identification and Successful Negotiation of a Metabolic Checkpoint in Direct Neuronal Reprogramming. *Cell Stem Cell* *18*, 1–14.

Gascón, S., Masserdotti, G., Russo, G.L., and Götz, M. (2017). Direct Neuronal Reprogramming: Achievements, Hurdles, and New Roads to Success. *Cell Stem Cell* *21*, 18–34.

Götz, M., Sirko, S., Beckers, J., and Irmeler, M. (2015). Reactive astrocytes as neural stem or

progenitor cells: In vivo lineage, In vitro potential, and Genome-wide expression analysis. *Glia* *63*, 1452–1468.

Grade, S., and Götz, M. (2017). Neuronal replacement therapy: previous achievements and challenges ahead. *Regen. Med.* *2*.

Graham, L.C., Eaton, S.L., Brunton, P.J., Atrih, A., Smith, C., Lamont, D.J., Gillingwater, T.H., Pennetta, G., Skehel, P., and Wishart, T.M. (2017). Proteomic profiling of neuronal mitochondria reveals modulators of synaptic architecture. *Mol. Neurodegener.* *12*, 77.

Harris, J.J., Jolivet, R., and Attwell, D. (2012). Synaptic Energy Use and Supply. *Neuron* *75*, 762–777.

Hartfuss, E., Galli, R., Heins, N., and Götz, M. (2001). Characterization of CNS Precursor Subtypes and Radial Glia. *Dev. Biol.* *229*, 15–30.

Heinrich, C., Blum, R., Gascón, S., Masserdotti, G., Tripathi, P., Sánchez, R., Tiedt, S., Schroeder, T., Götz, M., and Berninger, B. (2010). Directing Astroglia from the Cerebral Cortex into Subtype Specific Functional Neurons. *PLoS Biol.* *8*, e1000373.

Heinrich, C., Gascón, S., Masserdotti, G., Lepier, A., Sanchez, R., Simon-Ebert, T., Schroeder, T., Götz, M., and Berninger, B. (2011). Generation of subtype-specific neurons from postnatal astroglia of the mouse cerebral cortex. *Nat. Protoc.* *6*, 214–228.

Heinrich, C., Spagnoli, F.M., and Berninger, B. (2015). In vivo reprogramming for tissue repair. *Nat. Cell Biol.* *17*, 204–211.

Heins, N., Malatesta, P., Cecconi, F., Nakafuku, M., Tucker, K.L., Hack, M.A., Chapouton, P., Barde, Y.A., and Götz, M. (2002). Glial cells generate neurons: The role of the transcription factor Pax6. *Nat. Neurosci.* *5*, 308–315.

Herrero-mendez, A., Almeida, A., Fernández, E., Maestre, C., Moncada, S., and Bolaños, J.P. (2009). The bioenergetic and antioxidant status of neurons is controlled by continuous degradation of a key glycolytic enzyme by APC / C – Cdh1. *Nat. Cell Biol.* *11*, 747–754.

Hofmann, K., Rodriguez-Rodriguez, R., Gaebler, A., Casals, N., Scheller, A., and Kuerschner, L. (2017). Astrocytes and oligodendrocytes in grey and white matter regions of the brain metabolize fatty acids. *Sci. Rep.* *7*, 10779.

Hu, X., Weng, Z., Chu, C.T., Zhang, L., Cao, G., Gao, Y., Signore, A., Zhu, J., Hastings, T., Greenamyre, J.T., et al. (2011). Peroxiredoxin-2 protects against 6-hydroxydopamine-induced dopaminergic neurodegeneration via attenuation of the apoptosis signal-regulating kinase (ASK1) signaling cascade. *J. Neurosci.* *31*, 247–261.

Ito, K., and Suda, T. (2014). Metabolic requirements for the maintenance of self-renewing stem cells. *Nat. Rev. Mol. Cell Biol.* *15*, 243–256.

Janke, R., Dodson, A.E., and Rine, J. (2015). Metabolism and Epigenetics. *Annu. Rev. Cell Dev. Biol.* *31*, 473–496.

Johnson, D.T., Harris, R.A., Blair, P. V., and Balaban, R.S. (2007). Functional consequences of mitochondrial proteome heterogeneity. *Am. J. Physiol. Physiol.* *292*, C698–C707.

Kasischke, K.A., Vishwasrao, H.D., Fisher, P.J., Zipfel, W.R., and Webb, W.W. (2004). Neural activity triggers neuronal oxidative metabolism followed by astrocytic glycolysis. *Science* (80-. ). *305*, 99–103.

Khacho, M., Clark, A., Svoboda, D.S., Azzi, J., Maclaurin, J.G., Meghaizel, C., Sesaki, H., Lagace, D.C., Germain, M., Harper, M.-E., et al. (2016). Mitochondrial Dynamics Impacts Stem Cell Identity and Fate Decisions by Regulating a Nuclear Transcriptional Program. *Cell Stem Cell* *19*, 1–16.

Knobloch, M., Pilz, G.-A., Ghesquière, B., Kovacs, W.J., Wegleiter, T., Moore, D.L., Hruzova, M., Zamboni, N., Carmeliet, P., and Jessberger, S. (2017). A Fatty Acid Oxidation-Dependent Metabolic Shift Regulates Adult Neural Stem Cell Activity. *Cell Rep.* *20*, 2144–2155.

Li, H., and Chen, G. (2016). In Vivo Reprogramming for CNS Repair: Regenerating Neurons from Endogenous Glial Cells. *Neuron* *91*, 728–738.

Livak, K.J., and Schmittgen, T.D. (2001). Analysis of Relative Gene Expression Data Using Real-Time Quantitative PCR and the 2- $\Delta\Delta$ CT Method. *Methods* *25*, 402–408.

Lopez-Fabuel, I., Le Douce, J., Logan, A., James, A.M., Bonvento, G., Murphy, M.P., Almeida, A., and Bolaños, J.P. (2016). Complex I assembly into supercomplexes determines differential mitochondrial ROS production in neurons and astrocytes. *Proc. Natl. Acad. Sci. U. S. A.* *113*, 13063–13068.

Lovatt, D., Sonnewald, U., Waagepetersen, H.S., Schousboe, A., He, W., Lin, J.H.-C., Han, X., Takano, T., Wang, S., Sim, F.J., et al. (2007). The transcriptome and metabolic gene signature of

protoplasmic astrocytes in the adult murine cortex. *J. Neurosci.* *27*, 12255–12266.

Lu, C., and Thompson, C.B. (2012). Metabolic regulation of epigenetics. *Cell Metab.* *16*, 9–17.

Lunt, S.Y., and Vander Heiden, M.G. (2011). Aerobic Glycolysis: Meeting the Metabolic Requirements of Cell Proliferation. *Annu. Rev. Cell Dev. Biol.* *27*, 441–464.

Márquez, J., Tosina, M., de la Rosa, V., Segura, J.A., Alonso, F.J., Matés, J.M., and Campos-Sandoval, J.A. (2009). New insights into brain glutaminases: Beyond their role on glutamatergic transmission. *Neurochem. Int.* *55*, 64–70.

Masserdotti, G., Gillotin, S., Sutor, B., Drechsel, D., Irmeler, M., Jørgensen, H.F., Sass, S., Theis, F.J., Beckers, J., Berninger, B., et al. (2015). Transcriptional Mechanisms of Proneural Factors and REST in Regulating Neuronal Reprogramming of Astrocytes. *Cell Stem Cell* *17*, 74–88.

Misgeld, T., and Schwarz, T.L. (2017). Mitostasis in Neurons: Maintaining Mitochondria in an Extended Cellular Architecture. *Neuron* *96*, 651–666.

Miyake, S., Yamashita, T., Taniguchi, M., Tamatani, M., Sato, K., and Tohyama, M. (2002). Identification and characterization of a novel mitochondrial tricarboxylate carrier. *Biochem. Biophys. Res. Commun.* *295*, 463–468.

Mootha, V.K., Bunkenborg, J., Olsen, J. V, Hjerrild, M., Wisniewski, J.R., Stahl, E., Bolouri, M.S., Ray, H.N., Sihag, S., Kamal, M., et al. (2003). Integrated analysis of protein composition, tissue diversity, and gene regulation in mouse mitochondria. *Cell* *115*, 629–640.

Motori, E., Puyal, J., Toni, N., Ghanem, A., Angeloni, C., Malaguti, M., Cantelli-Forti, G., Berninger, B., Conzelmann, K.K., Götz, M., et al. (2013). Inflammation-induced alteration of astrocyte mitochondrial dynamics requires autophagy for mitochondrial network maintenance. *Cell Metab.* *18*, 844–859.

Murgia, M., Nagaraj, N., Deshmukh, A.S., Zeiler, M., Cancellara, P., Moretti, I., Reggiani, C., Schiaffino, S., and Mann, M. (2015). Single muscle fiber proteomics reveals unexpected mitochondrial specialization. *EMBO Rep.* *16*, 387–395.

Pagliarini, D.J., Calvo, S.E., Chang, B., Sheth, S.A., Vafai, S.B., Ong, S.-E., Walford, G.A., Sugiana, C., Boneh, A., Chen, W.K., et al. (2008). A Mitochondrial Protein Compendium Elucidates Complex I Disease Biology. *Cell* *134*, 112–123.

Panov, A., Orynbayeva, Z., Vavilin, V., and Lyakhovich, V. (2014). Fatty Acids in Energy Metabolism of the Central Nervous System. *Biomed Res. Int.* *2014*, 1–22.

Perevoshchikova, I. V, Quinlan, C.L., Orr, A.L., Gerencser, A.A., and Brand, M.D. (2013). Sites of superoxide and hydrogen peroxide production during fatty acid oxidation in rat skeletal muscle mitochondria. *Free Radic. Biol. Med.* *61*, 298–309.

Plucińska, G., and Misgeld, T. (2016). Imaging of neuronal mitochondria in situ. *Curr. Opin. Neurobiol.* *39*, 152–163.

Ryall, J.G., Cliff, T., Dalton, S., and Sartorelli, V. (2015). Metabolic Reprogramming of Stem Cell Epigenetics. *Cell Stem Cell* *17*, 651–662.

Schmitt, S., Saathoff, F., Meissner, L., Schropp, E.M., Lichtmanegger, J., Schulz, S., Eberhagen, C., Borchard, S., Aichler, M., Adamski, J., et al. (2013). A semi-automated method for isolating functionally intact mitochondria from cultured cells and tissue biopsies. *Anal. Biochem.* *443*, 66–74.

Schmitt, S., Eberhagen, C., Weber, S., Aichler, M., and Zischka, H. (2015). Isolation of Mitochondria from Cultured Cells and Liver Tissue Biopsies for Molecular and Biochemical Analyses. In *Methods in Molecular Biology* (Clifton, N.J.), pp. 87–97.

Schönfeld, P., and Reiser, G. (2013). Why does Brain Metabolism not Favor Burning of Fatty Acids to Provide Energy? - Reflections on Disadvantages of the Use of Free Fatty Acids as Fuel for Brain. *J. Cereb. Blood Flow Metab.* *33*, 1493–1499.

Schreiner, B., Romanelli, E., Liberski, P., Ingold-Heppner, B., Sobottka-Brillout, B., Hartwig, T., Chandrasekar, V., Johannssen, H., Zeilhofer, H.U., Aguzzi, A., et al. (2015). Astrocyte Depletion Impairs Redox Homeostasis and Triggers Neuronal Loss in the Adult CNS. *Cell Rep.* *12*, 1377–1384.

Souza, D.G., Almeida, R.F., Souza, D.O., and Zimmer, E.R. (2019). The astrocyte biochemistry. *Semin. Cell Dev. Biol.*

Spinelli, J.B., and Haigis, M.C. (2018). The multifaceted contributions of mitochondria to cellular metabolism. *Nat. Cell Biol.* *20*, 745–754.

Supplie, L.M., Düking, T., Campbell, G., Diaz, F., Moraes, C.T., Götz, M., Hamprecht, B., Boretius, S., Mahad, D., and Nave, K.-A. (2017). Respiration-Deficient Astrocytes Survive As Glycolytic Cells In Vivo. *J. Neurosci.* *37*, 4231–4242.

Tyanova, S., Temu, T., Sinitcyn, P., Carlson, A., Hein, M.Y., Geiger, T., Mann, M., and Cox, J. (2016). The Perseus computational platform for comprehensive analysis of (prote)omics data. *Nat. Methods* *13*, 731–740.

Völgyi, K., Gulyácssy, P., Háden, K., Kis, V., Badics, K., Kékesi, K.A., Simor, A., Györffy, B., Tóth, E.A., Lubec, G., et al. (2015). Synaptic mitochondria: A brain mitochondria cluster with a specific proteome. *J. Proteomics* *120*, 142–157.

Walcher, T., Xie, Q., Sun, J., Irmeler, M., Beckers, J., Ozturk, T., Niessing, D., Stoykova, A., Cvekl, A., Ninkovic, J., et al. (2013). Functional dissection of the paired domain of Pax6 reveals molecular mechanisms of coordinating neurogenesis and proliferation. *Development* *140*, 1123–1136.

Wang, X., and Michaelis, E.K. (2010). Selective neuronal vulnerability to oxidative stress in the brain. *Front. Aging Neurosci.* *2*, 12.

Weber, B., and Barros, L.F. (2015). The Astrocyte: Powerhouse and Recycling Center. *Cold Spring Harb. Perspect. Biol.* *7*, a020396.

Willems, P.H.G.M., Rossignol, R., Dieteren, C.E.J., Murphy, M.P., and Koopman, W.J.H. (2015). Redox Homeostasis and Mitochondrial Dynamics. *Cell Metab.* *22*, 207–218.

Wiśniewski, J.R., Zougman, A., Nagaraj, N., and Mann, M. (2009). Universal sample preparation method for proteome analysis. *Nat. Methods* *6*, 359–362.

Zhang, Y., Chen, K., Sloan, S.A., Bennett, M.L., Scholze, A.R., O’Keeffe, S., Phatnani, H.P., Guarnieri, P., Caneda, C., Ruderisch, N., et al. (2014). An RNA-sequencing transcriptome and splicing database of glia, neurons, and vascular cells of the cerebral cortex. *J. Neurosci.* *34*, 11929–11947.

Zheng, X., Boyer, L., Jin, M., Mertens, J., Kim, Y., Ma, L., Ma, L., Hamm, M., Gage, F.H., and Hunter, T. (2016). Metabolic reprogramming during neuronal differentiation from aerobic glycolysis to neuronal oxidative phosphorylation. *Elife* *5*, 1–25.

Zhou, H., Liu, J., Zhou, C., Gao, N., Rao, Z., Li, H., Hu, X., Li, C., Yao, X., Shen, X., et al. (2018). In vivo simultaneous transcriptional activation of multiple genes in the brain using CRISPR–dCas9-activator transgenic mice. *Nat. Neurosci.* *21*, 440–446.

Zischka, H., Laroche, N., Hoffmann, F., Hamo, D., Jägemann, N., Lichtmanegger, J., Jennen, L., Müller-Höcker, J., Roggel, F., Göttlicher, M., et al. (2007). Electrophoretic Analysis of the Mitochondrial Outer Membrane Rupture Induced by Permeability Transition. *Anal. Chem.* *80*, 5051–5058.

## Figure titles and legends

### **Figure 1. Cultured astrocytes and neurons from cerebral cortex differ in mitochondrial structure and function**

(A) Immunofluorescence microscopy images showing the mitochondrial network morphology in not reprogrammed astrocytes (*left*) versus induced neurons (*right*), 7 days after transduction with Ascl1-mitoGFP (green), respectively co-labeled with GFAP (white) or  $\beta$ -III-tubulin (red). Cells nuclei are labeled with DAPI (blue). Scale bar: 20 $\mu$ m. Inserts and magnification highlight the different mitochondrial structure. Scale bar: 6 $\mu$ m.

(B) Longitudinal traces of extracellular flux analysis measured by Seahorse XF analyzer, comparing the Oxygen Consumption Rate (*left*) and the Proton Production Rate (*right*), of astrocytes (green) versus neurons (red) over time, after challenging the cells with different electron transport chains or glycolysis inhibitors (Oligo = Oligomycin A; FCCP = Carbonyl cyanide-4-(trifluoromethoxy)phenylhydrazone; Rot = Rotenone; Ant = Antimycin A; 2-DG = 2-Deoxy-D-glucose). Values are normalized per 1000 cells. Each time point is shown as SD  $\pm$  mean. (n=3 for each group).

(C-H) Seahorse XF analyzer results comparing metabolism of astrocytes versus neuronal culture, showing basal OCR (C), basal PPR (D), oligomycin-dependent PPR (E), rotenone+antimycin-dependent PPR (F) and OCR/PPR ratio (G). Values are normalized per 1000 cells. Data are shown as median  $\pm$  IQR. Significance between median was tested using unpaired t-test, \*p  $\leq$  0.05, \*\*p  $\leq$  0.01, \*\*\* p  $\leq$  0.001. (n=3 for each group).

(H) Immunoblot detection of several mitochondrial proteins, in different fractions (8000g - nuclear; S.N. - cytosolic; 9000g - mitochondria and other organelles), of astrocytes versus neurons.

(I) Electron microscopy images showing the mitochondrial isolation composition at ultrastructural level. Scale bar: 5 $\mu$ m. Magnifications show single mitochondria morphology. Scale bar: 500nm.

### **Figure 2. Astrocytes and neurons exhibit profound differences in the mitochondria proteome**

(A) Principal components analysis on all identified mitochondrial proteins shows a clear separation between neuron (red) and astrocyte (green) samples.

(B) Volcano plot of the quantified mitochondrial proteins with the log<sub>2</sub> ratio of abundances astrocytes/neurons, given on the x-axis, and the  $-\log_{10}$  of the corresponding significance value, on the y-axis. Fold changes of 2-fold are indicated as vertical lines, the significance cut-off of p=0.05 is given as horizontal line. 2-fold significantly more abundant proteins in astrocytes are given in green, for neurons in red. Enlarged dots highlight relevant proteins.

(C) Heatmap cluster analysis of significantly and at least 2-fold differentially abundant mitochondrial proteins (n=3 for each group). Log<sub>2</sub> abundance ratios to the median abundance per protein were calculated across all samples, with positive values (higher than the median) given in yellow, and negative values (lower than the median) given in blue.

(D) GO terms have been elaborated with Genomatix generanker software. Top 35 biological processes are shown for neurons (red bars) and astrocytes (green bars). On the x-axis is shown the  $-\log_{10}$  of the p-value.

### **Figure 3. Mitochondrial protein changes during astrocyte-to-neuron reprogramming**

(A) Immunofluorescence microscopy images showing mitochondrial astrocytic marker (green, Sfxn5) in astrocytes (*arrowhead*) not reprogrammed versus converting neuronal cells (*arrow*), respectively co-labeled with GFAP (white) or  $\beta$ -III-tubulin (white). Cells were transduced with Neurog2-mitoRFP (red) and analyzed at 1, 3, 5 and 7 days post infection (DPI). Scale bar: 20 $\mu$ m.

(B) Immunofluorescence microscopy images showing mitochondrial neuronal marker (green, Gls) in astrocytes (*arrowhead*) not reprogrammed versus converting neuronal cells (*arrow*), respectively co-labeled with GFAP

(white) or  $\beta$ -III-tubulin (white). Cells were transduced with Neurog2-mitoRFP (red) and analyzed at 1, 3, 5 and 7 days post infection (DPI). Scale bar: 20 $\mu$ m

**Figure 4. dCas9-mediated induction of neuron-specific mitochondrial proteins potentially improves speed and efficiency of direct neuronal reprogramming**

(A) Scheme illustrating the dCas9-VPR combined with STAGr technique used to upregulate neuronal mitochondrial target in astrocytes.

(B) RNA PCR of sorted primary astrocytes, transduced with dCAS9-VPR and gRNAs, control or to upregulate Sod1 and Prdx2, 48 hours after transduction. Data are shown as SD $\pm$ mean.

(C) Reprogramming efficiency calculated as percentage of cells acquiring neuronal marker  $\beta$ -III-tubulin over total RFP<sup>+</sup>/GFP<sup>+</sup> only cells. Analysis was performed 6 days after transduction with Ascl1-RFP, dCas9-VPR and inducible GFP construct coding for control gRNAs (Stagr Cntrl) or for gRNAs to upregulate Sod1 and Prdx2 (Stagr P-S). Data shown as median  $\pm$  IQR. Significance between median was tested using upaired t-test, \*\*\*p  $\leq$  0.001. (n=7 for experimental condition).

(D) Time lapse graphs of cells undergoing reprogramming and acquiring neuronal morphology (y-axis) over time (x-axis), co-transduced with Stagr Cntrl (green line) or Stagr P-S (red line). Data are shown as mean  $\pm$  SD. Significance between mean was tested using upaired t-test, \*p  $\leq$  0.05, \*\*p  $\leq$  0.01. (n=3 for each time point and experimental condition).

(E) Immunofluorescence microscopy images showing cells co-transduced with Ascl1-RFP (red), dCas9-VPR and gRNAs (green), acquiring neuronal morphology,  $\beta$ -III-tubulin (white), over total population of cells (DAPI). Control (*left*) versus experimental condition upregulating Sod1 and Prdx2 (*right*) are compared. Arrowheads highlight neuronal cells. Scale bar: 200 $\mu$ m. Inserts and magnification highlight the different maturation of derived neurons in the two conditions. Scale bar: 20 $\mu$ m.

**Supplementary Figure 1. Cultured astrocytes and neurons from cerebral cortex differ in mitochondrial structure and function**

(A) Schematic illustration of mitochondrial isolation procedure based on pump-controlled cell rupture method, modified and adapted from (Schmitt et al., 2013).

(B) Immunoblot detection of contaminants proteins, in different fractions (8000g - nuclear; S.N. - cytosolic; 9000g - mitochondrial and other organelles) of astrocytes versus neurons.

(C) Graphs showing the vitality of isolated mitochondria for one hour upon isolation, measuring the membrane potential by Rhodamine 123 assay, and the swelling parameter by absorbance at 540nm, of astrocytes (green) versus neurons (red).

(D) GO terms have been elaborated with Genomatix generanker software. Top 35 molecular function are shown for neurons (red bars) and astrocytes (green bars). On the x-axis is shown the  $-\log_{10}$  of the p-value.

**Supplementary Figure 2. Mitochondrial protein exchange during astrocyte-to-neuron reprogramming**

(A) Immunofluorescence microscopy images showing mitochondrial astrocytic marker (green, Cpx) in astrocytes (*arrowhead*) not reprogrammed versus converting neuronal cells (*arrow*), respectively co-labeled with GFAP (magenta) or  $\beta$ -III-tubulin (white). Cells were transduced with Neurog2-RFP (red) and analyzed at 1, 3, 5 and 7 days post infection (DPI). Scale bar: 20 $\mu$ m.

(B) Immunofluorescence microscopy images showing mitochondrial neuronal marker (green, Prdx2) in astrocytes (*arrowhead*) not reprogrammed versus converting neuronal cells (*arrow*), respectively co-labeled with GFAP (violet) or  $\beta$ -III-tubulin (white). Cells were transduced with Neurog2-RFP (red) and analyzed at 1, 3, 5 and 7 days post infection (DPI). Scale bar: 20 $\mu$ m.

***Supplementary Figure 3. Mitochondrial protein exchange during astrocyte-to-neuron reprogramming (Ascl1)***

(A) Immunofluorescence microscopy images showing mitochondrial astrocytic marker (green, Sfxn5) in astrocytes (*arrowhead*) not reprogrammed versus converting neuronal cells (*arrow*), respectively co-labeled with GFAP (white) or  $\beta$ -III-tubulin (white). Cells were transduced with Ascl1-mitoRFP (red) and analyzed at 1, 3, 5 and 7 days post infection (DPI). Scale bar: 20 $\mu$ m.

(B) Immunofluorescence microscopy images showing mitochondrial neuronal marker (green, Gls) in astrocytes (*arrowhead*) not reprogrammed versus converting neuronal cells (*arrow*), respectively co-labeled with GFAP (white) or  $\beta$ -III-tubulin (white). Cells were transduced with Ascl1-mitoRFP (red) and analyzed at 1, 3, 5 and 7 days post infection (DPI). Scale bar: 20 $\mu$ m

***Supplementary Figure 4. Time-course expression of mitochondrial marker during direct neuronal reprogramming***

(A-F) Time course analysis at 1, 3, 5 and 7 DPI showing percentage of cells retaining mitochondrial markers expression tested by immunofluorescence, comparing cells acquiring neuronal morphology (Neurons, red) or maintaining astrocytic one (Astrocytes, green). Quantification was performed at each time-point for cells transduced with Neurog2-mitoRFP (A, B), Ascl1-mitoRFP (C, D) and Neurog2-RFP (E, F). (10-30 cells analyzed for each time-point and condition, from 2/3 biological replicates).

***Table 1. List of the 354 mitochondrial proteins, according to MitoCarta 2.0 database, more abundant in astrocytes or neurons, selected for a statistical significance of <0.05, and a two-fold enrichment. Specific proteins mentioned in the text underlined in yellow.***

***Supplementary Table 1. Full list of the 4755 proteins identified by LC-MS/MS analysis on isolated mitochondria of cortical astrocytes and neurons.***

***Supplementary Table 2. List of GO term analysis, performed with Genomatix Generanker, of the mitochondrial proteins enriched in astrocytes or neurons, divided each for GO terms from biological processes and molecular function.***

**Figure 1**

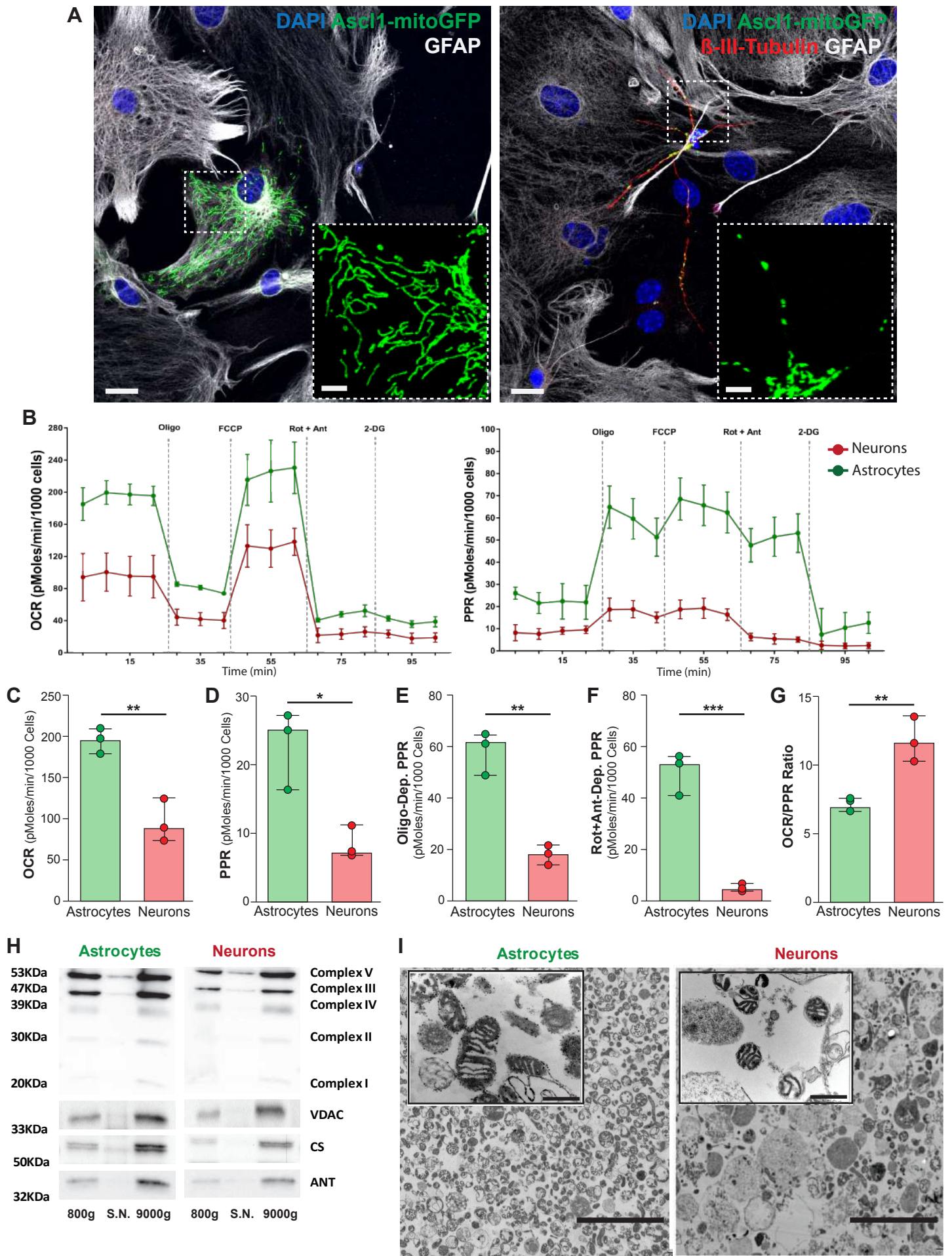


**Figure 2**

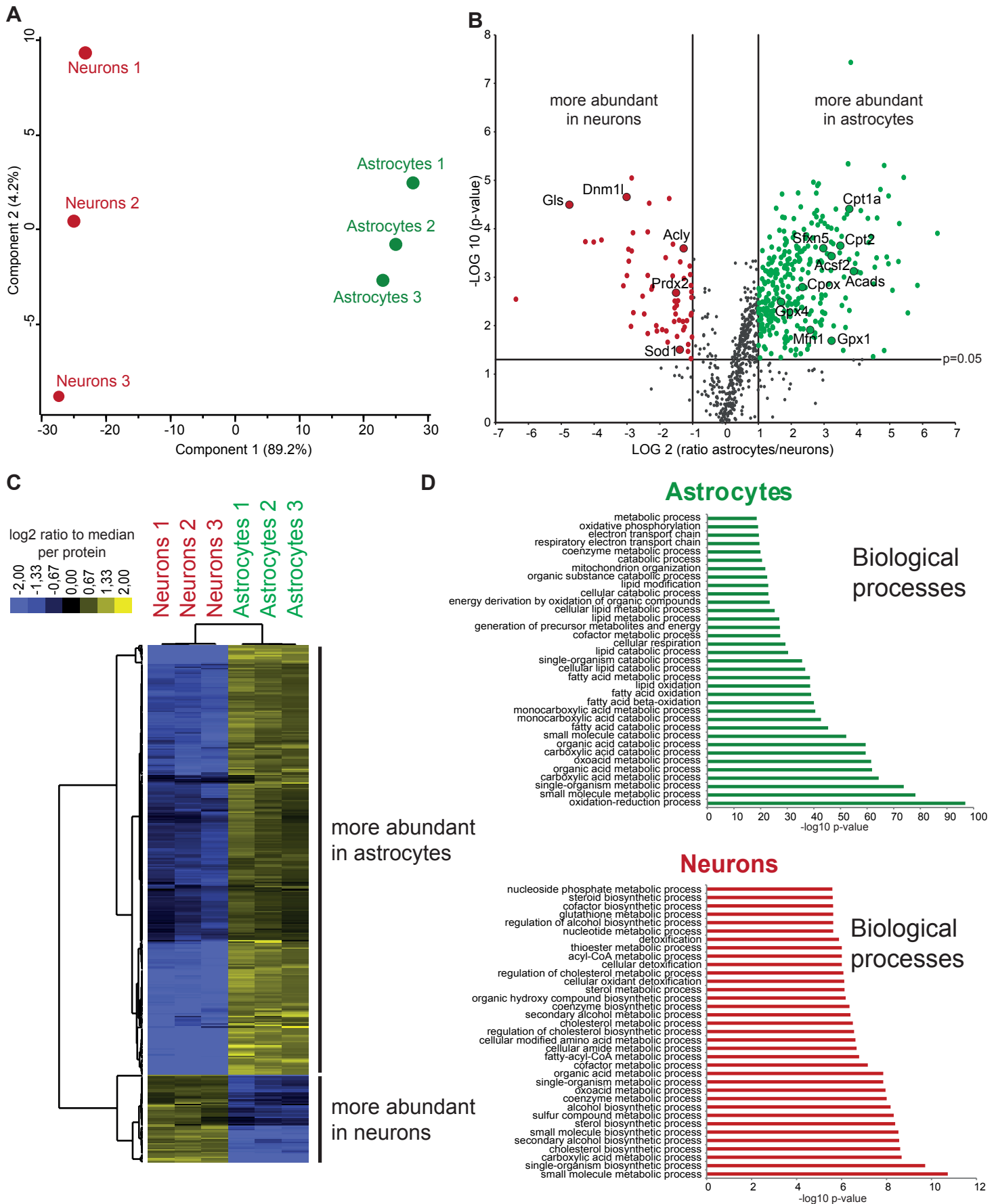
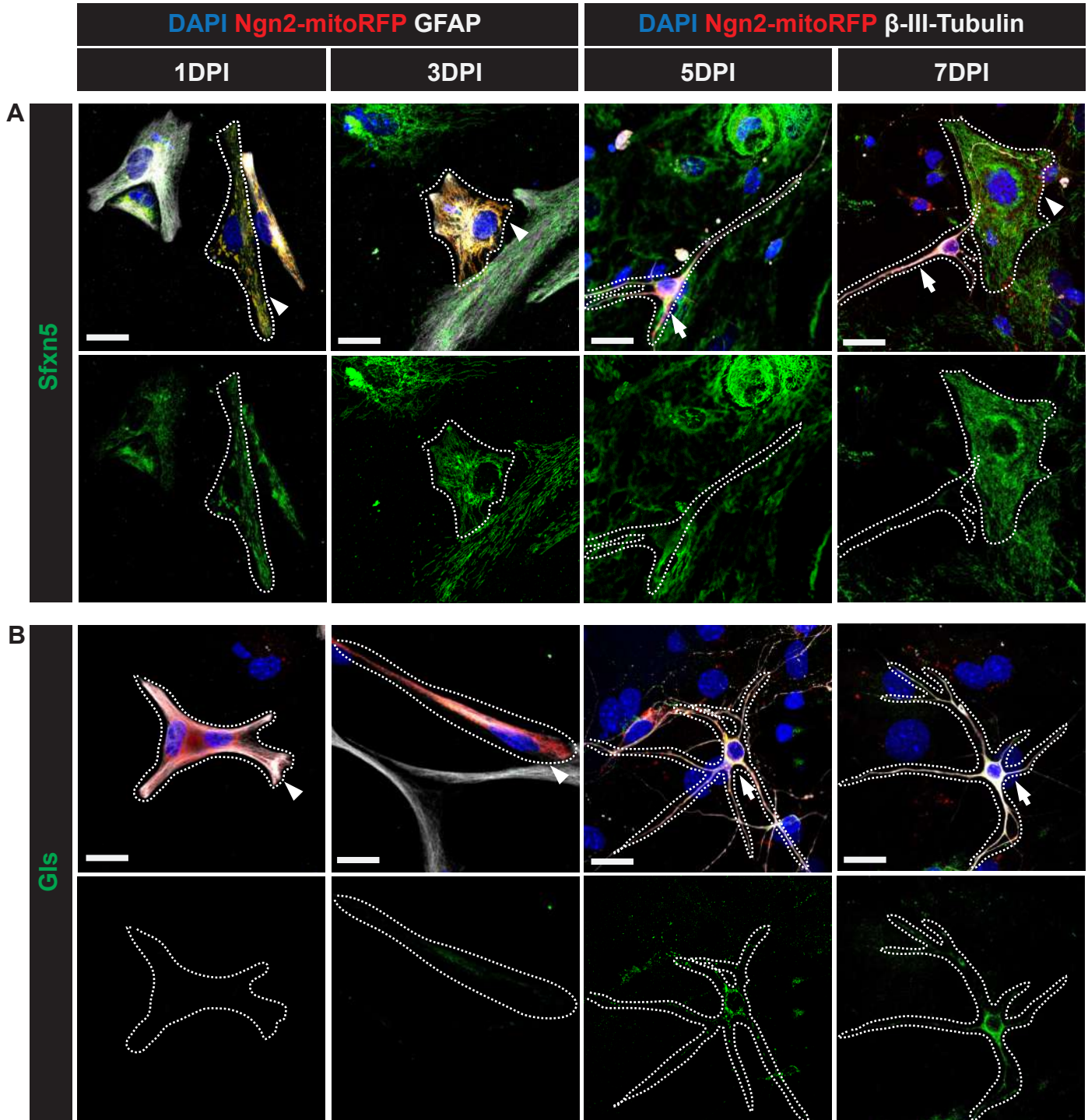
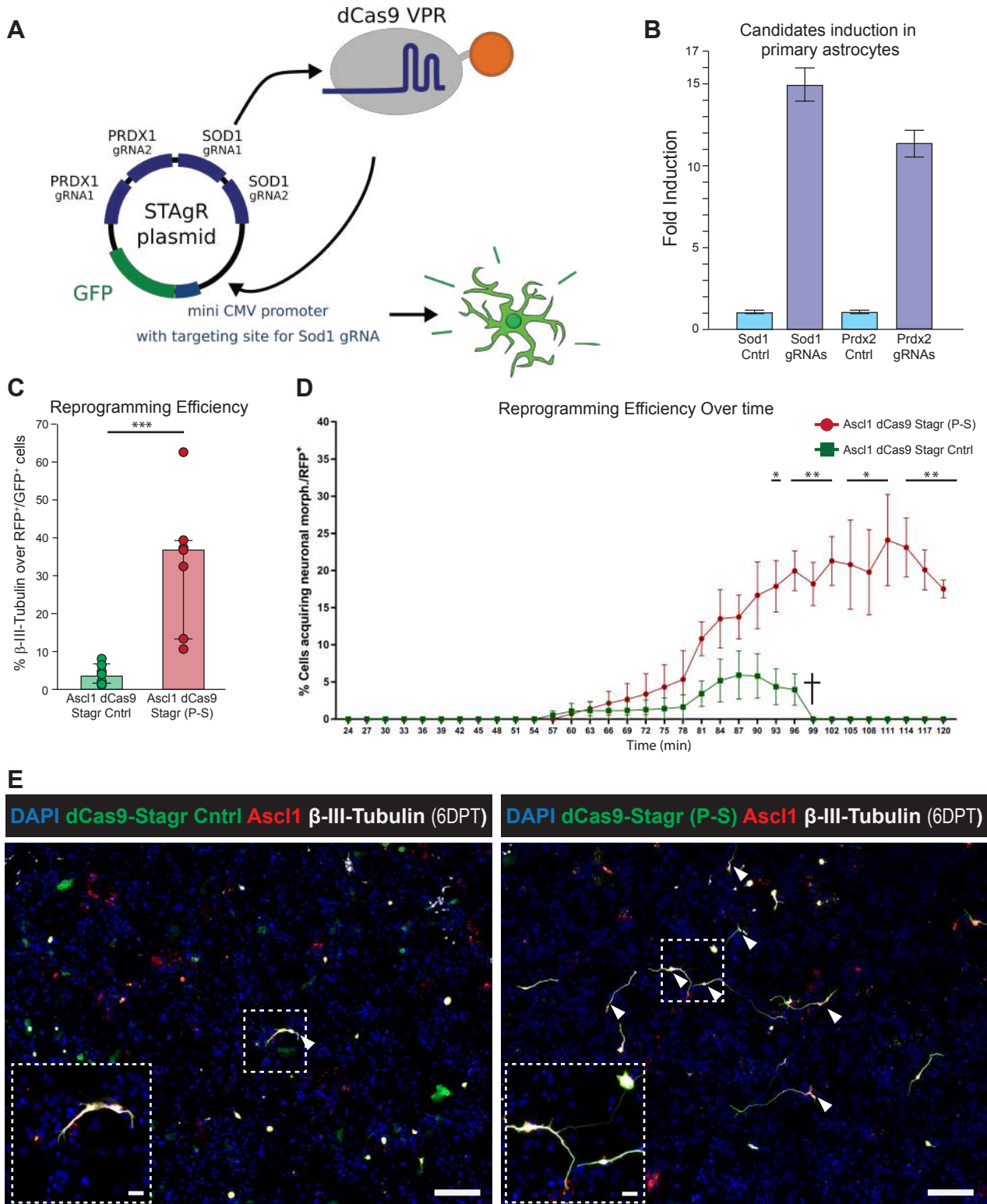


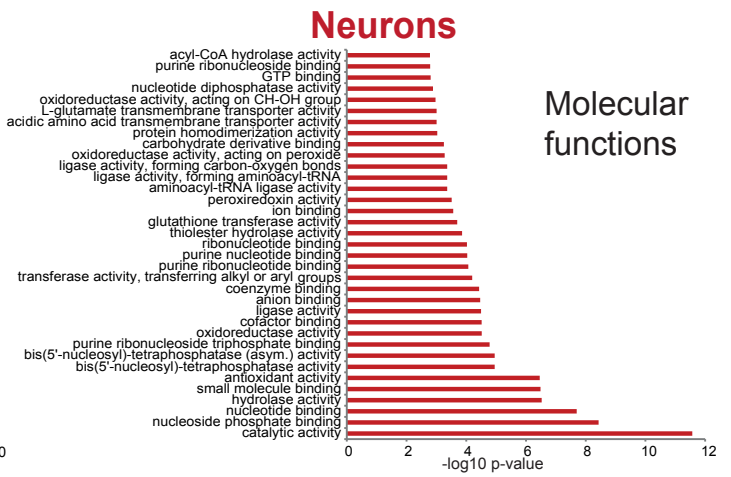
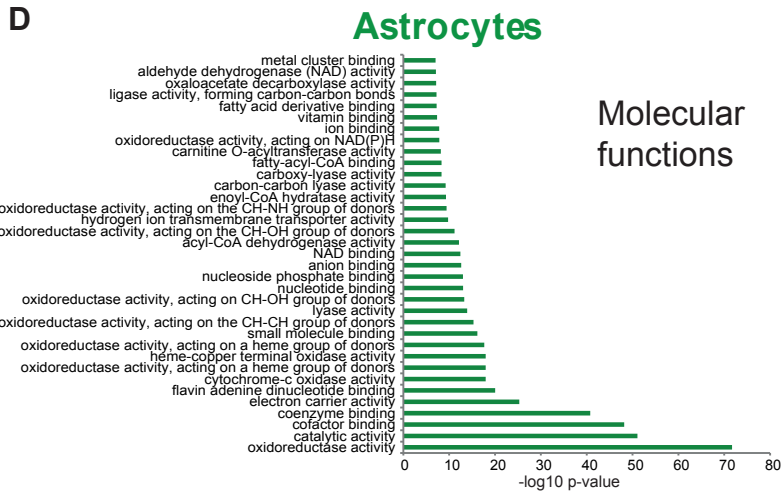
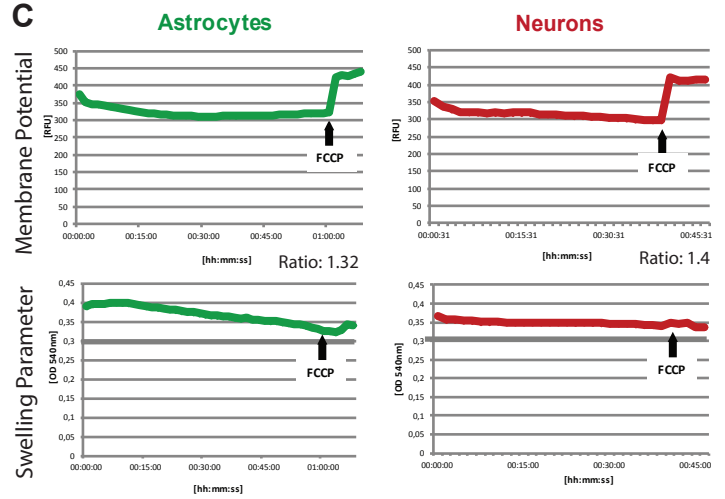
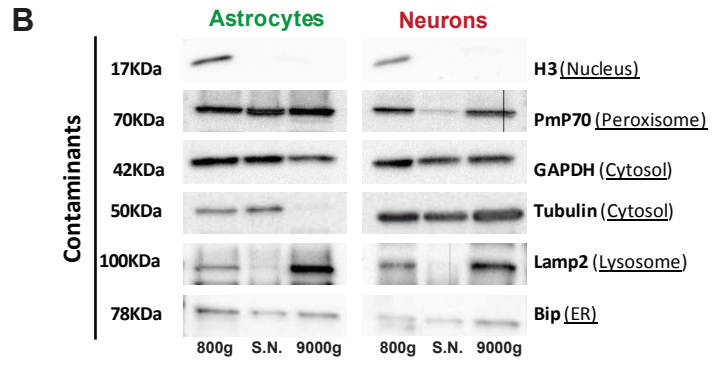
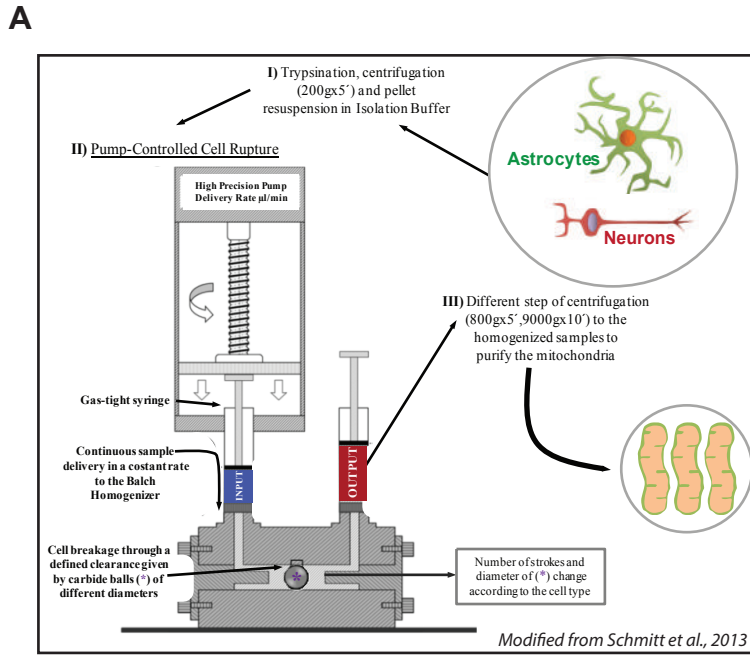
Figure 3



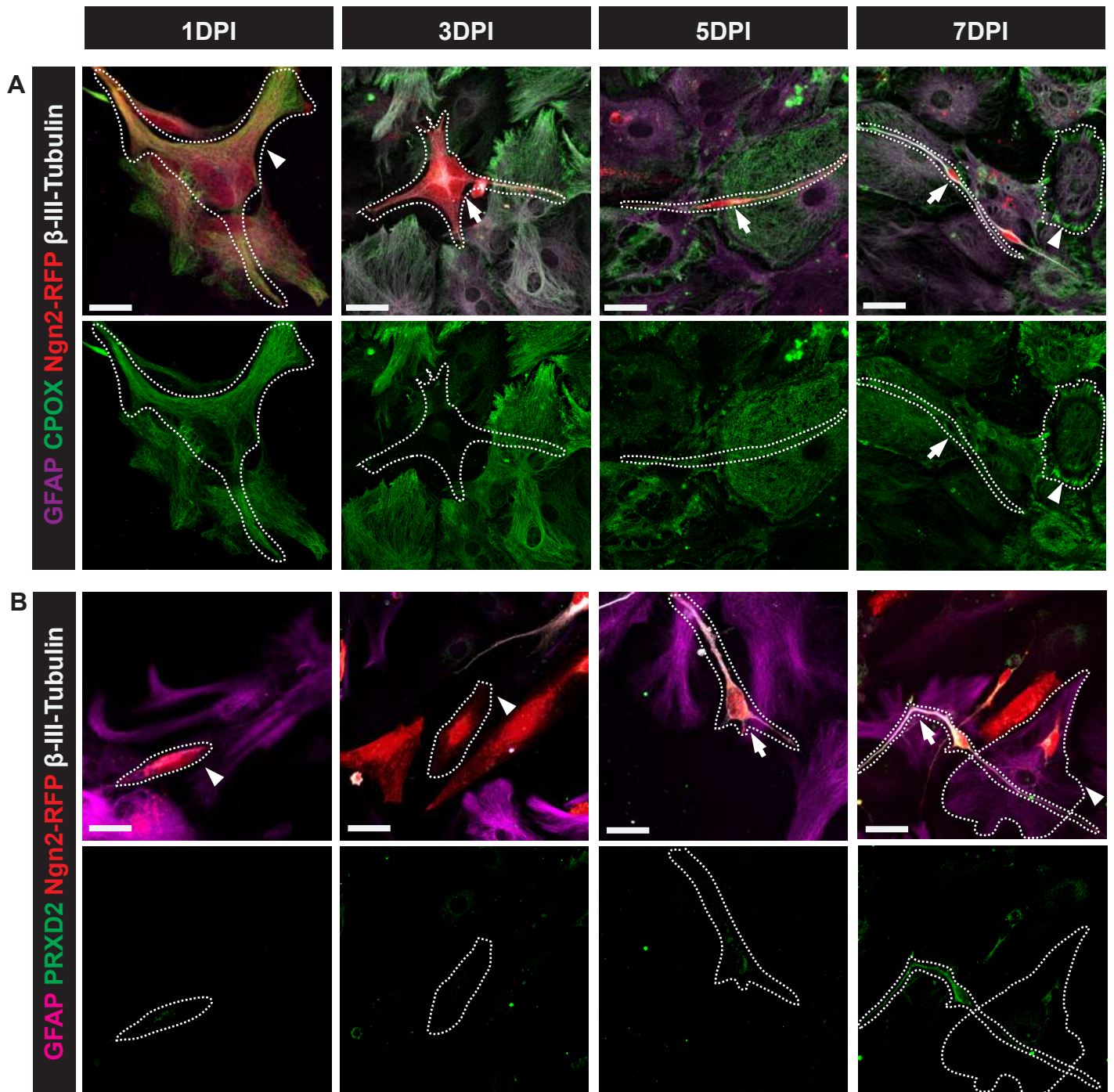
**Figure 4**



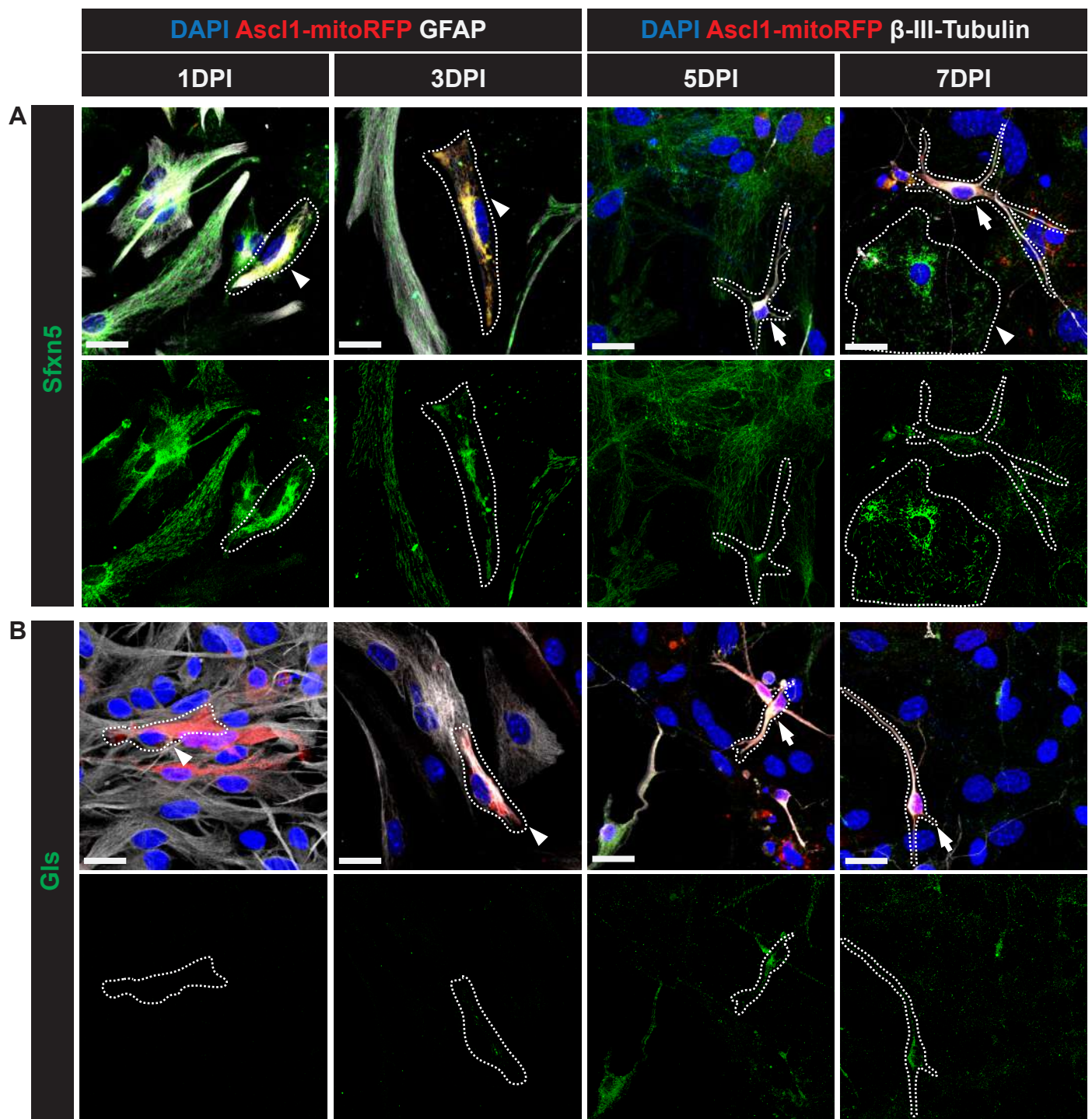
# Supplementary Figure 1



Supplementary Figure 2



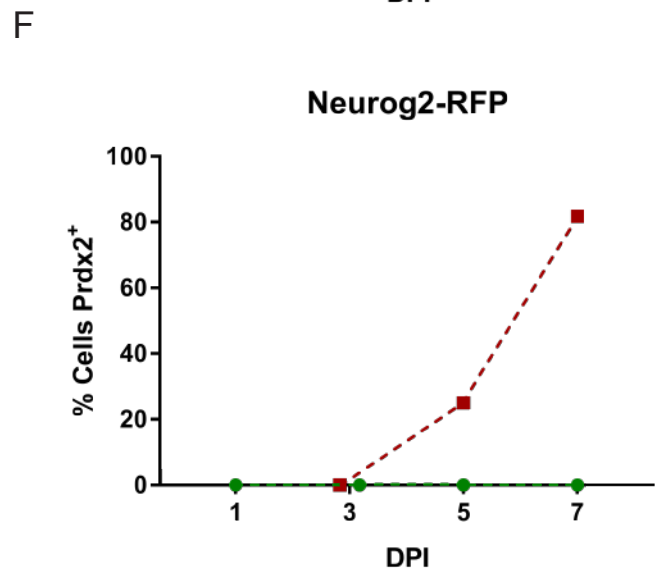
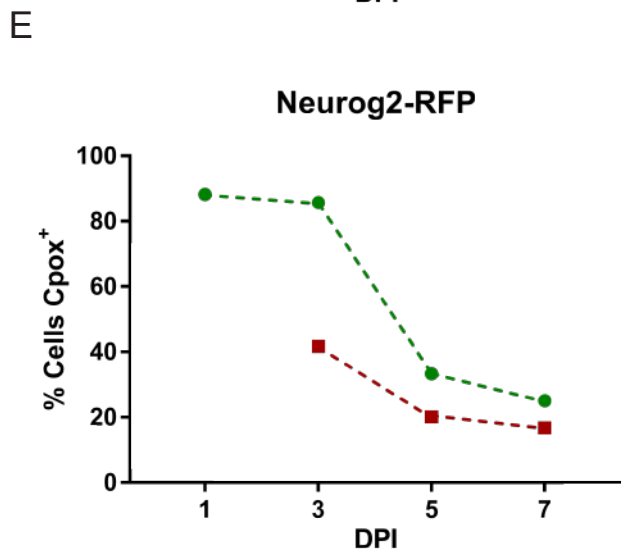
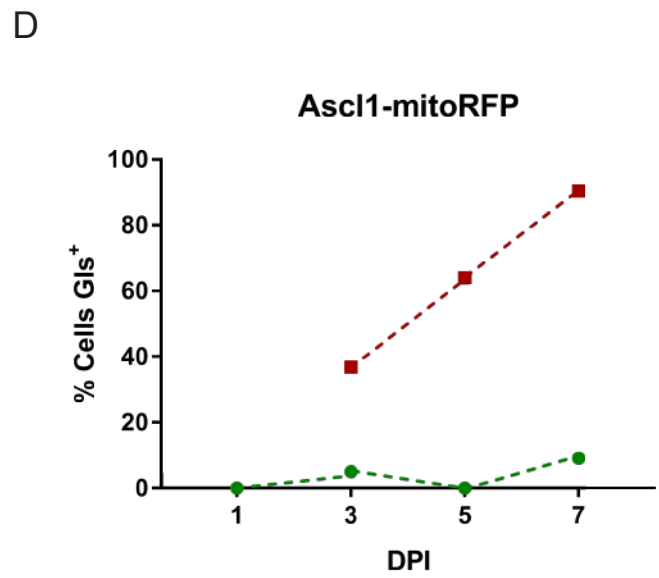
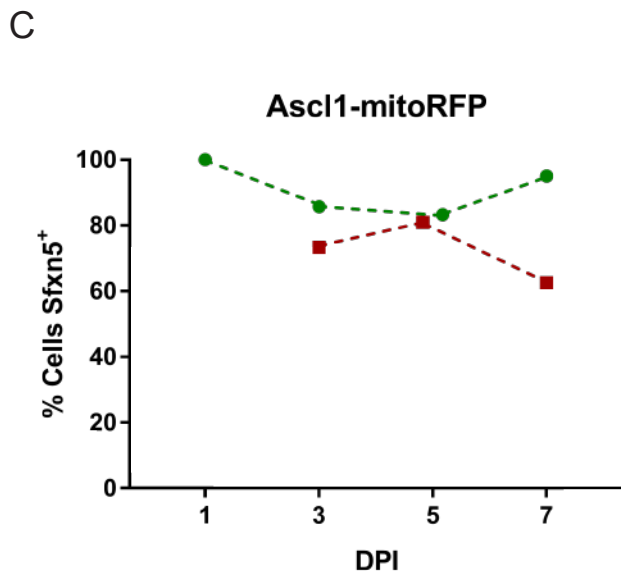
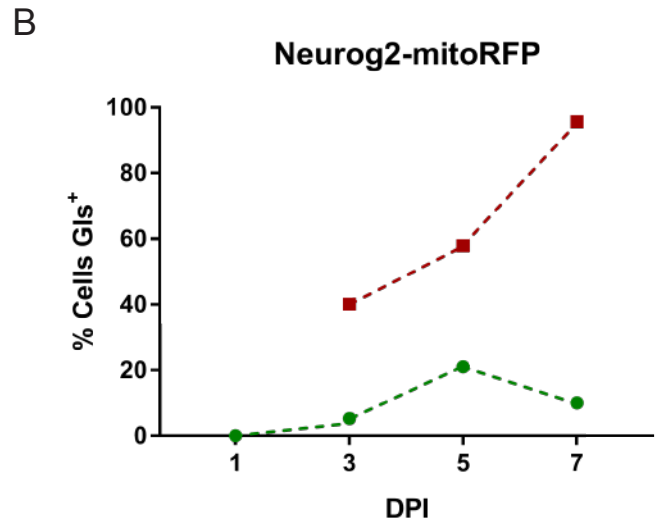
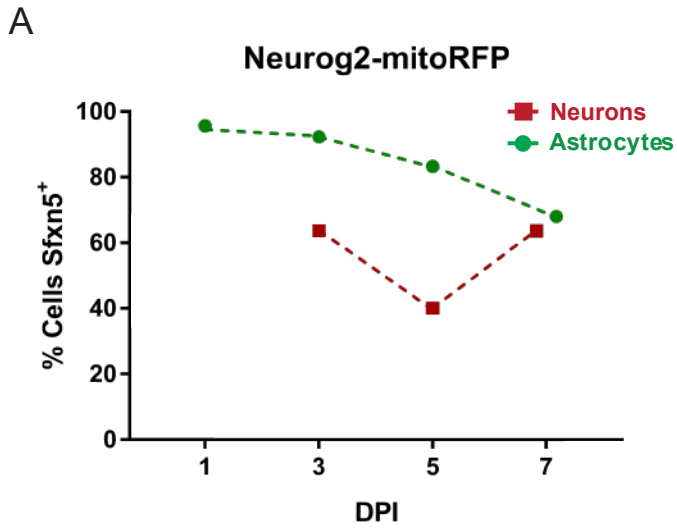
Supplementary Figure 3



# Supplementary Figure 4

## Mitochondrial Astrocytic Markers

## Mitochondrial Neuronal Markers



## Discussion

In my Ph.D. projects I could identify key hurdles and novel modulators to direct neuronal reprogramming of astrocytes. In particular, following the discovery from Gascon et al., that converting neurons face a dramatic burst in ROS, detrimental for the neuronal conversion, I could prove that modulating the metabolism of the converting cell further hampers the neuronal generation. Indeed, reducing ROS by pushing the metabolism toward a glycolytic phenotype could not improve the process, as a proper metabolic shift toward oxphos, functionally relying on ATP generation from the ETC, is essential for neuronal generation. Furthermore, investigating mitochondria composition of astrocytes and neurons in Russo et al., beyond identifying novel proteins and specific pathways of these two cortical cells, could demonstrate that, even if at a later stage, a shift in composition from astrocytes to neurons occurs. We further showed that mitochondria proteome reprogramming occurs, even if partial, as not all the astrocytic proteins are properly regulated in converting neurons. This suggests, at least from those markers tested, also a partial functional metabolic reprogramming. Furthermore, pushing with cas9 technology the early expression of neuronal mitochondrial proteins in converting astrocytes can greatly improve the generation of neurons, suggesting that metabolism modulation can be also a direct driving force, rather than a mere consequence, to cell fate change. These data require further attention when thinking about translating these findings *in vivo*. Mitochondrial composition *in vivo* is barely known and still many hurdles need to be dismantled to fully characterize the functionality of the *in vivo* generated neurons. Mattugini et al. seems to move the field a further step forward, as long-term surviving neurons and specific neuronal subtypes are generated. Interestingly, we found out that this process might be greatly affected by the delivery vector selected. We could indeed observe a different reaction of the environment to the viral vectors used to deliver the transcription factors, which can potentially affect the reprogrammed neurons engraftment and survival. A broader reactive gliosis and immune cells infiltration were observed with lentivirus or retrovirus, compared to AAV. Notably, the latter was associated with higher transduction rates and neuronal reprogramming efficiency.

Thus, combining techniques to reduce the potentially harmful immune reaction and glial activation, which increase inflammation, with buffering of ROS, potentially further induced by a malfunctioning metabolic shift, could greatly improve direct neuronal reprogramming. Another promising strategy, potentially complementary to these approaches, involves modulating the metabolic change by directly acting on mitochondria composition. Indeed, pushing an earlier mitochondrial composition shift during conversion from astrocytes to neurons could greatly improve the neuronal generation.

The potential implications of these findings for the field of direct neuronal reprogramming, and the gaps in knowledge which must still be filled to further boost the improvement of converted neurons, are here discussed and analyzed.

## Impact of viral vectors and inflammation on direct neuronal reprogramming

The paper from Mattugini et al. shows a degree of integration, maturity and survival hardly reached for reprogrammed neurons so far. This is achieved injecting the reprogramming factors encoded in AAV flex-switch virus in the grey and white matter of the somatosensory cortex 3 days following stab wound injury. The recombination occurs only in reactive astrocytes, as the mouse model used is a GFAP-cre line, with cre mediating the expression of the AAV selectively in astrocytes. Combined expression of the transcription factor nuclear receptor related 1 protein (Nurr1) and Neurog2 is essential for high efficiency reprogramming of astrocytes into neurons, which express appropriate lamina-specific hallmarks and long-distance axonal projections. Furthermore, these newly generated neurons mature with time and survive up to the last evaluated time point, 9 months. Interestingly reprogramming is successfully restricted to grey matter astrocytes, as white matter astrocytes do not convert, further highlighting the importance to target the correct starter cell (Heinrich et al., 2015) and to properly evaluate the environment in which the neurons are generated (Gascón et al., 2017).

My contribution to the project was evaluating a so far uninvestigated aspect of *in vivo* direct neuronal reprogramming, namely how viral vectors used to carry the transgenes can actually influence the environment and the reprogramming outcome. Indeed different vectors, such as lentivirus, retrovirus and adeno-associated virus have been widely used for reprogramming approaches, each of them with their own advantages and transduction rates (Gascón et al., 2017; Mancini and Horvath, 2018), as also described in the introduction. In general, our paradigm of direct neuronal reprogramming consists of viral vectors injection 3 days following unilateral stab-wound injury performed in the somatosensory cortex, reaching the grey and white matter. The first evaluation for neuronal generation is usually performed 10 days after viral injection, namely 13 days after stab wound injury.

Interestingly, we noticed that independently on the transcription factor expressed, whether is Neurog2 or GFP only, a huge difference in glial reactivity is observed. This difference depends on the viral vector used. In particular, retrovirus and lentivirus injections elicit, already at 3 days post-injection (DPI), a strong reactivity of astrocytes and microglia, characterized by GFAP<sup>+</sup> and Iba1<sup>+</sup> activation respectively (*data not shown*). Furthermore microglia acquire an amoeboid reactive morphology, accumulating at the injury site (Li and Barres, 2017), while astrocytes up-regulate GFAP reactivity but do not accumulate, in line with their behavior following injury (Bardehle et al., 2013). This highly reactive environment is also associated to massive leukocytes invasion, characterized by CD45<sup>+</sup> reactivity, which is further exacerbated at 10 DPI (Mattugini et al.), time point where first neurons are usually observed with retroviral-mediated reprogramming (Gascón et al., 2016). Surprisingly, this massive inflammation is much reduced following AAV injection, both at 10 DPI but also at later time points, as 24 DPI, when first neurons are actually observed with this viral vector (Mattugini et al.). Furthermore, we also analyzed the immune cell infiltrate 10 DPI following injection by magnetic-activated cell sorting (MACS) followed by fluorescent activated cell sorting (FACS) analysis. Dissecting leukocytes subpopulations we confirmed massive CD45<sup>+</sup> infiltration following LV and RV injection, compared to AAV, mostly characterized by monocytes/macrophages and activated lymphocytes, in particular T cells (*data not shown*).

Notably sham controls in which SW injury was followed by PBS injection showed almost no reactive gliosis and CD45<sup>+</sup> infiltration at 10 DPI, in line with TBI recovery observed in the absence of viral injections 3 days after injury (Frik et al., 2018; McKee and Lukens, 2016). This strongly suggests that despite the generation of viral vectors stripped of most of the original viral components, LV and RV in particular can still elicit a very strong inflammatory immune response which might explain the reduced reprogramming efficiency compared to the one following AAV injections (*Mattugini et al.*).

Interestingly, most studies showed that the outer components of the viral vector, like capsid or envelope proteins, necessary to mediate selective recognition and binding to the target cells, are the main inducers of an adaptive immune response. RV- and LV-based vectors, for example, often express envelope glycoproteins from other viruses, to improve their selective targeting, such as from VSV-G, Mukola virus or lymphocytic choriomeningitis virus (LCMV). These components, also present in the vectors used for reprogramming (*Gascón et al.*, 2016; Heinrich et al., 2014), are able to specifically elicit an adaptive immune response, which can not only be involved in the gliosis reaction (Kunitsyna et al., 2016), but also in the clearing and killing of transduced cells, drastically reducing the transduction rate (Drokhlyansky et al., 2016). The induction of microglia and astrocytes reactivity, monocytes/macrophages activation and recruitment of antigen-specific T lymphocytes can all be concomitant factors in the relative unsuccessful rate of reprogramming observed with LV and RV.

Advances in generating new viral vectors devoid of antigens able to elicit immune response or immunization against those components, inducers of adaptive immunity, are good strategies to produce improved vectors with high transduction rate and low immunogenicity, as demonstrated in some pivotal studies on virus infectivity in the brain (Drokhlyansky et al., 2016; Ewer et al., 2016). Despite the higher immunogenicity of RV and LV, is important to mention that also AAV-mediated overexpression of different transgenes can induce an inflammatory reaction within the brain (Lowenstein et al., 2007). Despite that, usually the inflammatory reaction is not linked to cell death, but rather to mild environmental inflammation, mostly associated to transgene-mediated recognition as foreign antigen or to pre-existing antibodies against the capsid proteins within the host (Chew et al., 2016; Mingozzi and High, 2013). A careful understanding of the viral vector and immune interactions is thus fundamental for the outcome of reprogramming and most importantly for the safety of the treatment.

In the field of neuronal transplantation most of the studies have been performed in immunodeficient or immunocompetent models receiving immunosuppressive drugs (Anderson et al., 2011), to allow engraftment of transplanted cells and avoiding cell rejection from the host immune system. An underestimation of the host immune system reaction has indeed led to death in some clinical trials for gene therapy (Thomas et al., 2003). Nowadays, transplantation of neuronal cells in primates and humans is always associated to immunosuppressive treatments, to avoid a pathological host response to the viral vector and the transgene carried (Curtis et al., 2018; Morizane et al., 2017). Translating these concepts to *in vivo* studies for direct neuronal reprogramming might be the key to further improve the process, bringing it closer to clinical translation. Using for example immunodeficient mice or

co-treatment with immunosuppressive drugs may support the neuronal integration, avoiding a likely detrimental immune response that would recognize and kill the infected cells, further increasing inflammation in the already injured brain parenchyma.

In line with the detrimental role that immune cells might exert on converting neurons, AAV-mediated reprogramming induces higher efficiency of transduction and neuronal survival (Torper et al., 2015; *Mattugini et al.*). Furthermore it is associated with lower inflammatory reactions of microglia and astrocytes and to reduced immune infiltration, compared to LV or RV injections (*Mattugini et al.*). It would be important to confirm whether this improved reprogramming is linked to the lowered immune response, for example by co-administering immunosuppressive drugs with the RV application, or whether it is due to internal viral vector properties, such as viral genes still active or different transgenes expressed (e.g. Bcl2 versus Nurr1).

Intrinsic viral vectors properties might also contribute to the higher success of AAV vectors in mediating neuronal conversion. Indeed, one of the main differences between LV/RV and AAV, beyond the packaging capacity, is associated with their peculiar replication mode. While AAVs remain episomal within the nucleus and require longer time to efficiently express the transgene, up to 10 days, genome-integrating RV and LV viral vectors express the genomic information at higher speed and rates, few days after transduction (*Gascón et al., 2016*; Mancini and Horvath, 2018; *Mattugini et al.*).

This could have important consequences for the timing in which we want to apply the reprogramming recovery strategy. Indeed, early treatments post-injury are usually linked to better recovery, limiting the spreading of cell death and reducing the damage. This was demonstrated for neural stem cells and neuronal cells transplantation following diverse types of injury, in which treatment in an early window following lesion, when inflammation is not yet at its peak and secondary cell death not yet occurred (Burda and Sofroniew, 2014), was associated to improved recovery (Bacigaluppi et al., 2016; Shear et al., 2011). Delaying the transplantation following injury could also help the engraftment of the cells, as the highly inflammatory reaction and immune infiltration which hampers new cells survival might be reduced, as demonstrated in other studies of stem cell transplantation following brain injuries (Karimi-Abdolrezaee et al., 2006; Péron et al., 2017). In the case of direct neuronal reprogramming, 3 days post-injury was selected as optimal time for retroviral injections, as this was the peak of glial cell proliferation (Simon et al., 2011), with the aim to target mainly proliferating cells for conversion. In this case, early and strong expression of the transgenes mediated by RV and LV might further challenge cell conversion and survival, as strong inflammation is still very active (Frik et al., 2018) and as we showed is further exacerbated by viral vectors themselves. The less immunogenic AAV vectors might further offer the advantage of inducing delayed expression of the transgene at a slower rate, coinciding with a less inflammatory environment, and being less demanding in term of energy requirements for the cell itself.

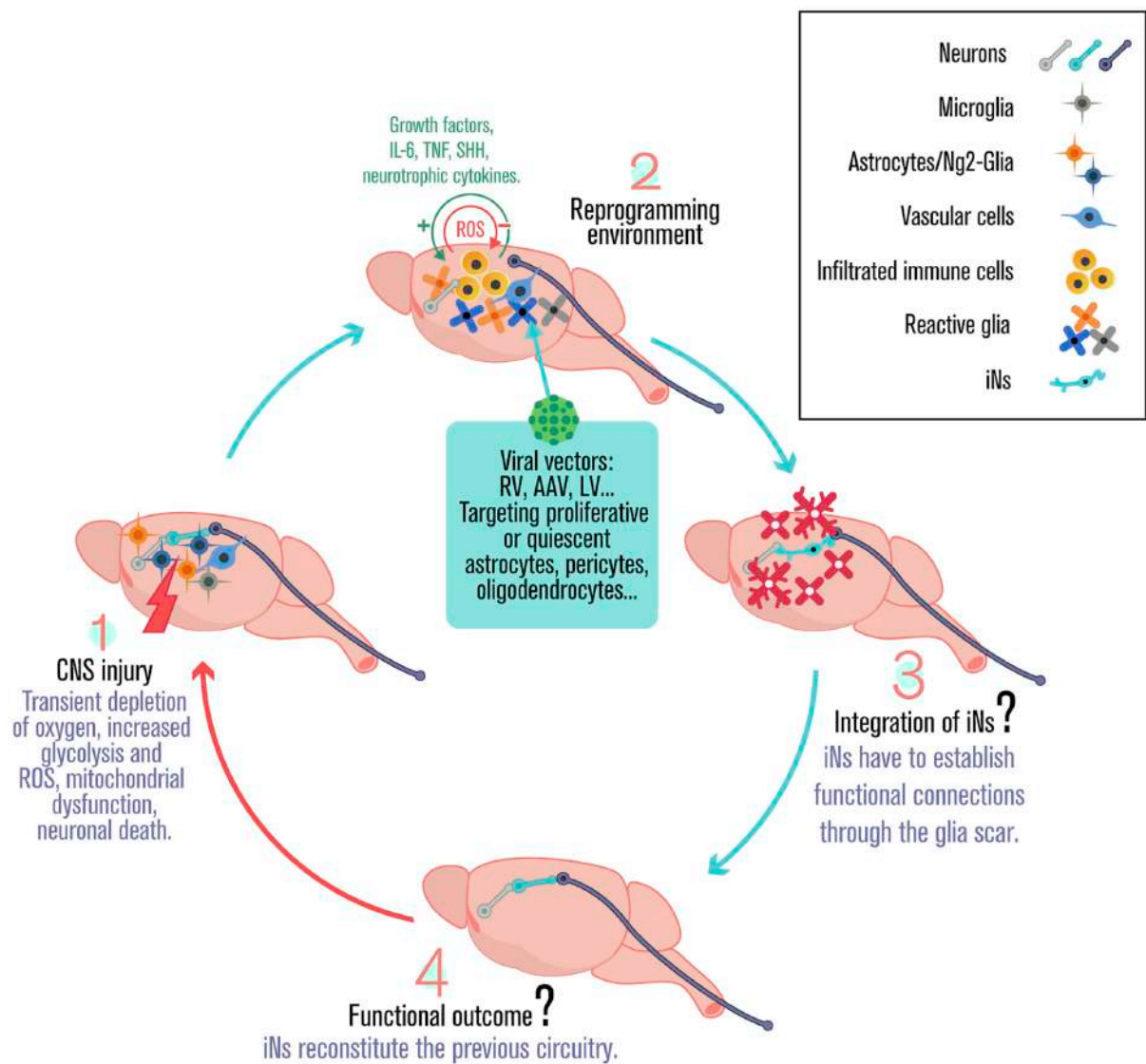


**Figure 5.** Effects of the *in vivo* environment on the process of neuronal generation and on the potential integration of converted neurons (Gascón et al., 2017).

All these pieces of information also raise the attention on the actual lesion in which direct neuronal reprogramming is tested, which is mostly traumatic brain injury (Gascón et al., 2017). Indeed, the discovery that the viral vectors so far used elicited a strong inflammation and immune cell recruitment challenges what we knew regarding the post stab-wound injury environment (Frik et al., 2018; Mattugini et al., 2018). In light of this high inflammatory activation, with adaptive immune cells further orchestrating the reaction, the pathological model is more coherent to one where specific viruses or pathogens infect the brain parenchyma (Russo and McGavern, 2015). This can have great impact on the challenges that our reprogrammed neurons must cope with for proper integration and survival, as the cells need to engraft in a much more reactive environment than the one initially considered following stab wound injury.

Thus, my contribution to Mattugini et al. was to evidence an underestimated role of the inflammation elicited by the viral vectors used. New studies evaluating the functional effects of immune cells and reactive gliosis to the reprogramming process, generation of improved

and less immunogenic delivery vectors, as well as a comprehensive understanding of the impact that different pathological environments could play on the neuronal conversion, might all represent fundamental steps for clinical translation of direct neuronal reprogramming.

### Role of ROS and metabolism in hampering direct neuronal reprogramming

One of the major hallmarks of inflammation is reactive oxygen species production. ROS are thus early mediator of damage following an injury, mostly secreted in the CNS by dying neurons or reactive microglia and infiltrating macrophages (Burda and Sofroniew, 2014; London et al., 2013). ROS also represent one of the major hurdles identified so far to successful direct neuronal reprogramming, *in vitro* as well as *in vivo* (Gascón et al., 2016).

Gascon et al., identified a critical time point during fate conversion into neurons, around 3 days after transduction or transfection, where most of the cells succumb to cell death. Interestingly, attempts to prevent induced neuronal death with different inhibitors identified ferroptosis and ROS accumulation as leading cause for the phenomenon. Indeed genetic manipulation, through co-expression with the neuronal transcription factors of pro-survival gene Bcl2, and chemical co-treatment with ROS scavengers or ferroptosis inhibitors drastically improve the neuronal generation. This drastic amelioration could also be translated *in vivo*, through co-injection of Neurog2 and Bcl2 and co-treatment with ROS scavengers, increasing neuronal generation from 10% up to 90% at 10 DPI. Furthermore, these neurons could survive up to 1 month, maturing and differentiating also in upper layer subtype.

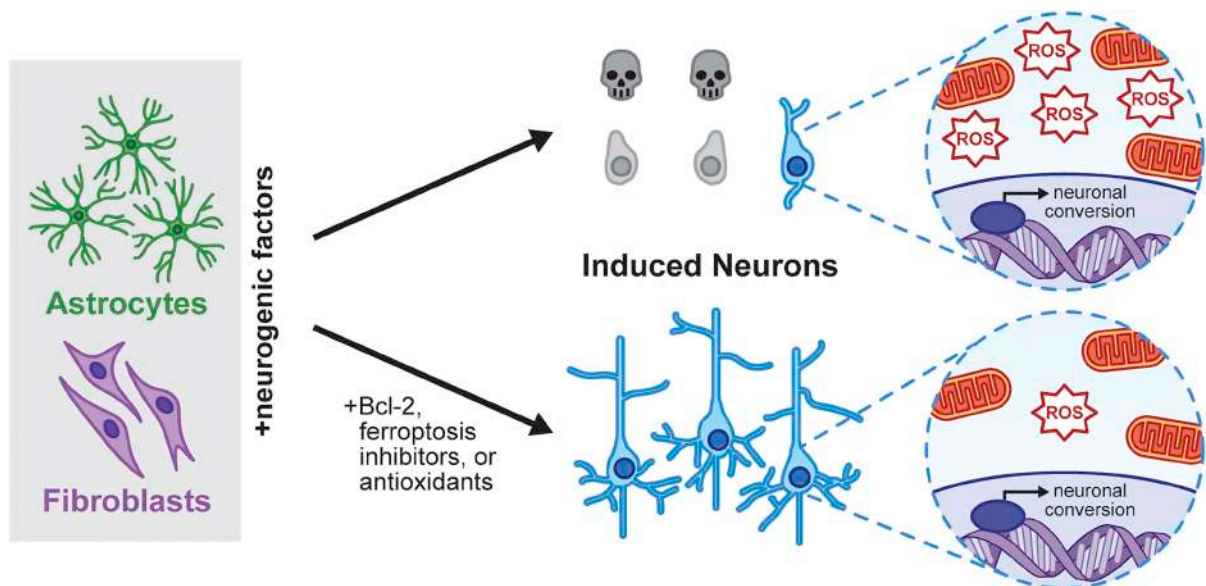


**Figure 6.** High oxidation levels hamper direct neuronal reprogramming (Quadrato et al., 2016. License Number: 4565520722239).

As ROS are byproducts of the respiratory chain activity characterizing oxphos metabolism, typical of neurons, while astrocytes in basal condition are mostly glycolytic, we wondered whether an active change in metabolism from astrocytes to neurons may affect or be associated to direct neuronal reprogramming.

We observed that astrocytes cultured in medium with oligomycin A, so-called glycolysis-only medium, blocking the generation of ATP from the ETC and allowing energy production only

through alternative pathways, preserved astrocytes features and almost totally interfered with their neuronal conversion, despite expression of the neuronal transcription factor. Furthermore, oligomycin treatment in astrocytes was not affecting cell survival. Interestingly, we recently observed an early decrease in expression levels of neuronal genes, while glial factors failed to be repressed, in converting astrocytes treated with oligomycin, compared to control cells in normal differentiation medium (*data not shown*). Notably, cells grown in glycolysis-only medium showed reduced ROS production, which we demonstrated was beneficial to improve reprogramming, but could not still convert. Conversely, pushing the metabolism toward a higher oxphos state providing only pyruvate and 2-deoxy-glucose, a competitive inhibitor for glucose, drove the converting astrocytes to even higher ROS production and total cell death. This suggests that ROS burst is just a maladaptive response of the converting cell to switch metabolism toward a higher oxphos state, which is somehow not functional and poses the cells to enormous stress. Notwithstanding, we demonstrated that the metabolic switch and reliance on an active ETC are necessary prerequisites for astrocyte conversion to neurons.

It has been widely studied that a proper metabolic change is necessary and sufficient for cell fate decision in spontaneous neurogenesis and iPSCs generation, but barely investigated in the field of direct neuronal reprogramming.

Indeed, understanding what happens from a metabolic point of view to astrocytes transitioning fate faces several technical challenges. A major limitation to reveal fine molecular changes at cellular level is associated to the fact that we convert with retroviruses only a limited numbers of astrocytes, out of the total transduced cells, producing a heterogeneous population of not converted astrocytes, neurons and intermediate transitioning cells (*Gascón et al., 2016; Masserdotti et al., 2015*). Furthermore, the majority of untransduced astrocytes still present in the culture impede the functional analysis of induced neurons metabolism, likely camouflaging metabolic differences between the two cell types. Indeed, as discussed in *Russo et al.*, these two cell types possess a different metabolism, but astrocytes possess a broader and more plastic metabolism, allowing them to rely both on oxphos and glycolysis. Furthermore, the different response of the converting cells and different outcome in neuronal subtype generated could further complicate a precise understanding of metabolic changes, especially *in vitro*. Thus, improvement in the reprogramming techniques and the quality of neurons generated could help unraveling new metabolic mechanisms. Notably, translating the findings regarding metabolic changes for iPSCs generation and neural stem cells differentiation might provide new knowledge for the field of reprogramming.

For example, in iPSCs reprogramming from fibroblasts, changes to a more glycolytic metabolism have been shown to occur (*Panopoulos et al., 2011; Prigione et al., 2014*) and also to be a driving force for the switch to happen, as pushing glycolytic metabolism by lowering O<sub>2</sub> or up-regulating key metabolic enzymes improves iPSCs generation (*Folmes et al., 2011; Yoshida et al., 2009*). Furthermore, acting directly on oxphos function with specific ETC inhibitors increases the glycolytic reliance of fibroblast, improving their conversion into iPSCs; while glycolysis inhibitors have the contrary effect (*Son et al., 2013*).

Notably, fibroblast conversion is associated to a transitory burst of ROS, which in this case is actually essential to drive the iPSCs formation, even if the final metabolism is still glycolytic, as its blockage hampers conversion (Kida et al., 2015). This burst of ROS needs to be controlled and be contained within a specific threshold, as its overactivation, exactly like for direct neuronal reprogramming, is detrimental for the process (Zhou et al., 2016). This could lead to the speculation that increased ROS activity, in iPSCs generation at least, may also be associated to functions that go beyond pure metabolism, as ROS are also important signaling mediators (Rafalski and Brunet, 2011). A better understanding of ROS function in the context of direct neuronal reprogramming might clarify unknown aspects of the process, as their tight association to metabolic pathways and to transcriptional regulation render them key determinants for cell fate change (Teslaa and Teitell, 2015).

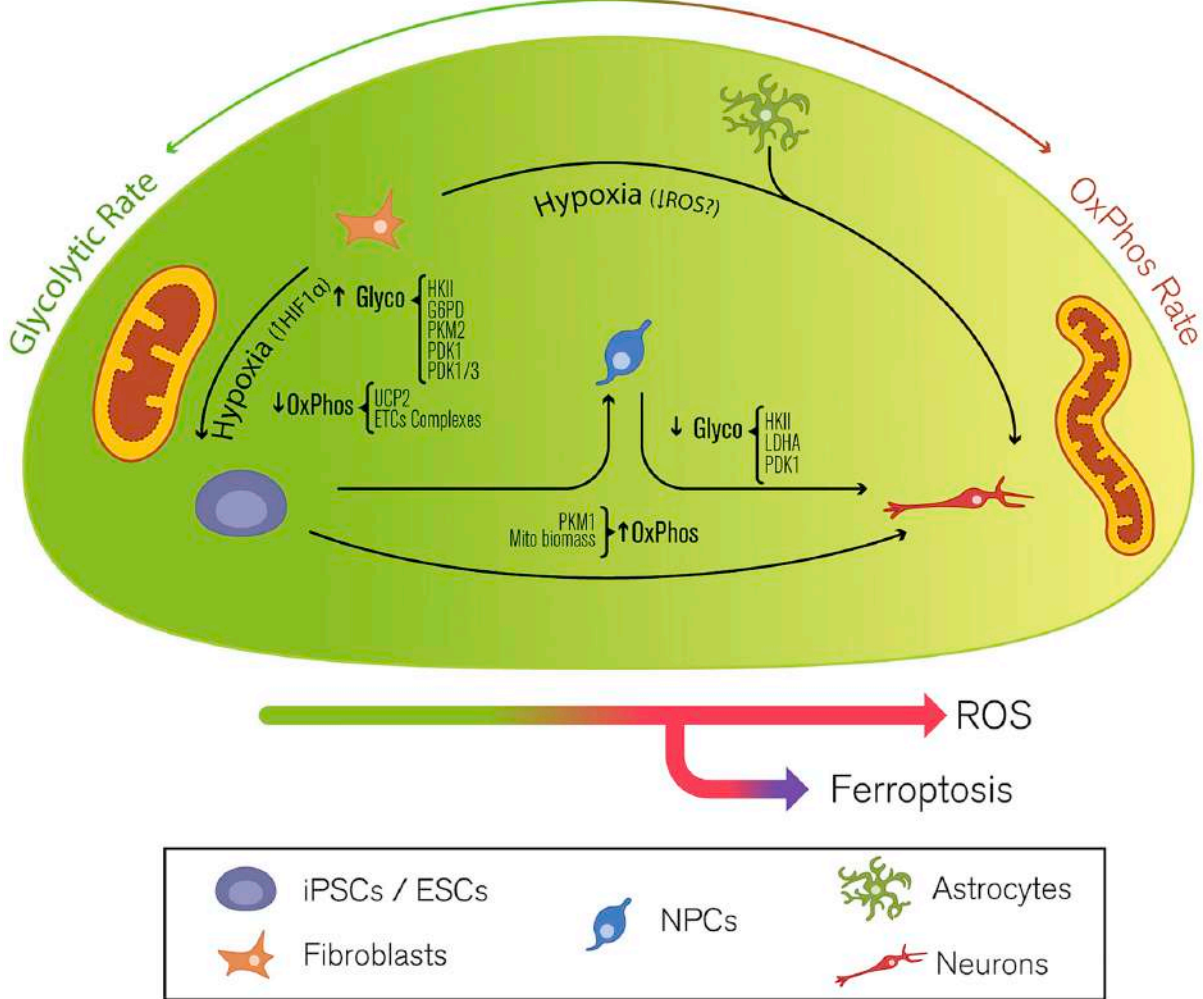


**Figure 7.** Metabolic changes during cell reprogramming to generate neurons (Gascón et al., 2017).

The role of ROS has also been investigated in neurogenesis, showing complicated and sometimes contrary mechanisms in response to their fine modulation, time of action, cellular specific context and dosage in which they act (Prozorovski et al., 2015). While the role of ROS in promoting neurogenesis is thus still a bit vague, that NSCs face a metabolic switch during differentiation is a consolidate knowledge.

Indeed, it has been shown that NSCs experience transcriptional changes from more glycolytic and lipid-based metabolism toward a more oxidative profile when differentiation in neurons occurs (Llorens-bobadilla et al., 2015; Shin et al., 2015), which is also physiologically coupled to an increased ROS production (Khacho et al., 2016). Interestingly, disruption of key proteins essential for proper mitochondrial function, as Drp1, involved in mediating fission of mitochondria (Steib et al., 2014), or TFAM, involved in mitochondria biogenesis (Beckervordersandforth et al., 2017), dramatically impairs neuronal generation, further confirming the necessity for neurons to have functional mitochondria to work. This was also demonstrated by several studies in which components of the oxphos machinery were ablated in different CNS cell types, proving broader metabolic adaptation for glial cells with major neuronal death if aerobic respiration is impaired (Diaz et al., 2012; Fünfschilling et al., 2012; Supplie et al., 2017).

Direct neuronal reprogramming has interesting correlates to endogenous neurogenesis. Despite that, reprogramming faces hurdles that neurogenesis does not, linked to epigenetic, genetic, metabolic and environmental barriers (Gascón et al., 2017).

Indeed it is fascinating that the physiological metabolic switch occurring in neurogenesis does not generally lead to cell death by ROS increase, as for reprogrammed neurons. This might be explained by different factors. First of all, we are not aware whether the ROS increase observed in direct conversion has a signaling function, as it is observed for NSCs differentiation (Le Belle et al., 2011), or is merely a side-effect of an occurring shift from glycolytic to oxidative metabolism. Indeed the strong transcriptional changes and protein synthesis induced by the transcription factors may dramatically alter the metabolism of the cell, causing ROS alteration (Lu and Thompson, 2012; Spinelli and Haigis, 2018).

Another likely possibility is that the endogenous neurons may better cope with the metabolic switch than induced ones because they already possess the metabolic machinery required for oxidative phosphorylation. It is known that NSCs already express the ETC components necessary for the neuronal metabolism, post-transcriptionally regulated with selective expression of inhibitors like ATP5IF1, which mimic oligomycin function. During NSCs differentiation these molecules are down-regulated, the ETC is activated and ROS increase at controlled levels to mediate transcriptional changes essential for neuronal generation (Khacho et al., 2016). Notwithstanding, big differences exist in mitochondria composition between different cell types, even if the ETC components are amongst the most preserved ones (Calvo and Mootha, 2010). However, also subtle differences in ETC subunit assembly, beyond their relative abundance, differentiate astrocytes and neurons in terms for example of ROS production (Lopez-Fabuel et al., 2016). We could also show that modulating mitochondrial proteome composition, underlying a functional metabolism (Johnson et al., 2007b), can be a driven force to improve the reprogramming process (*Russo et al.*).

The specific anti-oxidant system that each cell has could also contribute to a different outcome in neuronal generation from astrocytes or NSCs. We discussed in the introduction how neurons rely functionally on astrocytes both for substrates and anti-oxidant defense (Fernandez-Fernandez et al., 2012; Wang and Michaelis, 2010) and these cells indeed differ in term of specific anti-oxidant systems (*Russo et al.*). While the anti-oxidant molecules

typical for neurons are only late-induced during the conversion process of astrocytes, as for Prdx2 (Russo *et al.*), involved in important neuroprotective functions (Boulos *et al.*, 2007), neural stem cells might possess this machinery already from the beginning. Indeed the ordered and time-controlled process of physiological neurogenesis may be linked to better regulation of the machinery to cope and regulate oxidative stress.

Last but not least, a huge difference between neurogenesis and reprogramming is linked to the environment in which the cells integrate. While the neurogenic niches offer the perfect *milieu* of factors, cells and ECM to help newly generated neurons to integrate and survive (Doetsch, 2003; Falk and Götz, 2017), the process of reprogramming occurs in highly reactive tissue, filled with ROS and pro-inflammatory cytokines, which might be very hostile for the converted neurons to graft (Abdul-Muneer *et al.*, 2015; Glass *et al.*, 2010; Mattugini *et al.*).

Intriguingly reactive astrocytes, which acquire hallmarks of NSCs in the cortex following an injury (Sirko *et al.*, 2013) and share some aspects of their transcriptome (Götz *et al.*, 2015), require a functional ETC machinery to perform their function, as TFAM ablation prevents their activation (Fiebig *et al.*, 2019). Metabolic plasticity is thus essential not only for cell fate decision, as we demonstrated that preventing oxphos blocks direct neuronal reprogramming, but also to allow different function according to the cellular context, as it happens for immune cells activation (Ganeshan and Chawla, 2014).

As metabolic plasticity is mostly linked to mitochondria performance, a better understanding of the role that this organelle plays in the process of direct neuronal reprogramming is important. This is why I examined this previously uninvestigated aspect in the last part of my thesis.

### **Mitochondria reprogramming boosts astrocytes-to-glia conversion**

If ROS generation is a major hurdle to direct conversion of somatic cells into neurons, the role of mitochondria *per se* is rather underrated in the process. Since mitochondria are the main inducer of ROS and central hub for most of the metabolic pathways, regulating macromolecules synthesis and affecting transcriptional regulation, a careful estimation of their role in the reprogramming process is essential.

In Russo *et al.*, we first observed that a change in mitochondria morphology occurs from astrocytes to converted neurons, underlying changes in dynamic and function. To this aim, we decided to first evaluate if the metabolism of cortical astrocytes and e14-derived cortical neurons, as model for induced neurons, also *in vitro* was different, as suggested in literature. Indeed, we could observe profound functional differences with seahorse analysis between the two cell types analyzed, where astrocytes have a broader metabolic potential, relying both on oxphos and glycolysis, while neurons being able only to rely on oxphos for energy production. Digging more into the molecular characterization of these mitochondria, we decided to isolate functional organelles from both cell types, with good degree of purity, highlighting also at ultrastructural level through EM morphological differences, indicative of different metabolic profiles. We decided to perform proteomic analysis of independent biological replicates, identifying hundreds of differentially regulated proteins between neurons and astrocytes, leading to unique gene ontology terms. In particular, astrocytes GO

terms confirmed their higher metabolic plasticity, compared to neurons, and underlined that fatty acid oxidation is a peculiar pathway to this cortical glial cell. Interestingly, both cells showed higher representation of molecules involved in oxidative stress defense, even if their enzymatic machinery was not overlapping. Thus, we decided to evaluate astrocytic or neuronal mitochondrial protein expression during a time-course of astrocytes undergoing neuronal conversion. We demonstrated that neuron-specific mitochondrial proteins indeed appear in reprogrammed neurons, but are induced late during the process, around 5-7 days post-transduction. Surprisingly, the astrocyte-specific mitochondrial proteins are only partially down-regulated at this stage, demonstrating that a shift in mitochondria protein composition occurs, but only late and partial during the reprogramming process. This mitochondrial shift is also functional, as key enzymes involved in specific neuronal metabolic pathways, as glutaminase, appear also in reprogrammed neurons. As we also know that oxidative stress is an important hurdle to reprogramming, we decided to overexpress specific neuronal mitochondrial proteins involved in defense against ROS, early during the conversion of neurons. Indeed, the neuronal protein Prdx2 is up-regulated in reprogrammed neurons, but only at late stages of conversion. We took advantage of the recently developed dCas9 technology, where enzymatically dead dCas9 is fused with transcriptional activators, combined with gRNAs, targeting Sod1 and Prdx2 promoter region, to overexpress multiple endogenous genes. When combined with the proneural factor Ascl1, a seven-fold boost in the conversion of astrocytes into neurons was observed, further corroborated by time-lapse imaging analysis revealing increased survival and faster conversion. We thus reprogram for the first time mitochondria in a cell type-specific manner, proving a powerful effect on astrocyte-to-neuron conversion, suggesting mitochondria change to be a driving force for the process.

Astrocytes and neuronal metabolic functions have been widely investigated for decades, but a unanimous definition of their *in vivo* interplay has not yet been reached. As recently highlighted, understanding the cell-type specific function of mitochondria, involved beyond metabolic regulation also in mediating epigenetic, transcriptional and signaling events (Janke et al., 2015; Spinelli and Haigis, 2018), might greatly help understanding the functional effect on cell behavior. Despite the notion that specific mitochondrial function of astrocytes and neurons massively affect the physiology and pathology of the CNS (Fernandez-Fernandez et al., 2012; Willems et al., 2015), very few papers systematically evaluated the effect of the mitochondrial composition in the brain and its consequences on cell-specific function (Graham et al., 2017; Lopez-Fabuel et al., 2016); no one did in the field of direct neuronal reprogramming.

Intriguingly several papers unraveled a high degree of differences in mitochondria composition, with only between 50% and 70% of the mitochondrial proteins shared at similar levels between different organs (Mootha et al., 2003; Pagliarini et al., 2008). Obviously, similarly expressed mitochondrial proteins between organs and cells exist, like the proteins involved in the ETC machinery (Calvo and Mootha, 2010). Surprisingly, the mitochondrial proteome of the brain, the organ that consumes the biggest amount of energy and substrates within the body, has been rarely investigated, and mostly as whole tissue (Ingram and Chakrabarti, 2016). As we know that mitochondrial proteome composition can greatly affect

the organelle function as well as its response to physiological and pathological stimuli, it is important to clarify this also in the process of direct neuronal reprogramming.

Most studies evaluate broader changes in mitochondrial proteome from the whole tissue in pathological versus healthy conditions (Chou et al., 2011; Nilsen et al., 2007), clearly missing out substantial differences within different cell types which might contribute to the pathogenesis. Excitingly, recent studies on neurons investigated even sub-cellular differences in term of mitochondria composition, between synaptic and non-synaptic localization, showing dozens of proteins differentially expressed, underlying up to 30% difference in enzymatic activity (Graham et al., 2017; Völgyi et al., 2015). This clearly reveals how few we know of cell-type specific function of mitochondria. Our study evaluates and compares for the first time mitochondria proteome of cultured cortical neurons and astrocytes revealing profound differences with several cell-type specific pathways.

Some of the top GO terms of mitochondria from astrocytes are lipid metabolism and fatty acid  $\beta$ -oxidation, consistent with the expression of key enzymes regulating these pathways at transcriptomic level in adult cortical astrocytes (van Deijk et al., 2017; Hofmann et al., 2017). It is not fully understood why these pathways are specifically prominent in astrocytes, given that fatty acid oxidation requires higher oxygen levels compared to glycolysis (Schönfeld and Reiser, 2013), even if it produces more ATP at similar ROS rates (Darvey, 1998; Souza et al., 2019); but its importance in the brain is undeniable. Indeed 20% of the brain energy supply derives from fatty acid  $\beta$ -oxidation (Panov et al., 2014) and our *in vitro* data suggest that this pathway contributes to 30% of the total oxygen consumption within astrocytes, as shown by selectively blocking it with  $\beta$ -etomoxir (*data not shown*). Astrocyte dependence on this pathway might also vary according to the cellular context, as in a pathological environment with lack of glucose striatal astrocytes switch metabolism and start relying on fatty acid metabolism for energy production (Polyzos et al., 2019).

Interestingly, the role of fatty acid metabolism goes beyond regulating energy metabolism, as it has functional signaling effects, for example, in mediating diverse stem cell proliferative and quiescent state, as for NSCs and hematopoietic stem cells (Ito et al., 2012; Knobloch et al., 2012, 2017). It would be interesting to evaluate whether key enzymes that regulate fatty acid metabolism in mitochondrial astrocytes, such as Cpt1a or Acads, are actually down-regulated in converting neurons and which consequence their early down-regulation would have for neuronal conversion.

Other pathways more represented in astrocytes over neurons are linked to cellular respiration, mitochondria organization and respiratory electron transport chain. This is in line with the fact that Seahorse analysis results show a broader metabolic plasticity of astrocytes compared to neurons. Indeed a stronger reliance on oxphos in basal condition is present, but a compensatory mechanism with glycolysis for energy production is possible when oxphos is inhibited, on the contrary to neurons that lack this possibility. This is in line with evidence supporting higher reliance on oxphos for neurons (Bélanger et al., 2011; Kasischke et al., 2004), as also demonstrated by our OCR/ECAR ratio values, where neurons rely on double amount to oxphos compared to astrocytes already in basal condition. These data also underline that astrocytes in our culture have a stronger reliance on oxphos and fatty acid

oxidation for energy production, compared to *in vivo* where they seem mostly glycolytic in basal condition (Bélanger et al., 2011). Interestingly, region-specific heterogeneity of astrocytes has also been observed in term of reliance on metabolic substrates. Indeed, in a model of Huntington disease, astrocytes respond to neuronal vulnerability and overall reduced glucose level relying on different substrates for energy production, as fatty acids in the striatum or through amino acids metabolism in the cerebellum (Polyzos et al., 2019). This further supports the concept that astrocytes are more plastic in term of metabolic support than neurons and can use diverse metabolic substrates in challenging conditions.

Seahorse results reveal that both our cell types use their metabolism at their maximal rate, mostly linked to the *in vitro* condition and that neurons seem to have a lower metabolic activity compared to astrocytes. Even if this lower energy rate in neurons might not be intuitive, quantitative differences in term of ETC components within mitochondria amongst astrocytes and neurons might justify this relative difference. Another reason to justify this fact is the observation that our neuronal cultures are very pure, but may lack the fundamental glial components essential for neurons to receive the proper trophic and anti-oxidant support (Bélanger et al., 2011; Schreiner et al., 2015; Weber and Barros, 2015). This might thus limit the functionality of *in vitro* neurons, as well as their maturity. Indeed, even if our culture is differentiated until proper electrophysiological properties and mature markers arise, neurons could retain some properties of the stem cells from which they derive, as those are more immature in term of metabolic profile compared to adult post-mitotic neurons (Khacho et al., 2016; Llorens-bobadilla et al., 2015).

A more comprehensive study should anyway require more sophisticated isolation techniques of mitochondria, to further eliminate contaminants that are present in our isolation. This could improve a more defined discrimination of protein abundance. Indeed, even subtle differences in protein composition between astrocytes and neurons, like in the case of NDUFS1 subunit of Complex I, can lead to the formation of supercomplexes which generate diverse amount of ROS, contributing to specific cellular bioenergetic differences (Lopez-Fabuel et al., 2016). To discriminate and unravel novel protein function within mitochondria, cas9 technology can provide an easy solution and readout method in different cellular system (Arroyo et al., 2016; Jo et al., 2015), even for *in vivo* application (Zhou et al., 2018). Future studies should also take into account consistent processing and common databases for analysis (Calvo et al., 2016), to ease the identification of cell-specific metabolic pathways. Cell types selected for comparison, mitochondria from *in vitro* or *in vivo* cells, isolation techniques, statistical stringency and databases selected to define mitochondria proteins, should all be parameters to take into consideration when comparing results amongst different studies.

A further interesting correlate supporting our extrapolation of findings from neuronal culture to reprogrammed neurons comes from the observation of the mitochondrial morphology. Indeed, induced neurons, compared to the original astrocytes, display mitochondria with a smaller and roundish shape, less ramified, supporting their duty to provide energy in the long neuronal processes (Misgeld and Schwarz, 2017). In line with this, differential expression of mitochondrial proteins involved in regulating dynamic is observed, with a higher level of the fission regulator Drp1 in neurons and a higher level of the fusion regulator mitofusin1 in astrocytes. This would support the idea that astrocytes and neurons need different

mitochondrial network organization to support their own specific metabolic requirements, as also observed *in vivo* (Motori et al., 2013; Plucinska et al., 2012). Electron microscopy further sustains the idea of different mitochondrial dynamics between neurons and astrocytes, as the first appear smaller and roundish, while the second more ramified and elongated. Despite that, mitochondria ultrastructure in term of *cristae* organization and membrane invagination is comparably complex, supportive of mature organelles, as stem cells on the contrary have less complex and more immature mitochondria structural organization (Prigione et al., 2011).

This also implies that, beyond reorganizing mitochondrial proteome composition during direct neuronal conversion, the starter cell requires also the modification of its supramolecular structure for the functional change to occur. Thus, manipulating mitochondrial dynamic might greatly impact on neuronal generation. Indeed, impairment of its key molecular regulators has been shown to affect neurogenesis also *in vivo* (Ishihara et al., 2009; Oettinghaus et al., 2016; Steib et al., 2014). Proper mitochondrial dynamic changes can be further important for functional roles, properly distributing energy and molecules in all the compartments of the converting astrocyte into neuron, undergoing fast and drastic morphological reorganization. In iPSCs generation, for example, a transitory fission wave is essential for proper cell fate change (Martin et al., 2012; Prieto et al., 2016). Mitochondrial dynamic is also essential for proper cell function, as astrocytic mitochondria position next to the neuronal terminal when the energy demand is increased following activity or damage (Hayakawa et al., 2016; Jackson et al., 2014). Excitingly, some papers highlight also the possibility to modulate mitochondrial dynamic by the ability of mitochondria to be transferred between neighbor cells through nanotunnels (Wang and Gerdes, 2015). *In vivo* mitochondria transfer seems to occur and have a functional role in improving stroke recovery, as healthy mitochondria can be transferred from astrocytes to surrounding suffering neurons supporting their survival (Hayakawa et al., 2016). It could also be interesting to evaluate the role of autophagy, and consequently mitophagy, in supporting this process, as its modulation has been demonstrated to be essential for iPSCs generation (Ma et al., 2015; Wang et al., 2013) and in neuronal differentiation (Calvo-Garrido et al., 2019). In this study the autophagic adaptor p62 was demonstrated to be essential to forward neuro-epithelial stem cells in neurons differentiation, by allowing a metabolic switch from glycolysis to oxphos.

Thus, faster recycle of old mitochondria with a different metabolism and proteome composition, through increased dynamic and autophagic processes, could speed up the generation of mitochondria ready to support the new cell type generated. This can be particularly relevant for neurons, given the critical function that mitochondria play within this cell type to regulate multiple processes (Plucińska and Misgeld, 2016). Despite the fact that some of these results are difficult to reproduce, it suggests the exciting idea of modifying cell fate by direct modulation of mitochondria, as we also demonstrated to be functionally relevant for neuronal generation by overexpressing the neuronal mitochondrial proteins Prdx2 and Sod1.

Interestingly, mitochondria protein composition changes spontaneously during the transition from astrocytes to neurons, as we demonstrated by analyzing some markers by immunostaining over the process. Notably, this regulation of mitochondrial proteins is only partial and incomplete, as neuronal-enriched mitochondrial proteins up-regulate relatively late

during the conversion process, while astrocytes-enriched ones get only partially down-regulated, even at mature stages of conversion. This heterogeneous response in the switch in mitochondria composition may further influence the inefficient conversion process, inducing increased ROS production and cell death by ferroptosis (*Gascón et al., 2016*).

Despite that, the neuronal mitochondria proteins analyzed increased in expression when neuronal morphological features appeared, suggesting a functional metabolic switch to occur. This is the case for glutaminase, which catalyzes the hydrolysis of glutamine to glutamate and ammonia and is involved in generating neurotransmitters in neurons (Albrecht et al., 2010). This marker indeed appears already at 3 DPI, and by 7 DPI is represented in almost all of the analyzed neurons, independently from the neurogenic factors used for conversion, Neurog2 or Ascl1, suggesting a common mitochondria reorganization for glutamatergic or gabaergic neuronal cells.

On the contrary, the astrocytes-enriched mitochondria marker Sfxn5, a transporter for citrate, while correctly being retained in most of the non-converting astrocytes, is down-regulated in only 30% of the reprogrammed neurons. As we noticed that a switch in mitochondria marker composition increased with differentiation process, a further down-regulation of Sfxn5 at later stages of neuronal differentiation cannot be excluded, as we stopped our analysis at 7 DPI, time where usually mature neuronal features have been described (Heinrich et al., 2010; Masserdotti et al., 2015). Citrate is also an essential substrate to perform TCA cycle and oxphos, fundamental pathways within neurons. This suggests that a complete down-regulation of the transporter may not be an advantage for converting neurons, but the difference observed by proteomic analysis between neurons and astrocytes for this protein might be only quantitative, rather than functional.

Compared to the early induction of neuronal genes at transcriptomic levels, within 4 hours after activation of the neuronal program (Masserdotti et al., 2015), mitochondria remodeling seems to be far delayed, suggesting a more complicated proteomic regulation of these fundamental metabolic proteins. Important to note is that astrocytes undergoing conversion seem to face an intermediate confused stage in which not only astrocytic and neuronal markers overlap, as GFAP and  $\beta$ -III-tubulin, but also mitochondrial proteomic composition is changed at different pace, underlying metabolic pathways to be differentially replaced over time. The inefficiency in this process might further complicate the cell transition and increase ROS production. This prompted us to question whether modifying mitochondrial proteome composition earlier during the conversion could actually improve the process.

Interestingly, also Prdx2, an anti-oxidant protein enriched in neurons, involved in neuronal protection from oxidative stress and early expressed following injury (Boulos et al., 2007), is selectively increased in converting neurons only at late stages, while being absent from mitochondria of astrocytes. As this time-point is way beyond the peak in oxidative stress that induces death in converting astrocytes (*Gascón et al., 2016*), we asked what would happen if we overexpress this protein before the ROS wave occurs, together with the proneural transcription factor. Furthermore, resistance to oxidative stress was one of the common GO terms among astrocytes and neurons mito-proteome, consequent to specific expression of diverse anti-oxidant molecules. In particular beyond Prdx2, Sod1, a known scavenger of

superoxide radicals that when mutated lead to severe neurodegeneration (Bunton-Stasyshyn et al., 2015), was also found enriched in the mito-proteome of neurons.

To achieve expression of these proteins, we exploited the recently developed STAgR (String assembly gRNA cloning) and dCas9 technology (Breunig et al., 2018b), allowing synchronous overexpression of multiple endogenous targets. Up-regulating Sod1 and Prdx2 early in the reprogramming process, together with Ascl1, could greatly improve the generation of neurons, up to seven fold. Time-lapse experiments further revealed that these molecules had a dual mode of action, acting both on cell survival and neuronal maturation. In particular, the neuronal morphological features started to appear at the same time compared to control, but at a faster speed when the anti-oxidant molecules were expressed early. Control cells instead reached a *plateau* in differentiation within a few hours and were prone to death. It is important to mention that the very inefficient generation of neurons obtained in control cells, compared to other approaches previously published with retrovirus or lentivirus (Masserdotti et al., 2015; Rivetti di Val Cervo et al., 2017), is probably due to the triple transfection itself, usually associated to lower efficiency and higher mortality rate than other techniques.

Cas9 technology offers great advantages for direct neuronal reprogramming, as recently demonstrated by *in vivo* (Zhou et al., 2018) and *in vitro* (Black et al., 2016; Rubio et al., 2016) studies. It will be important to understand whether the powerful increase in reprogramming speed and efficiency achieved here, by activating only two neuron-specific mitochondrial genes, is specific or also true for other neuronal mitochondria genes. Genome-wide screening of mitochondrial proteins via CRISPR technology, as demonstrated for the OxPhos genes (Arroyo et al., 2016) or for epigenetic regulators in the brain *in vivo* (Swiech et al., 2015), could help answering this question and determining the mitochondrial proteins that are more relevant for the reprogramming process.

We just started to scratch the surface on understanding how manipulating the metabolism could affect cell fate decision and specifically neuronal generation from astrocytes. Greater knowledge in the function of mitochondria-related proteins in different cellular context, not only from a metabolic point of view, but also as signaling molecules and epigenetic regulators, could greatly benefit the field of neuronal reprogramming. Furthermore, it could also widen our knowledge on the physiological and pathological function of astrocytes and neurons within the *in vivo* environment.

Unraveling metabolic, mitochondria and environmental hurdles to the process could thus finally move the field of direct neuronal reprogramming from bench to clinic, being some of the greater challenges, but as well as opportunities, for the generation of functional neurons that properly integrated and survive in the brain tissue, supporting the recovery of the patient.

## Bibliography

- Abdul-Muneer, P.M., Chandra, N., and Haorah, J. (2015). Interactions of Oxidative Stress and Neurovascular Inflammation in the Pathogenesis of Traumatic Brain Injury. *Mol. Neurobiol.* *51*, 966–979.
- Akram, M. (2014). Citric Acid Cycle and Role of its Intermediates in Metabolism. *Cell Biochem. Biophys.* *68*, 475–478.
- Albert, M., Kalebic, N., Florio, M., Lakshmanaperumal, N., Haffner, C., Brandl, H., Henry, I., and Huttner, W.B. (2017). Epigenome profiling and editing of neocortical progenitor cells during development. *EMBO J.* *36*, 2642–2658.
- Albrecht, J., Sidoryk-Węgrzynowicz, M., Zielińska, M., and Aschner, M. (2010). Roles of glutamine in neurotransmission. *Neuron Glia Biol.* *6*, 263–276.
- Allaman, I., Bélanger, M., and Magistretti, P.J. (2011). Astrocyte–neuron metabolic relationships: for better and for worse. *Trends Neurosci.* *34*, 76–87.
- Altman, J. (1962). Are new neurons formed in the brains of adult mammals? *Science* *135*, 1127–1128.
- Alunni, A., and Bally-Cuif, L. (2016). A comparative view of regenerative neurogenesis in vertebrates. *Development* *143*, 741–753.
- Amamoto, R., and Arlotta, P. (2014). Development-inspired reprogramming of the mammalian central nervous system. *Science* (80-. ). *343*, 1239882.
- Amaral, A.I., Meisingset, T.W., Kotter, M.R., and Sonnewald, U. (2013). Metabolic aspects of Neuron-Oligodendrocyte-Astrocyte interactions. *Front. Endocrinol. (Lausanne)*. *4*, 1–5.
- Anderson, A.J., Haus, D.L., Hooshmand, M.J., Perez, H., Sontag, C.J., and Cummings, B.J. (2011). Achieving stable human stem cell engraftment and survival in the CNS: is the future of regenerative medicine immunodeficient? *Regen. Med.* *6*, 367–406.
- Anderson, M.A., Burda, J.E., Ren, Y., Ao, Y., O’Shea, T.M., Kawaguchi, R., Coppola, G., Khakh, B.S., Deming, T.J., and Sofroniew, M. V (2016). Astrocyte scar formation aids central nervous system axon regeneration. *Nature* *532*, 195–200.
- Arroyo, J.D., Jourdain, A.A., Calvo, S.E., Ballarano, C.A., Doench, J.G., Root, D.E., and Mootha, V.K. (2016). A Genome-wide CRISPR Death Screen Identifies Genes Essential for Oxidative Phosphorylation. *Cell Metab.* *24*, 875–885.
- Arundine, M., and Tymianski, M. (2004). Molecular mechanisms of glutamate-dependent neurodegeneration in ischemia and traumatic brain injury. *Cell. Mol. Life Sci.* *61*, 657–668.
- Avior, Y., Sagi, I., and Benvenisty, N. (2016). Pluripotent stem cells in disease modelling and drug discovery. *Nat. Rev. Mol. Cell Biol.* *17*, 170–182.
- Bacigaluppi, M., Russo, G.L., Peruzzotti-Jametti, L., Rossi, S., Sandrone, S., Butti, E., De Ceglia, R., Bergamaschi, A., Motta, C., Gallizioli, M., et al. (2016). Neural Stem Cell Transplantation Induces Stroke Recovery by Upregulating Glutamate Transporter GLT-1 in Astrocytes. *J. Neurosci.* *36*, 10529–10544.
- Bardhele, S., Krüger, M., Buggenthin, F., Schwausch, J., Ninkovic, J., Clevers, H., Snippert, H.J., Theis, F.J., Meyer-luehmann, M., Bechmann, I., et al. (2013). Live imaging of astrocyte responses to acute injury reveals selective juxtavascular proliferation. *Nat. Publ. Gr.* *16*, 580–586.
- Barrangou, R., Fremaux, C., Deveau, H., Richards, M., Boyaval, P., Moineau, S., Romero, D.A., and Horvath, P. (2007). CRISPR Provides Acquired Resistance Against Viruses in Prokaryotes. *Science* (80-. ). *315*, 1709–1712.
- Beckervordersandforth, R., Ebert, B., Schäffner, I., Moss, J., Fiebig, C., Shin, J., Moore, D.L., Ghosh, L., Trincherro, M.F., Stockburger, C., et al. (2017). Role of Mitochondrial Metabolism in the Control

of Early Lineage Progression and Aging Phenotypes in Adult Hippocampal Neurogenesis. *Neuron* 93, 560-573.e6.

Bélanger, M., Allaman, I., and Magistretti, P.J. (2011). Brain energy metabolism: Focus on Astrocyte-neuron metabolic cooperation. *Cell Metab.* 14, 724–738.

Le Belle, J.E., Orozco, N.M., Paucar, A.A., Saxe, J.P., Mottahedeh, J., Pyle, A.D., Wu, H., and Kornblum, H.I. (2011). Proliferative neural stem cells have high endogenous ROS levels that regulate self-renewal and neurogenesis in a PI3K/Akt-dependant manner. *Cell Stem Cell* 8, 59–71.

Benarroch, E.E. (2014). Brain glucose transporters: Implications for neurologic disease. *Neurology* 82, 1374–1379.

Berg, J.M., Tymoczko, J.L., and Stryer, L. (2002). *Biochemistry*. 5 edition. Section 30.1. Metabolism Consist of Highly Interconnected Pathways (W H Freeman).

Bergami, M., and Berninger, B. (2012). A fight for survival: The challenges faced by a newborn neuron integrating in the adult hippocampus. *Dev. Neurobiol.* 72, 1016–1031.

Birben, E., Sahiner, U.M., Sackesen, C., Erzurum, S., and Kalayci, O. (2012). Oxidative stress and antioxidant defense. *World Allergy Organ. J.* 5, 9–19.

Black, J.B., Adler, A.F., Wang, H.-G., D’Ippolito, A.M., Hutchinson, H.A., Reddy, T.E., Pitt, G.S., Leong, K.W., and Gersbach, C.A. (2016). Targeted Epigenetic Remodeling of Endogenous Loci by CRISPR/Cas9-Based Transcriptional Activators Directly Converts Fibroblasts to Neuronal Cells. *Cell Stem Cell* 19, 406–414.

Bolaños, J.P., and Almeida, A. (2009). The pentose-phosphate pathway in neuronal survival against nitrosative stress. *IUBMB Life* 62, NA-NA.

Boulos, S., Meloni, B.P., Arthur, P.G., Bojarski, C., and Knuckey, N.W. (2007). Peroxiredoxin 2 overexpression protects cortical neuronal cultures from ischemic and oxidative injury but not glutamate excitotoxicity, whereas Cu/Zn superoxide dismutase 1 overexpression protects only against oxidative injury. *J. Neurosci. Res.* 85, 3089–3097.

Breunig, C.T., Neuner, A.M., Giehl-Schwab, J., Wurst, W., Götz, M., and Stricker, S.H. (2018a). A Customizable Protocol for String Assembly gRNA Cloning (STAgR). *JoVE* e58556.

Breunig, C.T., Durovic, T., Neuner, A.M., Baumann, V., Wiesbeck, M.F., Köferle, A., Götz, M., Ninkovic, J., and Stricker, S.H. (2018b). One step generation of customizable gRNA vectors for multiplex CRISPR approaches through string assembly gRNA cloning (STAgR). *PLoS One* 10–12.

Brulet, R., Matsuda, T., Zhang, L., Miranda, C., Giacca, M., Kaspar, B.K., Nakashima, K., and Hsieh, J. (2017). NEUROD1 Instructs Neuronal Conversion in Non-Reactive Astrocytes. *Stem Cell Reports* 8, 1506–1515.

Buffo, A., Vosko, M.R., Erturk, D., Hamann, G.F., Jucker, M., Rowitch, D., and Gotz, M. (2005). Expression pattern of the transcription factor Olig2 in response to brain injuries: Implications for neuronal repair. *Proc. Natl. Acad. Sci.* 102, 18183–18188.

Buffo, A., Rite, I., Tripathi, P., Lepier, A., Colak, D., Horn, A.-P., Mori, T., and Götz, M. (2008). Origin and progeny of reactive gliosis: A source of multipotent cells in the injured brain. *Proc. Natl. Acad. Sci. U. S. A.* 105, 3581–3586.

Bunton-Stasyshyn, R.K.A., Saccon, R.A., Fratta, P., and Fisher, E.M.C. (2015). SOD1 Function and Its Implications for Amyotrophic Lateral Sclerosis Pathology. *Neurosci.* 21, 519–529.

Burda, J.E., and Sofroniew, M. V. (2014). Reactive gliosis and the multicellular response to CNS damage and disease. *Neuron* 81, 229–248.

Calvetti, D., and Somersalo, E. (2012). Ménage à Trois: The Role of Neurotransmitters in the Energy Metabolism of Astrocytes, Glutamatergic, and GABAergic Neurons. *J. Cereb. Blood Flow Metab.* 32, 1472–1483.

Calvo-Garrido, J., Maffezzini, C., Schober, F.A., Clemente, P., Uhlin, E., Kele, M., Stranneheim, H.,

- Lesko, N., Bruhn, H., Svenningsson, P., et al. (2019). SQSTM1/p62-Directed Metabolic Reprogramming Is Essential for Normal Neurodifferentiation. *Stem Cell Reports*.
- Calvo, S.E., and Mootha, V.K. (2010). The Mitochondrial Proteome and Human Disease. *Annu. Rev. Genomics Hum. Genet.* *11*, 25–44.
- Calvo, S.E., Clauser, K.R., and Mootha, V.K. (2016). MitoCarta2.0: an updated inventory of mammalian mitochondrial proteins. *Nucleic Acids Res.* *44*, D1251–D1257.
- Calzolari, F., Michel, J., and Baumgart, E.V. (2015). Fast clonal expansion and limited neural stem cell self-renewal in the adult subependymal zone.
- Carlén, M., Meletis, K., Göritz, C., Darsalia, V., Evergren, E., Tanigaki, K., Amendola, M., Barnabé-Heider, F., Yeung, M.S.Y., Naldini, L., et al. (2009). Forebrain ependymal cells are Notch-dependent and generate neuroblasts and astrocytes after stroke. *Nat. Neurosci.* *12*, 259–267.
- Carron, S.F., Alwis, D.S., and Rajan, R. (2016). Traumatic Brain Injury and Neuronal Functionality Changes in Sensory Cortex. *Front. Syst. Neurosci.* *10*, 47.
- Chavez, A., Scheiman, J., Vora, S., Pruitt, B.W., Tuttle, M., P R Iyer, E., Lin, S., Kiani, S., Guzman, C.D., Wiegand, D.J., et al. (2015). Highly efficient Cas9-mediated transcriptional programming. *Nat. Methods* *12*, 326–328.
- Chen, P.-C., Vargas, M.R., Pani, A.K., Smeyne, R.J., Johnson, D.A., Kan, Y.W., and Johnson, J.A. (2009). Nrf2-mediated neuroprotection in the MPTP mouse model of Parkinson's disease: Critical role for the astrocyte. *Proc. Natl. Acad. Sci.* *106*, 2933–2938.
- Chen, W.-W., Zhang, X., and Huang, W.-J. (2016). Role of neuroinflammation in neurodegenerative diseases. *Mol. Med. Rep.* *13*, 3391–3396.
- Chew, W.L., Tabebordbar, M., Cheng, J.K.W., Mali, P., Wu, E.Y., Ng, A.H.M., Zhu, K., Wagers, A.J., and Church, G.M. (2016). A multifunctional AAV–CRISPR–Cas9 and its host response. *Nat. Methods* *13*, 868–874.
- Cho, K.-O., Lybrand, Z.R., Ito, N., Bulet, R., Tafacory, F., Zhang, L., Good, L., Ure, K., Kernie, S.G., Birnbaum, S.G., et al. (2015). Aberrant hippocampal neurogenesis contributes to epilepsy and associated cognitive decline. *Nat. Commun.* *6*, 6606.
- Chou, J.L., Shenoy, D. V., Thomas, N., Choudhary, P.K., LaFerla, F.M., Goodman, S.R., and Breen, G.A.M. (2011). Early dysregulation of the mitochondrial proteome in a mouse model of Alzheimer's disease. *J. Proteomics* *74*, 466–479.
- Chouchane, M., Melo de Farias, A.R., Moura, D.M. de S., Hilscher, M.M., Schroeder, T., Leão, R.N., and Costa, M.R. (2017). Lineage Reprogramming of Astroglial Cells from Different Origins into Distinct Neuronal Subtypes. *Stem Cell Reports* *9*, 162–176.
- Chuquet, J., Quilichini, P., Nimchinsky, E.A., and Buzsaki, G. (2010). Predominant Enhancement of Glucose Uptake in Astrocytes versus Neurons during Activation of the Somatosensory Cortex. *J. Neurosci.* *30*, 15298–15303.
- Curtis, E., Martin, J.R., Gabel, B., Sidhu, N., Rzesiewicz, T.K., Mandeville, R., Van Gorp, S., Leerink, M., Tadokoro, T., Marsala, S., et al. (2018). A First-in-Human, Phase I Study of Neural Stem Cell Transplantation for Chronic Spinal Cord Injury. *Cell Stem Cell* *22*, 941-950.e6.
- Darvey, I.G. (1998). How does the ratio of ATP yield from the complete oxidation of palmitic acid to that of glucose compare with the relative energy contents of fat and carbohydrate?
- Davila, J., Chanda, S., Ang, C.E., Südhof, T.C., and Wernig, M. (2013). Acute reduction in oxygen tension enhances the induction of neurons from human fibroblasts. *J. Neurosci. Methods* *216*, 104–109.
- Davis, R.L., Weintraub, H., and Lassar, A.B. (1987). Expression of a single transfected cDNA converts fibroblasts to myoblasts. *Cell* *51*, 987–1000.
- van Deijk, A.-L.F., Camargo, N., Timmerman, J., Heistek, T., Brouwers, J.F., Mogavero, F.,

- Mansvelder, H.D., Smit, A.B., and Verheijen, M.H.G. (2017). Astrocyte lipid metabolism is critical for synapse development and function in vivo. *Glia* 65, 670–682.
- Díaz-García, C.M., and Yellen, G. (2018). Neurons rely on glucose rather than astrocytic lactate during stimulation. *J. Neurosci. Res.*
- Diaz, F., Garcia, S., Padgett, K.R., and Moraes, C.T. (2012). A defect in the mitochondrial complex III, but not complex IV, triggers early ROS-dependent damage in defined brain regions. *Hum. Mol. Genet.* 21, 5066–5077.
- Dimos, J.T., Rodolfa, K.T., Niakan, K.K., Weisenthal, L.M., Mitumoto, H., Chung, W., Croft, G.F., Saphier, G., Leibel, R., Golland, R., et al. (2008). Induced Pluripotent Stem Cells Generated from Patients with ALS Can Be Differentiated into Motor Neurons. *Science* (80-. ). 321, 1218–1221.
- Dimou, L., and Götz, M. (2014). Glial cells as progenitors and stem cells: new roles in the healthy and diseased brain. *Physiol Rev* 94, 709–737.
- Doetsch, F. (2003). A niche for adult neural stem cells. *Curr. Opin. Genet. Dev.* 13, 543–550.
- Drokhlyansky, E., Göz Aytürk, D., Soh, T.K., Chrenek, R., O’Loughlin, E., Madore, C., Butovsky, O., and Cepko, C.L. (2016). The brain parenchyma has a type I interferon response that can limit virus spread. *PNAS* E95–E104.
- Ewer, K.J., Lambe, T., Rollier, C.S., Spencer, A.J., Hill, A.V., and Dorrell, L. (2016). Viral vectors as vaccine platforms: from immunogenicity to impact. *Curr. Opin. Immunol.* 41, 47–54.
- Falk, S., and Götz, M. (2017). Glial control of neurogenesis. *Curr. Opin. Neurobiol.* 47, 188–195.
- Falkner, S., Grade, S., Dimou, L., Conzelmann, K.-K., Bonhoeffer, T., Götz, M., and Hübener, M. (2016). Transplanted embryonic neurons integrate into adult neocortical circuits. *Nature* 539, 248–253.
- Fang, D., Qing, Y., Yan, S., Chen, D., and Yan ShiDu, S. (2016). Development and Dynamic Regulation of Mitochondrial Network in Human Midbrain Dopaminergic Neurons Differentiated from iPSCs. *Stem Cell Reports* 7, 1–15.
- Fendt, S.-M., and Verstreken, P. (2017). Neurons eat glutamate to stay alive. *J. Cell Biol.* 216, 863–865.
- Fernandez-Fernandez, S., Almeida, A., and Bolaños, J.P. (2012). Antioxidant and bioenergetic coupling between neurons and astrocytes. *Biochem. J.* 443, 3–11.
- Fiebig, C., Keiner, S., Ebert, B., Schäffner, I., Jagasia, R., Lie, D.C., and Beckervordersandforth, R. (2019). Mitochondrial Dysfunction in Astrocytes Impairs the Generation of Reactive Astrocytes and Enhances Neuronal Cell Death in the Cortex Upon Photothrombotic Lesion. *Front. Mol. Neurosci.* 12, 40.
- Fishman, V.S., Shnayder, T.A., Orishchenko, K.E., Bader, M., Alenina, N., and Serov, O.L. (2015). Cell divisions are not essential for the direct conversion of fibroblasts into neuronal cells. *Cell Cycle* 14, 1188–1196.
- Folmes, C.D.L., Nelson, T.J., Martinez-Fernandez, A., Arrell, D.K., Lindor, J.Z., Dzeja, P.P., Ikeda, Y., Perez-Terzic, C., and Terzic, A. (2011). Somatic oxidative bioenergetics transitions into pluripotency-dependent glycolysis to facilitate nuclear reprogramming. *Cell Metab.* 14, 264–271.
- Forner, F., Foster, L.J., Campanaro, S., Valle, G., and Mann, M. (2006). Quantitative proteomic comparison of rat mitochondria from muscle, heart, and liver. *Mol. Cell. Proteomics* 5, 608–619.
- Frik, J., Merl-Pham, J., Plesnila, N., Mattugini, N., Kjell, J., Kraska, J., Gómez, R.M., Hauck, S.M., Sirko, S., and Götz, M. (2018). Cross-talk between monocyte invasion and astrocyte proliferation regulates scarring in brain injury. *EMBO Rep.* 19, e45294.
- Fünfschilling, U., Supplie, L.M., Mahad, D., Boretius, S., Saab, A.S., Edgar, J., Brinkmann, B.G., Kassmann, C.M., Tzvetanova, I.D., Möbius, W., et al. (2012). Glycolytic oligodendrocytes maintain myelin and long-term axonal integrity. *Nature* 485, 517–522.

- Gage, F.H. (2002). Neurogenesis in the adult brain. *J. Neurosci.* *22*, 612–613.
- Ganeshan, K., and Chawla, A. (2014). Metabolic regulation of immune responses. *Annu. Rev. Immunol.* *32*, 609–634.
- Gascón, S., Murenu, E., Masserdotti, G., Ortega, F., Russo, G.L., Petrik, D., Deshpande, A., Heinrich, C., Karow, M., Robertson, S.P., et al. (2016). Identification and Successful Negotiation of a Metabolic Checkpoint in Direct Neuronal Reprogramming. *Cell Stem Cell* *18*, 1–14.
- Gascón, S., Masserdotti, G., Russo, G.L., and Götz, M. (2017). Direct Neuronal Reprogramming: Achievements, Hurdles, and New Roads to Success. *Cell Stem Cell* *21*, 18–34.
- Glass, C.K., Saijo, K., Winner, B., Marchetto, M.C., and Gage, F.H. (2010). Mechanisms underlying inflammation in neurodegeneration. *Cell* *140*, 918–934.
- Gonçalves, J.T., Schafer, S.T., and Gage, F.H. (2016). Adult Neurogenesis in the Hippocampus: From Stem Cells to Behavior. *Cell* *167*, 897–914.
- Goodman, T., and Hajihosseini, M.K. (2015). Hypothalamic tanycytes—masters and servants of metabolic, neuroendocrine, and neurogenic functions. *Front. Neurosci.* *9*, 387.
- Götz, M., Sirko, S., Beckers, J., and Irmeler, M. (2015). Reactive astrocytes as neural stem or progenitor cells: In vivo lineage, In vitro potential, and Genome-wide expression analysis. *Glia* *63*, 1452–1468.
- Grade, S., and Götz, M. (2017). Neuronal replacement therapy: previous achievements and challenges ahead. *Regen. Med.* *2*.
- Graham, L.C., Eaton, S.L., Brunton, P.J., Atrih, A., Smith, C., Lamont, D.J., Gillingwater, T.H., Pennetta, G., Skehel, P., and Wishart, T.M. (2017). Proteomic profiling of neuronal mitochondria reveals modulators of synaptic architecture. *Mol. Neurodegener.* *12*, 77.
- Grande, A., Sumiyoshi, K., López-Juárez, A., Howard, J., Sakthivel, B., Aronow, B., Campbell, K., and Nakafuku, M. (2013). Environmental impact on direct neuronal reprogramming in vivo in the adult brain. *Nat. Commun.* *4*, 2373.
- Grath, A., and Dai, G. (2019). Direct cell reprogramming for tissue engineering and regenerative medicine. *J. Biol. Eng.* *13*, 14.
- Guo, Z., Zhang, L., Wu, Z., Chen, Y., Wang, F., and Chen, G. (2014). In Vivo Direct Reprogramming of Reactive Glial Cells into Functional Neurons after Brain Injury and in an Alzheimer's Disease Model. *Cell Stem Cell* *14*, 188–202.
- Gyoneva, S., and Ransohoff, R.M. (2015). Inflammatory reaction after traumatic brain injury: therapeutic potential of targeting cell-cell communication by chemokines. *Trends Pharmacol. Sci.* *36*, 471–480.
- Hallett, P.J., Deleidi, M., Astradsson, A., Smith, G.A., Cooper, O., Osborn, T.M., Sundberg, M., Moore, M.A., Perez-Torres, E., Brownell, A.-L., et al. (2015). Successful Function of Autologous iPSC-Derived Dopamine Neurons following Transplantation in a Non-Human Primate Model of Parkinson's Disease. *Cell Stem Cell* *16*, 269–274.
- Harris, J.J., Jolivet, R., and Attwell, D. (2012). Synaptic Energy Use and Supply. *Neuron* *75*, 762–777.
- Hayakawa, K., Esposito, E., Wang, X., Terasaki, Y., Liu, Y., Xing, C., Ji, X., and Lo, E.H. (2016). Transfer of mitochondria from astrocytes to neurons after stroke. *Nature* *535*, 551–555.
- Heinrich, C., Blum, R., Gascón, S., Masserdotti, G., Tripathi, P., Sánchez, R., Tiedt, S., Schroeder, T., Götz, M., and Berninger, B. (2010). Directing Astroglia from the Cerebral Cortex into Subtype Specific Functional Neurons. *PLoS Biol.* *8*, e1000373.
- Heinrich, C., Bergami, M., Gascón, S., Lepier, A., Viganò, F., Dimou, L., Sutor, B., Berninger, B., and Götz, M. (2014). Sox2-mediated conversion of NG2 glia into induced neurons in the injured adult cerebral cortex. *Stem Cell Reports* *3*, 1000–1014.
- Heinrich, C., Spagnoli, F.M., and Berninger, B. (2015). In vivo reprogramming for tissue repair. *Nat.*

Cell Biol. 17, 204–211.

Heins, N., Malatesta, P., Cecconi, F., Nakafuku, M., Tucker, K.L., Hack, M.A., Chapouton, P., Barde, Y.-A., and Götz, M. (2002). Glial cells generate neurons: the role of the transcription factor Pax6. *Nat. Neurosci.* 5, 308–315.

Herrero-mendez, A., Almeida, A., Fernández, E., Maestre, C., Moncada, S., and Bolaños, J.P. (2009). The bioenergetic and antioxidant status of neurons is controlled by continuous degradation of a key glycolytic enzyme by APC / C – Cdh1. *Nat. Cell Biol.* 11, 747–754.

Hofmann, K., Rodriguez-Rodriguez, R., Gaebler, A., Casals, N., Scheller, A., and Kuerschner, L. (2017). Astrocytes and oligodendrocytes in grey and white matter regions of the brain metabolize fatty acids. *Sci. Rep.* 7, 10779.

Hou, S.-W., Wang, Y.-Q., Xu, M., Shen, D.-H., Wang, J.-J., Huang, F., Yu, Z., and Sun, F.-Y. (2008). Functional Integration of Newly Generated Neurons Into Striatum After Cerebral Ischemia in the Adult Rat Brain. *Stroke* 39, 2837–2844.

Hu, W., Qiu, B., Guan, W., Wang, Q., Wang, M., Li, W., Gao, L., Shen, L., Huang, Y., Xie, G., et al. (2015). Direct Conversion of Normal and Alzheimer’s Disease Human Fibroblasts into Neuronal Cells by Small Molecules. *Cell Stem Cell* 17, 204–212.

Hu, X., Qin, S., Huang, X., Yuan, Y., Tan, Z., Gu, Y., Cheng, X., Wang, D., Lian, X.-F., He, C., et al. (2019). Region-Restrict Astrocytes Exhibit Heterogeneous Susceptibility to Neuronal Reprogramming. *Stem Cell Reports* 12, 290–304.

Ingram, T., and Chakrabarti, L. (2016). Proteomic profiling of mitochondria: what does it tell us about the ageing brain? *Aging (Albany, NY)*. 8, 3161–3179.

Ishihara, N., Nomura, M., Jofuku, A., Kato, H., Suzuki, S.O., Masuda, K., Otera, H., Nakanishi, Y., Nonaka, I., Goto, Y., et al. (2009). Mitochondrial fission factor Drp1 is essential for embryonic development and synapse formation in mice. *Nature* 11, 958–966.

Ito, K., Carracedo, A., Weiss, D., Arai, F., Ala, U., Avigan, D.E., Schafer, Z.T., Evans, R.M., Suda, T., Lee, C., et al. (2012). PML – PPAR-  $\delta$  pathway for fatty acid oxidation regulates hematopoietic stem cell maintenance. *Nat. Med.* 18, 1350–1358.

Ivanov, A.I., Malkov, A.E., Waseem, T., Mukhtarov, M., Buldakova, S., Gubkina, O., Zilberter, M., and Zilberter, Y. (2014). Glycolysis and oxidative phosphorylation in neurons and astrocytes during network activity in hippocampal slices. *J. Cereb. Blood Flow Metab.* 34, 397–407.

Jackson, J.G., O’Donnell, J.C., Takano, H., Coulter, D.A., and Robinson, M.B. (2014). Neuronal activity and glutamate uptake decrease mitochondrial mobility in astrocytes and position mitochondria near glutamate transporters. *J. Neurosci.* 34, 1613–1624.

Janke, R., Dodson, A.E., and Rine, J. (2015). Metabolism and Epigenetics. *Annu. Rev. Cell Dev. Biol.* 31, 473–496.

Jassam, Y.N., Izzy, S., Whalen, M., MCGavern, D.B., and El Khoury, J. (2017). Neuroimmunology of Traumatic Brain Injury: Time for a Paradigm Shift. *Neuron* 95, 1246–1265.

Jo, A., Ham, S., Lee, G.H., Lee, Y.-I., Kim, S., Lee, Y.-S., Shin, J.-H., and Lee, Y. (2015). Efficient Mitochondrial Genome Editing by CRISPR/Cas9. *Biomed Res. Int.* 2015, 1–10.

John Lin, C.-C., Yu, K., Hatcher, A., Huang, T.-W., Lee, H.K., Carlson, J., Weston, M.C., Chen, F., Zhang, Y., Zhu, W., et al. (2017). Identification of diverse astrocyte populations and their malignant analogs. *Nat. Neurosci.* 20, 396–405.

Johnson, D.T., Harris, R.A., French, S., Blair, P. V., You, J., Bemis, K.G., Wang, M., and Balaban, R.S. (2007a). Tissue heterogeneity of the mammalian mitochondrial proteome. *Am. J. Physiol. Physiol.* 292, C689–C697.

Johnson, D.T., Harris, R.A., Blair, P. V., and Balaban, R.S. (2007b). Functional consequences of mitochondrial proteome heterogeneity. *Am. J. Physiol. Physiol.* 292, C698–C707.

- Kandasamy, M., Roskopf, M., Wagner, K., Klein, B., Couillard-Despres, S., Reitsamer, H.A., Stephan, M., Nguyen, H.P., Riess, O., Bogdahn, U., et al. (2015). Reduction in Subventricular Zone-Derived Olfactory Bulb Neurogenesis in a Rat Model of Huntington's Disease Is Accompanied by Striatal Invasion of Neuroblasts. *PLoS One* *10*, e0116069.
- Karimi-Abdolrezaee, S., Eftekharpour, E., Wang, J., Morshead, C.M., and Fehlings, M.G. (2006). Delayed Transplantation of Adult Neural Precursor Cells Promotes Remyelination and Functional Neurological Recovery after Spinal Cord Injury. *J. Neurosci.* *16*, 2649–2658.
- Karow, M., Sánchez, R., Schichor, C., Masserdotti, G., Ortega, F., Heinrich, C., Gascón, S., Khan, M.A., Lie, D.C., Dellavalle, A., et al. (2012). Reprogramming of pericyte-derived cells of the adult human brain into induced neuronal cells. *Cell Stem Cell* *11*, 471–476.
- Kasahara, A., and Scorrano, L. (2014). Mitochondria: from cell death executioners to regulators of cell differentiation. *Trends Cell Biol.* *24*, 761–770.
- Kasischke, K.A., Vishwasrao, H.D., Fisher, P.J., Zipfel, W.R., and Webb, W.W. (2004). Neural activity triggers neuronal oxidative metabolism followed by astrocytic glycolysis. *Science* (80-. ). *305*, 99–103.
- Khacho, M., Clark, A., Svoboda, D.S., Azzi, J., Maclaurin, J.G., Meghaizel, C., Sesaki, H., Lagace, D.C., Germain, M., Harper, M.-E., et al. (2016). Mitochondrial Dynamics Impacts Stem Cell Identity and Fate Decisions by Regulating a Nuclear Transcriptional Program. *Cell Stem Cell* *19*, 1–16.
- Kida, Y.S., Kawamura, T., Wei, Z., Sogo, T., Jacinto, S., Shigeno, A., Kushige, H., Yoshihara, E., Liddle, C., Ecker, J.R., et al. (2015). ERRs mediate a metabolic switch required for somatic cell reprogramming to pluripotency. *Cell Stem Cell* *16*, 547–555.
- Knobloch, M., Braun, S.M.G., Zurkirchen, L., von Schoultz, C., Zamboni, N., Araúzo-Bravo, M.J., Kovacs, W.J., Karalay, Ö., Suter, U., Machado, R.A.C., et al. (2012). Metabolic control of adult neural stem cell activity by Fasn-dependent lipogenesis. *Nature* *493*, 226–230.
- Knobloch, M., Pilz, G.-A., Ghesquière, B., Kovacs, W.J., Wegleiter, T., Moore, D.L., Hruzova, M., Zamboni, N., Carmeliet, P., and Jessberger, S. (2017). A Fatty Acid Oxidation-Dependent Metabolic Shift Regulates Adult Neural Stem Cell Activity. *Cell Rep.* *20*, 2144–2155.
- Knott, A.B., Perkins, G., Schwarzenbacher, R., and Bossy-wetzel, E. (2008). Mitochondrial fragmentation in neurodegeneration. *Nat. Rev. Neurosci.* *9*, 505–518.
- Koyuncu, O.O., Hogue, I.B., and Enquist, L.W. (2013). Virus infections in the nervous system. *Cell Host Microbe* *13*, 379–393.
- Kunitsyna, T.A., Ivashkina, O.I., Roshchina, M.A., Toropova, K.A., and Anokhin, K. V. (2016). Lentiviral Transduction of Neurons in Adult Brain: Evaluation of Inflammatory Response and Cognitive Effects in Mice. *Bull. Exp. Biol. Med.* *161*, 316–319.
- Lake, B.B., Ai, R., Kaeser, G.E., Salathia, N.S., Yung, Y.C., Liu, R., Wildberg, A., Gao, D., Fung, H.-L., Chen, S., et al. (2016). Neuronal subtypes and diversity revealed by single-nucleus RNA sequencing of the human brain. *Science* (80-. ). *352*, 1586–1590.
- Lanjakornsiripan, D., Pior, B.-J., Kawaguchi, D., Furutachi, S., Tahara, T., Katsuyama, Y., Suzuki, Y., Fukazawa, Y., and Gotoh, Y. (2018). Layer-specific morphological and molecular differences in neocortical astrocytes and their dependence on neuronal layers. *Nat. Commun.* *9*, 1623.
- Lazarov, O., Mattson, M.P., Peterson, D.A., Pimplikar, S.W., and van Praag, H. (2010). When neurogenesis encounters aging and disease. *Trends Neurosci.* *33*, 569–579.
- Leker, R.R., and Shohami, E. (2002). Cerebral ischemia and trauma—different etiologies yet similar mechanisms: neuroprotective opportunities. *Brain Res. Rev.* *39*, 55–73.
- Letts, J.A., and Sazanov, L.A. (2017). Clarifying the supercomplex: the higher-order organization of the mitochondrial electron transport chain. *Nat. Struct. Mol. Biol.* *24*, 800–808.
- Li, Q., and Barres, B.A. (2017). Microglia and macrophages in brain homeostasis and disease. *Nat. Rev. Immunol.* *18*, 225–242.

- Li, X., Zuo, X., Jing, J., Ma, Y., Wang, J., Liu, D., Zhu, J., Du, X., Xiong, L., Du, Y., et al. (2015). Small-Molecule-Driven Direct Reprogramming of Mouse Fibroblasts into Functional Neurons. *Cell Stem Cell* 17, 195–203.
- Liddelw, S.A., and Barres, B.A. (2017). Reactive Astrocytes: Production, Function, and Therapeutic Potential. *Immunity* 46, 957–967.
- Lim, D.A., and Alvarez-Buylla, A. (2016). The Adult Ventricular-Subventricular Zone (V-SVZ) and Olfactory Bulb (OB) Neurogenesis. *Cold Spring Harb. Perspect. Biol.* 8, a018820.
- Liu, Y., Miao, Q., Yuan, J., Han, S., Zhang, P., Li, S., Rao, Z., Zhao, W., Ye, Q., Geng, J., et al. (2015). Ascl1 Converts Dorsal Midbrain Astrocytes into Functional Neurons In Vivo. *J. Neurosci.* 35, 9336–9355.
- Llorens-bobadilla, E., Zhao, S., Baser, A., Saiz-castro, G., Zwadlo, K., and Martin-Villalba, A. (2015). Single-Cell Transcriptomics Reveals a Population of Dormant Neural Stem Cells that Become Activated upon Brain Injury. *Cell Stem Cell* 17, 329–340.
- London, A., Cohen, M., and Schwartz, M. (2013). Microglia and monocyte-derived macrophages: functionally distinct populations that act in concert in CNS plasticity and repair. *Front. Cell. Neurosci.* 7, 34.
- Lopez-Fabuel, I., Le Douce, J., Logan, A., James, A.M., Bonvento, G., Murphy, M.P., Almeida, A., and Bolaños, J.P. (2016). Complex I assembly into supercomplexes determines differential mitochondrial ROS production in neurons and astrocytes. *Proc. Natl. Acad. Sci. U. S. A.* 113, 13063–13068.
- Lowenstein, P.R., Mandel, R.J., Xiong, W.-D., Kroeger, K., and Castro, M.G. (2007). Immune responses to adenovirus and adeno-associated vectors used for gene therapy of brain diseases: the role of immunological synapses in understanding the cell biology of neuroimmune interactions. *Curr. Gene Ther.* 7, 347–360.
- Lu, C., and Thompson, C.B. (2012). Metabolic regulation of epigenetics. *Cell Metab.* 16, 9–17.
- Lunt, S.Y., and Vander Heiden, M.G. (2011). Aerobic Glycolysis: Meeting the Metabolic Requirements of Cell Proliferation. *Annu. Rev. Cell Dev. Biol.* 27, 441–464.
- Luo, C., Keown, C.L., Kurihara, L., Zhou, J., He, Y., Li, J., Castanon, R., Lucero, J., Nery, J.R., Sandoval, J.P., et al. (2017). Single-cell methylomes identify neuronal subtypes and regulatory elements in mammalian cortex. *Science* (80-. ). 357, 600–604.
- Ma, T., Li, J., Xu, Y., Yu, C., Xu, T., Wang, H., Liu, K., Cao, N., Nie, B., Zhu, S., et al. (2015). Atg5-independent autophagy regulates mitochondrial clearance and is essential for iPSC reprogramming. *Nat. Cell Biol.* 17, 1379–1387.
- Mächler, P., Wyss, M.T., Elsayed, M., Stobart, J., Gutierrez, R., Von Faber-Castell, A., Kaelin, V., Zuend, M., San Martín, A., Romero-Gómez, I., et al. (2016). In Vivo Evidence for a Lactate Gradient from Astrocytes to Neurons. *Cell Metab.* 23, 94–102.
- Magistretti, P.J., and Allaman, I. (2015). A Cellular Perspective on Brain Energy Metabolism and Functional Imaging. *Neuron* 86, 883–901.
- Magnusson, J.P., Göritz, C., Tatarishvili, J., Dias, D.O., Smith, E.M.K., Lindvall, O., Kokaia, Z., Frisén, J., Sirko, S., Behrendt, G., et al. (2014). A latent neurogenic program in astrocytes regulated by Notch signaling in the mouse. *Science* 346, 237–241.
- Mall, M., Kareta, M.S., Chanda, S., Ahlenius, H., Perotti, N., Zhou, B., Grieder, S.D., Ge, X., Drake, S., Euong Ang, C., et al. (2017). Myt1l safeguards neuronal identity by actively repressing many non-neuronal fates. *Nature* 544, 245–249.
- Mancini, G., and Horvath, T.L. (2018). Viral Vectors for Studying Brain Mechanisms that Control Energy Homeostasis. *Cell Metab.* 27, 1168–1175.
- Marro, S., Pang, Z.P., Yang, N., Tsai, M.C., Qu, K., Chang, H.Y., Südhof, T.C., and Wernig, M. (2011). Direct lineage conversion of terminally differentiated hepatocytes to functional neurons. *Cell*

Stem Cell 9, 374–382.

Martin, A.V., Cufí, S., Faja, B.C., Oliveras, C., Vellon, L., and Menendez, J.A. (2012). Mitochondrial fusion by pharmacological manipulation impedes somatic cell reprogramming to pluripotency: New insight into the role of mitophagy in cell stemness. *Aging (Albany, NY)*. 4, 393–401.

Martino, G., and Pluchino, S. (2006). The therapeutic potential of neural stem cells. *Nat. Rev. Neurosci.* 7, 395–406.

Masserdotti, G., Gillotin, S., Sutor, B., Drechsel, D., Irmeler, M., Jørgensen, H.F., Sass, S., Theis, F.J., Beckers, J., Berninger, B., et al. (2015). Transcriptional Mechanisms of Proneural Factors and REST in Regulating Neuronal Reprogramming of Astrocytes. *Cell Stem Cell* 17, 74–88.

Masserdotti, G., Gascon, S., and Götz, M. (2016). Direct neuronal reprogramming: learning from and for development. *Development* 143, 2494–2510.

Matsuda, T., Irie, T., Katsurabayashi, S., Hayashi, Y., Nagai, T., Hamazaki, N., Adefuin, A.M.D., Miura, F., Ito, T., Kimura, H., et al. (2019). Pioneer Factor NeuroD1 Rearranges Transcriptional and Epigenetic Profiles to Execute Microglia-Neuron Conversion. *Neuron* 101, 472–485.e7.

Mattugini, N., Merl-Pham, J., Petrozziello, E., Schindler, L., Bernhagen, J., Hauck, S.M., and Götz, M. (2018). Influence of white matter injury on gray matter reactive gliosis upon stab wound in the adult murine cerebral cortex. *Glia* 66, 1644–1662.

McKee, C.A., and Lukens, J.R. (2016). Emerging Roles for the Immune System in Traumatic Brain Injury. *Front. Immunol.* 7, 556.

Mingozzi, F., and High, K.A. (2013). Immune responses to AAV vectors: overcoming barriers to successful gene therapy. *Blood* 122, 23–36.

Misgeld, T., and Schwarz, T.L. (2017). Mitostasis in Neurons: Maintaining Mitochondria in an Extended Cellular Architecture. *Neuron* 96, 651–666.

Mlody, B., and Prigione, A. (2016). A Glycolytic Solution for Pluripotent Stem Cells. *Stem Cell* 19, 419–420.

Montani, L., and Suter, U. (2018). Building lipids for myelin. *Aging (Albany, NY)*. 10, 861–862.

Mootha, V.K., Bunkenborg, J., Olsen, J. V., Hjerrild, M., Wisniewski, J.R., Stahl, E., Bolouri, M.S., Ray, H.N., Sihag, S., Kamal, M., et al. (2003). Integrated analysis of protein composition, tissue diversity, and gene regulation in mouse mitochondria. *Cell* 115, 629–640.

Morel, L., Chiang, M.S.R., Higashimori, H., Shoneye, T., Iyer, L.K., Yelick, J., Tai, A., and Yang, Y. (2017). Molecular and Functional Properties of Regional Astrocytes in the Adult Brain. *J. Neurosci.* 37, 8706–8717.

Morizane, A., Kikuchi, T., Hayashi, T., Mizuma, H., Takara, S., Doi, H., Mawatari, A., Glasser, M.F., Shiina, T., Ishigaki, H., et al. (2017). MHC matching improves engraftment of iPSC-derived neurons in non-human primates. *Nat. Commun.* 8, 385.

Motori, E., Puyal, J., Toni, N., Ghanem, A., Angeloni, C., Malaguti, M., Cantelli-Forti, G., Berninger, B., Conzelmann, K.K., Götz, M., et al. (2013). Inflammation-induced alteration of astrocyte mitochondrial dynamics requires autophagy for mitochondrial network maintenance. *Cell Metab.* 18, 844–859.

Murphy, M.P. (2009). How mitochondria produce reactive oxygen species. *13*, 1–13.

Naldini, L. (2011). Ex vivo gene transfer and correction for cell-based therapies. *Nat. Rev. Genet.* 12, 301–315.

Nath, S., and Villadsen, J. (2015). Oxidative phosphorylation revisited. *Biotechnol. Bioeng.* 112, 429–437.

Nilsen, J., Irwin, R.W., Gallaher, T.K., and Brinton, R.D. (2007). Estradiol In Vivo Regulation of Brain Mitochondrial Proteome. *J. Neurosci.* 27, 14069–14077.

- Niu, W., Zang, T., Zou, Y., Fang, S., Smith, D.K., Bachoo, R., and Zhang, C.-L. (2013). In vivo reprogramming of astrocytes to neuroblasts in the adult brain. *Nat. Cell Biol.* *15*, 1164–1175.
- Nudo, R.J. (2013). Recovery after brain injury: mechanisms and principles. *Front. Hum. Neurosci.* *7*, 887.
- Oettinghaus, B., Schulz, J.M., Restelli, L.M., Licci, M., Savoia, C., Schmidt, A., Schmitt, K., Grimm, A., Morè, L., Hench, J., et al. (2016). Synaptic dysfunction, memory deficits and hippocampal atrophy due to ablation of mitochondrial fission in adult forebrain neurons. *Cell Death Differ.* *23*, 18–28.
- Pagliarini, D.J., Calvo, S.E., Chang, B., Sheth, S.A., Vafai, S.B., Ong, S.-E., Walford, G.A., Sugiana, C., Boneh, A., Chen, W.K., et al. (2008). A Mitochondrial Protein Compendium Elucidates Complex I Disease Biology. *Cell* *134*, 112–123.
- Pang, Z.P., Yang, N., Vierbuchen, T., Ostermeier, A., Fuentes, D.R., Yang, T.Q., Citri, A., Sebastiano, V., Marro, S., Südhof, T.C., et al. (2011). Induction of human neuronal cells by defined transcription factors. *Nature* *476*, 220–223.
- Panopoulos, A.D., Yanes, O., Ruiz, S., Kida, Y.S., Diep, D., Tautenhahn, R., Herrerías, A., Batchelder, E.M., Plongthongkum, N., Lutz, M., et al. (2011). The metabolome of induced pluripotent stem cells reveals metabolic changes occurring in somatic cell reprogramming. *Cell Res.* *22*, 168–177.
- Panov, A., Orynbayeva, Z., Vavilin, V., and Lyakhovich, V. (2014). Fatty Acids in Energy Metabolism of the Central Nervous System. *Biomed Res. Int.* *2014*, 1–22.
- Papandreou, I., Cairns, R.A., Fontana, L., Lim, A.L., and Denko, N.C. (2006). HIF-1 mediates adaptation to hypoxia by actively downregulating mitochondrial oxygen consumption. *Cell Metab.* *3*, 187–197.
- Pekny, M., and Pekna, M. (2014). Astrocyte Reactivity and Reactive Astroglia: Costs and Benefits. *Physiol. Rev.* *94*, 1077–1098.
- Pellerin, L., and Magistretti, P.J. (1994). Glutamate uptake into astrocytes stimulates aerobic glycolysis: a mechanism coupling neuronal activity to glucose utilization. *Proc. Natl. Acad. Sci. U. S. A.* *91*, 10625–10629.
- Pellerin, L., Pellegrini, G., Bittar, P.G., Charnay, Y., Bouras, C., Martin, J.-L., Stella, N., and Magistretti, P.J. (1998). Evidence Supporting the Existence of an Activity-Dependent Astrocyte-Neuron Lactate Shuttle. *Dev. Neurosci.* *20*, 291–299.
- Perevoshchikova, I. V., Quinlan, C.L., Orr, A.L., Gerencser, A.A., and Brand, M.D. (2013). Sites of superoxide and hydrogen peroxide production during fatty acid oxidation in rat skeletal muscle mitochondria. *Free Radic. Biol. Med.* *61*, 298–309.
- Péron, S., Droguerre, M., Debarbieux, F., Ballout, N., Benoit-Marand, M., Francheteau, M., Brot, S., Rougon, G., Jaber, M., and Gaillard, A. (2017). A Delay between Motor Cortex Lesions and Neuronal Transplantation Enhances Graft Integration and Improves Repair and Recovery. *J. Neurosci.* *37*, 1820–1834.
- Pfeiffer, T., Schuster, S., and Bonhoeffer, S. (2001). Cooperation and Competition in the Evolution of ATP-Producing Pathways. *Science* (80-. ). *292*, 504–507.
- Plucinska, G., Paquet, D., Hruscha, A., Godinho, L., Haass, C., Schmid, B., and Misgeld, T. (2012). In Vivo Imaging of Disease-Related Mitochondrial Dynamics in a Vertebrate Model System. *J. Neurosci.* *32*, 16203–16212.
- Plucińska, G., and Misgeld, T. (2016). Imaging of neuronal mitochondria in situ. *Curr. Opin. Neurobiol.* *39*, 152–163.
- Politis, M., and Lindvall, O. (2012). Clinical application of stem cell therapy in Parkinson's disease. *BMC Med.* *10*, 1.
- Polyzos, A.A., Lee, D.Y., Datta, R., Hauser, M., Budworth, H., Holt, A., Mihalik, S., Goldschmidt, P., Frankel, K., Trego, K., et al. (2019). Metabolic Reprogramming in Astrocytes Distinguishes Region-

Specific Neuronal Susceptibility in Huntington Mice. *Cell Metab. 0*.

Poskanzer, K.E., and Molofsky, A. V. (2018). Dynamism of an Astrocyte In Vivo: Perspectives on Identity and Function. *Annu. Rev. Physiol. 80*, 143–157.

Prieto, J., León, M., Ponsoda, X., Sendra, R., Bort, R., Ferrer-Lorente, R., Raya, A., López-García, C., and Torres, J. (2016). Early ERK1/2 activation promotes DRP1-dependent mitochondrial fission necessary for cell reprogramming. *Nat. Commun. 7*, 11124.

Prigione, A., Fauler, B., Lurz, R., Lehrach, H., and Adjaye, J. (2010). The Senescence-Related Mitochondrial / Oxidative Stress Pathway is Repressed in Human Induced Pluripotent Stem Cells. *Stem Cells 28*, 721–733.

Prigione, A., Hossini, A.M., Lichtner, B., Serin, A., Fauler, B., Megges, M., Lurz, R., Lehrach, H., Makrantonaki, E., Zouboulis, C.C., et al. (2011). Mitochondrial-Associated Cell Death Mechanisms Are Reset to an Embryonic-Like State in Aged Donor-Derived iPS Cells Harboring Chromosomal Aberrations. *PLoS One 6*, e27352.

Prigione, A., Rohwer, N., Hoffmann, S., Mlody, B., Katharina, D., Bukowiecki, R., Blümlein, K., Wanker, erich e., Ralser, M., Cramer, T., et al. (2014). Hif1a modulates cell fate reprogramming through early glycolytic shift and upregulation of PDK1-3 and PKM2. *Stem Cells 364–376*.

Prigione, A., Ruiz-Pérez, M.V., Bukowiecki, R., and Adjaye, J. (2015). Metabolic restructuring and cell fate conversion. *Cell. Mol. Life Sci. 72*, 1759–1777.

Prozorovski, T., Schneider, R., Berndt, C., Hartung, H.-P., and Aktas, O. (2015). Redox-regulated fate of neural stem progenitor cells. *Biochim. Biophys. Acta 1850*, 1543–1554.

Quadrato, G., Zhang, A.C., and Arlotta, P. (2016). Stressed out? Healing Tips for Newly Reprogrammed Neurons. *Cell Stem Cell 18*, 297–299.

Quaegebeur, A., Segura, I., Schmieder, R., Verdegem, D., Decimo, I., Bifari, F., Dresselaers, T., Eelen, G., Ghosh, D., Davidson, S.M., et al. (2016). Deletion or inhibition of the oxygen sensor PHD1 protects against ischemic stroke via reprogramming of neuronal metabolism. *Cell Metab. 23*, 280–291.

Rafalski, V.A., and Brunet, A. (2011). Energy metabolism in adult neural stem cell fate. *Prog. Neurobiol. 93*, 182–203.

Rajkovic, O., Potjewyd, G., and Pinteaux, E. (2018). Regenerative Medicine Therapies for Targeting Neuroinflammation After Stroke. *Front. Neurol. 9*, 734.

Rivetti di Val Cervo, P., Romanov, R.A., Spigolon, G., Masini, D., Martín-Montañez, E., Toledo, E.M., La Manno, G., Feyder, M., Pifl, C., Ng, Y.-H., et al. (2017). Induction of functional dopamine neurons from human astrocytes in vitro and mouse astrocytes in a Parkinson's disease model. *Nat. Biotechnol. 35*, 444–452.

Robel, S., Berninger, B., and Götz, M. (2011). The stem cell potential of glia: lessons from reactive gliosis. *Nat. Rev. Neurosci. 12*, 88–104.

Rowe, R.G., and Daley, G.Q. (2019). Induced pluripotent stem cells in disease modelling and drug discovery. *Nat. Rev. Genet. 1*.

Rubio, A., Luoni, M., Giannelli, S.G., Radice, I., Iannielli, A., Cancellieri, C., Di Bernardino, C., Regalia, G., Lazzari, G., Menegon, A., et al. (2016). Rapid and efficient CRISPR/Cas9 gene inactivation in human neurons during human pluripotent stem cell differentiation and direct reprogramming. *Sci. Rep. 6*, 37540.

Russo, M. V, and McGavern, D.B. (2015). Immune Surveillance of the CNS following Infection and Injury. *Trends Immunol. 36*, 637–650.

Saab, A.S., Tzvetanova, I.D., and Nave, K.A. (2013). The role of myelin and oligodendrocytes in axonal energy metabolism. *Curr. Opin. Neurobiol. 23*, 1065–1072.

Schönfeld, P., and Reiser, G. (2013). Why does Brain Metabolism not Favor Burning of Fatty Acids to Provide Energy? - Reflections on Disadvantages of the Use of Free Fatty Acids as Fuel for Brain. *J.*

Cereb. Blood Flow Metab. 33, 1493–1499.

Schreiner, B., Romanelli, E., Liberski, P., Ingold-Heppner, B., Sobottka-Brillout, B., Hartwig, T., Chandrasekar, V., Johannssen, H., Zeilhofer, H.U., Aguzzi, A., et al. (2015). Astrocyte Depletion Impairs Redox Homeostasis and Triggers Neuronal Loss in the Adult CNS. *Cell Rep.* 12, 1377–1384.

Sena, L.A., and Chandel, N.S. (2012). Physiological roles of mitochondrial reactive oxygen species. *Mol. Cell* 48, 158–166.

Shear, D.A., Tate, C.C., Tate, M.C., Archer, D.R., LaPlaca, M.C., Stein, D.G., and Dunbar, G.L. (2011). Stem cell survival and functional outcome after traumatic brain injury is dependent on transplant timing and location. *Restor. Neurol. Neurosci.* 29, 215–225.

Shi, Y., Inoue, H., Wu, J.C., and Yamanaka, S. (2017). Induced pluripotent stem cell technology: a decade of progress. *Nat. Rev. Drug Discov.* 16, 115–130.

Shin, J., Berg, D.A., Zhu, Y., Shin, J.Y., Song, J., Bonaguidi, M.A., Enikolopov, G., Nauen, D.W., Christian, K.M., Ming, G.L., et al. (2015). Single-Cell RNA-Seq with Waterfall Reveals Molecular Cascades underlying Adult Neurogenesis. *Cell Stem Cell* 17, 360–372.

Silver, J., Schwab, M.E., and Popovich, P.G. (2014). Central nervous system regenerative failure: role of oligodendrocytes, astrocytes, and microglia. *Cold Spring Harb. Perspect. Biol.* 7, a020602.

Simon, C., Götz, M., and Dimou, L. (2011). Progenitors in the adult cerebral cortex: Cell cycle properties and regulation by physiological stimuli and injury. *Glia* 59, 869–881.

Sirko, S., Behrendt, G., Johansson, P.A., Tripathi, P., Costa, M.R., Bek, S., Heinrich, C., Tiedt, S., Colak, D., Dichgans, M., et al. (2013). Reactive Glia in the Injured Brain Acquire Stem Cell Properties in Response to Sonic Hedgehog. *Cell Stem Cell* 12, 426–439.

Sofroniew, M. V., and Vinters, H. V (2010). Astrocytes: biology and pathology. *Acta Neuropathol.* 119, 7–35.

Son, M.J., Jeong, B.R., Kwon, Y., and Cho, Y.S. (2013). Interference with the mitochondrial bioenergetics fuels reprogramming to pluripotency via facilitation of the glycolytic transition. *Int. J. Biochem. Cell Biol.* 45, 2512–2518.

Southwell, D.G., Nicholas, C.R., Basbaum, A.I., Stryker, M.P., Kriegstein, A.R., Rubenstein, J.L., and Alvarez-Buylla, A. (2014). Interneurons from Embryonic Development to Cell-Based Therapy. *Science* (80-. ). 344, 1240622–1240622.

Souza, D.G., Almeida, R.F., Souza, D.O., and Zimmer, E.R. (2019). The astrocyte biochemistry. *Semin. Cell Dev. Biol.*

Spinelli, J.B., and Haigis, M.C. (2018). The multifaceted contributions of mitochondria to cellular metabolism. *Nat. Cell Biol.* 20, 745–754.

Steib, K., Scha, I., Jagasia, R., Ebert, B., and Lie, D.C. (2014). Mitochondria Modify Exercise-Induced Development of Stem Cell-Derived Neurons in the Adult Brain. *J. Neurosci.* 34, 6624–6633.

Stincone, A., Prigione, A., Cramer, T., Wamelink, M.M.C., Campbell, K., Cheung, E., Olin-Sandoval, V., Grüning, N.M., Krüger, A., Tauqeer Alam, M., et al. (2015). The return of metabolism: Biochemistry and physiology of the pentose phosphate pathway. *Biol. Rev.* 90, 927–963.

Stricker, S.H., and Götz, M. (2018). DNA-Methylation: Master or Slave of Neural Fate Decisions? *Front. Neurosci.* 12, 5.

Supplie, L.M., Düking, T., Campbell, G., Diaz, F., Moraes, C.T., Götz, M., Hamprecht, B., Boretius, S., Mahad, D., and Nave, K.-A. (2017). Respiration-Deficient Astrocytes Survive As Glycolytic Cells In Vivo. *J. Neurosci.* 37, 4231–4242.

Swiech, L., Heidenreich, M., Banerjee, A., Habib, N., Li, Y., Trombetta, J., Sur, M., and Zhang, F. (2015). In vivo interrogation of gene function in the mammalian brain using CRISPR-Cas9. *Nat. Biotechnol.* 33, 102–106.

Takahashi, K., and Yamanaka, S. (2006). Induction of Pluripotent Stem Cells from Mouse Embryonic

and Adult Fibroblast Cultures by Defined Factors. *Cell* 126, 663–676.

Takahashi, K., Tanabe, K., Ohnuki, M., Narita, M., Ichisaka, T., Tomoda, K., and Yamanaka, S. (2007). Induction of Pluripotent Stem Cells from Adult Human Fibroblasts by Defined Factors. *Cell* 131, 861–872.

Tanabe, K., Ang, C.E., Chanda, S., Olmos, V.H., Haag, D., Levinson, D.F., Südhof, T.C., and Wernig, M. (2018). Transdifferentiation of human adult peripheral blood T cells into neurons. *Proc. Natl. Acad. Sci.* 115, 6470–6475.

Tang, B.L. (2016). The astrocyte scar - not so inhibitory after all? *Neural Regen. Res.* 11, 1054–1055.

Teslaa, T., and Teitell, M.A. (2015). Pluripotent stem cell energy metabolism : an update. *EMBO J.* 34, 138–153.

Thomas, C.E., Ehrhardt, A., and Kay, M.A. (2003). Progress and problems with the use of viral vectors for gene therapy. *Nat. Rev. Genet.* 4, 346–358.

Torper, O., Pfisterer, U., Wolf, D.A., Pereira, M., Lau, S., Jakobsson, J., Bjorklund, A., Grealish, S., and Parmar, M. (2013). Generation of induced neurons via direct conversion in vivo. *Proc. Natl. Acad. Sci.* 110, 7038–7043.

Torper, O., Ottosson, D.R., Pereira, M., Cardoso, T., Grealish, S., Parmar, M., Torper, O., Ottosson, D.R., Pereira, M., Lau, S., et al. (2015). In Vivo Reprogramming of Striatal NG2 Glia into Functional Neurons that Integrate into Local Host. *Cell Rep.* 12, 1–8.

Valvona, C.J., Fillmore, H.L., Nunn, P.B., and Pilkington, G.J. (2015). The Regulation and Function of Lactate Dehydrogenase A: Therapeutic Potential in Brain Tumor. *Brain Pathol.* 26, 3–17.

Vannucci, S.J., Clark, R.R., Koehler-Stec, E., Kang, L., Smith, C.B., Davies, P., Maher, F., and Simpson, I.A. (1998). Glucose Transporter Expression in Brain: Relationship to Cerebral Glucose Utilization. *Dev. Neurosci.* 20, 369–379.

Verkhatsky, A., and Nedergaard, M. (2018). Physiology of Astroglia. *Physiol. Rev.* 98, 239–389.

Victor, M.B., Richner, M., Hermanstynne, T.O., Ransdell, J.L., Sobieski, C., Deng, P.-Y., Klyachko, V.A., Nerbonne, J.M., and Yoo, A.S. (2014). Generation of Human Striatal Neurons by MicroRNA-Dependent Direct Conversion of Fibroblasts. *Neuron* 84, 311–323.

Vierbuchen, T., Ostermeier, A., Pang, Z.P., Kokubu, Y., Südhof, T.C., and Wernig, M. (2010). Direct conversion of fibroblasts to functional neurons by defined factors. *Nature* 463, 1035–1041.

Völgyi, K., Gulyássi, P., Háden, K., Kis, V., Badics, K., Kékesi, K.A., Simor, A., Györfy, B., Tóth, E.A., Lubec, G., et al. (2015). Synaptic mitochondria: A brain mitochondria cluster with a specific proteome. *J. Proteomics* 120, 142–157.

Wang, X., and Gerdes, H. (2015). Transfer of mitochondria via tunneling nanotubes rescues apoptotic PC12 cells. *Cell Death Differ.* 22, 1181–1191.

Wang, X., and Michaelis, E.K. (2010). Selective neuronal vulnerability to oxidative stress in the brain. *Front. Aging Neurosci.* 2, 12.

Wang, S., Xia, P., Ye, B., Huang, G., Liu, J., and Fan, Z. (2013). Transient Activation of Autophagy via Sox2-Mediated Suppression of mTOR Is an Important Early Step in Reprogramming to Pluripotency. *Cell Stem Cell* 13, 617–625.

Weber, B., and Barros, L.F. (2015). The Astrocyte: Powerhouse and Recycling Center. *Cold Spring Harb. Perspect. Biol.* 7, a020396.

Wernig, M., Zhao, J.-P., Pruszak, J., Hedlund, E., Fu, D., Soldner, F., Broccoli, V., Constantine-Paton, M., Isacson, O., and Jaenisch, R. (2008). Neurons derived from reprogrammed fibroblasts functionally integrate into the fetal brain and improve symptoms of rats with Parkinson's disease. *Proc. Natl. Acad. Sci.* 105, 5856–5861.

Willems, P.H.G.M., Rossignol, R., Dieteren, C.E.J., Murphy, M.P., and Koopman, W.J.H. (2015). Redox Homeostasis and Mitochondrial Dynamics. *Cell Metab.* 22, 207–218.

- Wilson, D.F. (2017). Oxidative phosphorylation: regulation and role in cellular and tissue metabolism. *J. Physiol.* *595*, 7023–7038.
- Winblad, B., Amouyel, P., Andrieu, S., Ballard, C., Brayne, C., Brodaty, H., Cedazo-Minguez, A., Dubois, B., Edvardsson, D., Feldman, H., et al. (2016). Defeating Alzheimer’s disease and other dementias: a priority for European science and society. *Lancet Neurol.* *15*, 455–532.
- Wu, Y., Zhang, X., Kang, X., Li, N., Wang, R., Hu, T., Xiang, M., Wang, X., Yuan, W., Chen, A., et al. (2013). Oxidative stress inhibits adhesion and transendothelial migration, and induces apoptosis and senescence of induced pluripotent stem cells. *Clin. Exp. Pharmacol. Physiol.* *40*, 626–634.
- Xu, J., Du, Y., and Deng, H. (2015). Direct lineage reprogramming: Strategies, mechanisms, and applications. *Cell Stem Cell* *16*, 119–134.
- Yasuhara, T., Kameda, M., Sasaki, T., Tajiri, N., and Date, I. (2017). Cell Therapy for Parkinson’s Disease. *Cell Transplant.* *26*, 1551–1559.
- Yoo, A.S., Sun, A.X., Li, L., Shcheglovitov, A., Portmann, T., Li, Y., Lee-Messer, C., Dolmetsch, R.E., Tsien, R.W., and Crabtree, G.R. (2011). MicroRNA-mediated conversion of human fibroblasts to neurons. *Nature* *476*, 228–231.
- Yoshida, Y., Takahashi, K., Okita, K., Ichisaka, T., and Yamanaka, S. (2009). Hypoxia Enhances the Generation of Induced Pluripotent Stem Cells. *Cell Stem Cell* *5*, 237–241.
- Zhang, J., Nuebel, E., Daley, G.Q., Koehler, C.M., and Teitell, M.A. (2012). Metabolic regulation in pluripotent stem cells during reprogramming and self-renewal. *Cell Stem Cell* *11*, 589–595.
- Zhang, Y., Chen, K., Sloan, S.A., Bennett, M.L., Scholze, A.R., O’Keeffe, S., Phatnani, H.P., Guarnieri, P., Caneda, C., Ruderisch, N., et al. (2014). An RNA-sequencing transcriptome and splicing database of glia, neurons, and vascular cells of the cerebral cortex. *J. Neurosci.* *34*, 11929–11947.
- Zhou, G., Meng, S., Li, Y., Ghebre, Y.T., and Cooke, J.P. (2016). Optimal ROS Signaling Is Critical for Nuclear Reprogramming. *Cell Rep.* *15*, 919–925.
- Zhou, H., Liu, J., Zhou, C., Gao, N., Rao, Z., Li, H., Hu, X., Li, C., Yao, X., Shen, X., et al. (2018). In vivo simultaneous transcriptional activation of multiple genes in the brain using CRISPR–dCas9-activator transgenic mice. *Nat. Neurosci.* *21*, 440–446.
- Zhu, S., Li, W., Zhou, H., Wei, W., Ambasudhan, R., Lin, T., Kim, J., Zhang, K., and Ding, S. (2010). Reprogramming of human primary somatic cells by OCT4 and chemical compounds. *Cell Stem Cell* *7*, 651–655.

# Curriculum Vitae Gianluca Luigi Russo

## ***Personal Data***

Date of birth: June 23, 1989

Nationality: Italian

Address: Zeppelinstrasse 45, München, Germany

Cell phone: +49 176 2831 8472

E-mail: [gianluca.l.russo@gmail.com](mailto:gianluca.l.russo@gmail.com)

## ***Professional Experience***

---

09.2014-08.2019      **PhD student in Neuroscience**, laboratory of Prof. Dr. Magdalena Götz, Ludwig-Maximilians University, Munich:

- Independent organization of scientific experiments, coordinating and setting up multiple collaborations among different research institutes in Munich
- Project supervisor of different master students in a big laboratory with multi-national background
- Handling of three different projects focused on neuro-regenerative approaches with time-management organizational approach and optimization of resources
- Monthly presentations about my projects and papers in front of a big audience using fluent English
- Publication as first author and co-author of 4 papers in high impact factors journals

11.2013-08.2014      **Research assistant**, laboratory of Prof. Dr. Gianvito Martino, San Raffaele Scientific Institute, Milan:

- Critical reading of papers and routine laboratories skills acquisition
- Scientific English writing and revision of thesis, papers, grants
- Big amount of data handling and critical prioritization of work

## ***Education***

---

2015-2018      **PhD in Neuroscience**, Graduate School of Systemic Neuroscience, at the Ludwig-Maximilians University, Munich

2011-2013      **Master of Science in Molecular and Cellular Medical Biotechnology**, at the University Vita-Salute San Raffaele, Milano. *Mark: 110/110 cum laude*

2008-2011      **Bachelor of Science in Medical and Pharmaceutical Biotechnology**, at the University Vita-Salute San Raffaele, Milano. *Mark: 110/110 cum laude*

2003-2008      **High school Diploma specializing in scientific education**, at Liceo Scientifico Statale Barsanti e Matteucci, Viareggio (LU). *Mark: 100/100*

## ***Organization and leadership***

---

11.2017-05.2018      Co-organizer of the event in Munich for scientific divulgation to the public **Pint of Science 2018**

01.2017-05.2017      Co-organizer of the event in Munich for scientific divulgation to the public **Pint of Science 2017**

- Fundraising and sponsorship
- Selection and recruitment of speakers
- Logistic organization of the event

11.2015-11.2016 Co-organizer of the international conference **Interact 2016: Life Science Symposium**, 3-4 November, Munich:

- Contacting and securing several industrial and academic sponsorship
- Collection and allocation of a total budget of 31.000 euro
- Organization of sponsored goods and major awards
- End-to-end management and extending support to the company representatives at the company fair
- Conflict management and negotiation skills

### Awards and Scholarship

2015 Selected as PhD student at the **Graduate School of Systemic Neuroscience**, LMU, Munich, supporting conferences, travels and salary (admission rate 7%)

### Scientific skills

Preparation and culture of murine adult and embryonal neural stem cells, astrocytes, oligodendrocyte precursor cells, human and murine fibroblasts.

Animal handling and i.p./i.v. injections. Stereotaxic and i.c.v. injections. Animal sacrifice, perfusion and tissues extraction, cryostat and vibratome tissue cut, tissue and cellular staining (IF, IHC). (FELASA international certificate for animal handling)

Live imaging (spinning disk microscope), epifluorescence and confocal microscope images acquisition and processing.

RNA extraction and retrotranscription, RT-PCR Taqman, PCR for genotyping. Western Blotting and ELISA. DNA Cloning and lentivirus production. Proteomic data analysis.

### Poster/Oral Presentations

Poster presentation and/or oral talk at the the following conferences;

- December 2018: Cell Symposia, *Metabolites as signaling molecules*, Seattle, Washington, USA.
- June 2017: Keystone Symposium, *Neuroinflammation*, Keystone, Colorado, USA.
- April 2017: Abcam Symposium, *Programming and Reprogramming of the Brain*, Munich, Germany.
- September 2016: Cell Symposium, *10 Years of iPSCs*, Berkeley, USA.
- April 2014: 8th Symposium on Neuroprotection and Neurorepair, Magdeburg, Germany.

### Software

#### **Windows and MAC OS**

Excel, Powerpoint, Word, Pages

#### **Imaging**

LasAF, ImageJ, Fiji, Photoshop, ZEN software, Neurolucida, Stereo Investigator

#### **Statistical and Others**

GraphPad Prism, DAVID, Gorilla, Endnote, Mendeley

### Language skills

Italian (Mother tongue)

English (Advanced level, Cambridge First Certificate, ESOL, B.2)

German (Intermediate level, IUCM B.2 certificate)

Spanish (Basic level)

## Publications

- **Russo, G.L.**, Sonsalla, G., Breunig, C.T., Merl-Pham, J., Schmitt, S., Jastroch, M., Zischka, H., Stricker, S., Hauck, S.M., Masserdotti, G. and Götz M. Mitochondrial reprogramming using dCas9 boosts glia-to-neuron conversion. *Manuscript in preparation*
- Mattugini, N.,\* Bocchi, R.\*, **Russo, G.L.**, Torper, O., Lao, C.L. and Götz M. Region and layer specific differences in astrocyte-to-neuron reprogramming. *Unver second revision in Neuron*.
- (Review) Gascon, S.,\* Masserdotti, G.\*, **Russo, G.L.\*** and Götz M. (2017). Direct neuronal reprogramming: achievements, hurdles and new roads to success. *Cell Stem Cell*, 21(1), 18-34.
- (Book Chapter) Bacigaluppi, M., **Russo, G.L.** and Martino G. (2017). Neuroregeneration after stroke, chapter *Current Development in Stroke*, Bentham eBooks. Rev 02, Issue 01.
- Gascon, S., Murenu, E., Masserdotti, G., Ortega, F., **Russo, G. L.**, Petrik, D., ... Götz, M. (2016). Identification and Successful Negotiation of a Metabolic Checkpoint in Direct Neuronal Reprogramming. *Cell Stem Cell*, 18(3): 396-409.
- Bacigaluppi, M., **Russo, G. L.**, Peruzzotti-Jametti, L., Rossi, S., Sandrone, S., Butti, E., ... Martino, G. (2016). Neural Stem Cell Transplantation Induces Stroke Recovery by Upregulating Glutamate Transporter GLT-1 in Astrocytes. *Journal of Neuroscience*, 36(41), 10529–10544.

Eidesstattliche Versicherung/Affidavit

Hiermit versichere ich an Eides statt, dass ich die vorliegende Dissertation **“Unraveling and overcoming hurdles in direct neuronal reprogramming”** selbstständig angefertigt habe, mich außer der angegebenen keiner weiteren Hilfsmittel bedient und alle Erkenntnisse, die aus dem Schrifttum ganz oder annähernd übernommen sind, als solche kenntlich gemacht und nach ihrer Herkunft unter Bezeichnung der Fundstelle einzeln nachgewiesen habe.

I hereby confirm that the dissertation **“Unraveling and overcoming hurdles in direct neuronal reprogramming”** is the result of my own work and that I have only used sources or materials listed and specified in the dissertation.

München, den  
Munich, date

06.09.2019

Unterschrift  
Signature

Gianluca Luigi Russo

## Declaration of Author Contribution

1. **Russo, G.L.**, Sonsalla, G., Breunig, C.T., Merl-Pham, J., Schmitt, S., Jastroch, M., Zischka, H., Stricker, S., Hauck, M.S., Masserdotti, G. and Götz M. Mitochondrial reprogramming using dCas9 boosts glia-to-neuron conversion. *Manuscript ready for submission.*

M.G. conceived and designed the project. **G.L.R. shaped the project and performed most of the experiments and analysis.** G.S. contributed to some immunostainings. C.T.B. and S.S. provided the CRISPR Cas expertise, developed and designed the STAgR approach, and C.B. helped with cloning of the constructs. J.M-P. and S.M.H. provided the proteomic expertise, experiments and analysis. S.S. and H.Z. performed the mitochondrial isolation and electron microscopy. M.J. provided expertise in metabolism and Seahorse analysis. G.M. provided expertise and training of G.L.R. in reprogramming and was also involved in directing the project together with M.G. **G.L.R. and M.G. wrote the manuscript and all authors contributed corrections and comments.**

2. Mattugini, N.,\* Bocchi, R.\*, **Russo, G.L.**, Torper, O., Lao, C.L. and Götz M. Region and layer specific differences in astrocyte-to-neuron reprogramming. *Unver revision in Neuron.*

M.G., N.M. and R.B. conceived the experiments, discussed the data and wrote the manuscript. N.M. and R.B. performed almost all experiments and analyzed the data. **G.L.R. tested the immune response to viral vectors.** O.T. provided AAV expertise and scientific inputs. C.L. prepared viral vectors.

3. Gascon, S., Murenu, E., Masserdotti, G., Ortega, F., **Russo, G.L.**, Petrik, D., ... Götz, M. (2016). Identification and Successful Negotiation of a Metabolic Checkpoint in Direct Neuronal Reprogramming. *Cell Stem Cell*, 18(3): 396-409.

S.G. and M.G. conceived and designed the experiments; S.G., E.M., and M.G. designed in vivo experiments; E.M. performed in vivo experiments; S.G., F.O., A.D., **G.L.R.**, and M.K. **performed in vitro experiments;** D.P. performed electrophysiological recordings; M.I., S.G., M.G., and G.M. performed genome-wide experiments and analysis; S.G., E.M., G.M., F.O., A.D., and **G.L.R. analyzed data;** G.M., M.I., J.B., J.P.F.A., M.C., C.B., T.S., and S.R. contributed reagents/materials/analysis tools; and M.G., S.G., E.M., and B.B. wrote the paper. **All authors discussed the manuscript.**

Signature

Prof. Dr. Magdalena Götz

PhD candidate: Gianluca Luigi Russo

## Acknowledgements

I perfectly remember the first time I landed in Munich, almost five years ago, excited and scared about a new chapter of my life waiting for me. Will I like the city? Will I ever learn German? Will I be a successful researcher? And yet, five years later, I still find myself at the same place where I started, with most of these questions answered (I will never learn this language properly), and new doubts coming out in my head. Thus, I still find myself facing those mixed feelings of excitement and fear about what the future might hold for me, with a surprisingly enhanced feeling of *italianity* within myself.

Nevertheless, I am also totally different from the person I was 5 years ago. I have reached a level of maturity, satisfaction and consciousness of who I am and who I want to become, thanks to all the skills I have learnt, that I could have hardly imagined when I started this journey. As much as I may like to believe I was the only player in this path of personal and professional growth, the Ph.D. experience was the fundamental step in this process. But the Ph.D. itself could not have taught me so much, if it were not for the people who accompanied me in this long journey. And as crazy as it might sound for someone, or maybe for even myself, when I will read these words in the future, it has been the best experience of my life (so far).

The first person I need to acknowledge is definitely Magdalena. Your passion, your enthusiasm, your excitement for science, that I have rarely seen in any scientists I have met, gave me the stronger will to pursue my Ph.D. and to succeed. You gave me the chance to test myself in different tasks and projects, with daily challenges, guiding me, directly or indirectly, to understand what are my strength and weakness. I will be always grateful for the chance you gave me.

On the same line of professional acknowledgements I have to say thank you to my second supervisor, Giacomo Masserdotti. Thank you for always been there to answer my questions and doubts, your patience and your support.

Thanks to all the smart colleagues and collaborators, which allowed me to produce or being part of projects of which I am very proud of.

Of course I have to thank all the members of the lab for their professional support, the technicians for the great technical help, the secretaries and the members of my TAC for the precious feedback and inputs. Special thanks also to the people who allowed me to be part of the GSN and its staff, I am very grateful for all the support you provide to the students to become better scientists and professionals. You also allowed me to meet beautiful people, now friends.

As the professional growth goes hand by hand with personal improvement, nothing of this would have been possible without my precious colleagues, which

became part of my Munich family with time. Thanks to Radhika, for cheering me up every time I speak with you, with a meme or with an endless vocal message, and for having one of the warmest heart I have ever met. I am lucky you did not send me to hell the first time we met and I offended you saying your food looked like parrot food. Thanks to Luisa, for your joyful, open-minded and determined spirit, for always being present for me when I needed, and always giving personal and professional advices. Thanks to Sofia, for standing my jokes on your age all the time, you are the smartest, sweetest and youngest (inside) of all of us, and I am very proud of having you as a friend. Thanks to Daisy, for her cheerful smiles and support, and still standing me after such a long time. You were the first friend I had in Munich, and I am very happy we still share so many beautiful moments together. Thanks to Judith, for her warm comprehension and understanding, her emotional support and german lessons. Thanks Amel for being my partner in crime and never judging me, helping me in first place to judge myself less. Thanks Gia for your professional and personal help, and always having a hug ready when needed. Thanks Allwyn for standing me and my racist jokes, you are the best. Thanks also to all the other members of my present and past offices, for sharing an encouraging word or just a laugh when needed, you made the lab life always easier and more pleasant.

Of course thanks to Nico, we had to move 1000km far from home to get to know each other and become friends. I am very happy you ignored me in high school, otherwise probably by now we would have not been so close. I think age suits us very well, *I mejo dei mejo für immer*. On this line, sincere thanks go to my extended Italian family in Munich. Thanks to Giorgia, my favourite travel buddy. Your honesty and your friendship is truly worth to me, you are a reference point for me in Munich and I am looking forward more trips and experiences to share. Thanks to Benedetta, for being so smart and sophisticated, but also crazy and alternative, thanks for your constant psychological support and for teaching me a new point of view on the world. Luckily I did not kill you the first time we had a party together and I smashed you on the tables of the drinks. Thanks to Valeria, since the first time we met at the german class, for enduring our friendship despite our failed attempts to improve german together. Thanks Silvia, my favourite over-seas travel buddy! Last but not least, thanks to Elisabetta, for our 10 years friendship and for being the best *girlfriend* and roommate I could have wished for.

Thanks also to Admir, you helped me seeing myself from a perspective I never considered; your lesson and your friendship will always be part of me. Thanks Manu, you gave me so much more than just a place where I could write my thesis in peace. Thanks to the community that cheered up my evenings, my trips, parties, BBQ on the Isar, and much more, making me feel special and loved. Thanks to, in random order, to Fortunato, Matteo, Gerardo, Coco, Ketu, Veriko, Carmen, Sachith, Flo, Shehjar, Pablo, Ulrico, Aurore and many more! Special

thanks to Arcan, you truly inspired me to be myself, in a moment where I was clearly lost.

Thanks to my Italian family living in Italy, composed by my long-life friends and by my Family. Wherever I have been, in every stage of my life, you always made me feel home and loved. I cannot see my life without you. Thanks to Jessica for being so true to yourself and so open to support me in every situation. You make me feel like part of your family, and I am proud to be uncle to beautiful Luna, *caciottina!* Thanks to Mara, my evil twin sister, for always making me laugh and encouraging me, you are very special. Thanks Laura for always being there since I basically can remember, I am proud we are in each others life and we keep on sharing beautiful memories together. Thanks to Marco e Alessandro, for listening and being part of my closer friends, every time I go back to Italy you make me feel like Home. Thanks to Vale D.C., I am so proud of who you have become and to have you with me in this new chapter of my life.

Of course, biggest acknowledgements go to my family, whose support and love never missed, I am very lucky to have you as inspiration and role models! Thanks to my Dad, for his strength, pragmatism, unconditional love and drive to make me ambitious. Thanks to my Mom, my role model, for her emotional support, her empathy, her strength, her being herself always and teaching me to accept and love myself. Thanks Mari, for always loving me as if I was your son, I do not see a life without your support and affection. Thanks to Davide, for being my brother, differences in age or character never set us apart and never will.

And of course thanks to me, myself and I, for enduring, succeeding, pursuing, and improving myself, accepting to love the way I am. Keep on working on yourself, there is always time and space to become a better human being.

München, 06.05.2019

Gianluca Luigi Russo